Performance Steel Castings

David R. Poweleit and Raymond W. Monroe

Steel Founders' Society of America (SFSA)

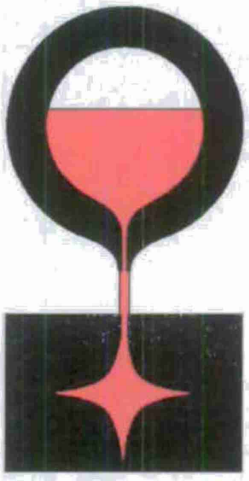

Final Report
Report # PSC-2012
November 3, 2006 to June 30, 2012

Research was sponsored by the U.S. Army Benet Laboratories and was accomplished under Cooperative Agreement Number W15QKN-08-2-0007. The views and conclusions contained in this document are those of the authors and should not be interpreted as representing the official policies, either expressed or implied, of U.S. Army Benet Laboratories or the U.S. Government. The U.S. Government is authorized to reproduce and distribute reprints for Government purposes notwithstanding any copyright notation heron.

Title

Report #: PSC-2012

Report title: Performance Steel Castings

Submitted by: David R. Poweleit and Raymond W. Monroe

Performed by: Steel Founders' Society of America (SFSA), 780 McArdle Dr Unit G, Crystal Lake, IL 60014

Final technical report for November 3, 2006 to June 30, 2012

Cooperative Agreement #: W15QKN-08-2-0007, W15QKN-06-R-0501, and MIPR funds from DLA R&D and ARL

Sponsored by: the U.S. Army Benet Laboratories; US Army JM&L LCMC Acquisition Center, AMSML-AQ-JA Bldg 10, Picatinny Arsenal, NJ 07806-5000

Subject descriptors: steel, casting, modeling, performance, rapid tooling, sand, armor, alloys, foundry, muzzle brake, supply center, tooling, sources

Notice

Format Information

Report created in Microsoft Word

Report Documentation

Appendix A: SF 298

Contents

Acknowledgments

Research was sponsored by the U.S. Army Benet Laboratories and was accomplished under Cooperative Agreement Number W15QKN-08-2-0007. The views and conclusions contained in this document are those of the authors and should not be interpreted as representing the official policies, either expressed or implied, of U.S. Army Benet Laboratories or the U.S. Government. The U.S. Government is authorized to reproduce and distribute reprints for Government purposes notwithstanding any copyright notation heron.

SFSA would also like to acknowledge the team that supported this effort: Benét Laboratories, Army Research Laboratories, DLA R&D J335, University of Iowa, Iowa State University, University of Northern Iowa, Non-Ferrous Founders' Society, QuesTek, buyCASTINGS.com, Spokane Industries, Nova Precision Casting, Waukesha Foundry and the members of Steel Founders' Society of America.

Abstract

Weapon system designers and builders need advanced steel casting technology to achieve the performance goals required for new systems. The dramatic reduction in weight and increase in capability will require high performance components with complex geometries. SFSA combined the latest developments in technology to improve the design and manufacturing of steel castings for improved weapon system reliability. SFSA developed innovative casting design and manufacturing processes for high performance parts. SFSA is uniquely positioned through its industry leadership steel casting R&D to assume a prominent role in the development of industry-ready, performance steel casting technology. R&D led to innovative capability to simulate the steel casting applications, manufacture short run tooling, and acquire advanced sand properties for modeling. SFSA developed the initial thrust on encapsulated ceramic armor tiles through steel casting. SFSA provided technical support and technology tools, including sourcing and tooling, to support the procurement of castings, which provided a benefit through facilitating a robust supply chain while minimizing cost and lead-time.

Introduction

Weapon system designers and builders need advanced steel casting technology to achieve the performance goals required for new systems. The dramatic reduction in weight and increase in capability will require high performance components with complex geometries. Steel castings are not effectively used to produce the needed components because of uncertainties in performance and inefficiencies in production.

Support of legacy weapon systems faces a multitude of challenges. Diminishing manufacturing sources, low-volume procurement, out-dated specifications, and broken supply chains. Research to develop technology tools to rapidly identify tooling and sources is one opportunity to support the warfighter's mission. Enhancing capability in quality and cost reduction through foundry process improvement will better enable industry to support legacy cast parts.

Steel castings have been used in structural applications for fighting vehicles because of their extraordinary performance and capability. These components have design flexibility with robust mechanical properties. Applying new steel casting technology will achieve the highest levels of weapon system performance. Steel castings can exploit proven manufacturing technology to significantly reduce weight and improve reliability of structural components in future systems. The perception of steel castings as heavy, low performance components stems from the use of old designs that fail to fully utilize the material properties and aggressive design strategies to achieve performance.

This program developed the technology that will be deployed in legacy weapon systems, next generation system designs and future system concepts. This technology utilizes high performance parts that reduce weight and enhance capabilities.

The program was directed by the Steel Founders' Society of America (SFSA). SFSA is the world leader in developing steel casting technology and leverages over a century of service to ensure R&D is relevant and rapidly deployed in foundries. Member foundries, such as Rock Island Arsenal, will be able to utilize the developed technology. SFSA will utilize military part production experience at steel foundries that support the DOD.

The first year's efforts harvested some near term technology for fast success. The extensive development of manufacturing models of flow and solidification has been advanced dramatically by the University of Iowa (UI). The manufacturing models are integrated with design at the UI by Dr. Christoph Beckermann as an expansion of their efforts to integrate performance and quality in steel casting design. Several legacy parts and components were examined for improvement in the casting design or for replacement by a casting.

The advanced manufacturing effort was developed at the Iowa State University (ISU) by Dr. Frank Peters as an extension of their program on efficient steel casting manufacturing. The team at ISU has worked directly with steel foundries to improve the quality of manufacturing and the quality of the castings produced. They worked with foundries to optimize production of

components designed and optimized by UI.

Rapid tooling and pattern making for prototype components will be performed at the University of Northern Iowa (UNI). Professor Jerry Thiel will lead their team to take solid model designs and construct patterns required for component production using advanced prototyping and pattern making technologies. UNI's Metal Casting Center for applied foundry research will be utilized to make cast prototypes. UNI is the premiere research institute for sand technology. The development of sand properties is one key to unlocking higher integrity in casting simulation.

The program developed an approach for encapsulating a ceramic tile with cast steel to enable the development of low cost, high performance, light weight armor. The metal matrix will serve as a mechanism for joining the tiles together. The challenge is to develop a process that maintains the integrity of the ceramic tile, while providing zero tolerance adhesion between the metal and ceramic at a cost that will enable application on a large scale. This initiative also investigated a couple of wrought alloys as candidates for armor material.

Under this program, a task performed to provide technical support and technology tools to support the procurement of castings for the DLA and their DOD partners such as Benet Labs. Assistance was provided to sustain casting activities at the DLA Supply Centers. Support leveraged developed casting technology to enable casting procurements to deliver parts to the US warfighter. The continued development and application of tools such as the NFFS tooling and sourcing databases provided a benefit to facilitating a robust supply chain while minimizing cost and lead-time. This activity took advantage of best practices for casting acquisition by centers such as Benet Labs, Defense Supply Center Columbus and Defense Supply Center Richmond. The project demonstrated the benefit of a government-industry partnership, such as between Benet and SFSA, to provide premiere weapon system capability.

The entire effort leveraged work sponsored by the Defense Logistics Agency to sustain casting supply for their logistics needs and the Department of Energy to reduce energy consumption for manufacturing parts, along with the expertise of SFSA.

Results and Discussion

Development of Breech Nozzle Mesh

Dr. Richard Hardin worked with Prof. Matt Frank at Iowa State University to develop a solid model of the cast version of the breech nozzle which could be meshed using ABAQUS-CAE in order to perform finite element stress analysis (fea). Numerous iterations were required because of problem areas such as those highlighted in Figure 1 containing problems such as imprecise vertices, small edges and unmatched surfaces. Ultimately, a valid solid model was developed that could be properly meshed using ABAQUS-CAE after carefully repairing these problems through trial and error. The finite element mesh shown in Figure 2 was used to perform the stress analysis on the casting design using ABAQUS Standard. As shown in Figure 2, half symmetry was assumed in the analysis, and the boundary conditions and load applied were identical to those used by Benet Lab to analyze the original breech nozzle. The mesh density is similar to that used in the original analysis provided by Benet Lab, but has a higher number of elements (approximately 245,000 elements) than the original design (about 214,00 elements) due to the solid tube in the cast design. The same type of elements was used in ABAQUS simulations at the University of Iowa as in the Benet Lab simulations, 4-node linear tetrahedrons.

Elastic stress analysis was performed for the new design just as it was for the original design at Benet Lab. The original design fea run was repeated at the University of Iowa to generate output results for comparison with the new design. Elastic analysis material properties for AISI 8630 used were used: Young's modulus (205 GPa) and Poisson ratio (0.29). These were also used in the original Benet Lab fea run. Von Mises stress was considered as the design comparison criteria between the new casting design and original design. The Von Mises stress results on the fea mesh of for the new design is shown in Figure 3. The stress distributions for the original and casting designs are compared on the mid-plane of the nozzle in Figures 4 a) and b), respectively. A closer view of the highest stressed areas is shown in Figure 5. The maximum Von Mises Stress is 1043 MPa as shown in Figure 5 a) for the original design, and 854 MPa for the casting design as shown in Figure 5 b). An additional simulation was performed using elastic properties for stainless steel 17-4: 0.29 for Poisson ratio and 196 GPa for elastic modulus. Because the simulation is elastic, the strains increase by 4.4% for 17-4 and the stresses remain the same.

The fatigue life prediction software fe-safe was used with fatigue properties from the literature for 8630 and from research at the University of Iowa. The shortest fatigue life observed was 948 cycles as shown in Figure 6.

Casting simulations were run at Sivyer to develop a risering method for the casting, where only a small amount (1% to 2%) feeding shrinkage was predicted. The CAD models of the risering method (see Figure 7) was then transferred to U. of Iowa, where it was re-simulated using a finer mesh, with filling, and with thermo-physical properties generated using software at U. of Iowa. The feeding shrinkage predictions were about the same as Sivyer found, see Figures 8 and 9. The casting was also simulated using an advanced porosity prediction module for MAGMAsoft undergoing development and testing at the U. of Iowa. Four images of these results are shown in Figure 10. We believe these results to be more realistic and more sensitive; since they are based on simulating the feeding flow of liquid through the solidifying mush of liquid and solid. These results seem to agree with the standard MAGMAsoft in that the value is about 1%.

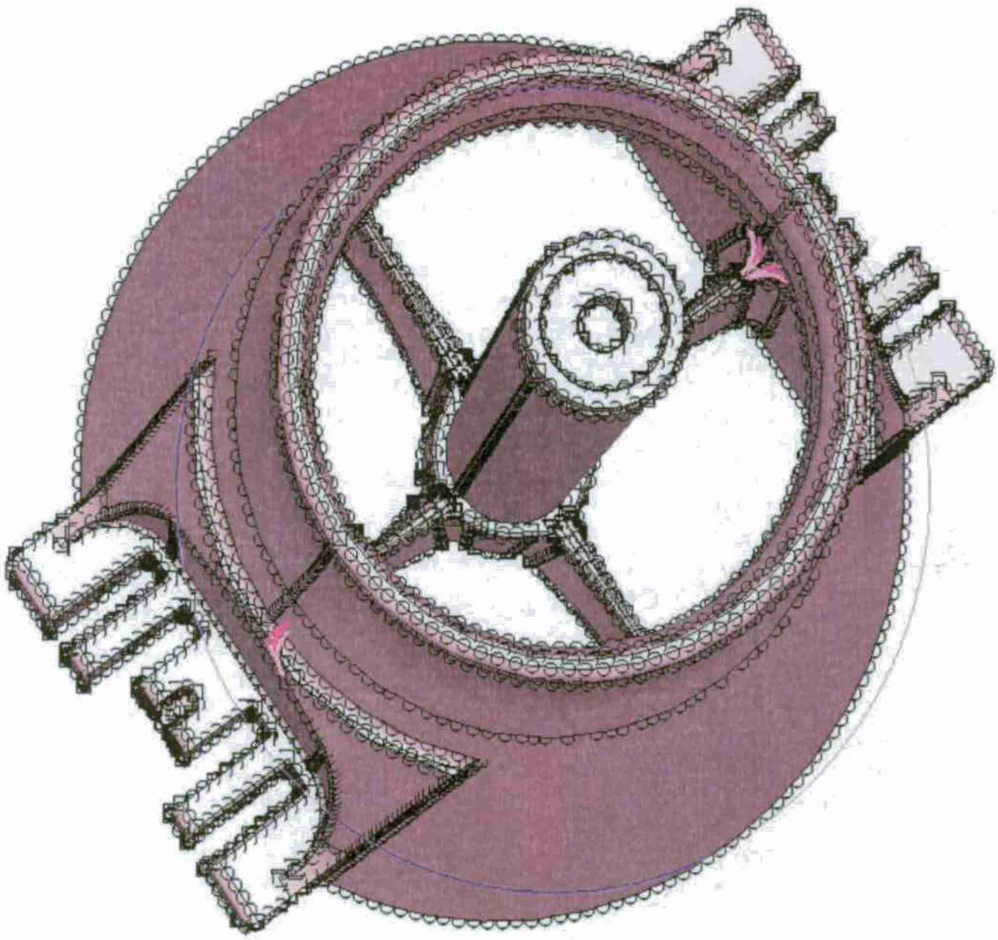

Figure 1 Highlighted areas indicate types of small surfaces where problems were encountered when trying to mesh the part in ABAQUS-CAE

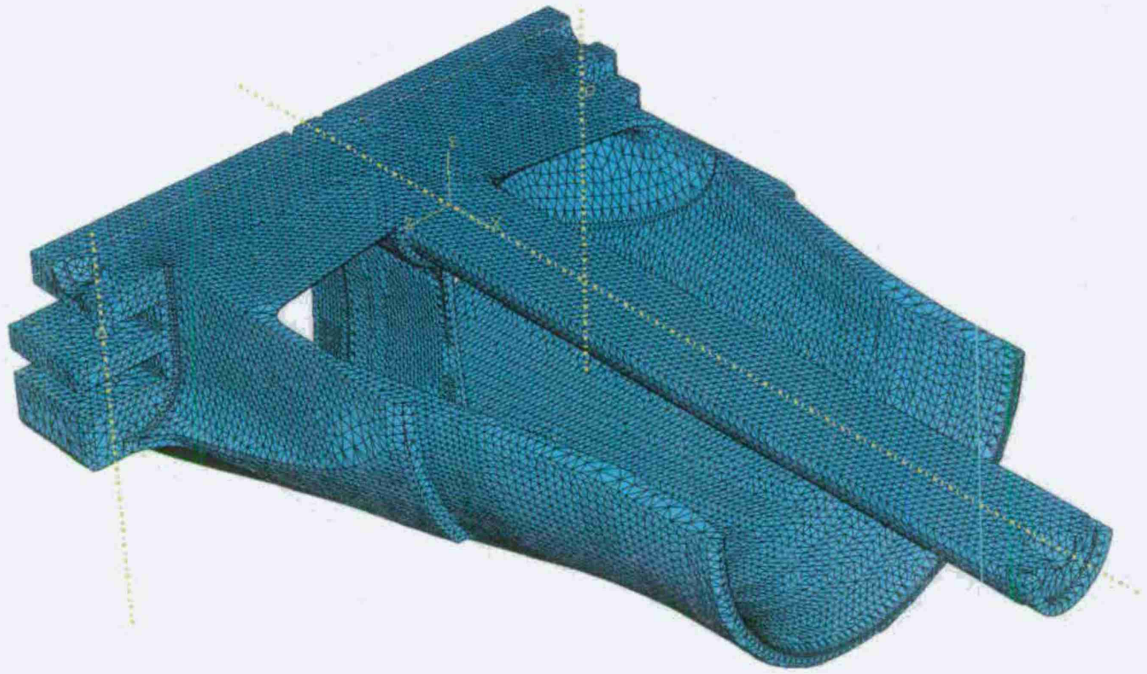

Figure 2 Finite element mesh used to analyze the breech nozzle casting design.

Figure 3 Von Mises stress distribution results on casting design.

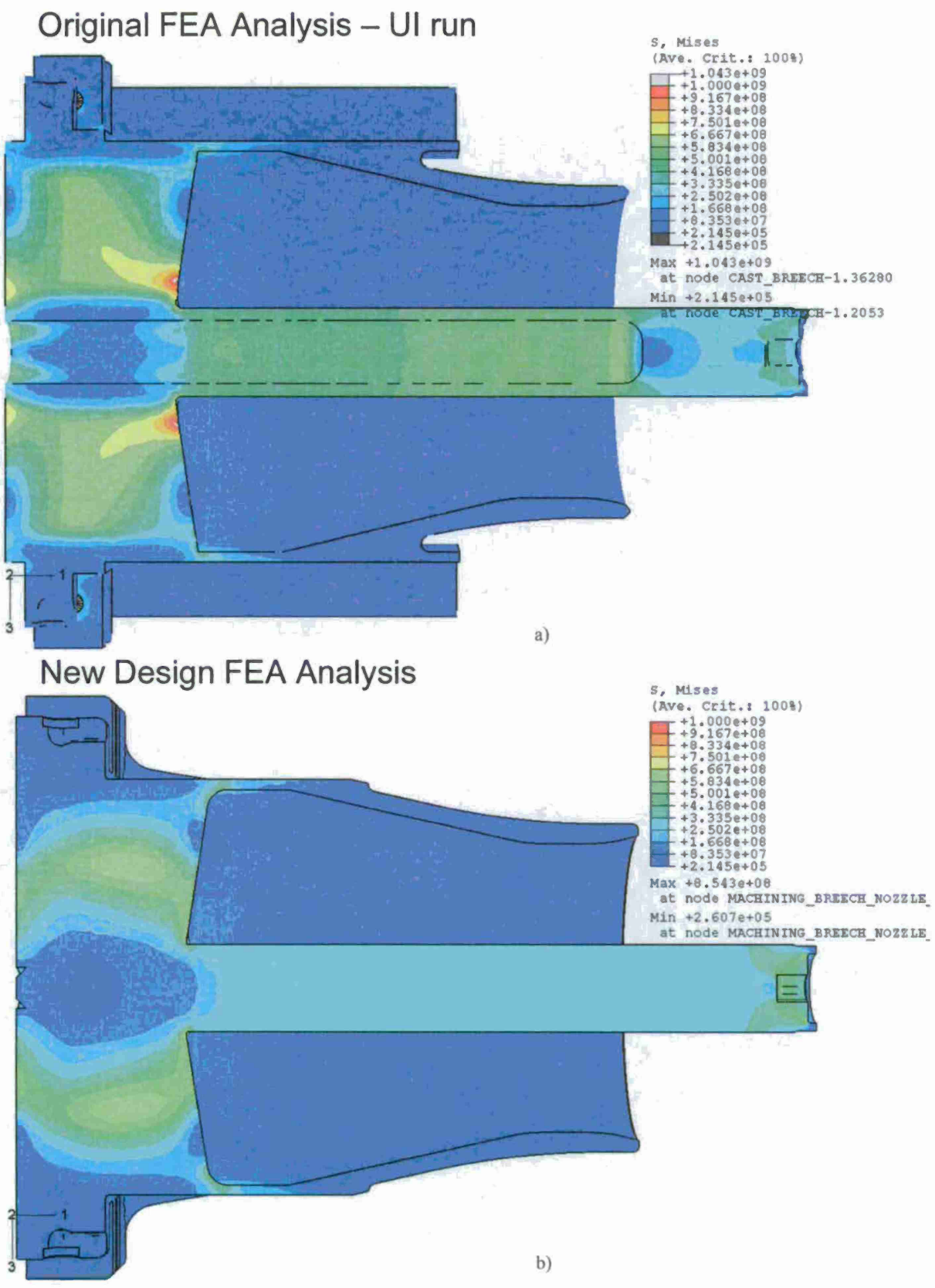

Figure 4 Von Mises stress distribution for a) original design and b) for casting design.

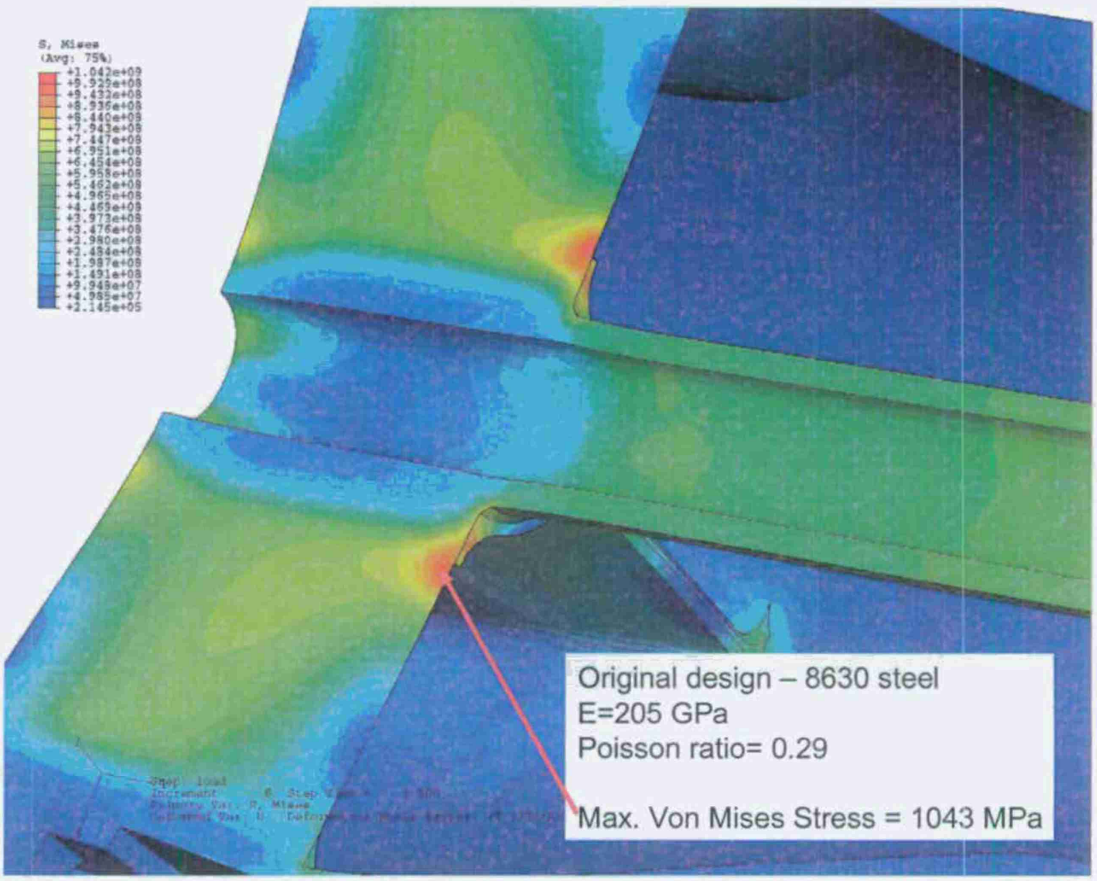

a)

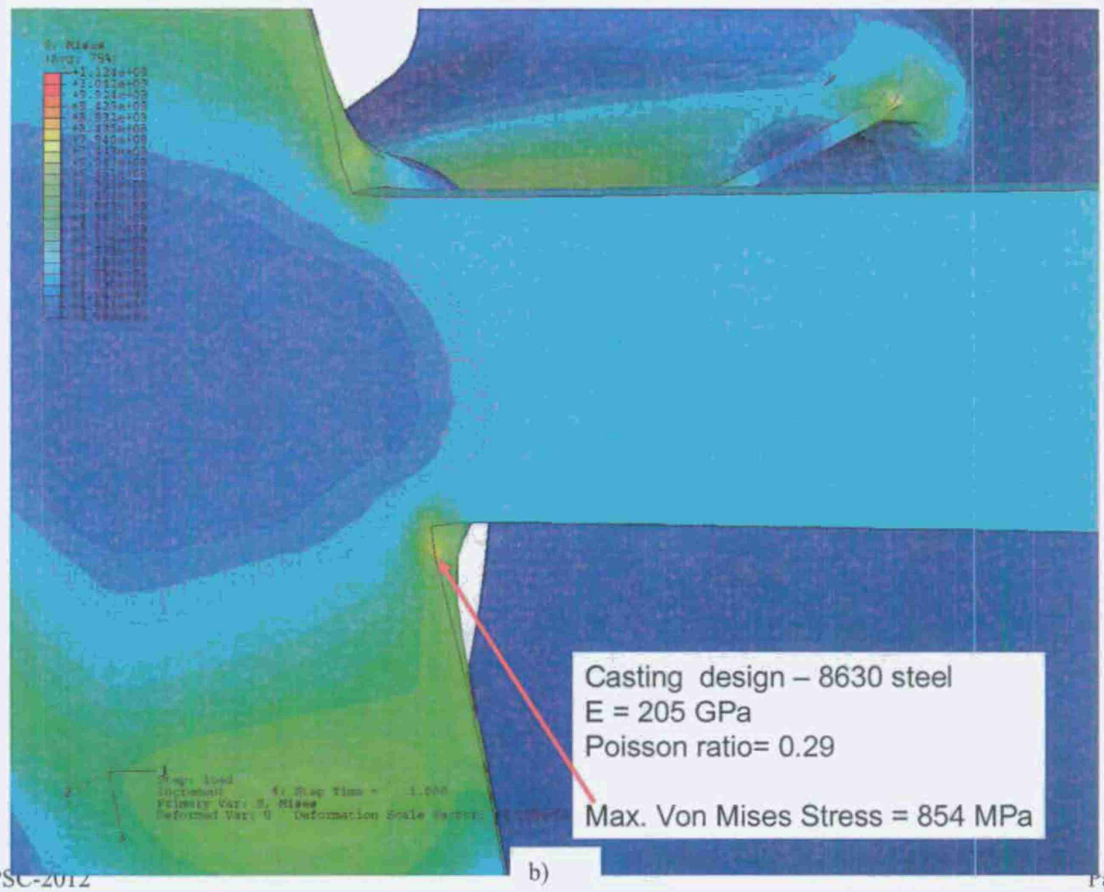

b)

Figure 5 Von Mises stress at location of highest stress for a) original design and b) for casting design.

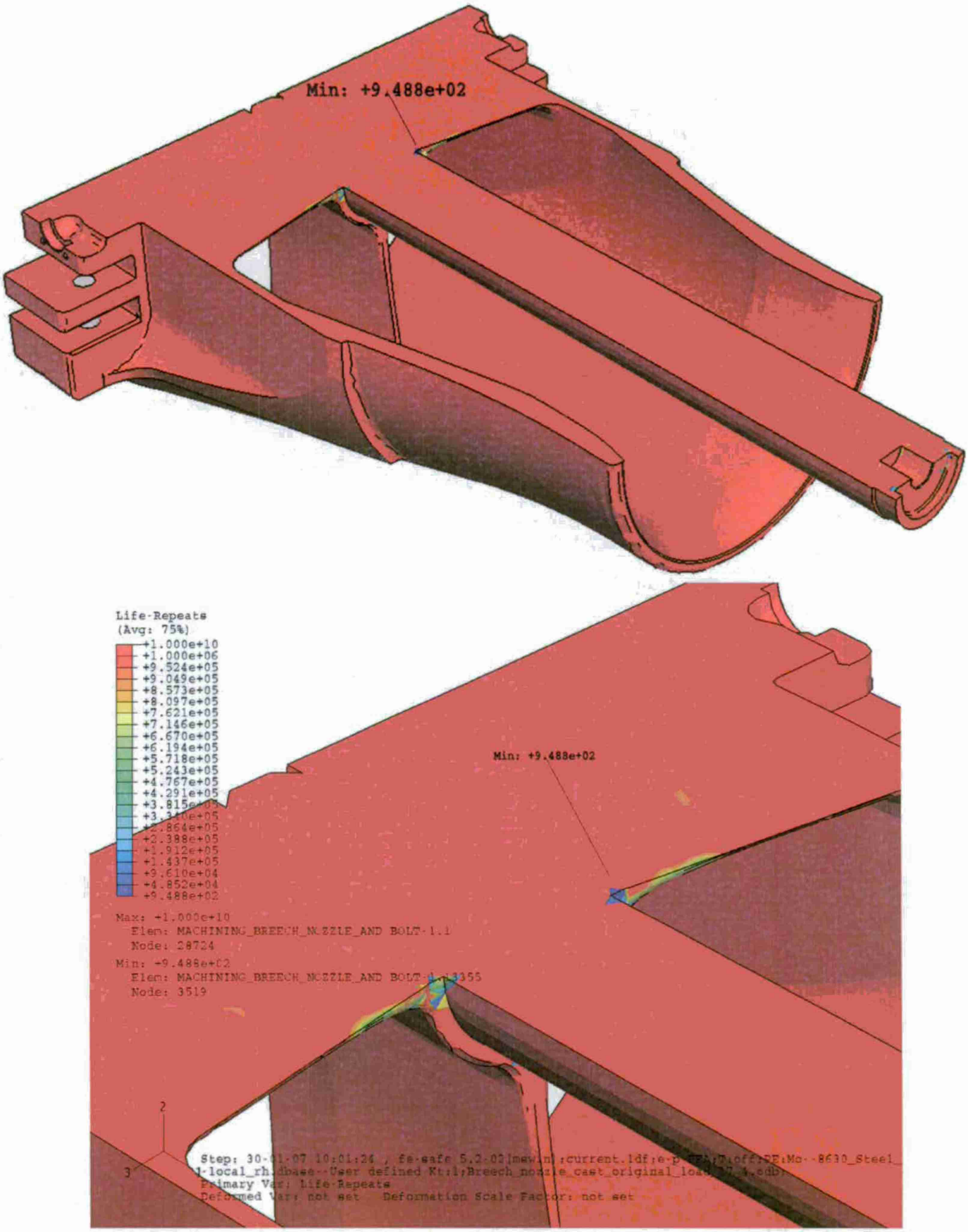

Figure 6 Fatigue life prediction results from simulation program "fe-safe" using strain-life prediction. Shortest life is predicted to be 948 cycles at location of highest strain (or stress).

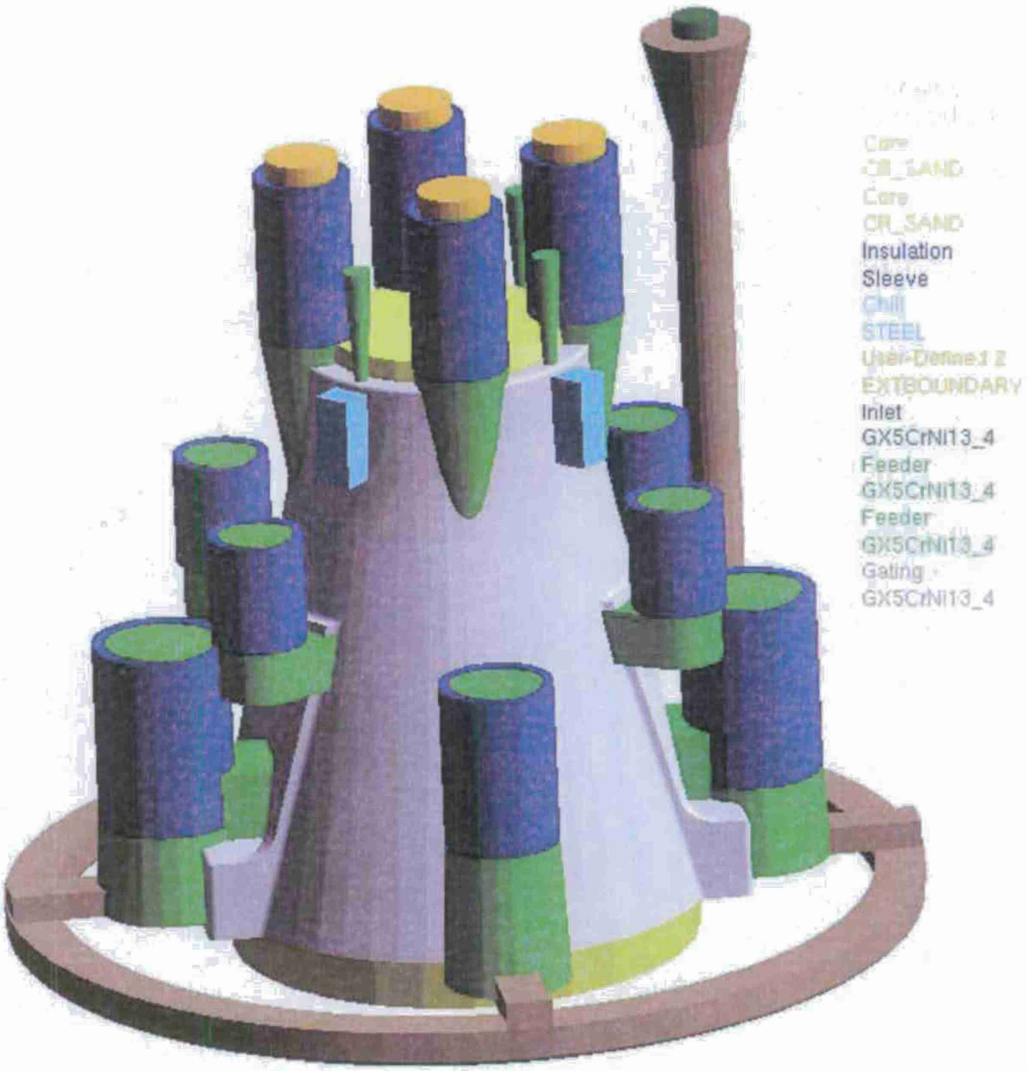

Figure 7 Casting rigging as designed by Sivyer Steel.

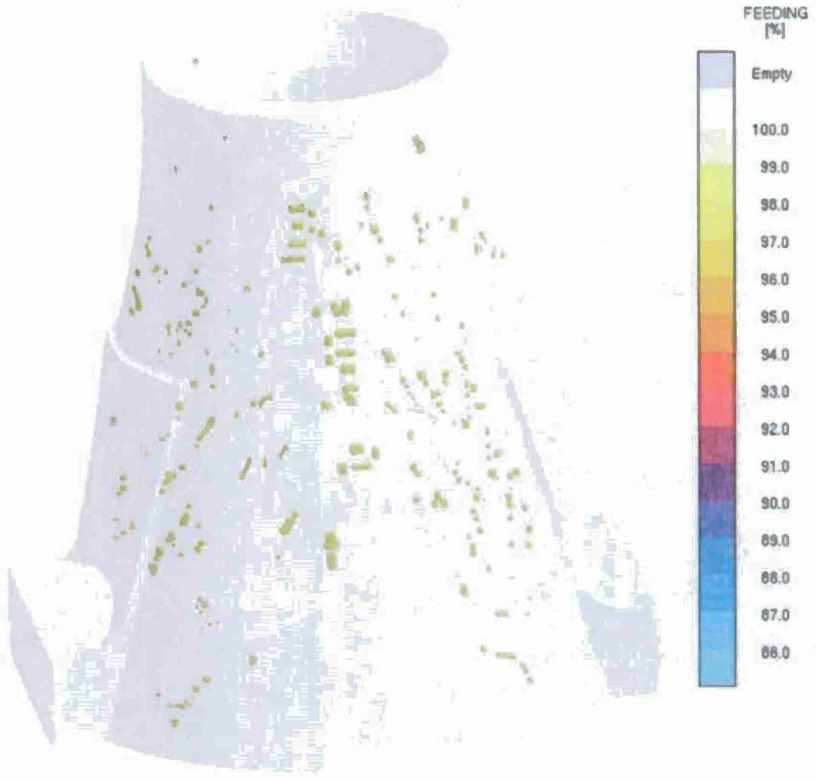

Figure 8 Predicted incomplete feeding/shrinkage in casting shown in an x-ray view.

Figure 9 Additional slice views showing feeding shrinkage in risers and much smaller amounts in casting.

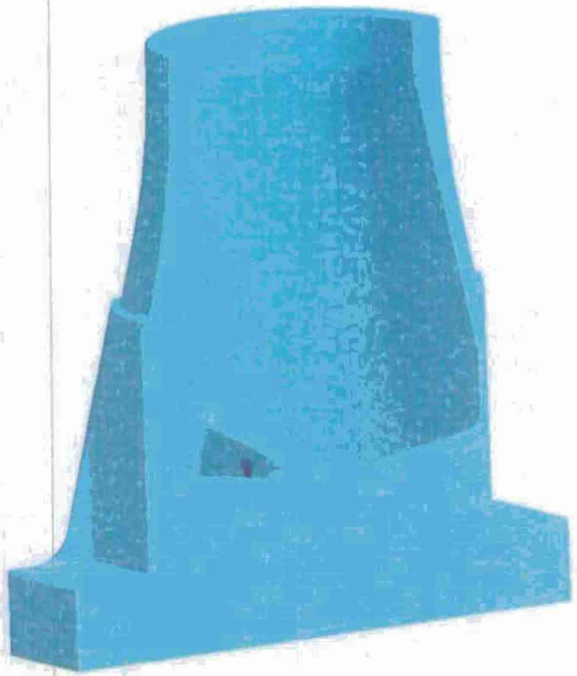

a)

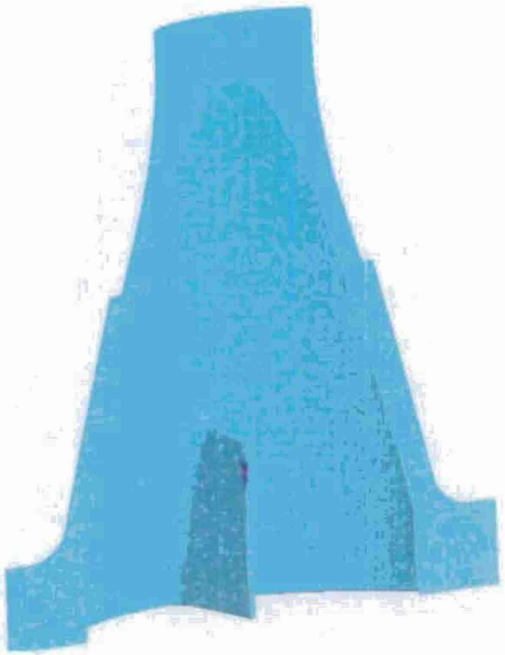

b)

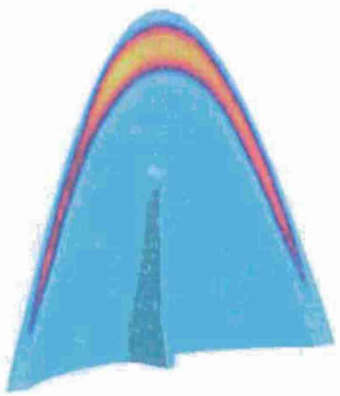

c)

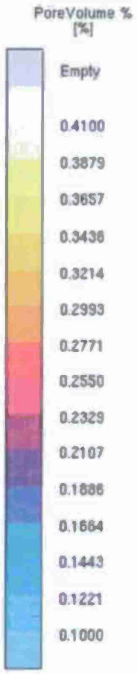
PoreVolume %
[%]
Empty
0.4100
0.3879
0.3657
0.3436
0.3214
0.2993
0.2771
0.2550
0.2329
0.2107
0.1886
0.1664
0.1443
0.1221
0.1000

d)

Model Development for Predicting Fatigue Life

In the area of hot tear modeling, Charlie Monroe and Prof. Beckermann are developing a mechanical constitutive model implement in ABAQUS as a user defined material subroutine (UMAT). This should allow for more accurate predictions than the previously used standard material models available in ABAQUS. Mr. Monroe will present his model results at the Steel Founders' Society of America (SFSA) Carbon and Low Alloy (CLA) Research Review Committee meeting on July 19. During next quarter he will travel to Aachen, Germany and collaborate with software developers at MAGMA GMBH to implement the model in their MAGMAstress software. Before he leaves, the model should be sufficiently complete in its ABAQUS implementation to simulate the breech nozzle casting; analyzing it for hot tear prediction.

In July, Charlie Monroe and Dr. Hardin will travel to the University of Northern Iowa (UNI) to spend one day setting up and a second day executing a hot tear experiment at the Metal Casting Center. This allowed Dr. Hardin to see first hand how the experiments are performed, so he can execute them himself in the future and determine how they might be modified or improved.

Dr. Beckermann and Antonio Melendez worked on improving the inclusion prediction model capabilities. They also arranged with Harrison Steel Castings to produce and radiograph plates with inclusions to compare with the model results. The model predicts the formation, growth and agglomeration of inclusions. Measured data, such as average inclusion diameter shown in Figure 1, can be compared with the model. The inclusion number and size distribution statistics development is predicted based on physics and several reasonably assumed parameters such as initial inclusion diameter d_{inc}, initial spacing, number density n_{inc}, a length scale for the growth model L_c and an agglomeration length parameter L_{agg}. The model parameters and results from a simulation of the Harrison-cast plate is given in Figure 2. Predicted inclusion size (diameter d_{inc}) distribution for the model compares favorably with the average measured diameter of about 2.25 mm. The measured particle volume faction was f_{inc} = 239.42 ppm or 0.41 in^3/ft^3 and the model predicts f_{inc} =370 ppm or 0.63 in^3/ft^3. For these model parameters, the results are very encouraging.

We will use the inclusion model on the breech nozzle casting as soon as possible, but the long computer execution time for the casting has prevented us from running that simulation this quarter. Also, next quarter, Dr. Hardin will simulate the effect of pressurizing the risers of the breech nozzle casting and report on those results.

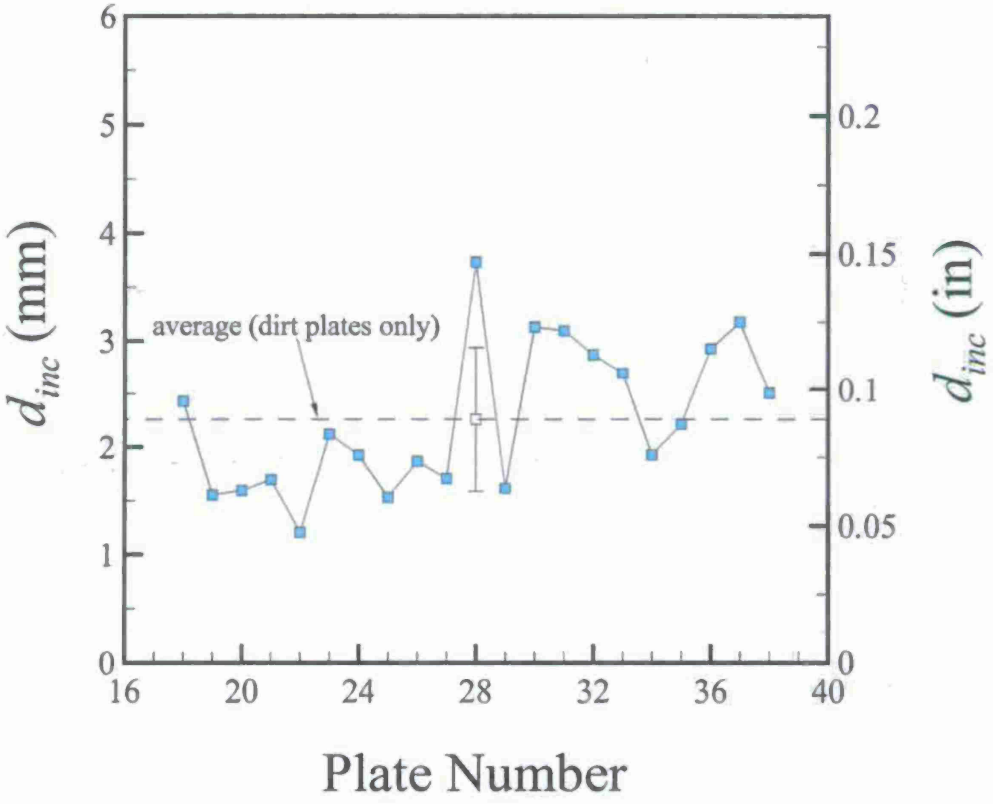

Figure 1 Average inclusion diameter d_{inc} measured in each of the plates with inclusions. The dashed line indicates the average inclusion diameter.

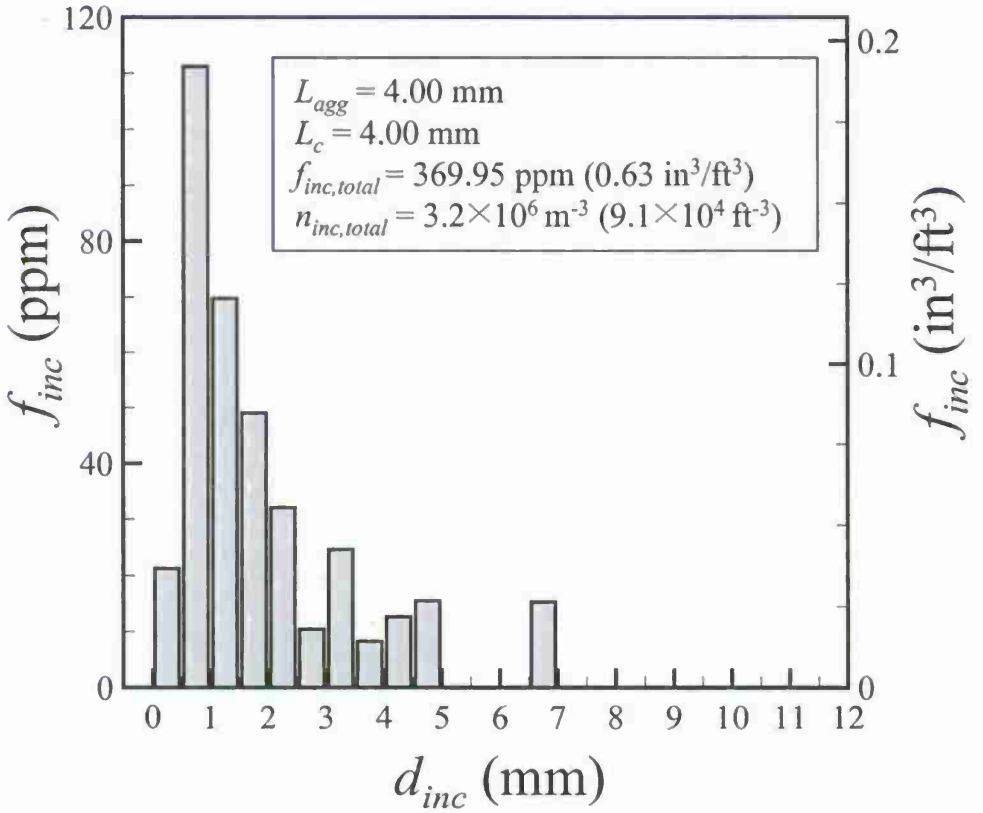

Figure 2 Predicted inclusion size (diameter) d_{inc} distribution for model parameters given in inset box. The measured particle volume faction was f_{inc} = 239.42 ppm or 0.41 in^3/ft^3. The model predicts f_{inc} =370 ppm or 0.63 in^3/ft^3.

Fatigue Life Prediction for Breech Nozzle

Dr. Hardin simulated the effect of pressurizing the risers on the soundness on the breech nozzle casting. Porosity levels were relatively unaffected. In part this is because the porosity in the casting was already low level microporosity. Also because there is a delay required to apply pressure in order for the casting to form a solid shell of sufficient strength to support and contain the pressure, most of the regions with microporosity were too solid to push additional feeding liquid steel into those regions.

Dr. Hardin simulated the effects of the porosity formed in the casting process on fatigue life of the breech nozzle. Because of the format of the ABAQUS finite element model and the method of transferring the results to fe-safe, the ABAQUS user post-processing programs to interface the results with fe-safe required special modifications. After this was accomplished the model could be run in fe-safe using fatigue properties developed for 8630 steel as part of the AMC Castings for Improved Readiness project. The property data should be a reasonable approximation for the steel being used to cast the breach nozzle. The process and results of this study will be outlined below. The advanced porosity prediction module in MAGMAsoft was applied to the breach nozzle as shown in Figure 1. Only a small amount of macro-porosity (that is visible without magnification) is seen on the outside surface of the casting at some riser contacts (shown in Figure 1 a) and Figure 2. The remaining porosity in the casting is limited to microporosity at the centerline of the housing seen in an x-ray view in Figure 1 b). The MAGMAlink program was used to transfer the porosity onto the FEA mesh node points. This requires loading the FEA model (shown in magenta in Figure 3) into the preprocessor in MAGMA and correctly positioning it over the casting. The transformation matrix necessary for the transfer between the models is computed by MAGMAlink. Here the FEA mesh is an ABAQUS input file (*.inp). The models are correctly positioned in Figure 4 and the results are transferred to the FEA mesh. In this case since the central cylinder is added to the casting later, that geometry returns warnings from MAGMAlink because that part of the breech nozzle is external to the casting (shown in blue in Figure 5). Dr. Hardin has written a custom program to automatically remove bad porosity and the error values for nodes that fall outside of the casting, and create the porosity field for analysis in ABAQUS and fe-safe.

In Figure 6 the porosity field at the FEA nodes is shown. An elastic stress analysis simulation is run in ABAQUS using an elastic modulus E that is locally dependent on the porosity at the nodes ϕ. As part of our AMC work, we determined this relationship to be $E(\phi) = E_0 \left(1-\phi/0.5\right)^{2.5}$ where E_0 is the elastic modulus of the sound material and ϕ is the porosity volume fraction. In Figure 6 note that the volume fraction is plotted instead of the percentage that is the output from MAGMAsoft. For the breech nozzle, the stress field with porosity is essentially unchanged from the "sound" run. The highest stressed locations are predicted to be sound in MAGMAsoft (see Figure 7), and the resulting life predictions are also unchanged from the sound component (see Figure 8). The predicted life in fe-safe is computed using the strain-life method with properties determined as part of the AMC program; this life is typically thought of as crack initiation life in a component. Cracks can be expected to form at the lowest life points indicated in Figure 8 starting at around 5000 cycles, or firings in this case. The fatigue notch factor field resulting from the porosity is shown in Figure 9. A histogram of the 5% lowest lived nodes from the strain-life fatigue calculations from fe-safe for entire breech nozzle is given in Figure 10. It is recommended to monitor the areas of lowest life during testing of the breech nozzle for crack initiation and growth. Good toughness characteristics would be desirable in the steel used to resist this crack growth and extend the life of the nozzle.

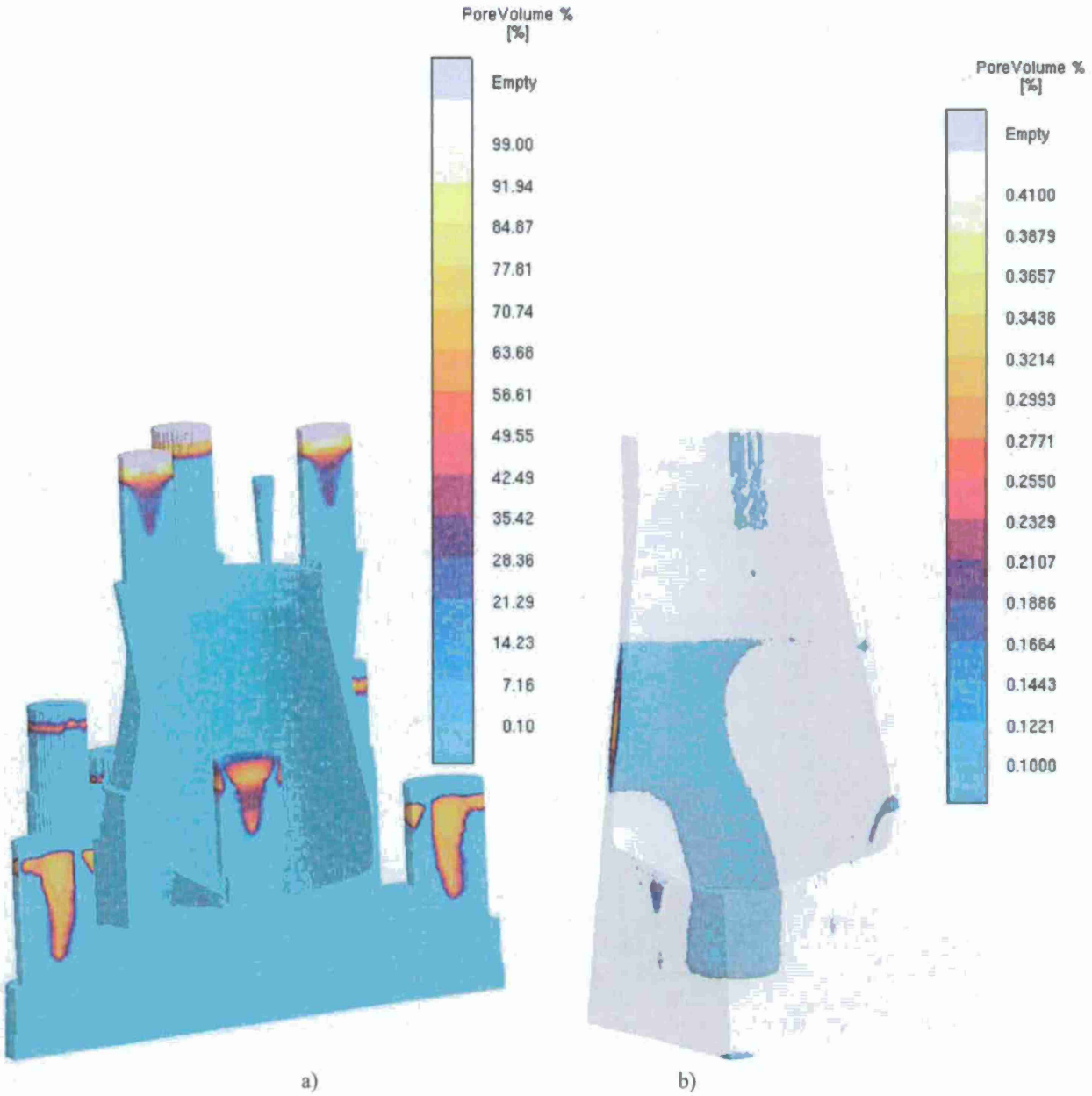

Figure 1 Porosity prediction from advanced porosity module in MAGMAsoft. Macroporosity is predicted in the risers in a) and at two small locations of riser contacts on the casting surface. The x-ray view in b) shows locations of dispersed microporosity in nozzle wall, and in the vanes.

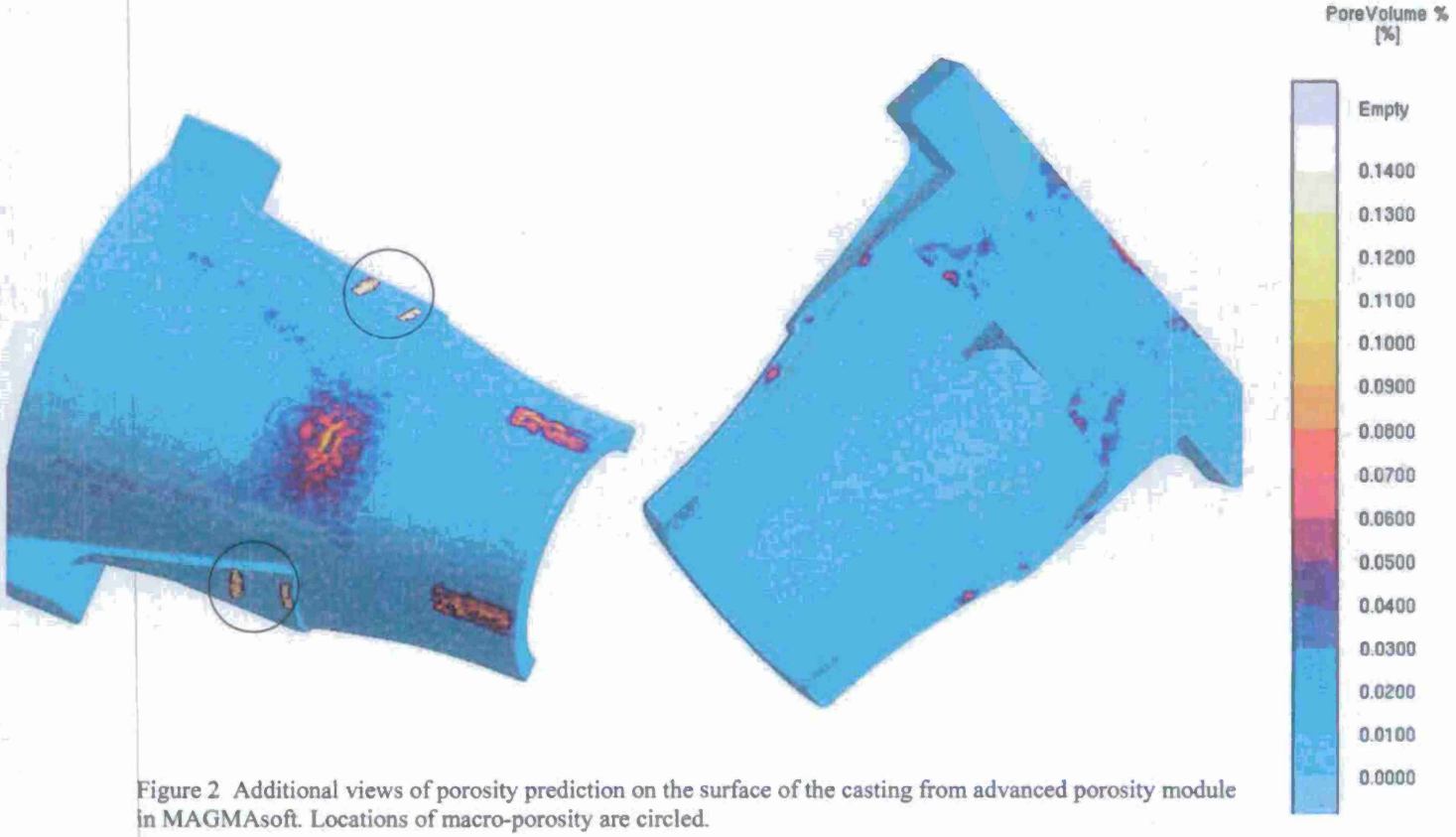

Figure 2 Additional views of porosity prediction on the surface of the casting from advanced porosity module in MAGMAsoft. Locations of macro-porosity are circled.

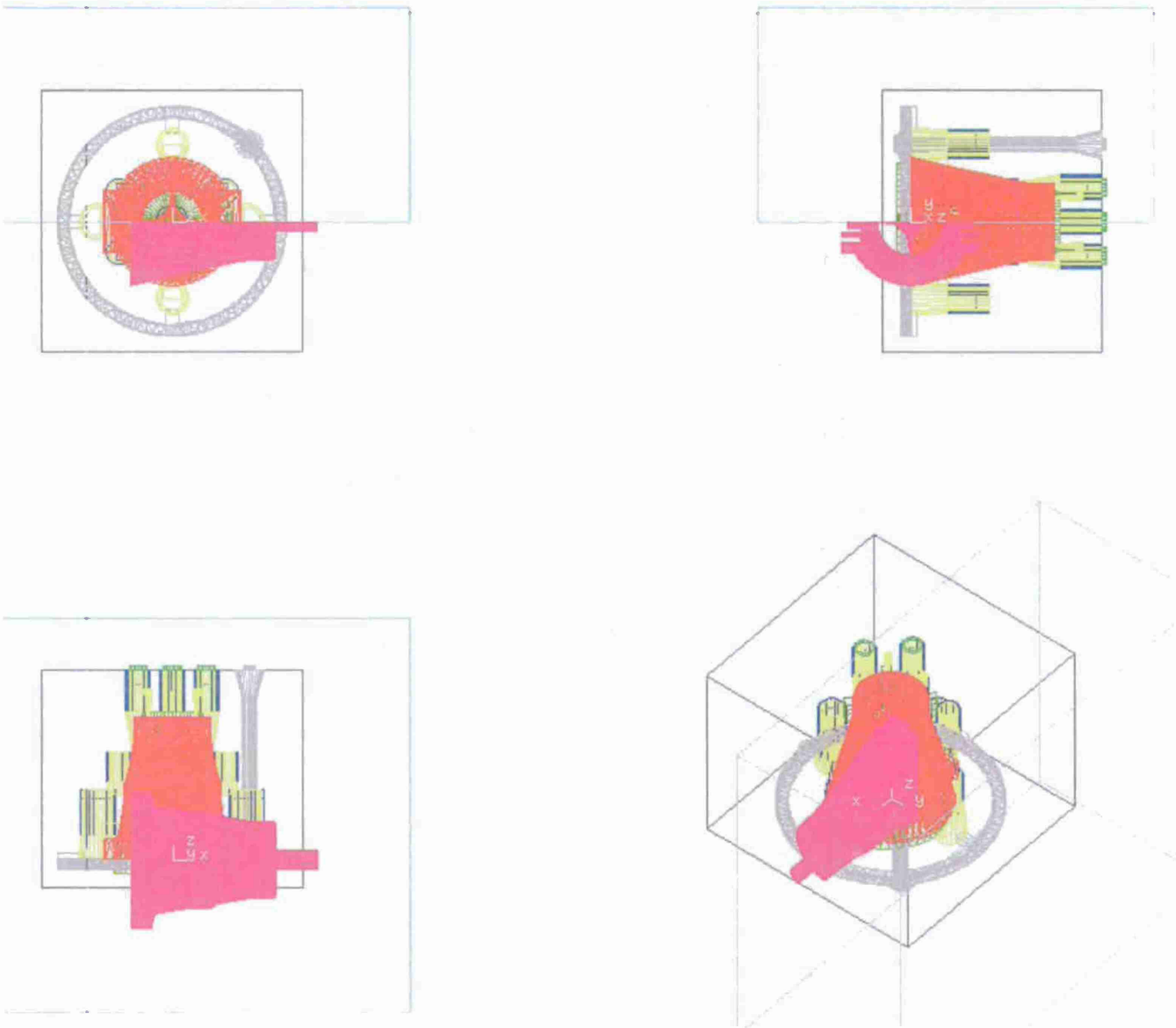

Figure 3 Finite element mesh (shown in magenta) brought into the MAGMAlink program as an ABAQUS input (inp) file. Note that FEA model must be positioned (translated and rotated) to fit the MAGMAsoft model in order to transfer results onto FEA mesh.

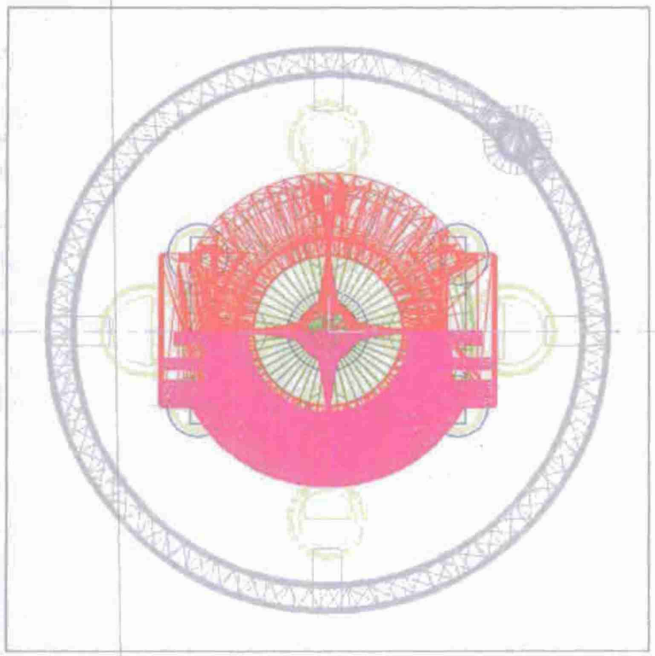

Top View

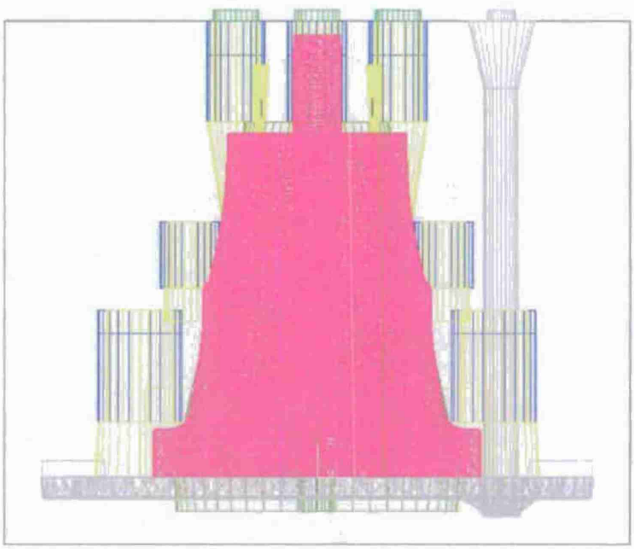

Side View

Figure 4 Top and side views of correctly positioned finite element mesh (shown in magenta) brought into the MAGMAlink program as an ABAQUS input (inp) file.

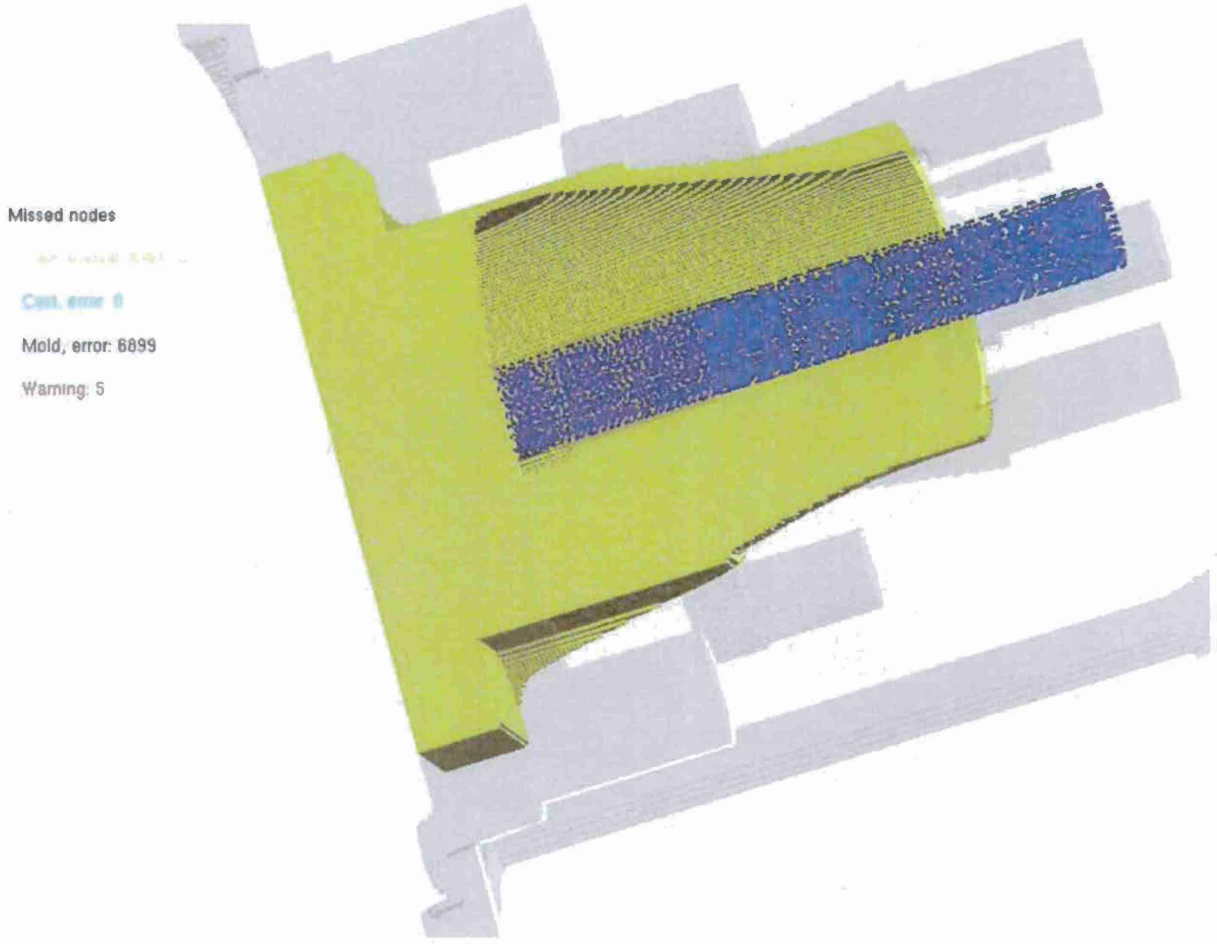

Figure 5 Note that the central tube portion of the FEA mesh returns mold errors on all nodes because they fall in the mold. The central tube is not part of the casting, and is assumed to be 100% sound material. The remainder of the casting transfers data to the FEA mesh successfully.

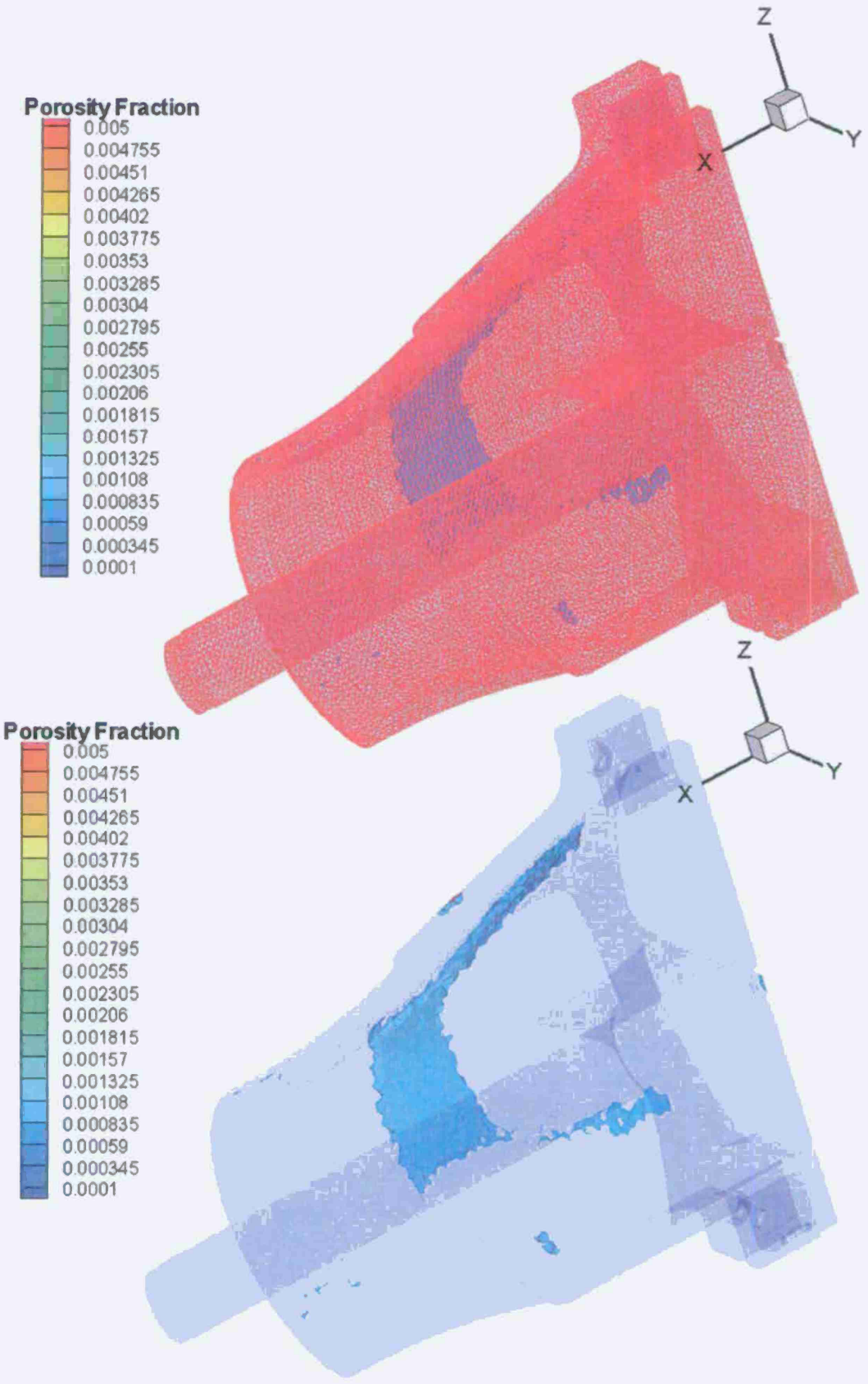

Figure 6 Porosity field from MAGMAsoft advanced porosity module transferred to FEA mesh. FEA mesh shown above and x-ray view shown below. Note that porosity filed is converted from % to pore fraction before performing calculations in ABAQUS and fe-safe.

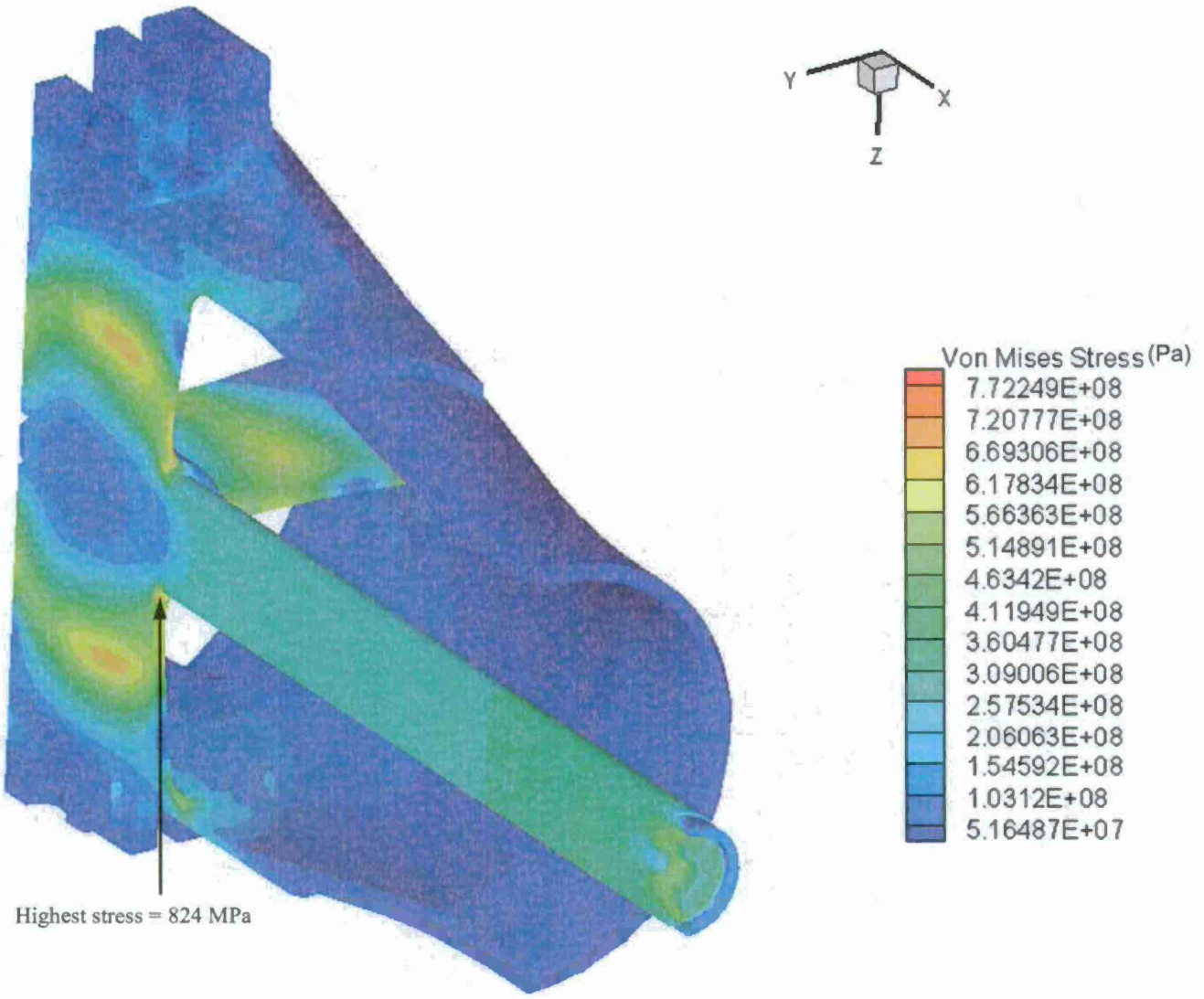

Figure 7 Von Mises stress (Pa) from ABAQUS simulation using porosity filed imported from MAGMAsoft and elastic properties dependent on porosity. No appreciable change is stress field observed.

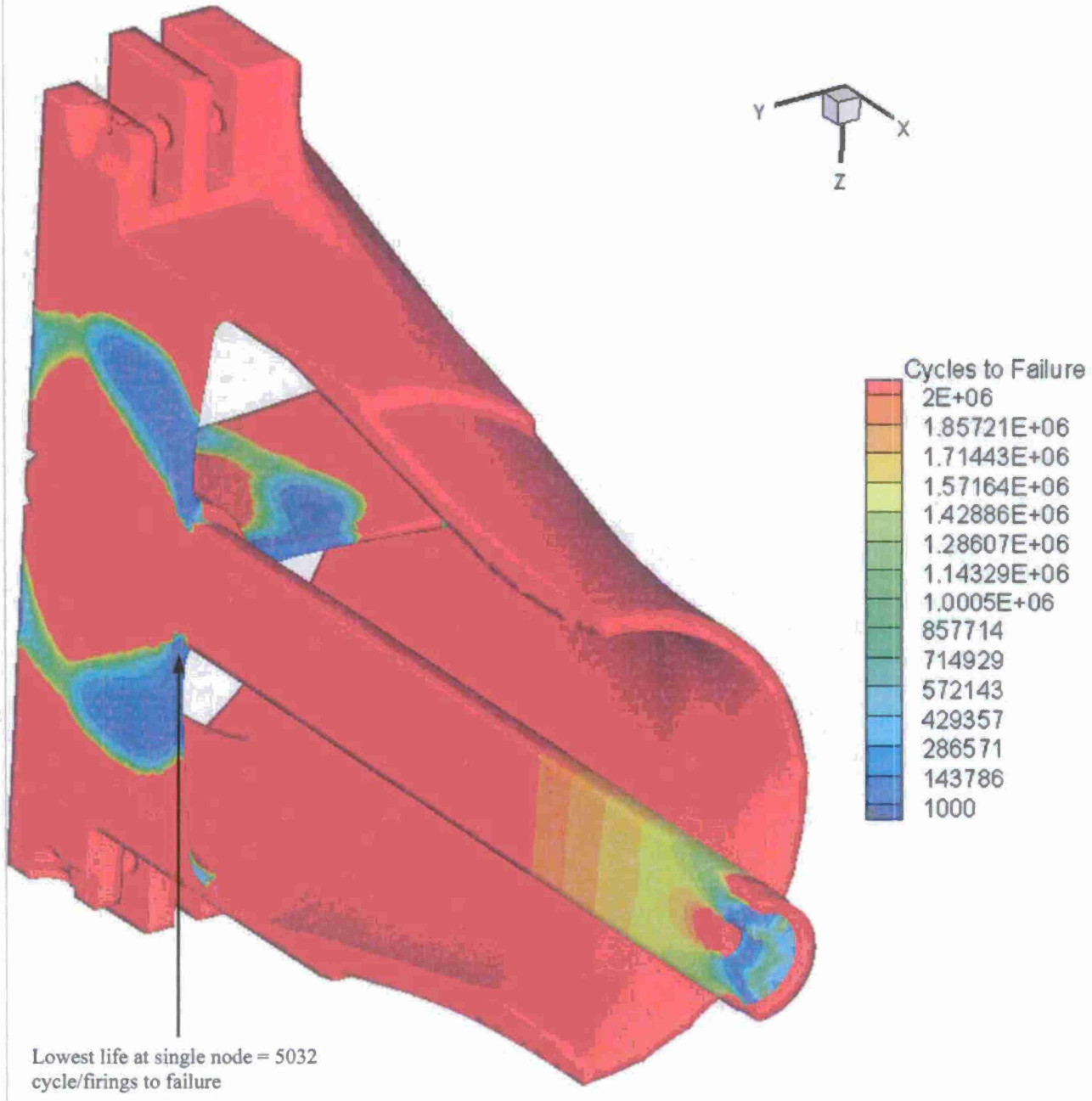

Figure 8 Strain-life fatigue calculations from fe-safe using ABAQUS stress results and porosity field imported from MAGMAsoft. Fatigue properties used were for 8630 steel developed from specimens with porosity from AMC project.

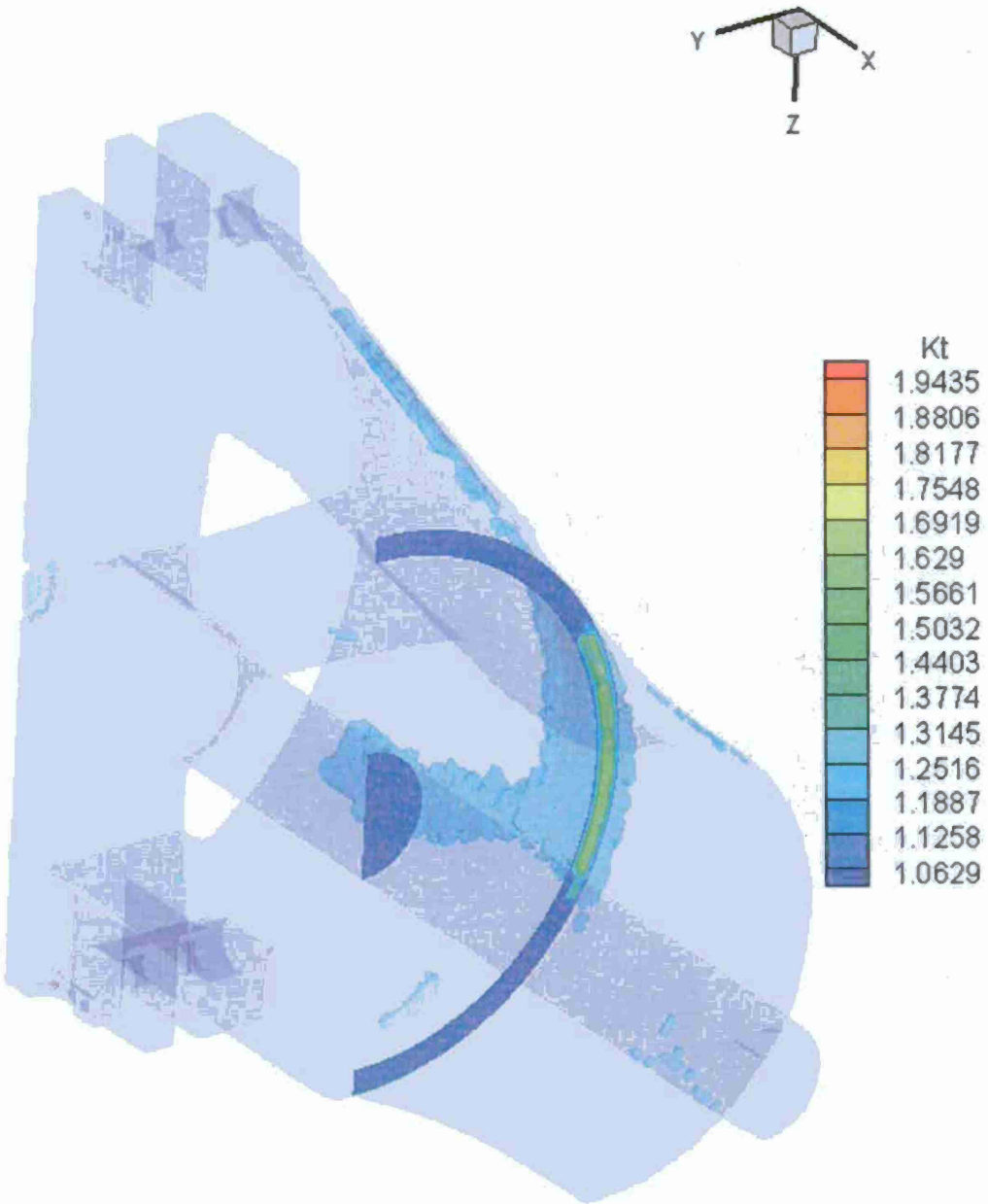

Figure 9 Fatigue notch factor data used in fe-safe strain-life calculations.

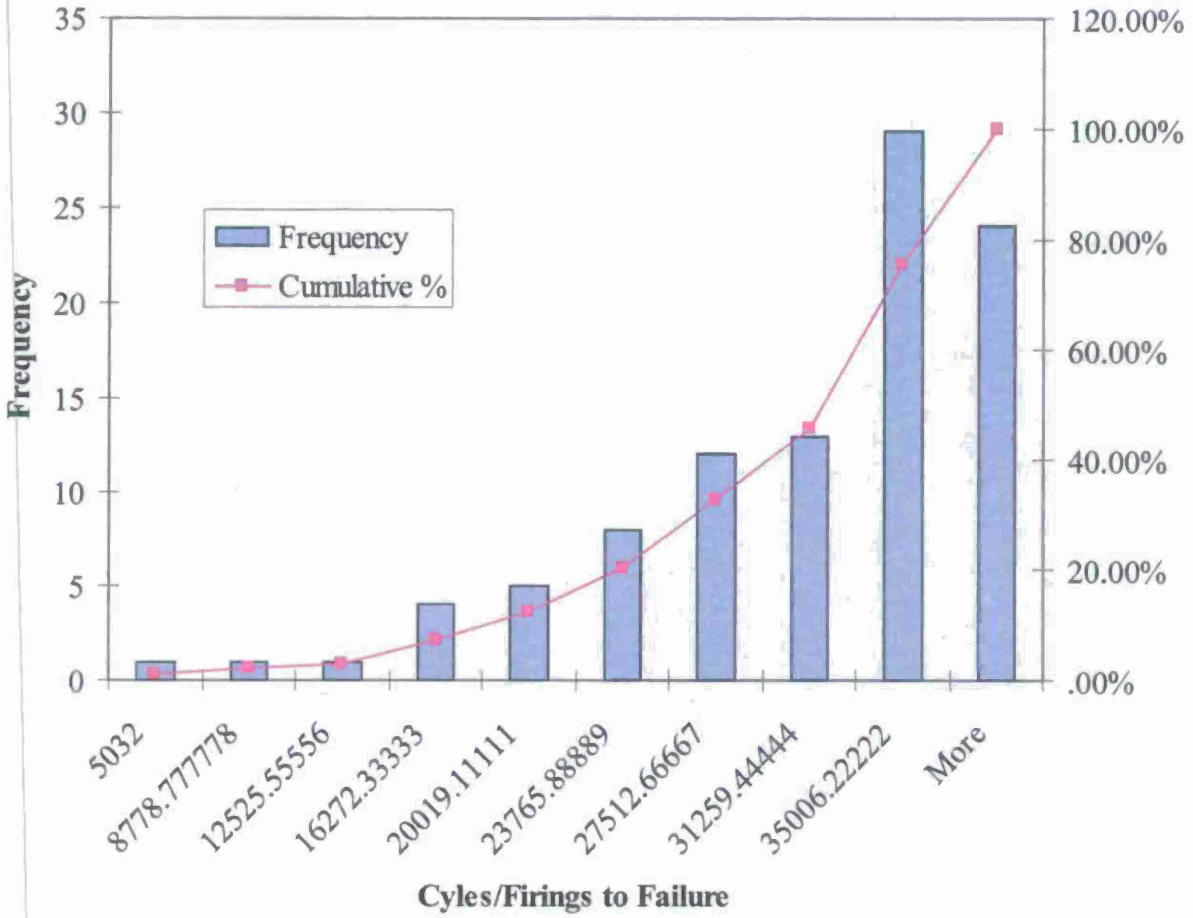

Figure 10 Histogram of nodes having the 5% lowest lives of entire breech nozzle from the strain-life fatigue calculations from fe-safe.

120mm Mortar Baseplate Modeling

We are using a partner development version of MAGMAsoft that includes advanced porosity prediction capability. This has the capability to predict micro-shrinkage in steel castings. We would anticipate that such porosity is likely to form in a thin rangy casting such as this mortar base plate. Figure 1 shows the best porosity-free section of the casting at its mid-symmetry plane. Figures 2 through 4 show sections having the most porosity predicted in s the simulation, which is approximately 1%. These locations would be difficult but not impossible to feed soundly. In order to make these locations sound the casting would have to be padded up and more extensively risered. Because of the thin sections involve with this part, it is anticipated that the metal will actually contract to prevent this porosity from forming.

The first effort to cast the base plate was performed at ACIPCO. However, an alloy different from what UI had simulated was poured, and the 12 second fill time and the 100 C minimum superheat that we found to be critical in filling the part were not achieved. The superheat was too low and the fill time of 32 seconds was much too long. The first test casting had numerous problems and defects. Unfortunately after this first test casting, ACIPCO has decided to try and produce it using a different approach they will develop based on what casting parameters they can achieve.

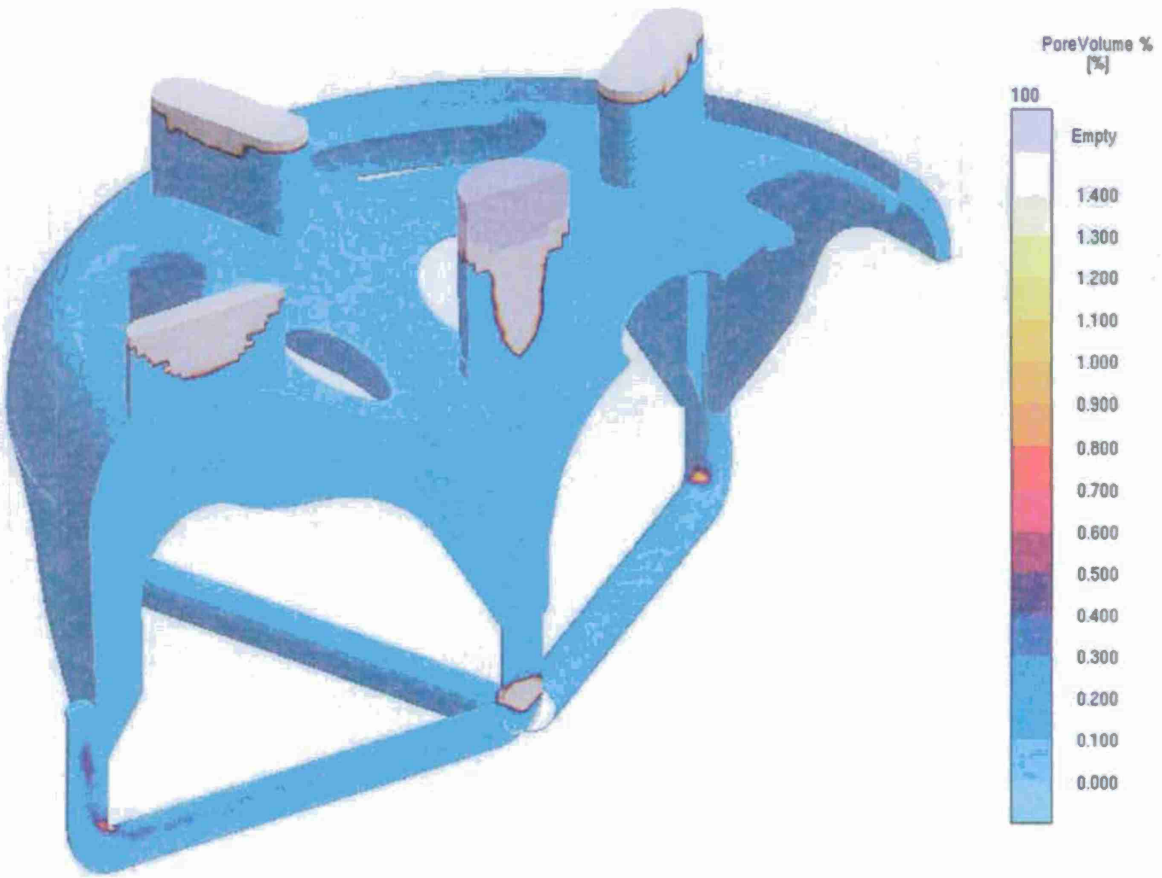

Figure 1 Porosity prediction for rigging used in mortar baseplate casting simulated using the advanced feeding development model in MAGMAsoft. Mid-section of casting is porosity-free.

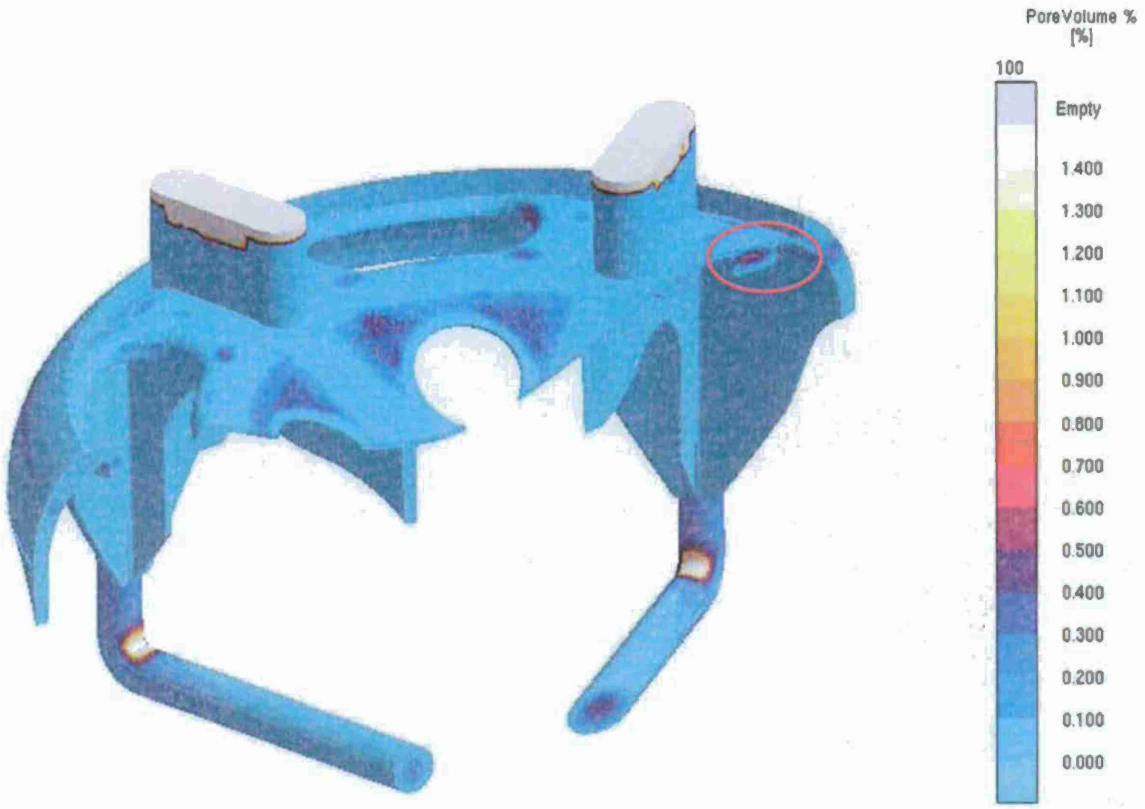

Figure 2 Porosity prediction for mortar baseplate casting simulated using the advanced feeding development model in MAGMAsoft. Worst porosity for section indicated.

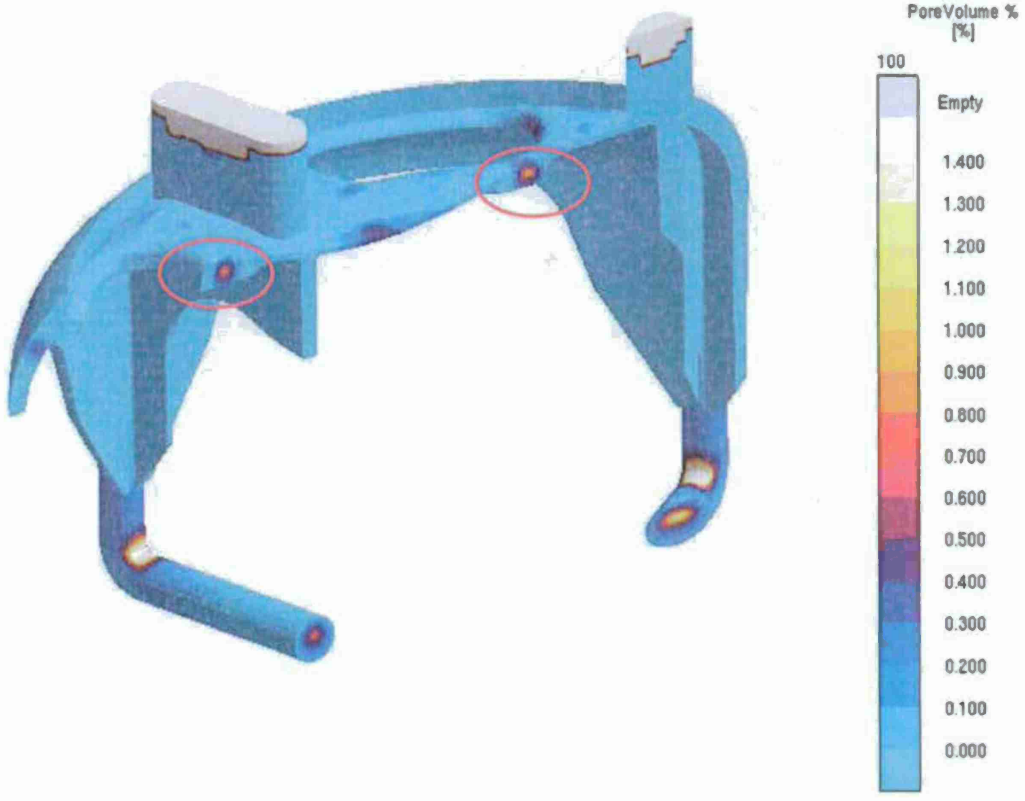

Figure 3 Porosity prediction in mortar baseplate casting simulated using the advanced feeding development model in MAGMAsoft. Worst porosity for section is indicated indicated.

Figure 4 Porosity prediction in mortar baseplate casting simulated using the advanced feeding development model in MAGMAsoft. Worst porosity for section is indicated indicated.

RAVEN Breech Nozzle Redesign

A second RAVEN breech nozzle will be produced for Benet Labs. It was decided that modifications would be made to the design to strengthen the support vanes and, if possible, reduce the part weight. Examining the typical stress pattern predicted in the part, shown in Figure 5, one can readily identify that the nozzle wall is subject to low stresses, about 40 MPa. The highest stress region is the center sections of the support vanes. A redesign of the breech nozzle was performed using the surface-only CAD model that was provided by ISU. Unfortunately, this CAD part had to be formed into a solid part by stitching the surfaces together, and resulted in a part file that could not the meshed in ABAQUS after many attempts. Nevertheless, the initial redesign was performed to see if the part weigh could be reduced while strengthening the support vanes.

The first breech nozzle casting is shown in Figure 6; it weighs about 365 kg assuming the density of steel is 7827 kg/m^3. Once material is removed from the outside of the breech nozzle, and the recuperator supports, while increasing the thickness of the support vanes to twice their minimum thickness, the part weight is reduced by 11% to 327 kg. The support vanes will have to be tapered so this was just an estimate of the final vane redesign. The redesigned nozzle is shown in Figure 7 for comparison to Figure 6. Cross sections of the original and redesigned nozzle are shown in Figures 8 and 9, respectively. Note that the section thickness of the redesigned nozzle wall in Figure 9 is essentially equal to the minimum section found in the original design, as indicated in Figure 8. The image of the original nozzle in Figure 10, shows the taper required to feed the vane section soundly. The challenge facing us in the redesign is to add as much thickness as possible to the central highly stressed sections of the vanes (see Figure 11) while providing enough taper to feed these sections soundly when the casting is produced, all while minimizing the weight add to the part. The final redesign will only be possible using a solid and native parametric ProE CAD part file. It is hope this can be provided to the UI team during the next project quarter either by our partners at Iowa State University or by Benet Labs.

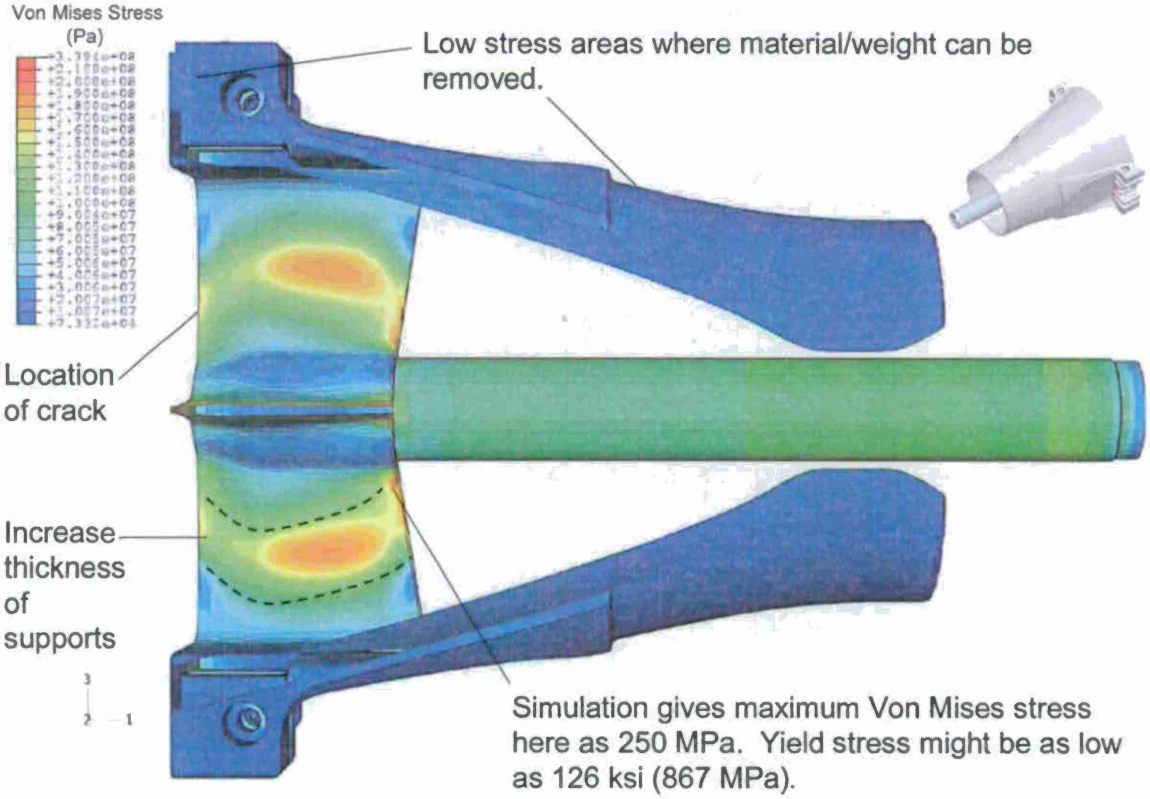

Figure 5 Stress pattern in breech nozzle. Areas where material can be removed and where it is required to be added are indicated. Location of the crack formation at the trailing edge of the vane is also shown.

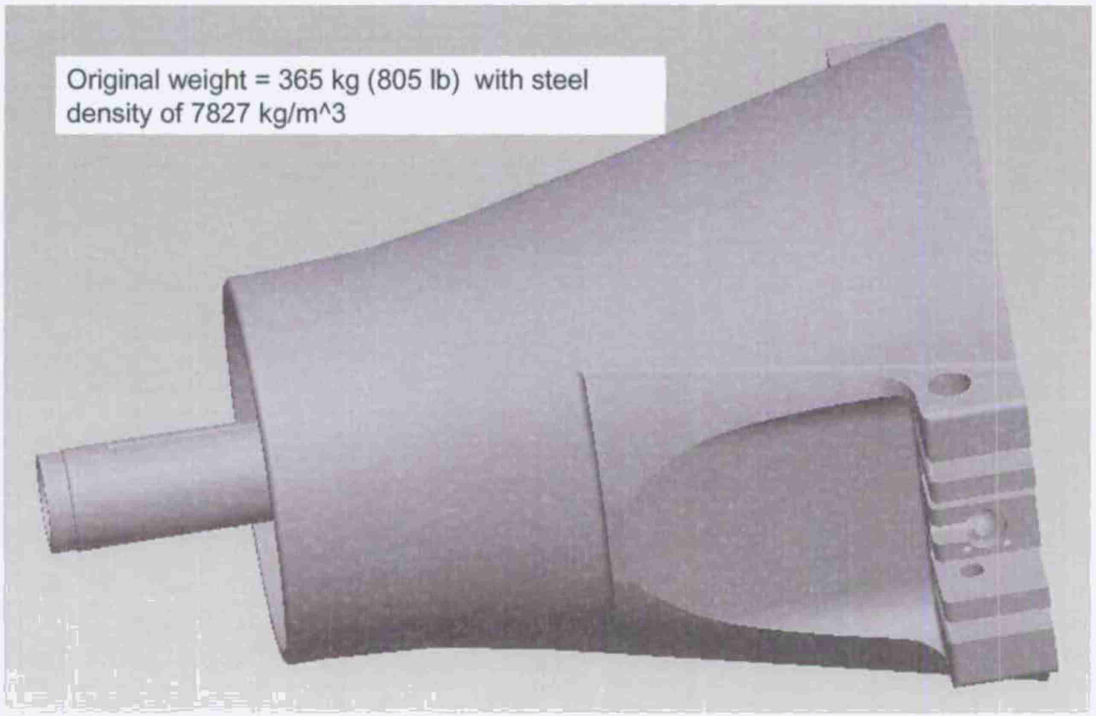

Figure 6 View of the first breech nozzle casting weighing 365 kg.

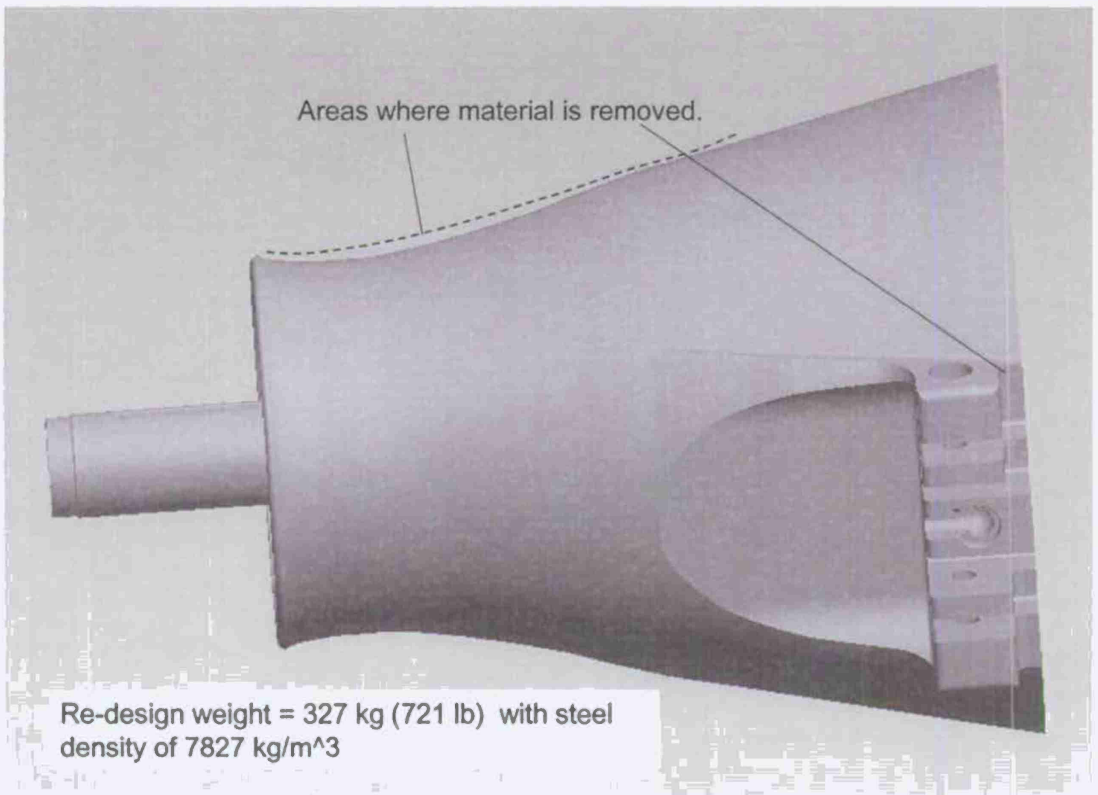

Figure 7 View of redesigned breech nozzle similar to Figure 6 showing where material is removed from outside of nozzle wall and surface and from recuperator supports to reduce weight and allow material to be added to the support vanes. Weight reduction is about 11%.

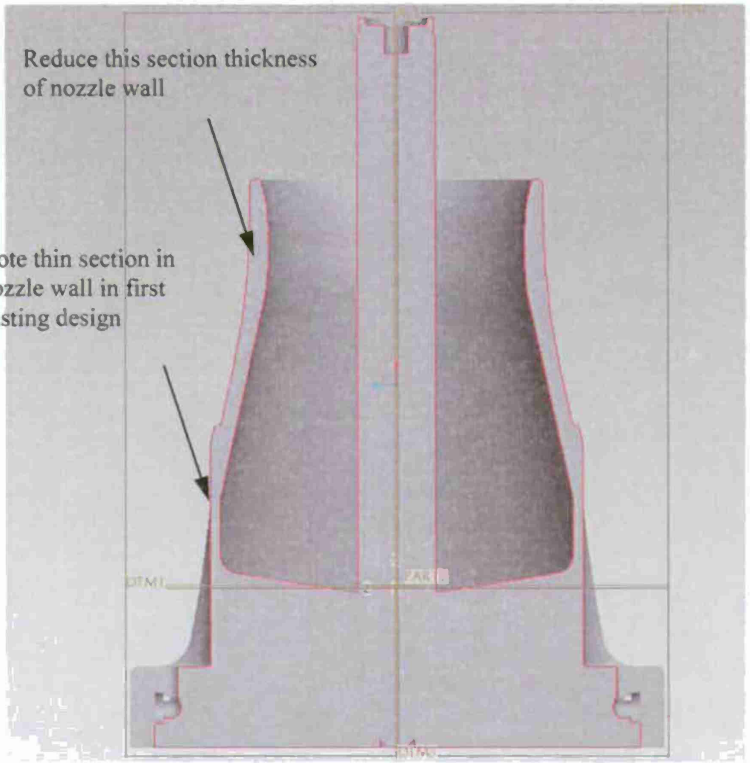

Figure 8 Cross section of first breech nozzle casting design showing wall section to be reduced and the section of nozzle wall that has smallest thickness, indicating the opportunity to reduce the overall wall thickness to this thin section.

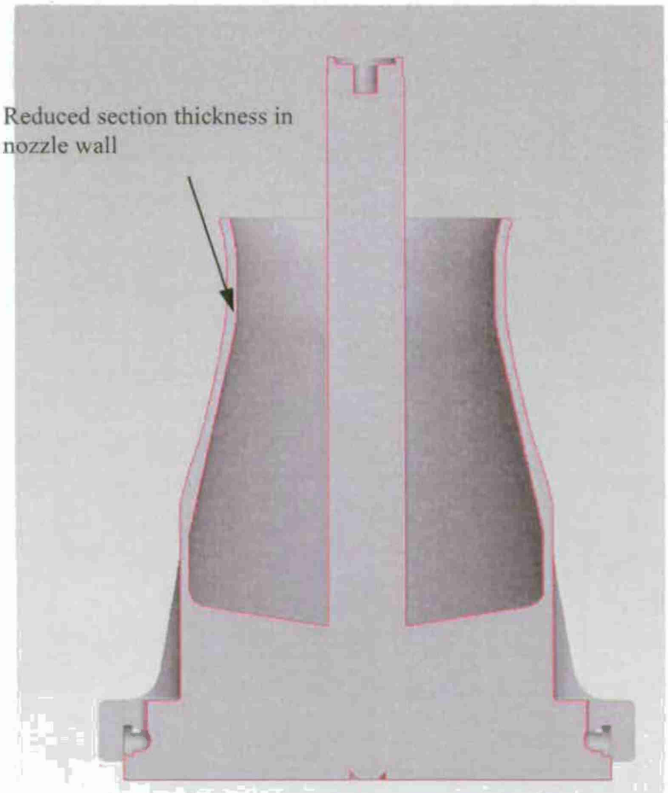

Figure 9 Same cross section as shown in Figure 8 for redesigned breech nozzle showing reduction in wall thickness taken from outside of nozzle.

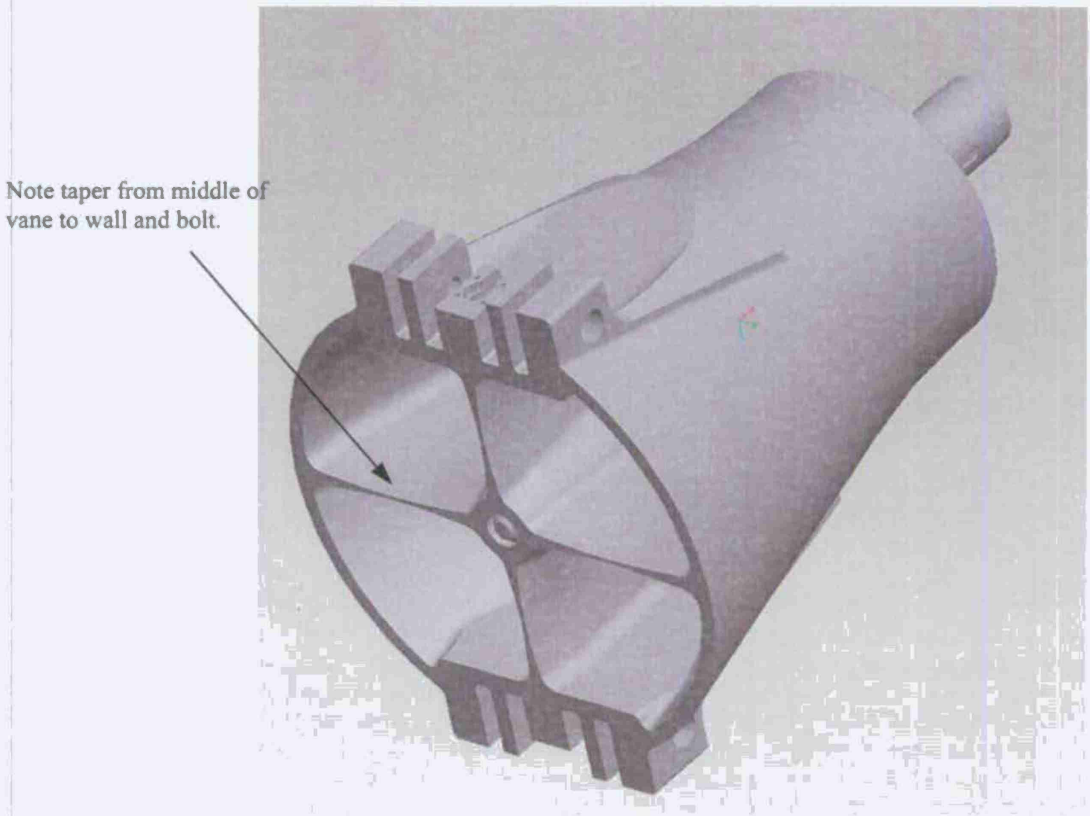

Figure 10 View of support vanes from first casting design. Note taper from minimum thickness at vane center to thick section at breech bolt and nozzle wall.

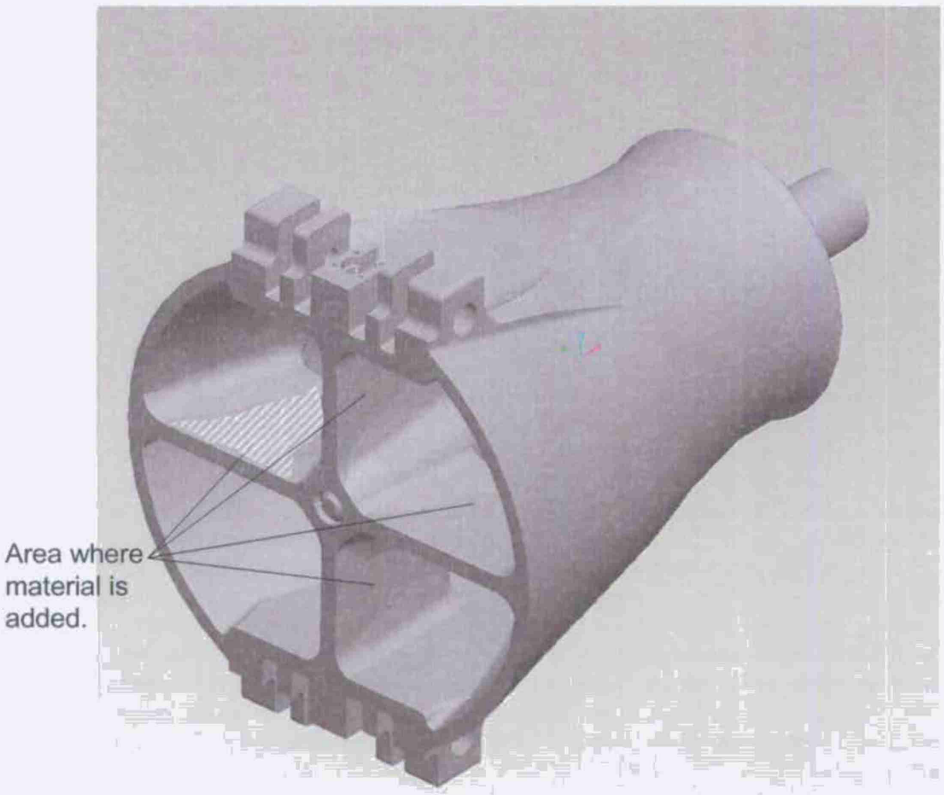

Figure 11 View of support vanes from new casting design indicating areas where additional material will be added to decrease stress levels. Model does not show the taper to be added to assure vane soundness.

Advanced Modeling Characteristics and Demonstration

This project included the development of experimental test apparatus for the measurement of high temperature sand mold properties. Such data is critically important to correctly predict hot tears in castings. Baseline measurements of the elastic and plastic properties of mold sand led to the decision to focus on measurement of elastic properties at elevated temperature first, before moving on to measure plastic properties. Measurement of elastic modulus from 100 C to 500 C was performed on a sand and no bake binder system typically used in steel foundries. Fatigue life of the new breech nozzle design was predicted using the porosity prediction for the rigging designed at the University of Iowa. Fatigue life of the 120 mm mortar base plate casting was predicted using the porosity prediction for the rigging we designed at the University of Iowa.

Sand Mold Property Measurements

Accurate data for the mechanical properties of sand-binder systems is a key component in the prediction of hot tearing and deformation in sand castings. Previous experimental work for this project compared measurements and predictions for the casting experiment shown in Figure 1. Here note that the casting is restrained by bolts at the ends of the arms of the casting. The restraint forces are measured at the bolts, and the displacements of the tabs are measured using quartz rod-attached LVDTs . Using finite element modeling of the thermo-mechanical process with the loads measured at the bolts as the boundary conditions, comparisons were made between predictions and measurements using several assumed stiffness versus temperature relationships for the sand-binder system in the simulations. As shown in Figure 2 (a), the stiffness of the mold decreases with increasing temperature in general. In the current recommended modeling property data, the stiffness decreases to a constant value between 1500 and 2000 MPa as shon in Figure 2(a). We found, however, that this data gave poor agreement with the experimentally observed displacements of the tabs seen from comparison between the thick curve in Figure 2 (b) and the prediction of curve (iii) made using the constant high temperature stiffness. In the experimental curve note that the contraction of the casting during solidification initially causes the tabs to move toward each other decreasing the gap in-between them (negative direction displacement) until about 1200 seconds when they begin to displace in the positive direction (moving away from each other). The prediction made using constant high temperature stiffness greatly over predicts the reversal in the tab displacements. By allowing the stiffness to decrease further with temperature above 400 C, to a complete lack of stiffness, progressively better agreement was found between the predictions and measurements as seen in Figures 2(a) and 2(b) by curve (ii) and then by (i), where the greatest drop in stiffness produced the best agreement.

During the current reporting period an experimental setup was developed by Mr. Jacob Thole (a graduate student in our M.S. program) to measure the properties of a sand-binder system at elevated temperatures. The apparatus is shown in Figure 3. It is basically a three point bend test fixture which is placed in a furnace. It is shown in detail in the image to the right in Figure 3. The load and LVDT displacement sensors have to be located outside the furnace due to the high temperatures. As in the casting experiment described in the previous paragraph, a quart rod attaches the displacement sensor to the three point bend fixture since its dimensions are unaffected by the high temperature. The sand binder system chosen for study was silica sand, a Phenolic-Urethane No Bake binder (PUNB) at 1.25% by total weight and a 60/40 ratio of part 1 and part 2 (PUNB is a 2 part system). In addition, the sand has 3% Black Iron Oxide. Rectangular block test specimens were produced in a small mold box. The testing began with room temperature tests, and twenty specimens were tested by loading them to failure to examine variability of specimens and the testing process. In Figure 4 the elastic modulus measured in the twenty room temperature tests as function of test specimen porosity and testing strain rate are shown. The error bar shows ± 1 standard deviation in the data scatter. The porosity in the specimens was found to vary from 32% to just over 36%. Generally, there is a trend of decreasing elastic modulus with increasing porosity, but no correlation is drawn. There was no trend seen in the measurements with the strain rate. In Figures 5 through 7 the strain hardening coefficient, yield stress, ultimate stress, strain at yield, and ultimate strain are given, respectively, as functions of specimen porosity and testing strain rate. There does not appear to be a systematic dependence in these properties on the porosity of the specimens of the testing strain rate.

After acquiring this initial room temperature data, it was decided to focus on the elastic modulus temperature dependency before examining plastic properties' temperature dependence. The elevated temperature tests were run in an inert nitrogen atmosphere, and all elevated temperature tests were initially loaded at room temperature to obtain a room temperature benchmark modulus. Measurements made by this project for elastic modulus as a function of temperature are given in Figure 8 (left side), and similar measurements made at the University of Northern Iowa (UNI), and in the German foundry literature are shown in Figure 8 (right side). Room temperature data with standard deviation error bar also shown. The elastic modulus data from Figure 8 are divided by the room temperature modulus data taken before heating and plotted as a function of temperature in Figure 9. While the UNI data has a similar room temperature modulus to this study, the German data does not, and non-dimensionalization with the room temperature allows for a even comparison of the effect of temperature. This also reduces some of the scatter in the data. The very low modulus measurement at 150 C is due to a chemical reaction; this behavior is also seen in the UNI data but at a higher temperature. It is believed that either the German data was made with a binder not having this reaction, or they missed the reaction by not taking data at smaller temperature intervals. We strongly feel this is a real effect, and will try to reproduce these results in future measurements. This result is also encouraging vis-à-vis the discussion surrounding Figure 2, where we found previously that a great reduction in mold stiffness was required at higher temperatures to achieve better agreement between measurements and predictions of casting distortion.

Mr. Thole will continue with future testing to examine the temperature dependent modulus at finer temperature increments around the points of interest. Other planned tests include studying the recoverability of elastic modulus from an elevated temperature, the dependency of elastic modulus on time held at elevated temperature, and the effect of different strain rates at elevated temperature on the measured elastic modulus of this sand-binder system.

RAVEN Breech Nozzle Fatigue Life Prediction

In our previous work on the breech nozzle redesign, we performed elastic simulations. This quarter we performed elastic-plastic simulations and fatigue life predictions without and with the presence of porosity. During the firing cycle, we predicted a small amount of plastic strain as shown in Figure 10.

Using the predicted porosity in the casting (shown in two views in Figures 11 and 12), a fatigue notch distribution is calculated. We made this particular calculation extremely sensitive including all porosity predicted down to 0.01%. This results in the fatigue notch factor distribution appearing much more sensitive than the porosity distribution. The resulting fatigue life is shown in two views in Figures 15 and 16, where in each view the life without porosity is shown in the left side image and the life with porosity on the right side of the figures. Generally, designers are concerned if the life prediction is below 10^7 cycles, for an infinite life design goal. Here a cycle is one firing, and the planned life of the part should survive the remaining testing, which conservatively should be on the order of 100 firings. Without considering porosity, the crack initiation fatigue life is predicted to be about 250,000 cycles. With porosity, the minimum fatigue life in the parts is 6,430 cycles, and there are 20 nodes having lives less than, 10,000 cycles. In our validation of the modeling approach we predict within one decade (one power of ten) in this low cycle fatigue regime. This, and the conservative level of porosity considered, means we have reasonable confidence that no cracks should form at less than 600 cycles. Lowest life areas of the breech nozzle are circled in Figures 15 and 16.

120 mm Mortar Base Plate Fatigue Life Prediction

Elastic stress simulations were performed assuming 8630 steel properties for the mortar base plate. The ABAQUS input deck files used were provided by Benet Labs for four load cases: 45 degrees over spade, 45 degrees over no spade, 80 degrees over no spade, and 80 degrees over spade. These cases refer to the angle of the mortar and its orientation relative to the spades. The four cases are shown in Figures 17 through 20, respectively. The 45 degree loads cases give higher peak stresses, and the highest stress areas generally are seen around the circular holes and on the underside at the spade reinforcing ribs also near the circular holes.

Because we never received data from the base plate producer on the final rigging used to produce the part, we were left predicting the fatigue life with the presence of porosity produced using the rigging we designed. This rigging and some of the key locations where we predict porosity are shown in Figures 21 through 23. Areas of the casting

with higher levels of porosity are indicated in Figures 22 and 23. For the fatigue calculations, a fatigue notch distribution is calculated using an assumed pore size no smaller than 200 micron in diameter. We use this as a conservative estimate given our observation that pores that large are the maximum likely size to form whenever there is detectable microporosity. This results in a fairly constant fatigue notch factor of about 1.65 wherever microporosity is predicted. This is shown in Figure 24. Just as a representative load case, predicted fatigue life was predicted for the 80 degrees over no spade case. For this case, the minimum fatigue life predicted in the base plate without porosity is 12,900 cycles, while 20 nodes have lives less than 40,000 cycles. Generally then, given the nature of fatigue life prediction, the predicted crack initiation life is 10,000 to 20,000 cycles. When porosity is considered in the life prediction, the is a much larger region with lower lives as shown in Figure 26. The minimum life for this case with porosity is 2,400 cycles, and twenty nodes have lives less than 3,500 cycles. This means the crack initiation life is on the order of 1,000 to 5,000 cycles in the presence of porosity. To understand the service conditions better, strain measurements are usually made. Here we have just used one of the load cases, but have demonstrated that the porosity can be expected to reduce the fatigue life by a decade, and has moved the expected location of the failure from the reinforcing ribs to the circular holes.

More case studies like the breech nozzle and the base plate are needed to establish the accuracy and refine the fatigue life predictions. The parts performance should be carefully tracked to determine the actual fatigue life of the parts in service and locations where crack form in the parts.

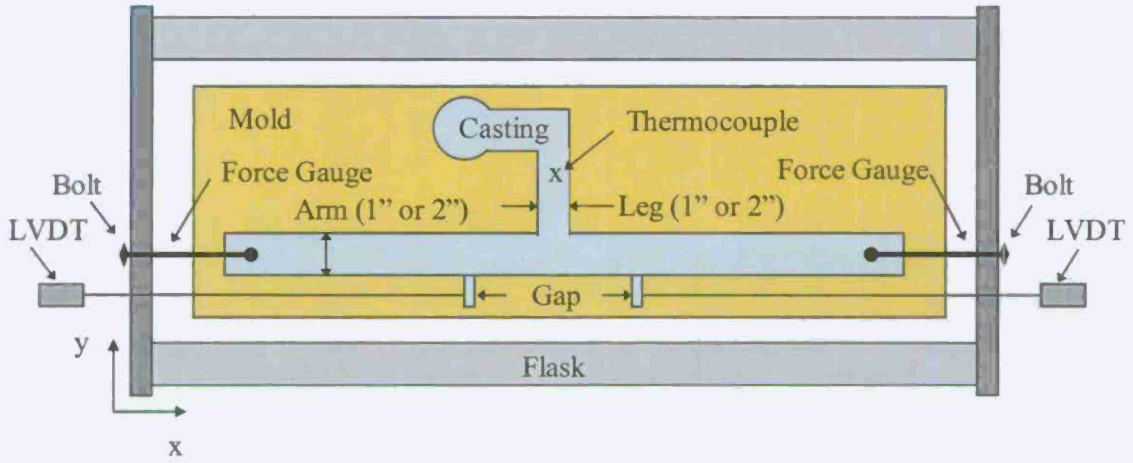

Figure 1 Casting experiment for the study of deformation and hot tearing of steel castings. Casting is restrained by bolts at the ends of the arms. The restraint forces measured at the bolts, and displacements of the tabs are measured using quartz rod-attached LVDTs .

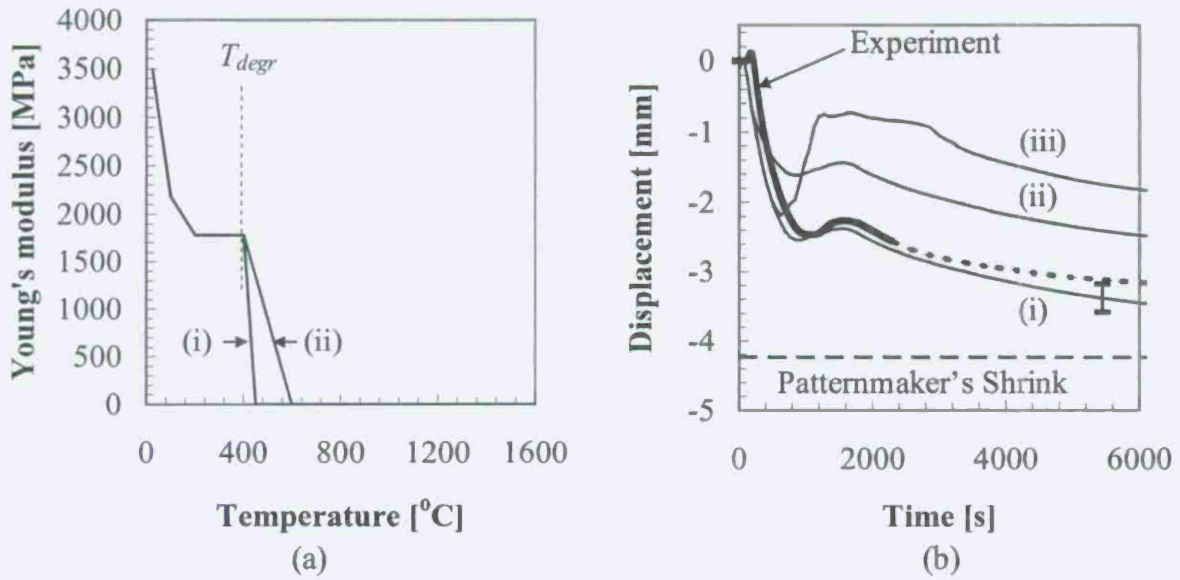

Figure 2 (a) Previously, it was assumed that the stiffness of the mold decreased with increasing temperature until it reach a constant value, between 1500 and 2000 MPa. However, it was found that a further degradation in the mold stiffness above 400 C (curve (i) and (ii) in Figure 2 (a)) was found to give better agreement between predicted and the measured displacements of the tabs as seen in Figure 2(b) by comparing curves (i) and (ii) with the bold measured curve.

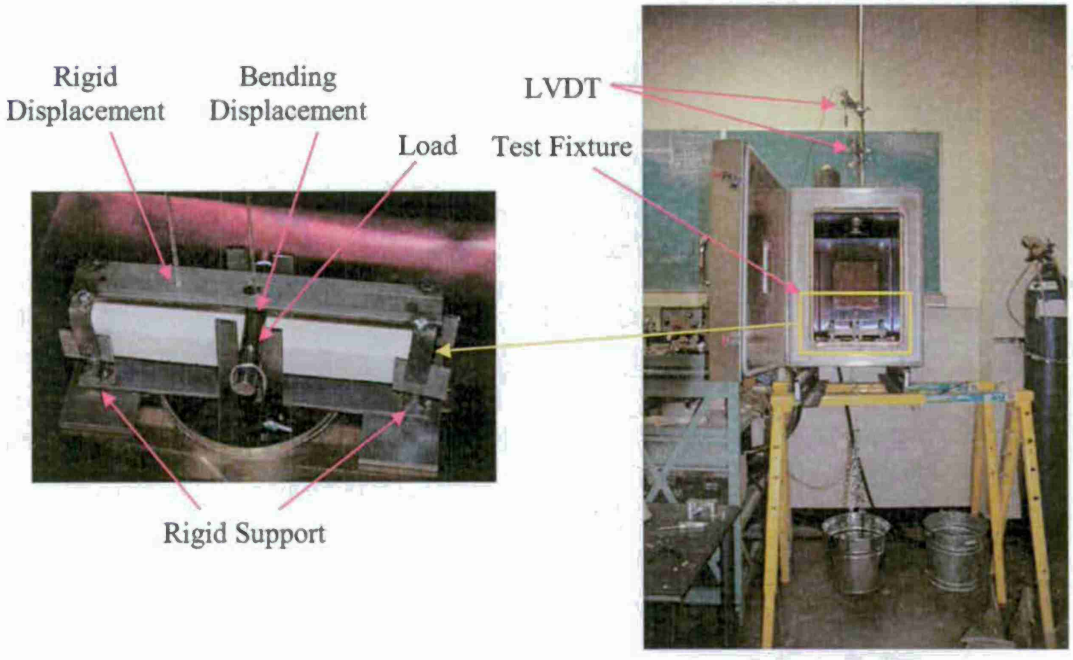

Figure 3 Experimental apparatus developed to measure the properties of a sand-binder system at elevated temperatures: a three point bend test fixture (shown in detail at right), and furnace with external load and displacement sensors.

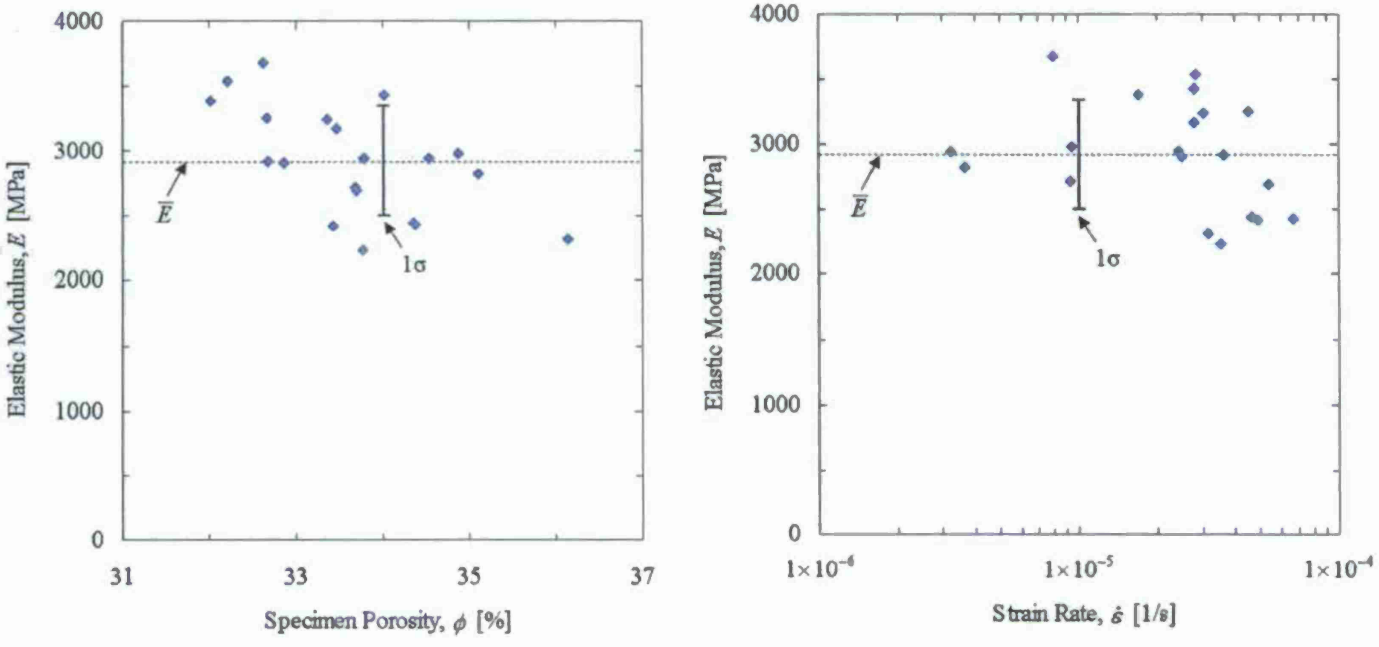

Figure 4 Elastic modulus measured in twenty room temperature tests as function of test specimen porosity and testing strain rate. Error bar shows ± 1 standard deviation.

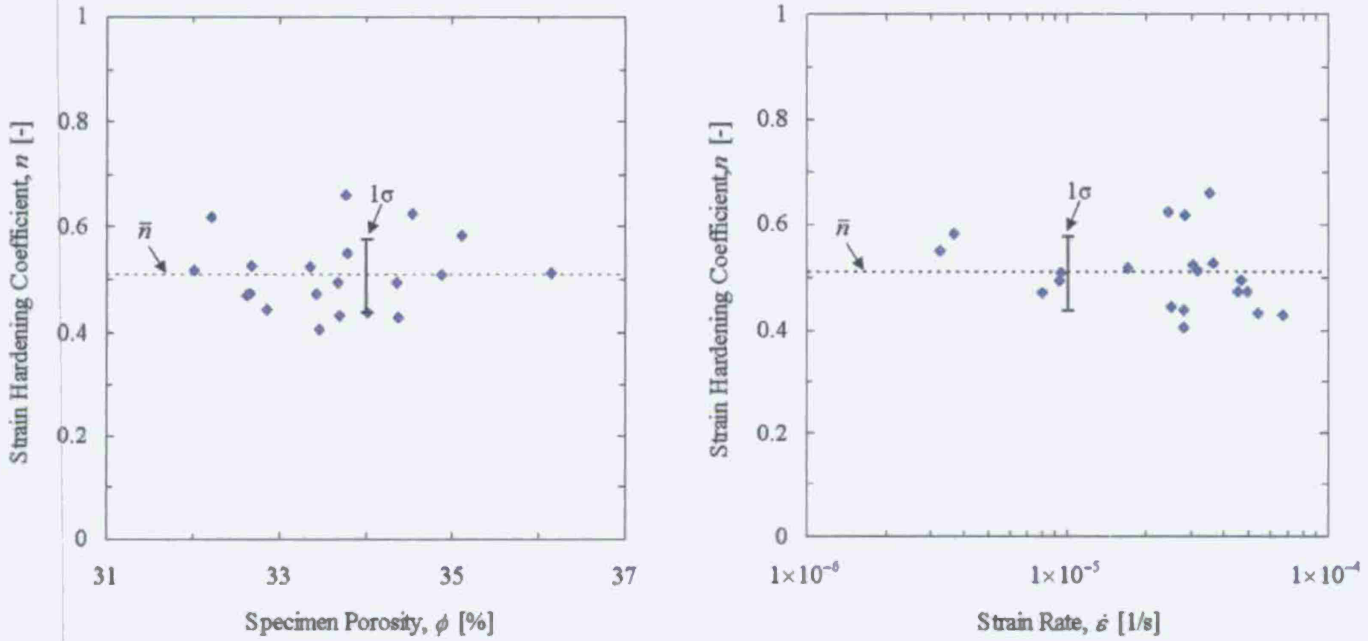

Figure 5 Strain hardening coefficient measured in twenty room temperature tests as function of test specimen porosity and testing strain rate. Error bar shows ± 1 standard deviation.

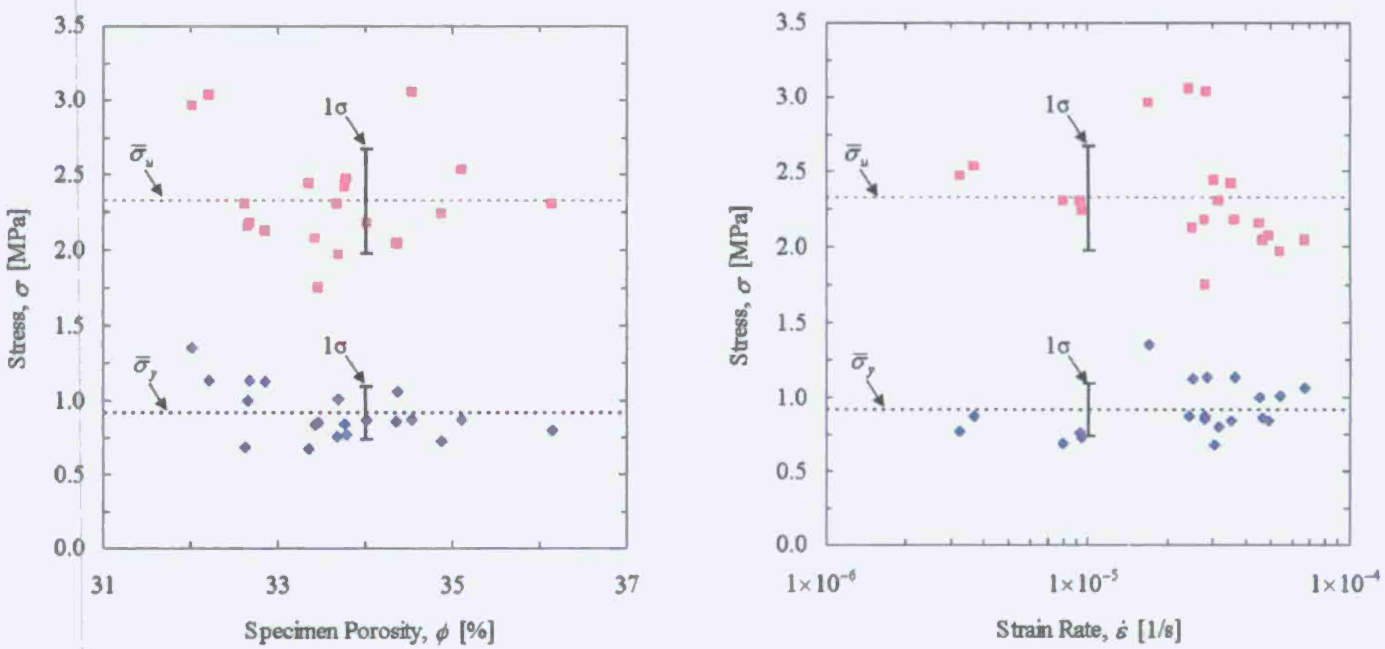

Figure 6 Ultimate stress and yield stress measured in twenty room temperature tests as function of test specimen porosity and testing strain rate. Error bar shows ± 1 standard deviation.

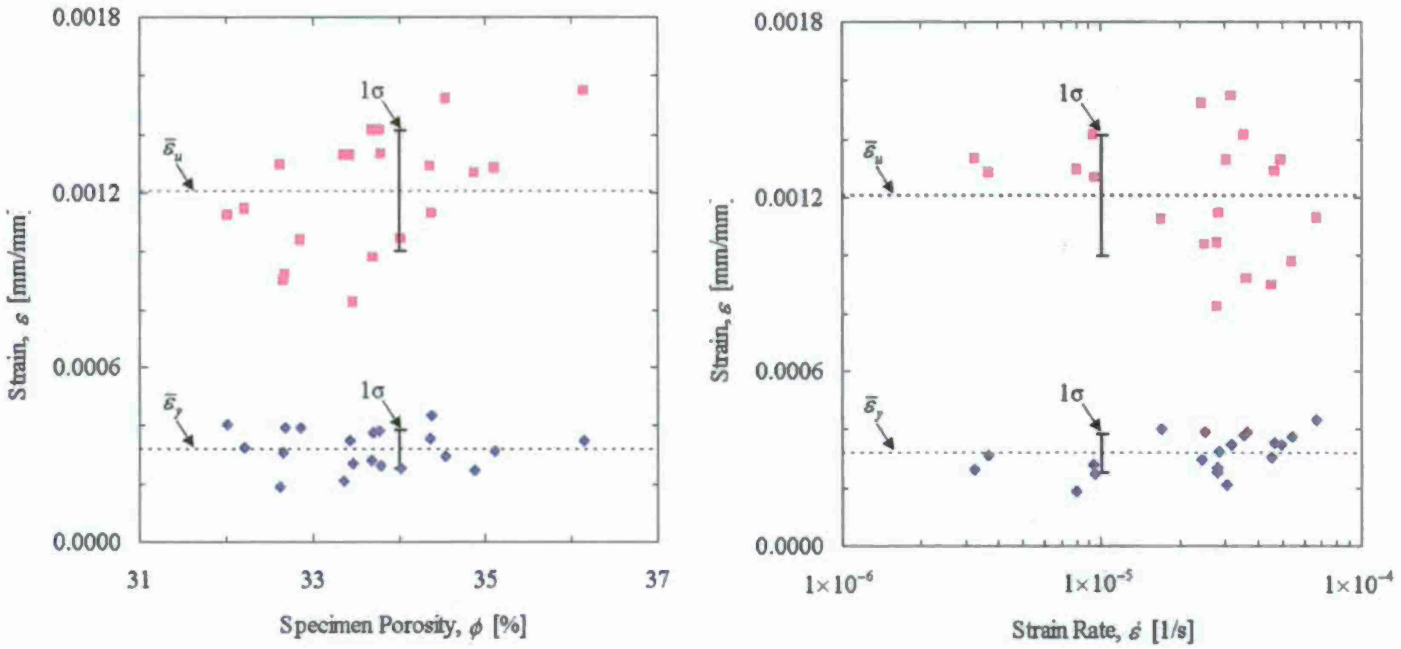

Figure 7 Ultimate strain and yield strain measured in twenty room temperature tests as function of test specimen porosity and testing strain rate. Error bar shows ± 1 standard deviation.

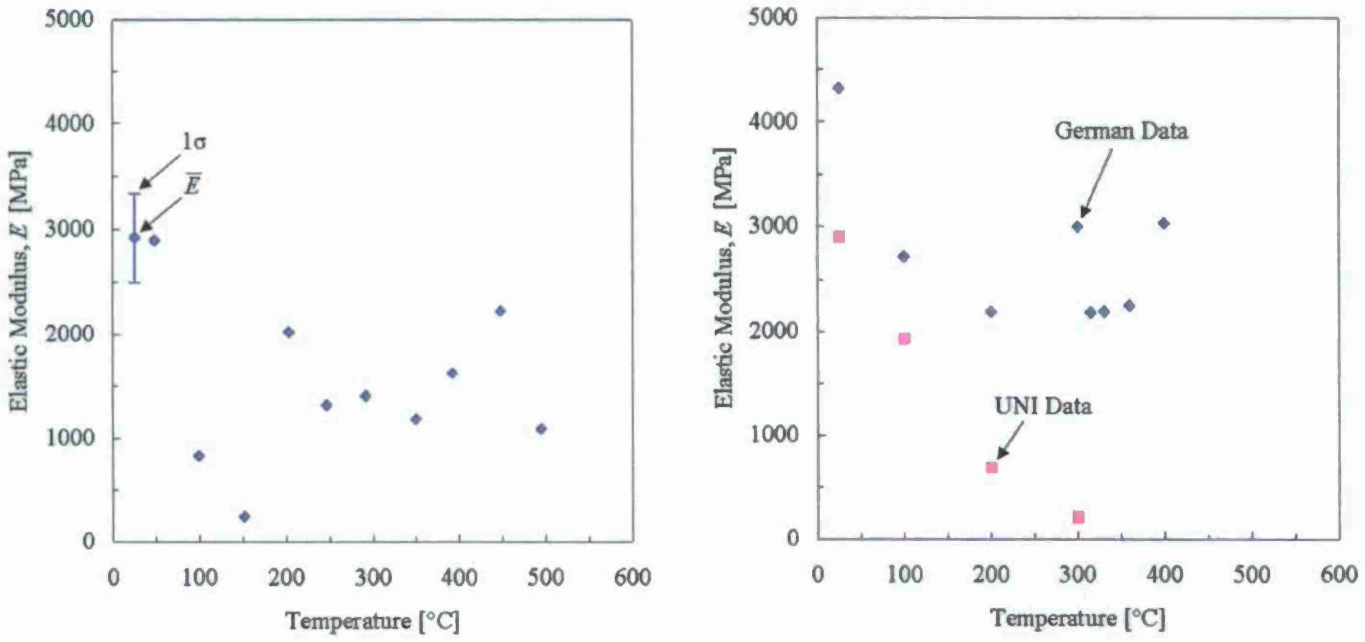

Figure 8 Measurements made by during this reporting quarter for elastic modulus and function of temperature(above left), and similar measurements made at the University of Northern Iowa, and in the German foundry literature (above right). Room temperature data from Figure 4 with standard deviation error bar also shown.

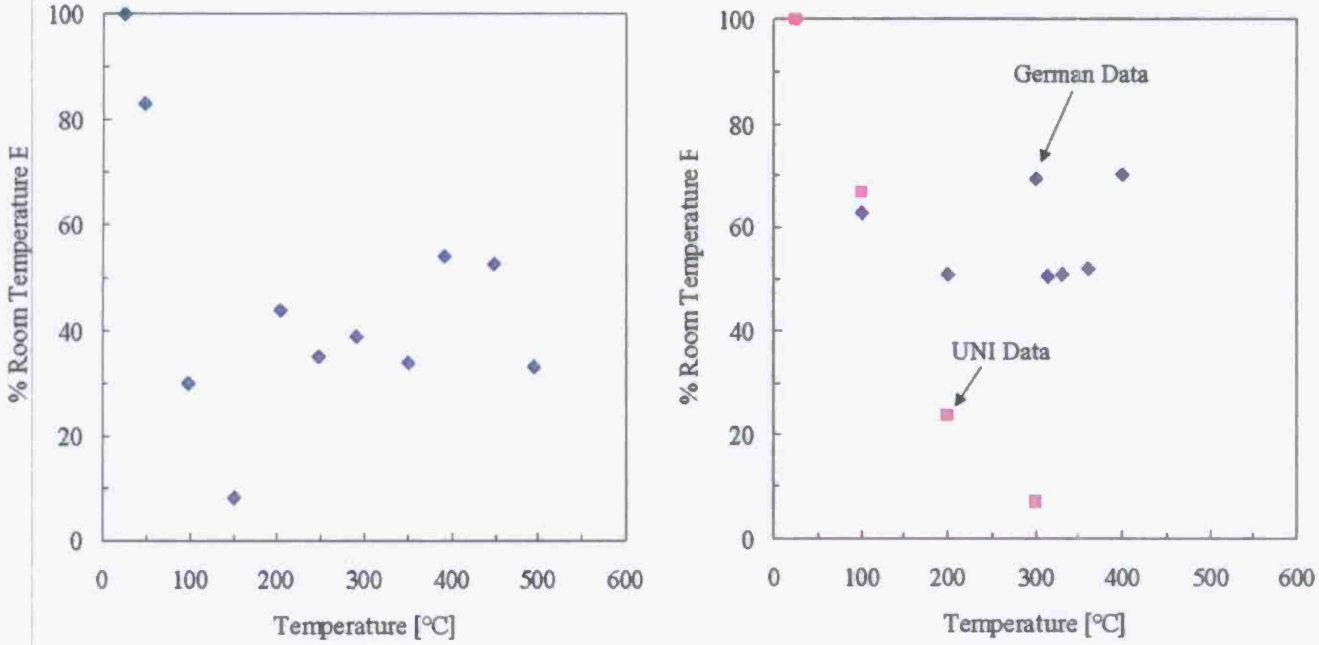

Figure 9 (above left) Elastic modulus data from Figure 8 divided by its room temperature value measured for each test prior to heating the furnace plotted as function of temperature. (above right) The UNI and German data divided by their respective room temperature values for comparison.

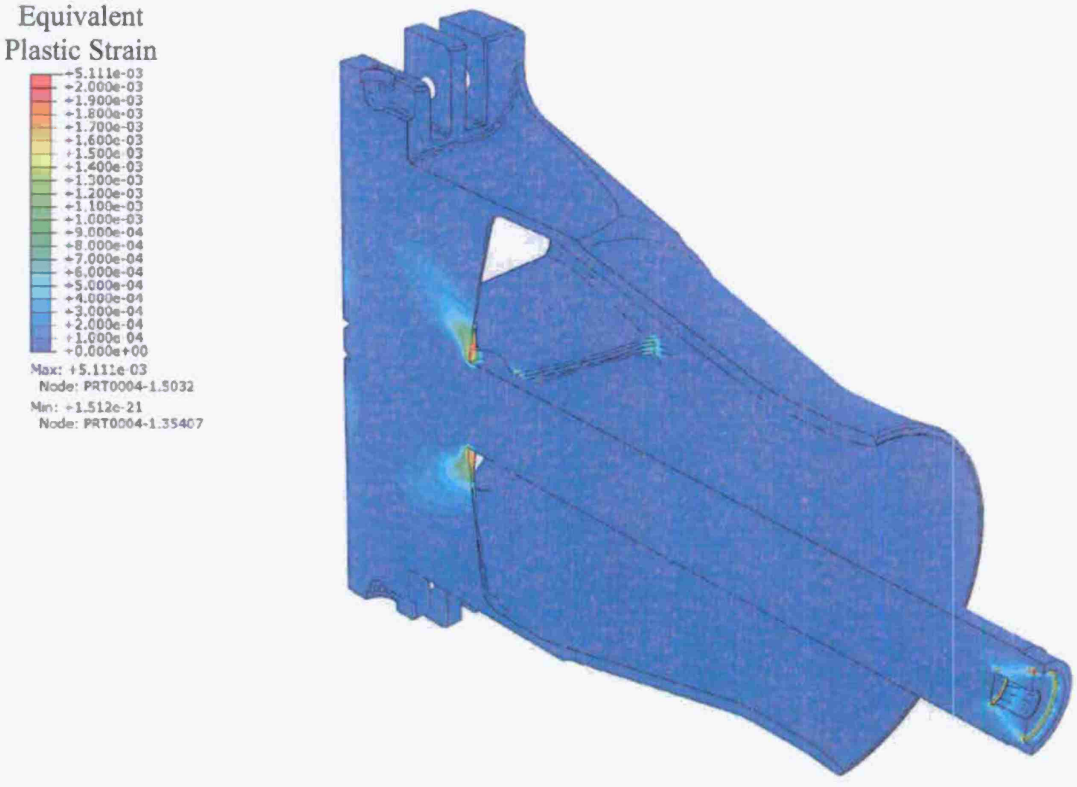

Figure 10 Equivalent plastic strain for re-designed breech nozzle using elastic-plastic analysis.

Figure 11 Porosity fraction for re-designed breech nozzle mapped onto ABAQUS finite element mesh.

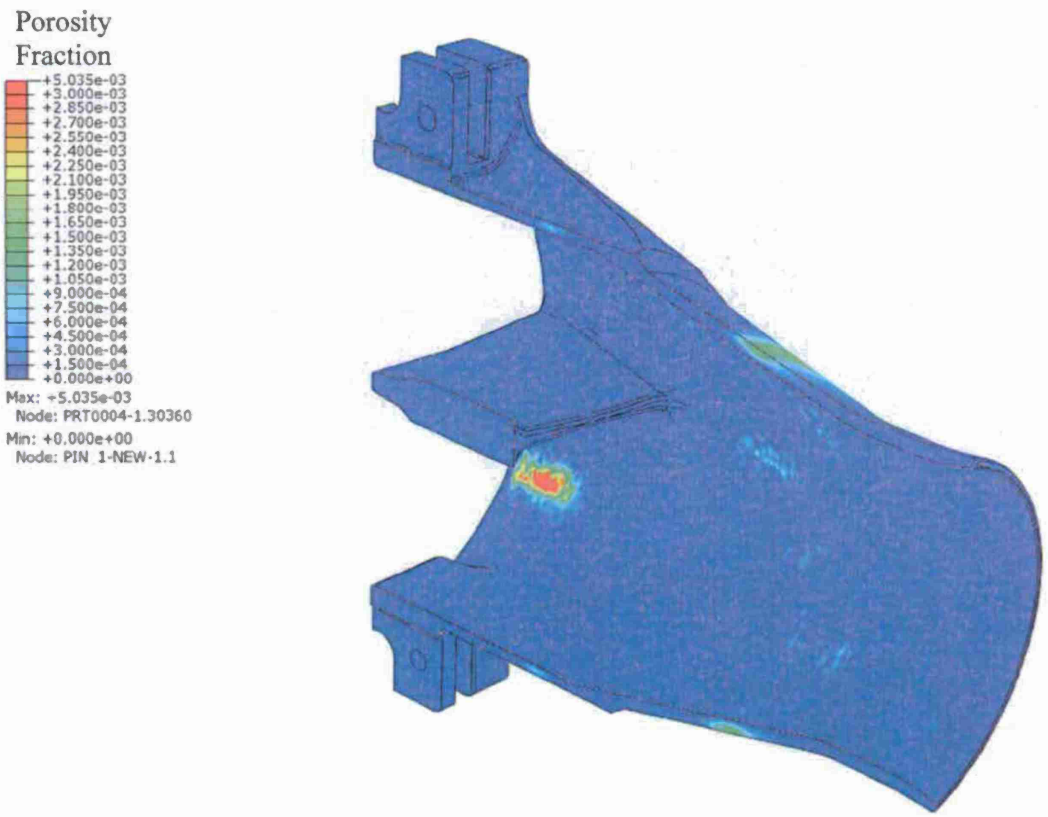

Figure 12 Porosity fraction for re-designed breech nozzle mapped onto ABAQUS finite element mesh with center tube cut away showing higher level of porosity.

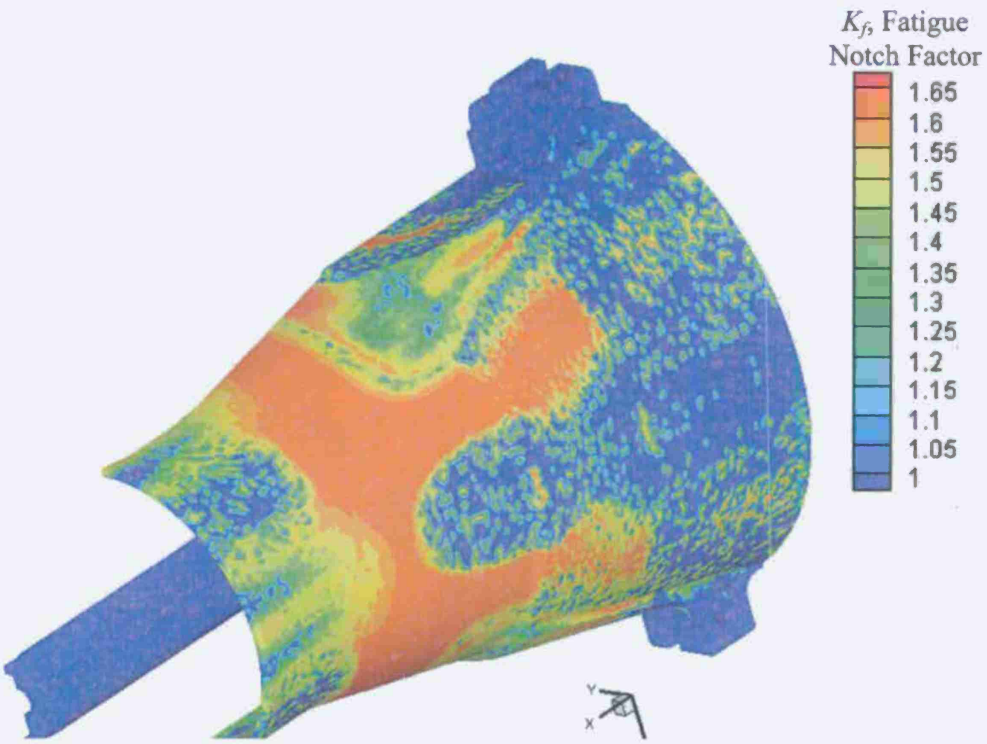

Figure 13 Fatigue notch factor distribution calculated from porosity field and finite element mesh, view 1.

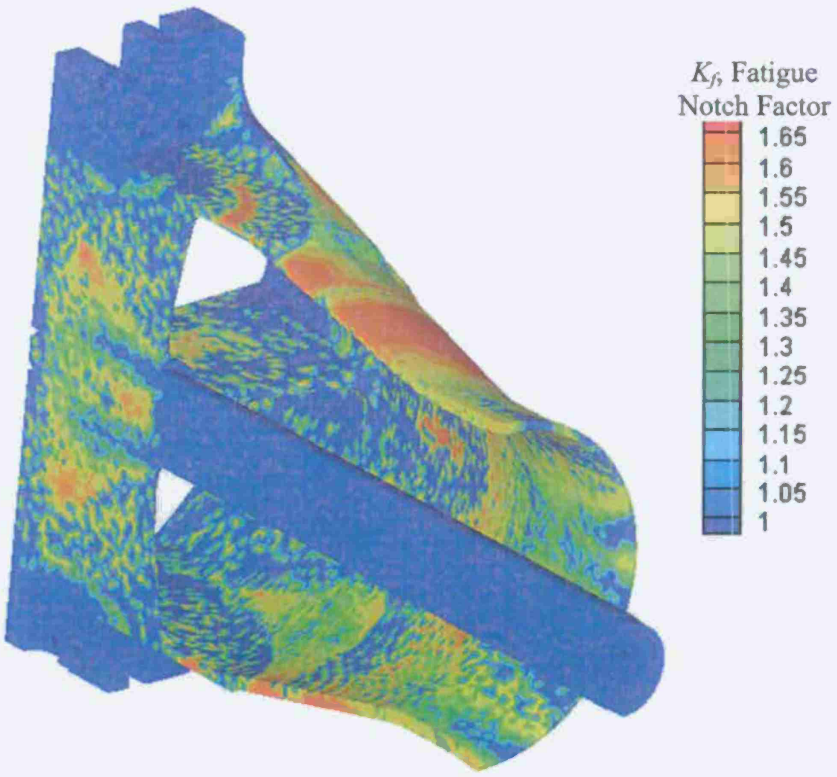

Figure 14 Fatigue notch factor distribution calculated from porosity field and finite element mesh, view 2.

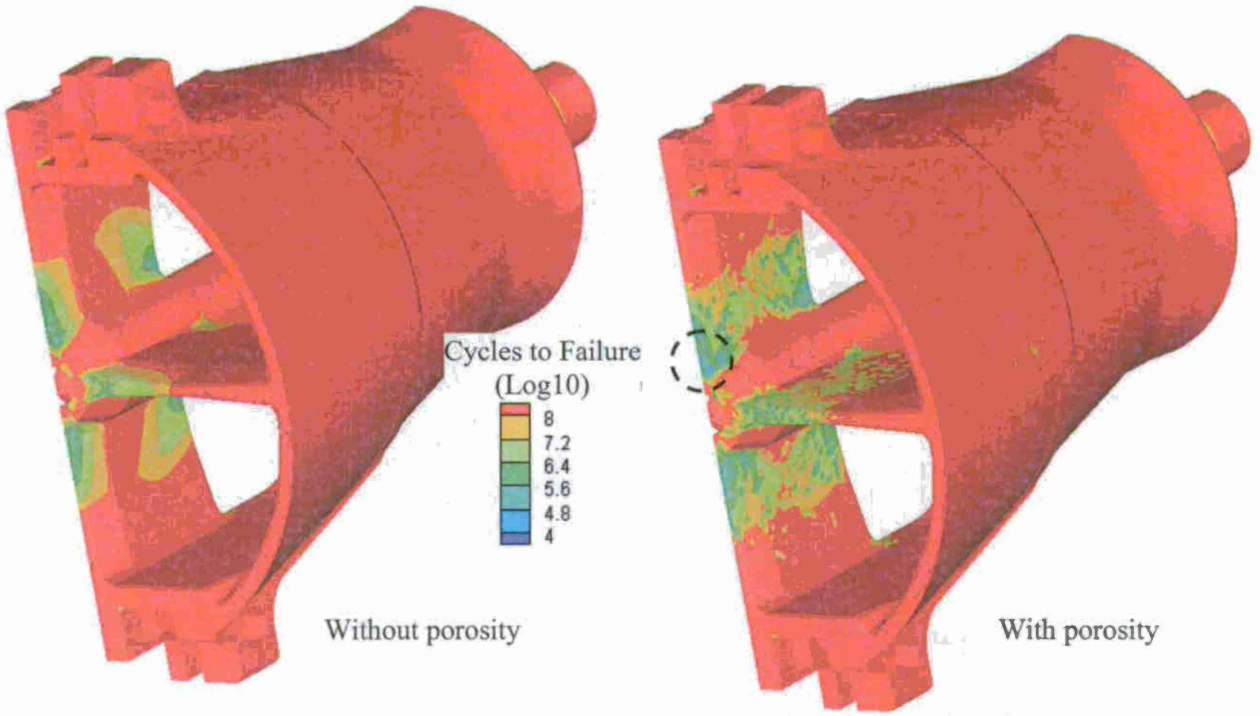

Figure 15 Fatigue life prediction without and with porosity results included in the analysis, view 1.

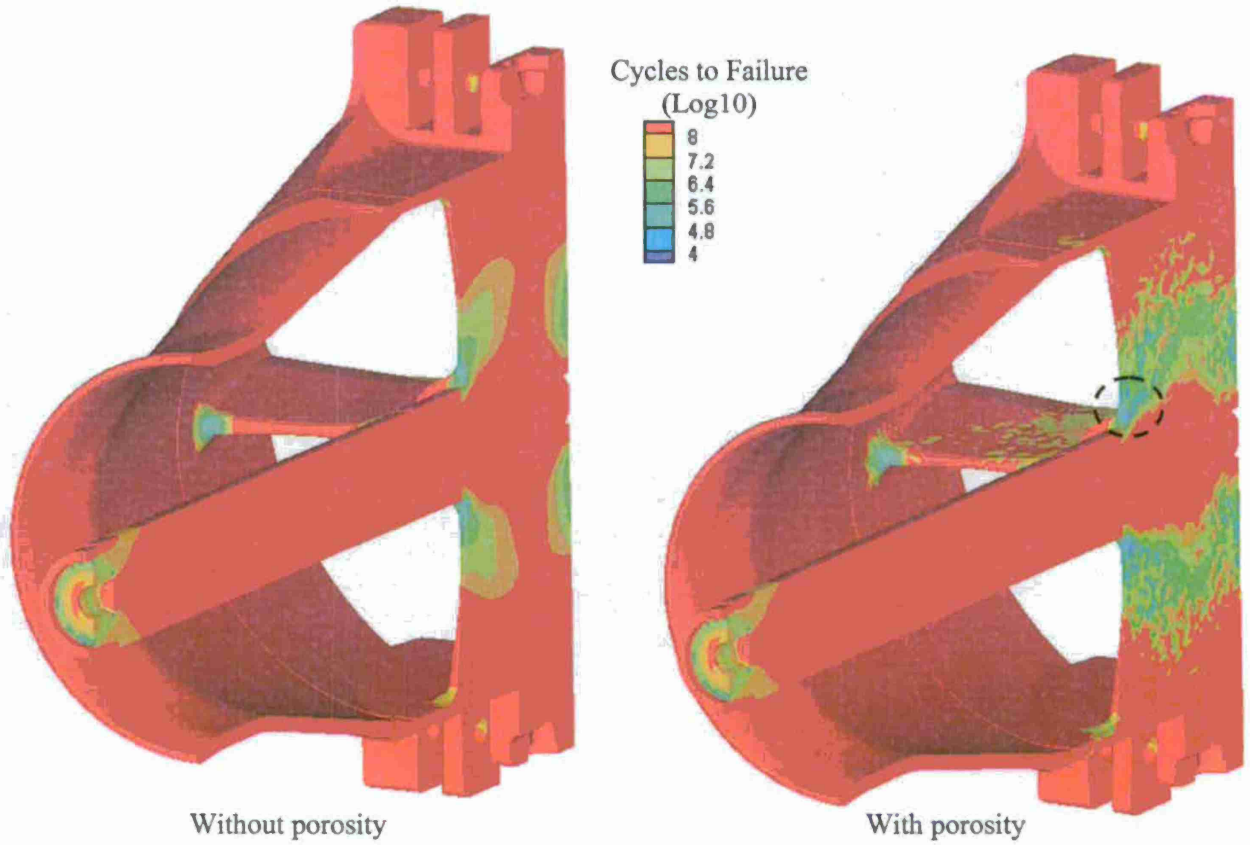

Figure 16 Fatigue life prediction without and with porosity results included in the analysis, view 2.

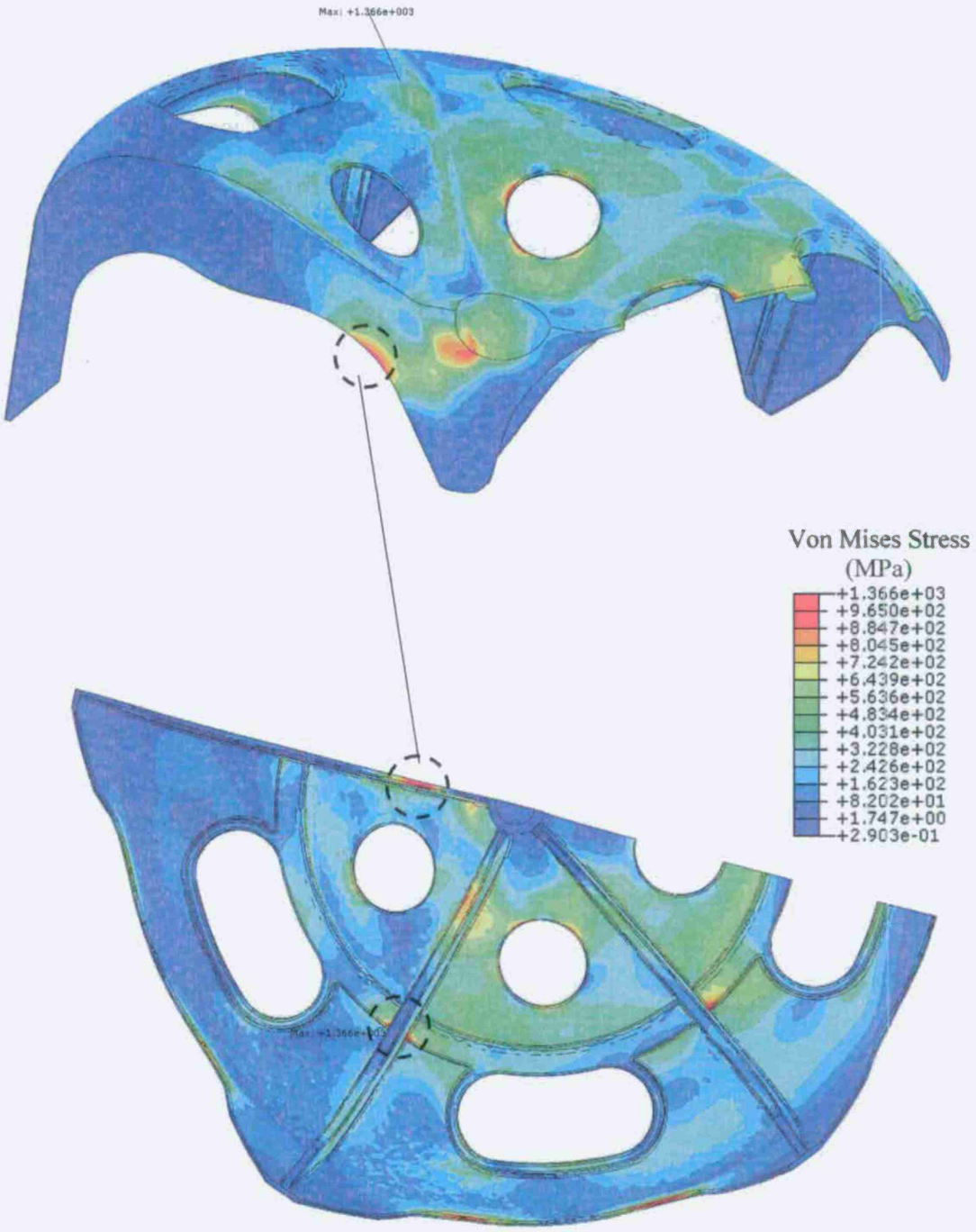

Figure 17 Von Mises stress distribution for load case 45 degrees over spade.

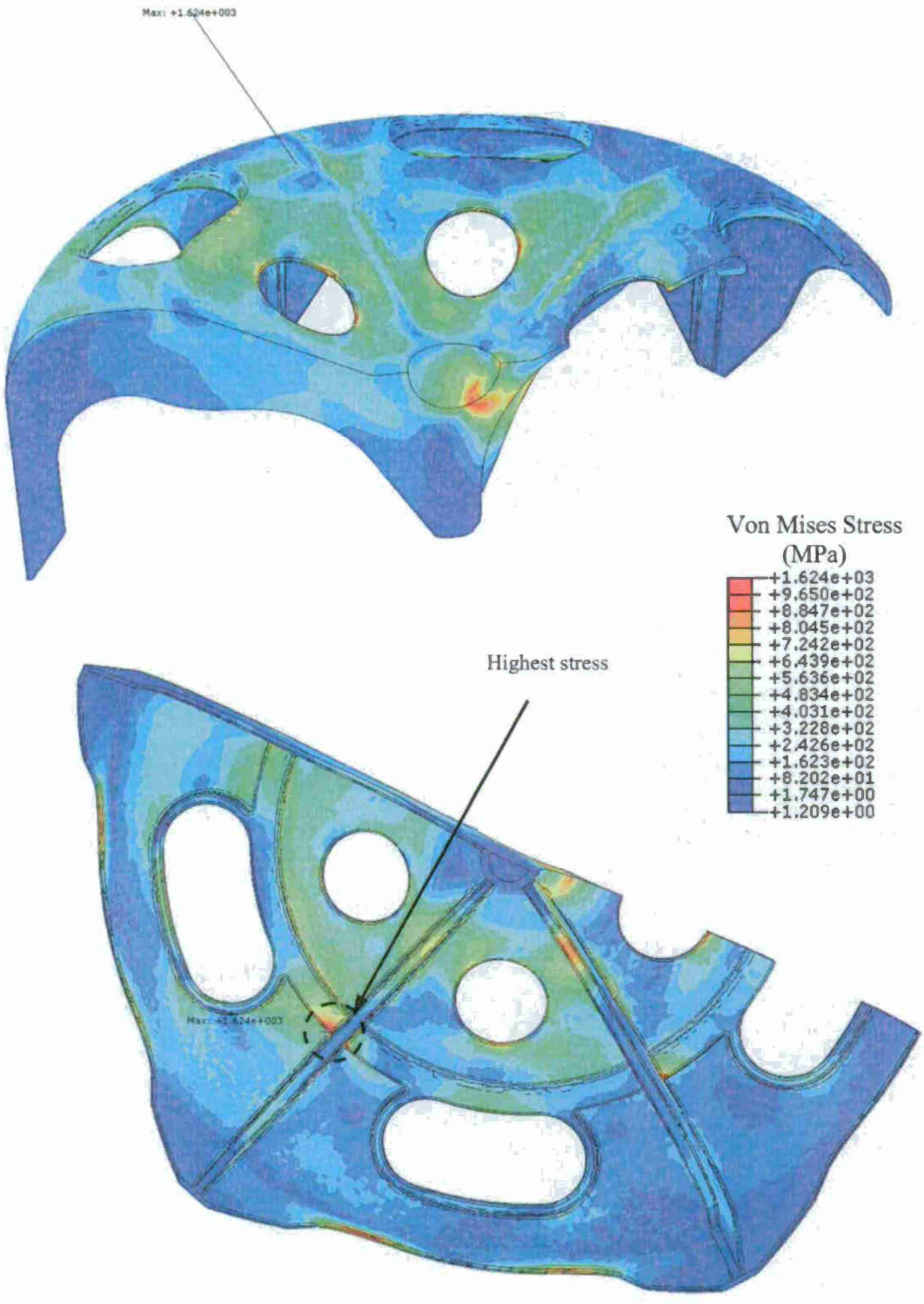

Figure 18 Von Mises stress distribution for load case 45 degrees over no spade.

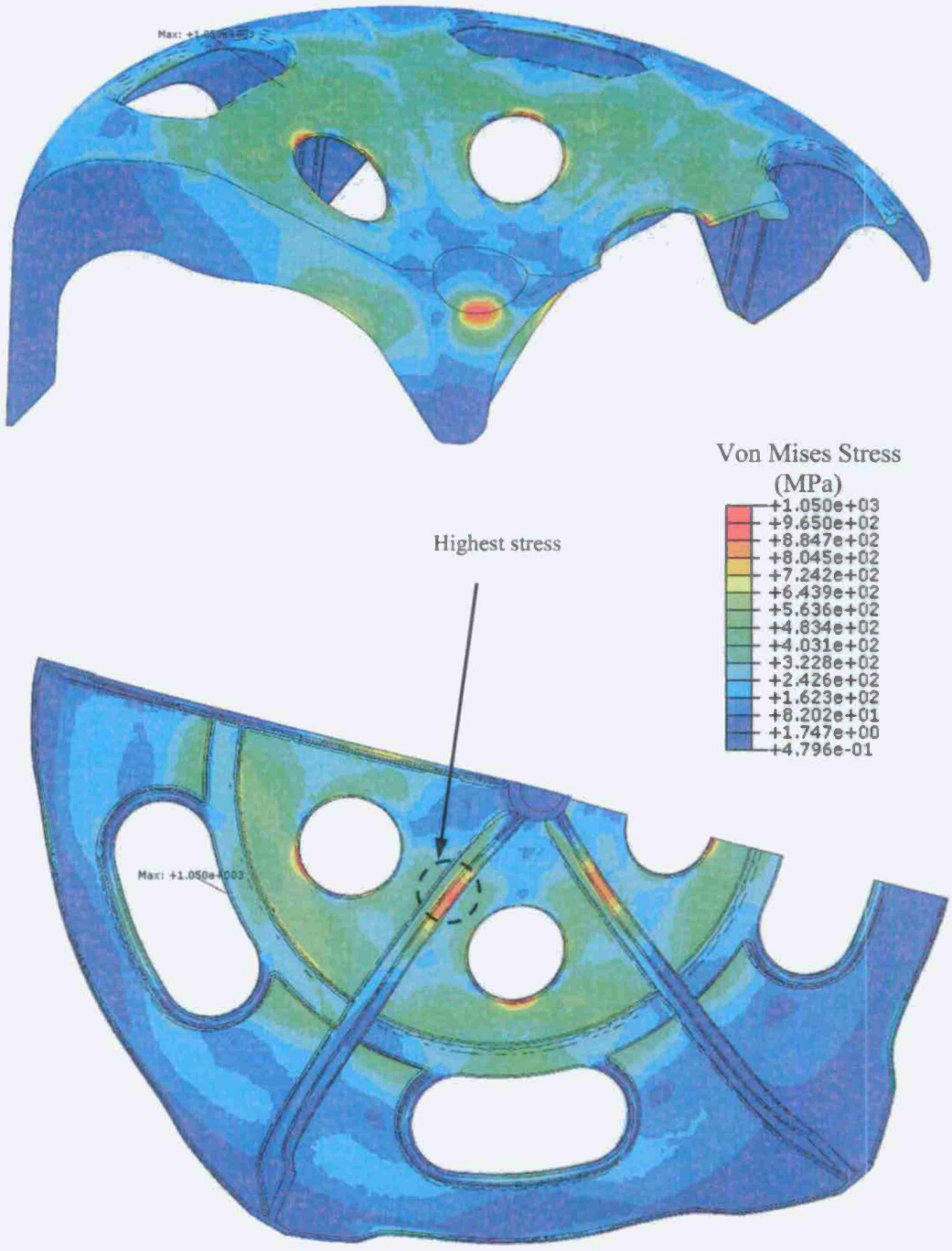

Figure 19 Von Mises stress distribution for load case 80 degrees over no spade

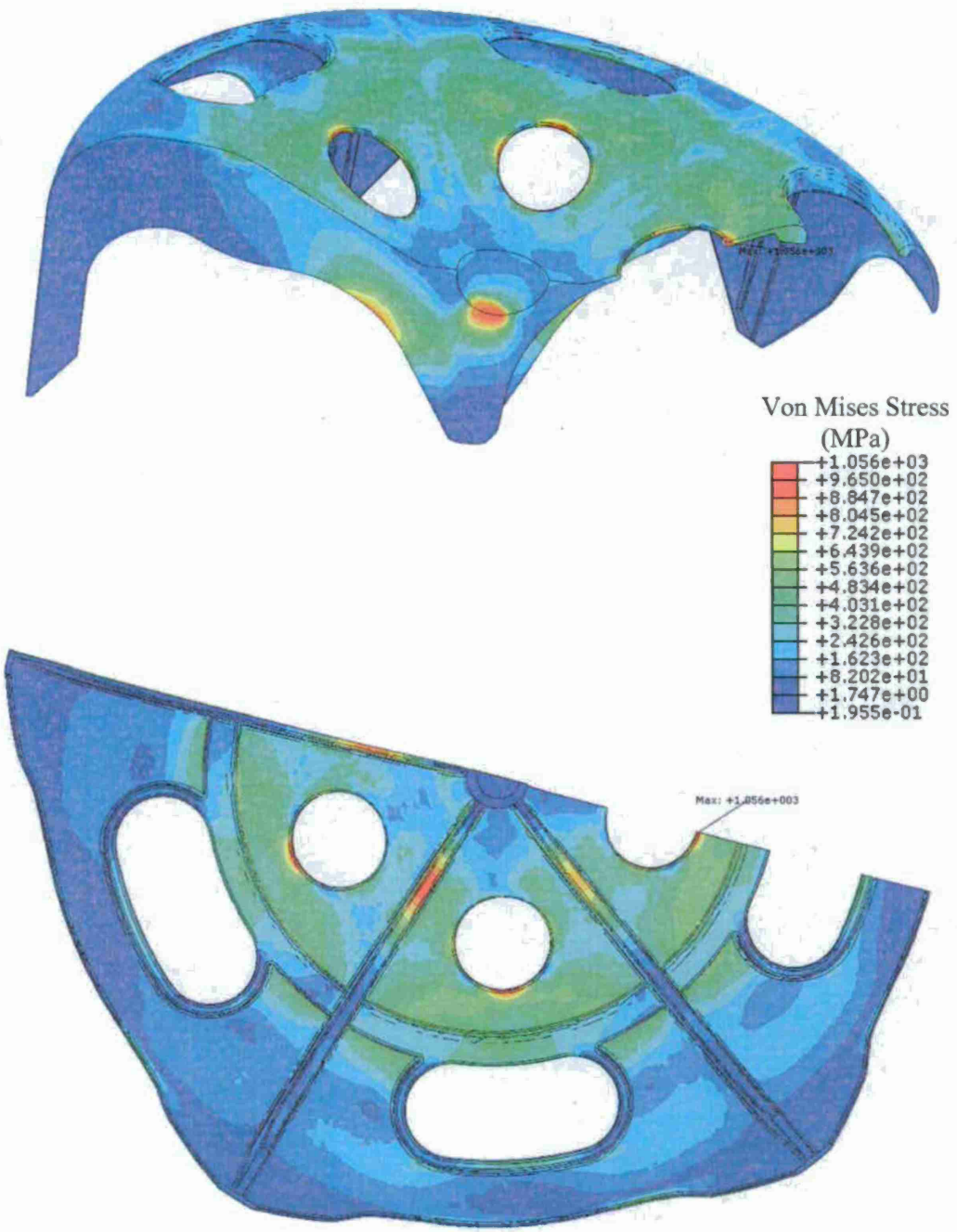

Figure 20 Von Mises stress distribution for load case 80 degrees over spade

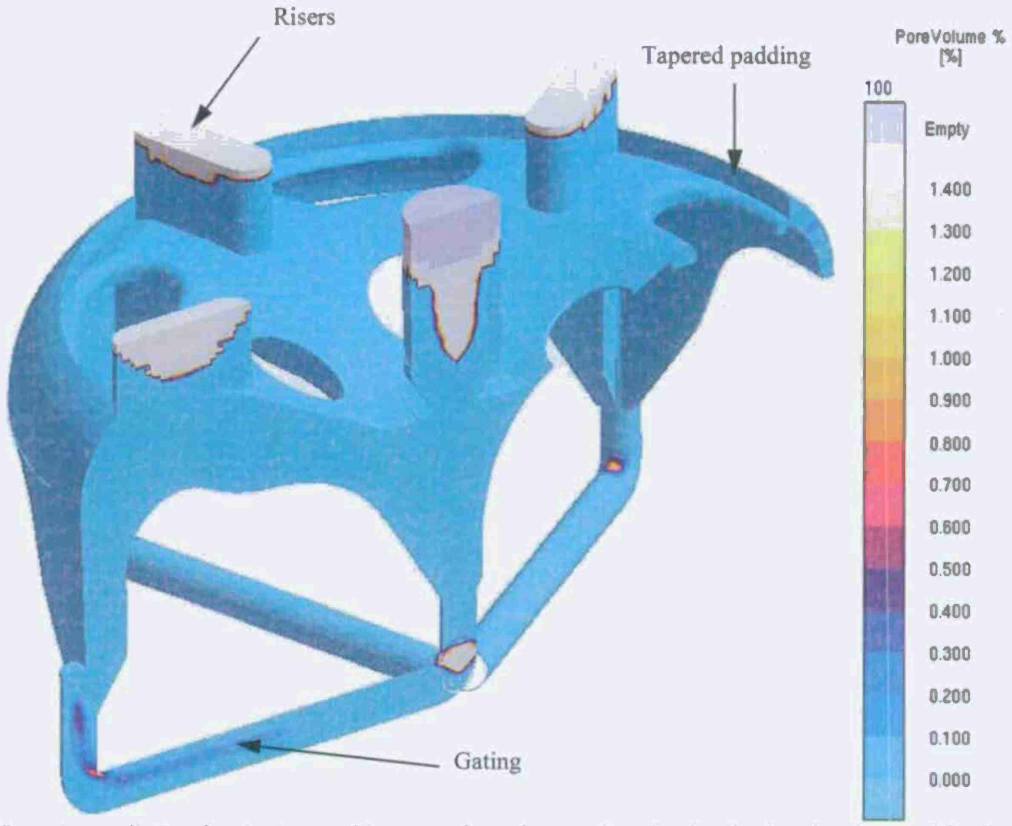

Figure 21 Porosity prediction for rigging used in mortar baseplate casting simulated using the advanced feeding development model in MAGMAsoft. Mid-section of casting is porosity-free.

Figure 22 Porosity prediction for mortar baseplate casting simulated using the advanced feeding development model in MAGMAsoft. Worst porosity for section indicated in red circle.

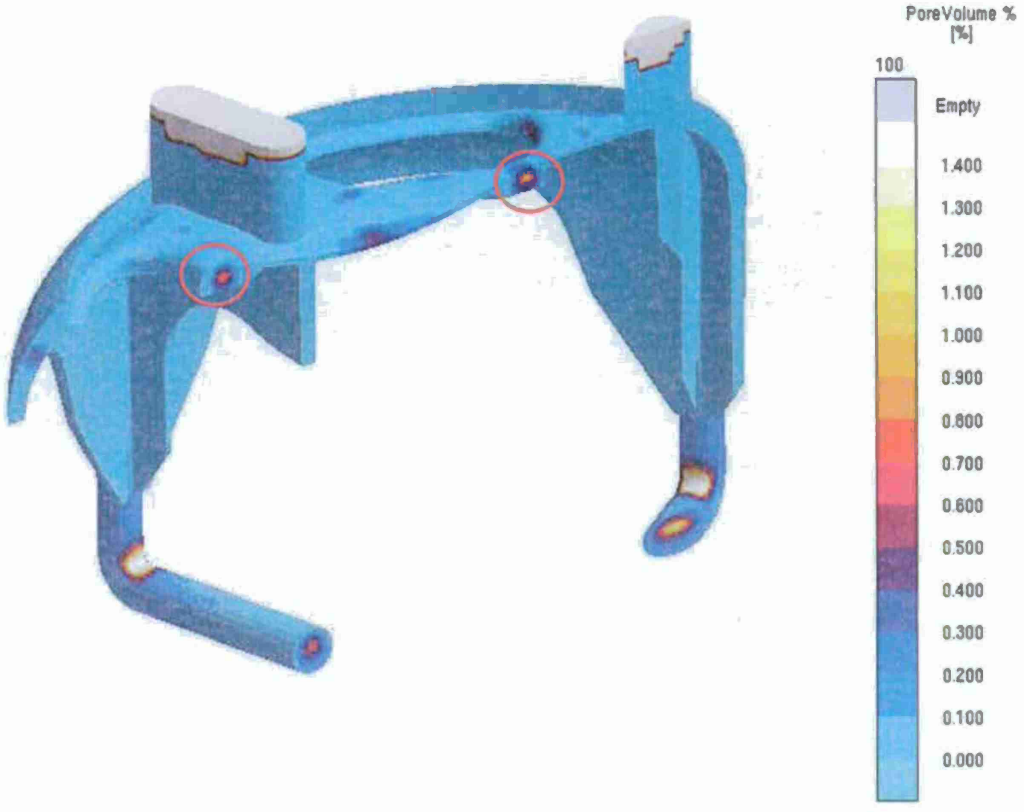

Figure 23 Porosity prediction in mortar baseplate casting simulated using the advanced feeding development model in MAGMAsoft. Worst porosity for section is indicated.

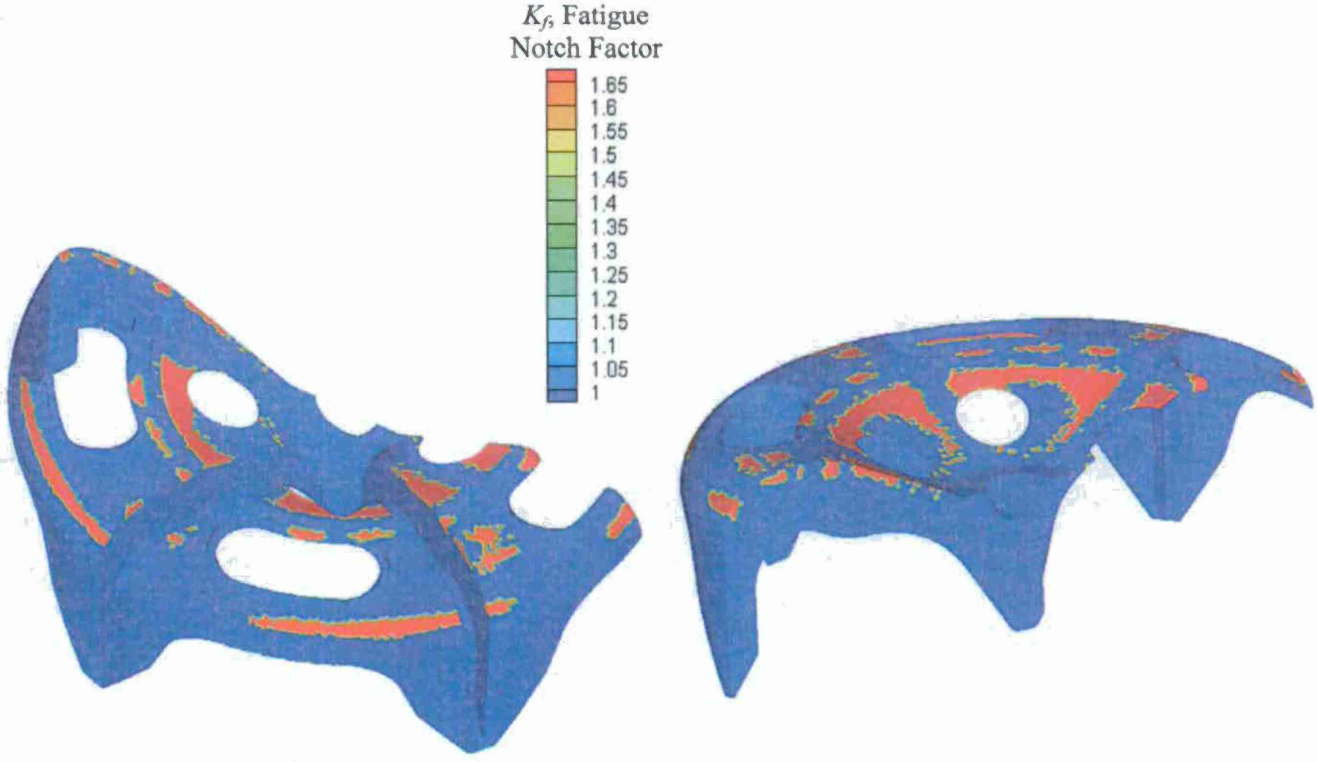

Figure 24 Fatigue notch factor resulting from porosity prediction and pore size model for mortar baseplate casting simulated using the advanced feeding development model in MAGMAsoft.

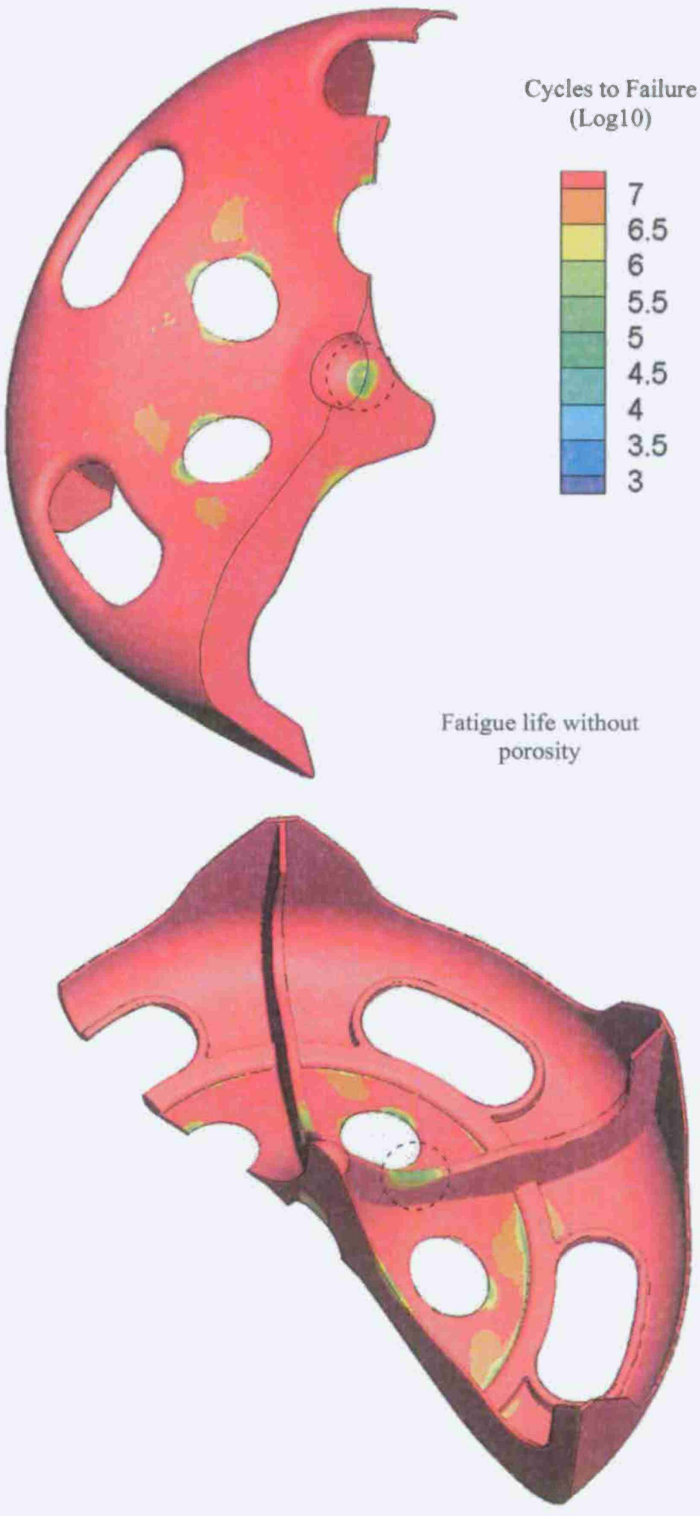

Figure 25 Fatigue life prediction without including effects of porosity gives minimum fatigue life of 12,900 cycles of load case 80 degrees over no spade. Also twenty nodes had lives < 40,000 cycles.

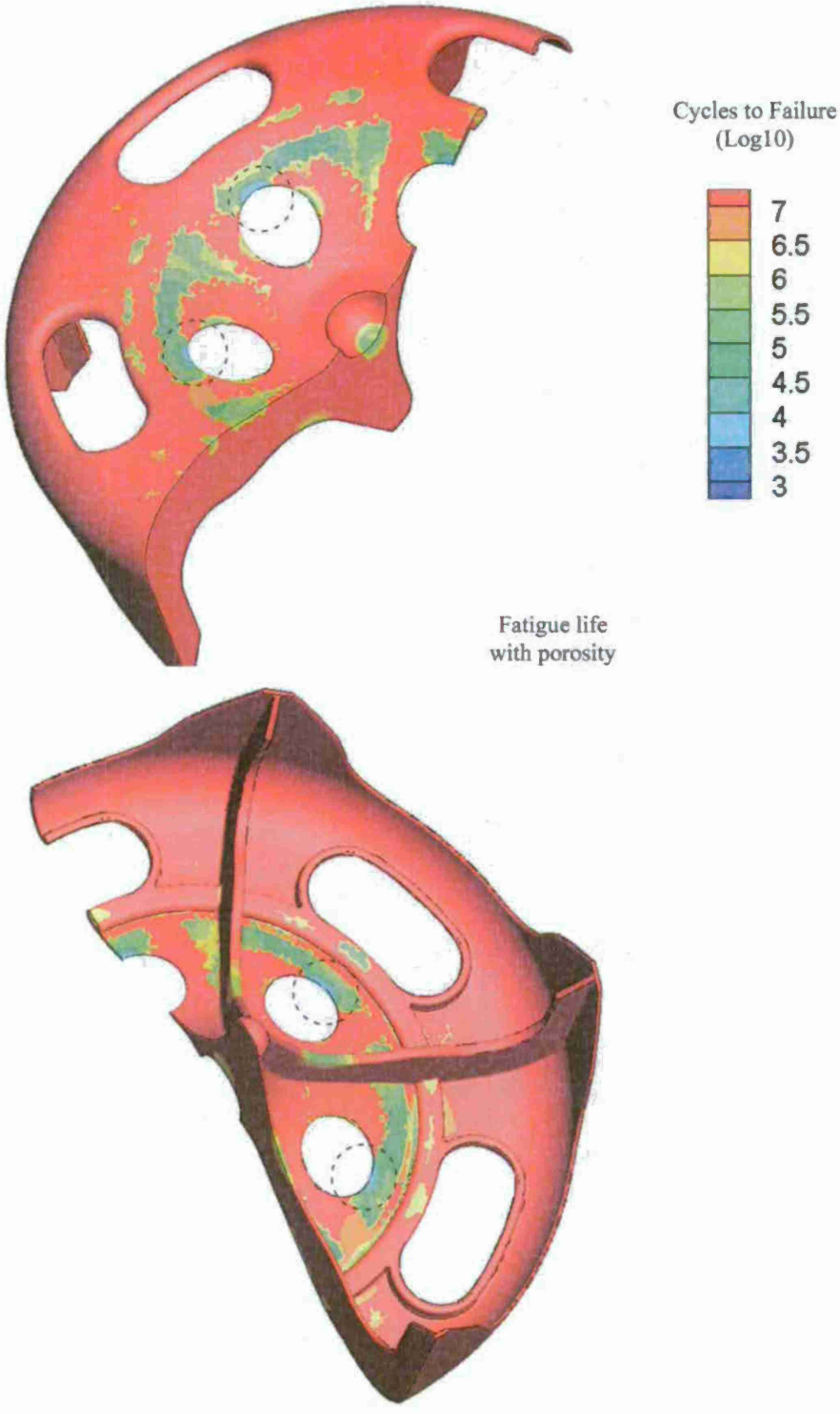

Figure 26 Fatigue life prediction including effects of porosity gives minimum fatigue life of 2,400 cycles of load case 80 degrees over no spade. Also twenty nodes had lives < 3,500 cycles.

Simulation Technology Transition and Demonstration

Visit to Benet Labs

Dr. Hardin traveled to the Watervliet NY area on May 4th and met one-on-one with an engineer who might be taking on the role as the lab's casting simulation analyst using MAGMAsoft. He discussed casting simulation with her and went through a presentation he would give the following day on the topic. He visited Benet Labs on May 5th. The next morning he gave a seminar presenting three topics: Introduction to Casting Process Simulation and MAGMAsoft, A Method for Predicting Effects of Porosity on the Performance of Steel Castings, and on Case Studies of Casting Design Evaluation using MAGMAsoft, ABAQUS and fe-safe. In particular he was asked to and addressed the advantages of using casting simulation in the design process, its limitations and pitfalls, the data and information required to run casting simulations, and the common assumptions made when performing the simulations. Future project work was planned and it was decided to perform casting simulation and performance prediction for the FAS muzzle brake.

FAS Muzzle Brake Casting

We received a technical data package from Benet Labs that is required to analyzed the part (drawings, CAD and ABAQUS files) and began to work on the FAS muzzle break casting, A teleconference was held with engineers at Waukesha Foundry, who will be producing the as-cast part, the SFSA and the University of Iowa. It was determined that a confidentiality agreement would be put in effect between the University of Iowa and Waukesha. Following is in place before any information on the casting process is transferred to the University of Iowa. Following that work should proceed swiftly. Near the end of the quarter the agreement was said to be in the signing process at the University of Iowa.

Hexagonal Ceramic Armor

During this quarter, simulations were performed using MAGMAsoft and MAGMAstress to determine the temperature and stress characteristics of a hexagonal ceramic cast-in steel armor plate. Two types of ceramic, SiC and Al_2O_3, are being considered for the casting ceramic plate. As shown in Figure 1, the hexagonal ceramic plate is centered in a mold in which steel is poured. The dimensions defining the armor plate are the ceramic hex's width and height (shown in Figure 1), and the side spacing, and top and bottom thickness of steel cast around the ceramic. In the simulation results that follow 1/12th symmetry is assumed about the hexagon, and one half symmetry of the thickness is also assumed (i.e. to the mid-thickness of the ceramic). The following parameters are being investigated and analyzed to determine their effects on stresses and hot tear susceptibility arising during the casting production process for the armor: preheating temperature of ceramic and shell mold, cast-in steel wall thickness (top, bottom and side), casting method (sand or shell mold), and steel composition. Computer models of the ceramic block and surrounding casting geometry were created in Pro/E and imported into MAGMAsoft. No gating is considered in the simulations run thus far, and no filling is simulated. Therefore, it is assumed that molten steel surrounds ceramic, filling the casting space about the ceramic, at start of simulation. We also assume that the ceramic is perfectly centered and suspended in the metal. The following cases have been simulated:

Ceramic geometry
SiC having Width = 4", Height = 3/4"
Al_2O_3 having Width = 3 7/8", Height = 1 5/16"

Cast steel thickness
Case 1 has Side spacing = 1/8", Top/Bottom spacing = 1/4"
Case 2 has Side spacing = 1/4", Top/Bottom = 1/2"

Also, in the simulations the mold has been assumed to be shell mold surrounds steel with a 10 mm wall thickness.

Comparing stress, strain and hot tear criteria results for simulations run with various parameters, we performed a study examining which combinations parameters produce the lowest stresses, strain and least hot tear damage. Typical results generated during the previous reporting period for Von Mises stress and hot tear damage (or tendency) are shown in Figures 2 and 3. These results are for C19Mn5 cast steel surrounding a SiC ceramic plate

after casting and cooling to room temperature. The preheat temperature used for ceramic is 700C (this is the initial temperature of the ceramic in the simulation). Higher values of the hot tear tendency in Figure 3 denote worse tearing. So far our results show preheat to be the most important variable in the process, but additional simulations, and a more in depth sensitivity study is necessary to determine a best/recommended process for this cast-in ceramic armor. We plan to perform this in future work in the upcoming quarter.

Measurement of Displacement and Forces During Casting of a 12x1x1 inch Bar

During this quarter, experiments were performed to provide good data for validating models of displacement (contraction) and stresses (forces) during and after solidification. These were in-situ experiments for a 12" long x 1" thick x 1" wide bar with free (unrestrained) and restrained ends as shown in Figure 4. In Figure 5, the top and side views of the unrestrained 12" long x 1" thick x 1" wide bar used in the stress displacement experiments are given to show the locations of thermocouple temperature sensors (T.C.) and position sensors (LVDT). Plots of measured temperature (red lines) and displacement/contraction versus time of the experiment for the steel (blue lines) and for sand (in violet) in the unrestrained casting are shown in Figure 6. Note how contraction begins to develop at the start of solidification, and the final measured contraction is 6.5 mm for steel. In Figure 7, the measured contraction versus temperature for the steel in the unrestrained casting is shown. A schematic diagram for the restrained casting is shown in Figure 8. Locations of thermocouple temperature sensors are same as in Figure 5 and force sensors (load cells, L.C.) and position sensors (LVDT) are indicated in Figure 8. The load cells are attached to the bolts embedded in the casting ends shown in Figure 8. In Figure 9 plots of measured temperature (red lines) and displacement (blue lines) versus time for the steel in the restrained casting are given. Note that the final displacement for the restrained casting is about 3 mm. Compare this to the displacement of 6.5 mm for the unrestrained casting shown earlier. In Figure 10 the measured temperature (red line) and force (magenta) versus time for the steel in the restrained casting are shown. Note how restraining force begins to develop close to, but not at, the end of solidification. The maximum forced developed at the restraints is about 4750 N (mean between the two sensors). In Figure 11, plots of measured contraction and force versus temperature for the steel in the restrained casting are given. Comparing Figure 5 and Figure 11, the restrained casting contraction was measured to be 1% and the unrestrained casting was 2.1%. In both experiments, the casting was made of WCB Steel, the mold was made from IL5W silica lake sand, and the binder was a bio-urethane no bake. In future work, during the upcoming quarter, we plan to cast a restrained casting using a turnbuckle to apply a load shortly after a solid skin has formed. This will give data on applying an active/varying force to the casting during the process. We will also work with simulations to match experimental temperatures and distortions.

Internal/External Shrink in Casting of Steel in Blind Risers

Our MAGMA simulations with the advanced feeding module are capable of predicting internal shrinkage porosity (voids within the casting) and external porosity (surface deformations, caused by the casting surface sucking in to compensate for the shrinkage). In the last quarter, we developed and cast four experimental castings to obtain data to compare with these model predictions. The castings chosen for these experiments are blind riser castings as shown in the diagram in Figure 12. As shown in the top and side views of Figure 12, each casting used in this internal/external shrinkage study has two blind risers. The downsprue is not shown in Figure 12, and it was designed to freeze off well before horizontal bar connecting the two blind "risers" so it can be removed from the simulations. In Figure 12, note that the locations of B-type thermocouples are indicated by circles. Out of the four experimental castings produced, three had measurable surface shrinkage. A picture of one of the three (out of four) castings determined to have visible surface sinking. This indicates the "external" shrink predicted by the advanced feeding module. Note the thermocouple locations are seen at the dark round holes. The cast steel, mold sand and binder using were the same as those of the cast steel bar discussed in the previous section. In future work during the upcoming quarter, we plan to x-ray and cut the four castings to quantify surface shrink and internal porosity. It is also planned to run MAGMA simulations with advanced feeding module to compare its results with the experiments.

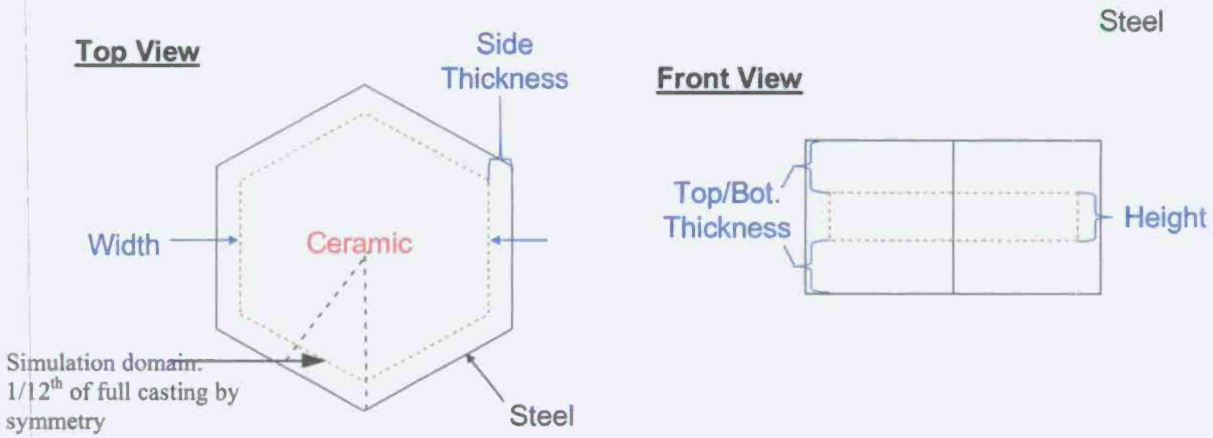

Figure 1 Diagram of hexagonal ceramic plate cast into steel. Note simulation domain is one-twelfth of cast-in ceramic armor.

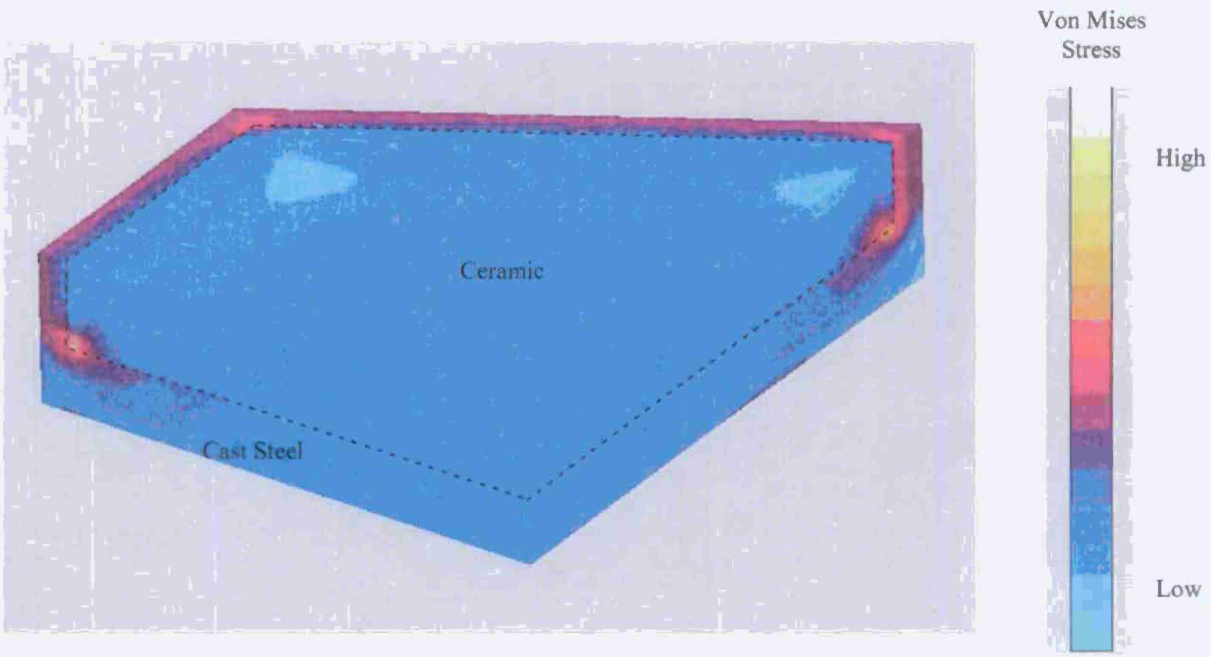

Figure 2 Von Mises stress distribution showing hot spots in the corners of the cast steel surrounding the ceramic plate. One-twelfth section at mid-thickness of armor shown. Preheat for SiC ceramic is 700C.

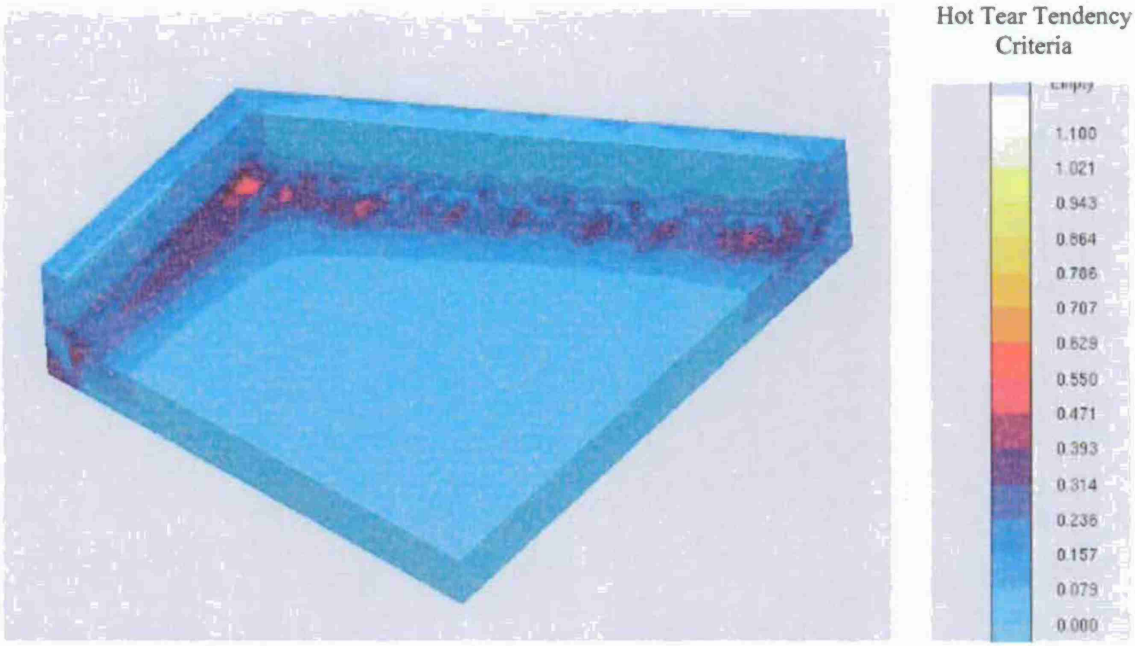

Figure 3 Hot tear tendency criteria for cast steel surrounding a ceramic armor plate. Higher value denotes worse tearing. One-twelfth section of the cast steel is shown. Preheat for SiC ceramic is 700C.

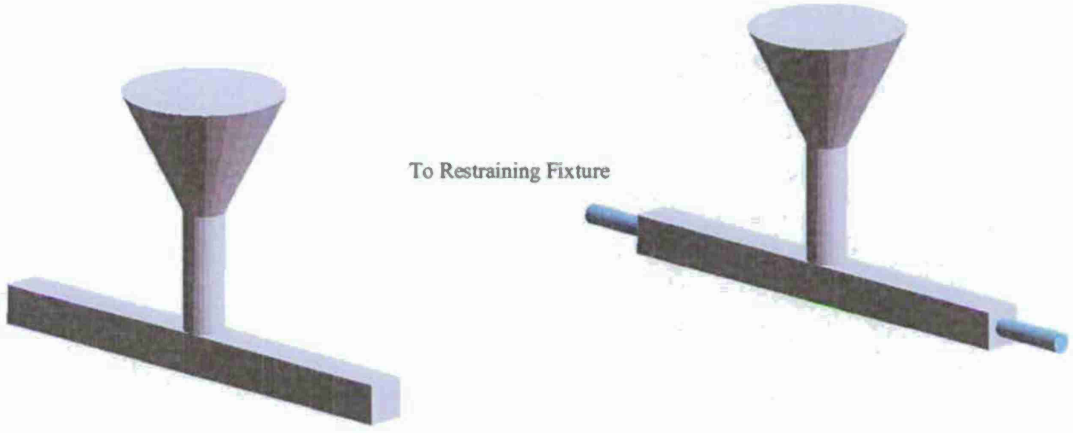

Figure 4 Images of 12" Length x 1" Thickness x 1" Width bar showing unrestrained geometry (above left) and restrained geometry with bolts cast into ends (above right).

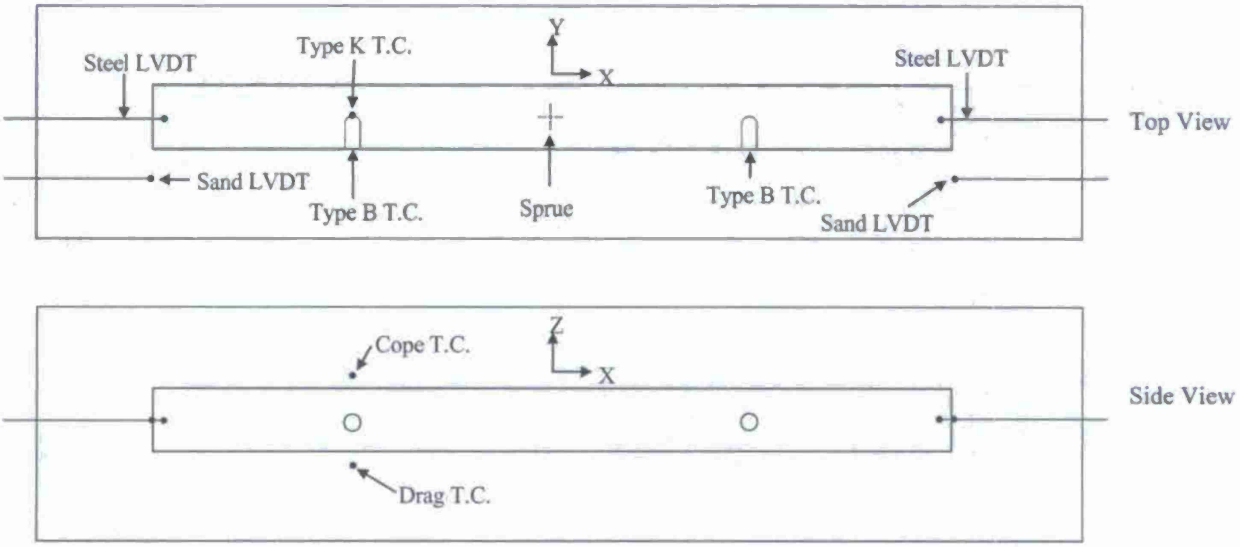

Casting Dimensions: 12" x 1" x 1" Mold Dimensions: 16" x 5" x 6"

Figure 5 Top and side views of the unrestrained 12" long x 1" thick x 1" wide bar used in the stress displacement experiments. Locations of thermocouple temperature sensors (T.C.) and position sensors (LVDT) are indicated.

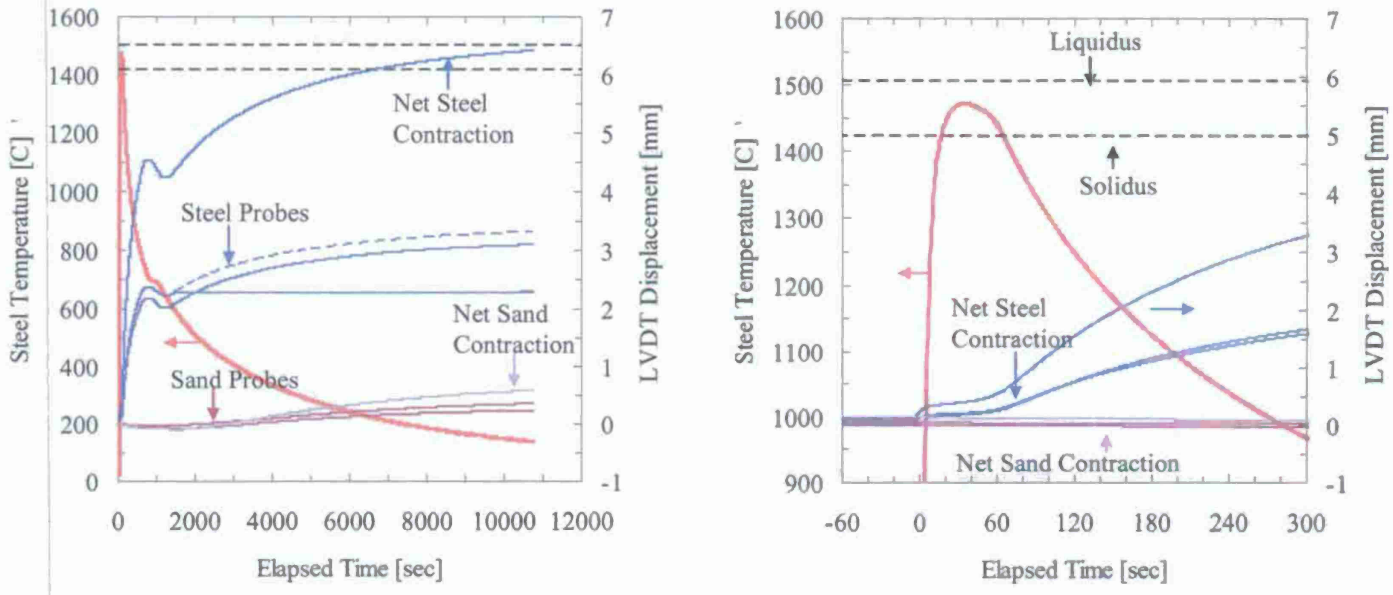

Figure 6 Plots of measured temperature (red lines) and displacement/contraction (blue lines are steel, violet lines are sand) versus time for the steel in the unrestrained casting. Temperature scale at right shows high temperature range (from 1200 C to 1500 C). Note how contraction begins to develop at the start of solidification.

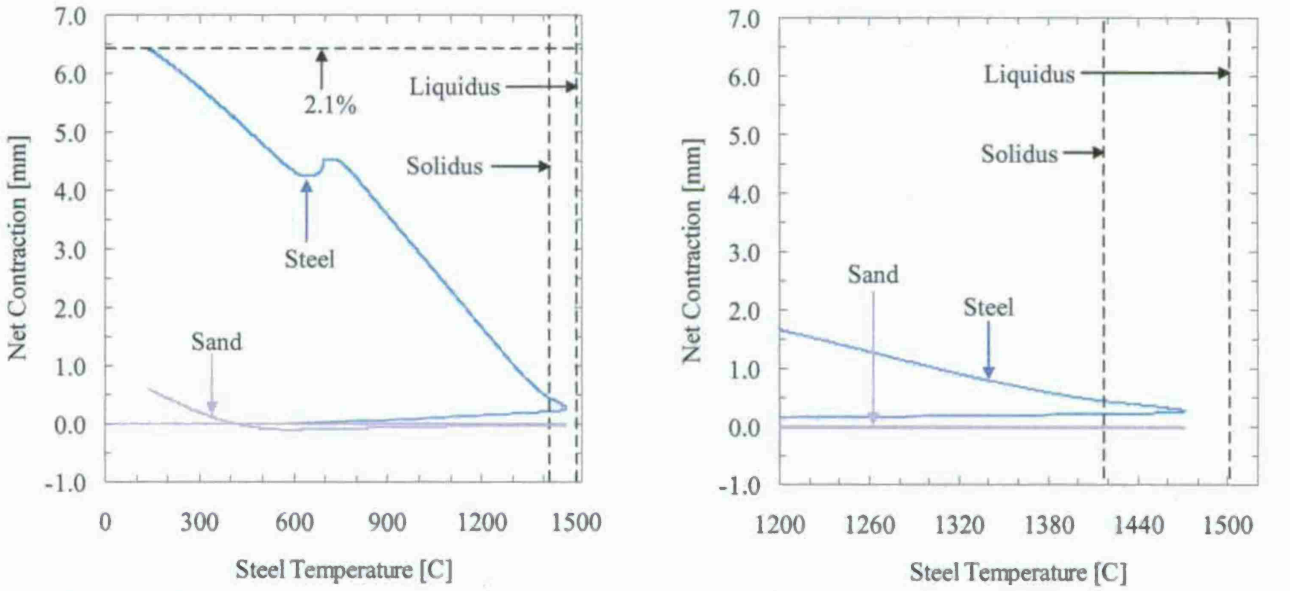

Figure 7 Plots of measured contraction versus temperature for the steel in the unrestrained casting. Temperature scale at right shows high temperature range (from 1200 C to 1500 C).

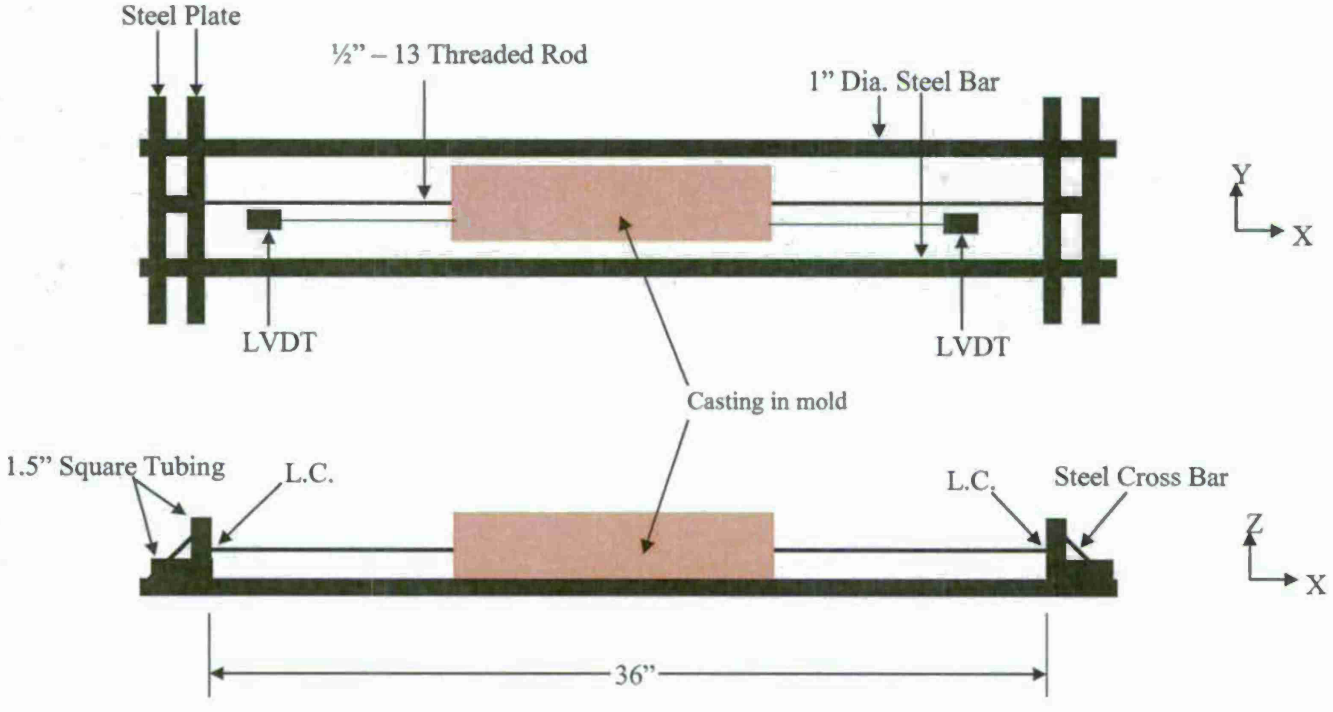

Figure 8 Top and side views of the restrained 12" long x 1" thick x 1" wide bar used in the stress displacement experiments. Locations of thermocouple temperature sensors are same as in Figure 5 and force sensors (load cells, L.C.) and position sensors (LVDT) are indicated.

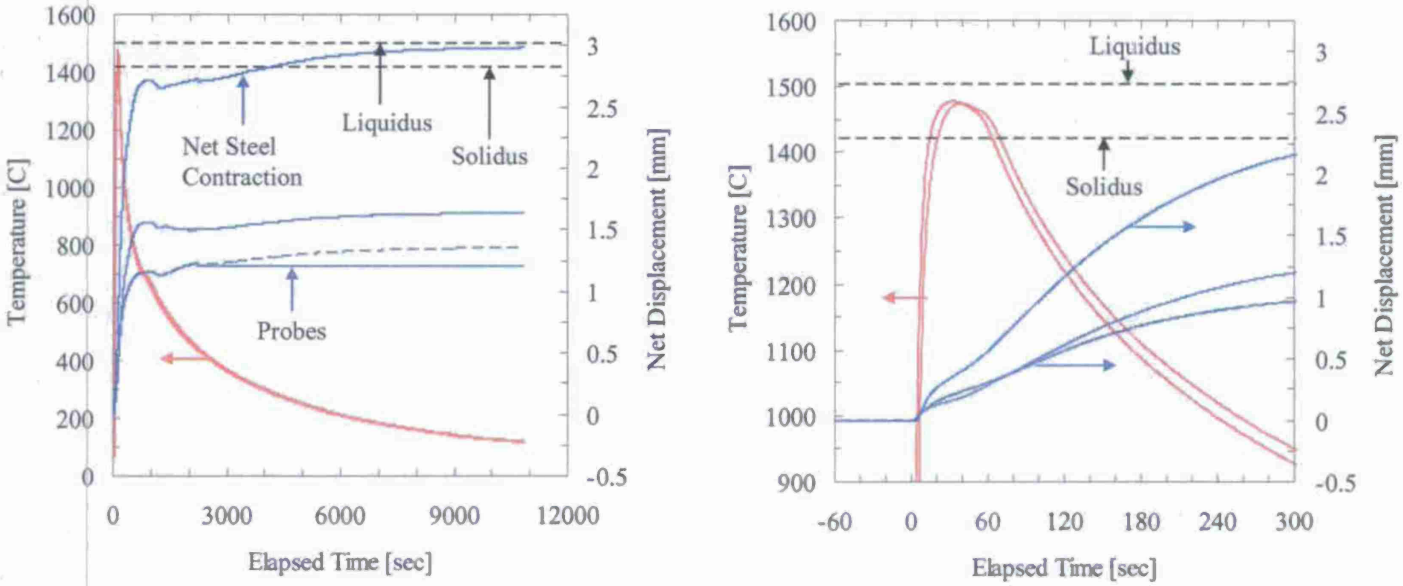

Figure 9 Plots of measured temperature (red lines) and displacement/contraction (blue lines) versus time for the steel in the restrained casting. Temperature scale at right shows high temperature range (from 1200 C to 1500 C). Note how contraction begins to develop at the start of solidification.

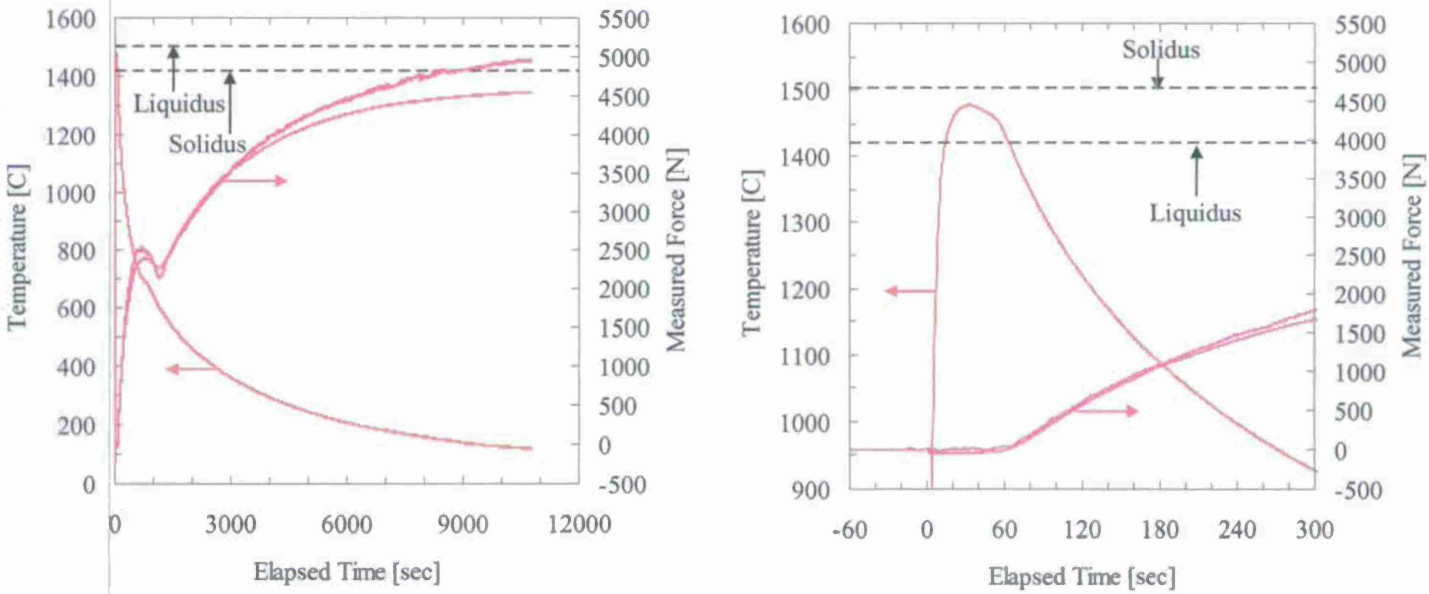

Figure 10 Plots of measured temperature (red line) and force (magenta) versus time for the steel in the restrained casting. Temperature scale at right shows high temperature range (from 1200 C to 1500 C). Note how restraining force begins to develop close to, but not at, the end of solidification.

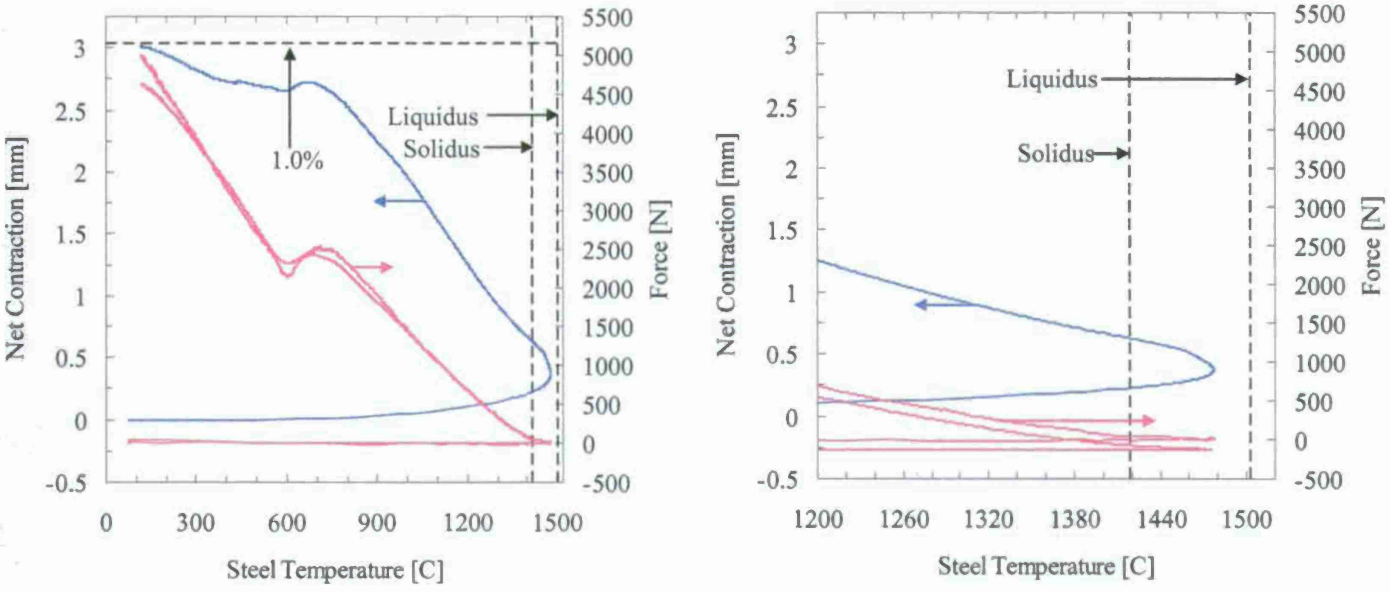

Figure 11 Plots of measured contraction and force versus temperature for the steel in the restrained casting. Temperature scale at right shows high temperature range (from 1200 C to 1500 C).

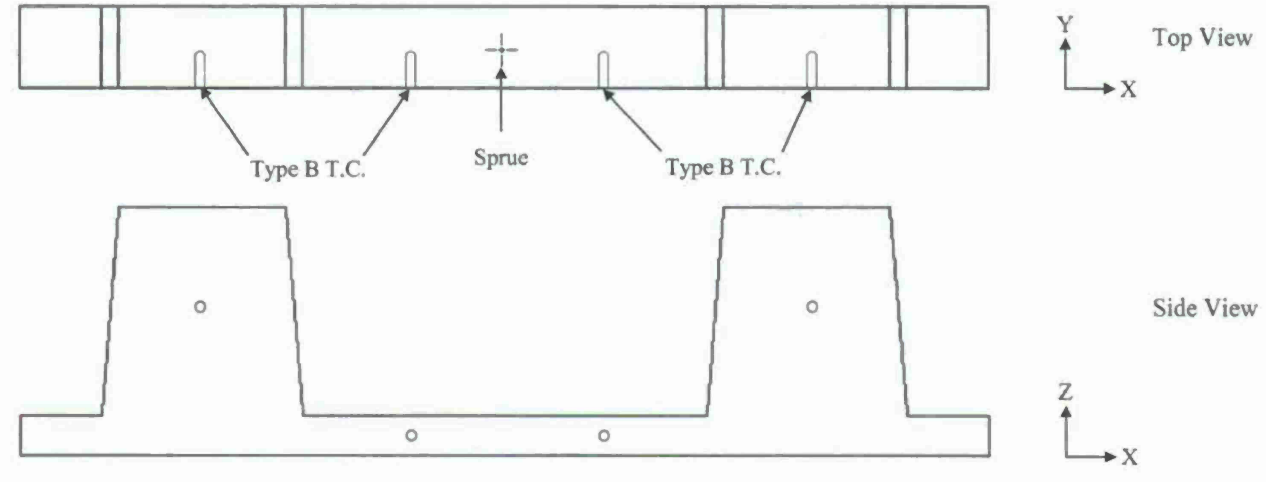

Figure 12 Top and side views of blind riser casting used in the internal/external shrinkage study. Downsprue is not shown. Locations of B-type thermocouples are shown by circles.

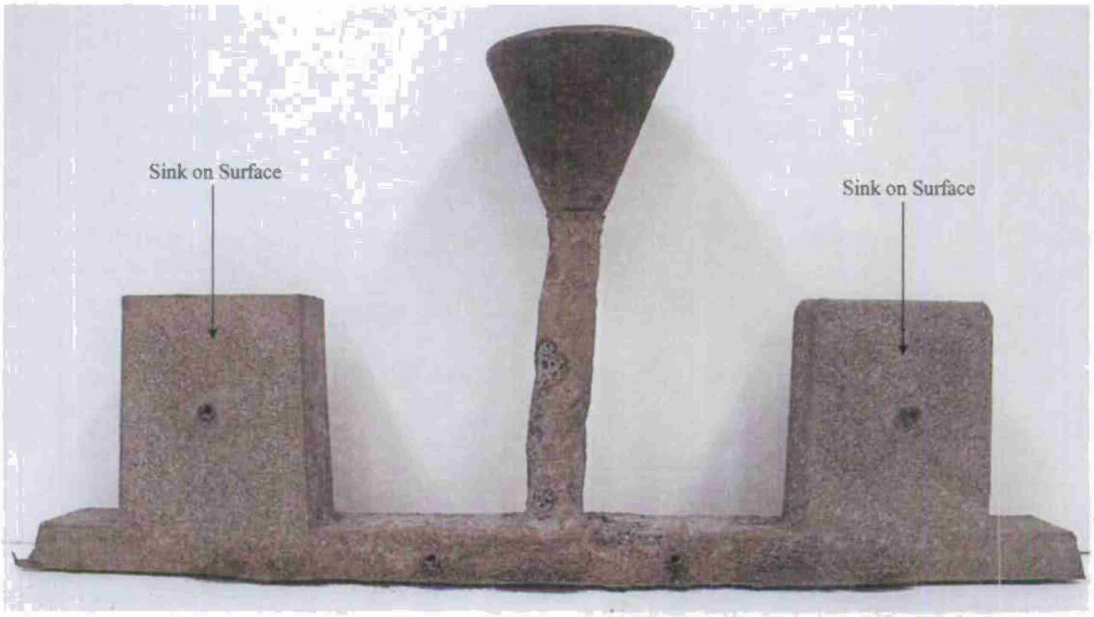

Figure 13 Picture of one of the three (out of four) castings determined to have visible surface sinking. This indicates external shrink. Note the thermocouple locations are seen at the dark round holes.

Dimension Prediction and Demonstration

FAS Muzzle Brake Casting

MAGMAsoft casting simulations and part performance simulations (with and without porosity defects in the part) were performed for the FAS muzzle brake casting. The casting was specified as ASTM A487 Grade 10. This chemistry is very similar to AISI 4330, for which we have developed accurate properties in our lab. So the AISI 4330 property data was used. The pouring conditions for the metal entering the inlet of the downsprue were: inlet temperature 1600 C (2912 F), and fill time 15 seconds. For MAGMAsoft's feeding percentage porosity predictor the feeding effectivity is set to 50%.
MAGMAsoft's shell mold sand properties were used for the shell and dry silica sand for the backing material.

Four porosity prediction methods were applied in the simulations of this casting. Two of these are available in the current commercially released version of MAGMAsoft. A brief description of them is below:

- Niyama Criterion: This is a thermal criterion function defined as the temperature gradient divided by the cooling rate of a computational cell at the end of solidification. It is compared to some critical value below which shrinkage
  porosity occurs. It has units of $(°C\ sec)^{1/2}/(mm)$ in MAGMAsoft. For these units
  and this steel, values below 0.1 should correspond to formation of macroporosity (visible on a cut section with the unaided eye, and possibly on an x-ray) and values of about 0.7 to microporosity (visible only under magnification).

- Feeding Percentage: This porosity predictor is determined from an algorithm where all solidifying metal cells are checked to see if their adjacent cells have reached the critical solid fraction (the feeding effectivity, here 50%) above which no liquid metal can flow through them to feed the shrinkage porosity (arising from the liquid to solid density change). Regions of the casting isolated, and cut off from risers, form feeding zone where porosity can form. In other words, feeding zones form shrinkage if there is no open feed path to the riser. This predictor has been carefully designed to predict riser shrinkage pipes and hot spots well.

In addition to the two porosity predictors discussed above, our lab has advanced modules which we have developed together with MAGMA GMBH. These two additional porosity models available in our lab are:

- Advanced Feeding (AF) Pore Volume: This model predicts porosity from the fundamental physics of pore nucleation and growth arising from the pressure field and flow of liquid in the solidifying metal. The concentration of gas in the liquid metal is a model variable, and hence it can predict both gas and shrinkage porosity. The results presented here were run using no gas, so they reflect solidification shrinkage only.

- Microporosity Predictor: This model predicts microporosity according to a new dimensionless criteria developed in our lab. This criteria can be thought of as a dimensionless "Niyama" Criteria, but it gives an amount of porosity formed rather than a criteria value. The amount of gas in this model is also a variable in this criteria, and it was set to 0 for these results.

Results by the four porosity prediction methods will show that there is microporosity predicted in the casting, and possibly borderline macroporosity. The microporosity at this level may be difficult to detect by NDE. Porosity is predicted at three locations in the casting; there is more than one region of porosity at these locations in the casting as you will see below. Location 1 is on the top ring (in the "collar" at the mid-points between the four risers, location 2 is on the baffle face surfaces opposite the chills, and location 3 is on the centerline of the rings forming the openings of the two baffles. In Figure 1 these three locations can be seen as predicted using the Niyama Criterion, and the porosity at location 1 is predicted to be the worst, and might be detectable by radiography. The regions at location 2 (six regions in the part altogether) might be masked by surface conditions, and the porosity at location 3 would have to cut, sectioned and examined under magnification to be seen. The second commercially available porosity predictor in MAGMAsoft, the Feeding Percentage, predicted no porosity in the casting, only in the riser and gating

as seen in Figure 2. Here the riser shrinkage pipes look good, and the risers and necks could probably be reduced in size. Note the risers also looked good in Figure 1 using the Niyama Criteria. This demonstrates the limitations of the Feeding Percentage model (no porosity predicted in the casting).

Using the advanced feeding (AF) pore volume, as shown in Figures 3 and 4, porosity is predicted at all three locations and, although not shown here, the AF model also predicts the riser shrinkage pipes. In Figure 3 the horizontal slice through the porosity indications at location 1 (image on the right) clearly show the indications between the four risers. This porosity predicted at location 1 between the upper risers might not be of concern to performance, but it could be eliminated by placing chills between the upper risers. Note the risers are not shown in the image on the left in Figure 3. Figure 4 is provided to show the worse sections of the porosity indications at locations 2 and 3. Again the porosity predicted by the AF model appears to be microporosity, and should not affect the strength, or stiffness, or produce stress redistribution. Though we anticipate it will affect fatigue life. In Figure 5, the Microporosity Percentage predictions are shown at three slices through the casting and they show similar levels of porosity predicted at locations 1, 2 and 3 as was seen in Niyama Criterion and AF. The advanced feeding (AF) results will be mapped into the finite element model and used in the stress analysis and fatigue life predictions.

An advanced inclusion prediction model was also used to simulate the reoxidation inclusions in this casting. These reoxidation inclusions (so called because they form during pouring after the melt is deoxidized) form from the melt reacting with oxygen on the free surface or with entrained air in the melt. This advanced inclusion prediction model is another model we have developing with MAGMAsoft, and is not yet in their commercial package. These results, however, have not been used with performance predictions to predict the effect the inclusions will have on performance. The inclusion model was run to see if it predicts inclusions that might be observed during production. It might also be used to develop a gating system which produces fewer inclusions, if a "cleaner" casting is required. Two results from the inclusion prediction model are typically examined: the size (diameter) of the inclusions and the area fraction of inclusions. Since the inclusion model predicts nucleation, growth and agglomeration of the inclusions (as they collide and combine to form larger inclusions), the inclusion diameter result is useful in visualizing where the largest diameter inclusions end up in a casting. The area fraction can be large if there are many small inclusions or a few large inclusions in a given area, and so it gives the results from a different perspective. The inclusion diameter results for the casting are shown in Figure 6. It is even more useful to look at an animation of the inclusions as they form and grow during the filling process. The largest inclusions appear to be about 7 mm diameter. The cope surface appears to have the most inclusions that larger than 2 mm diameter, and the middle baffle has a number of larger inclusions as well. The lower baffle appears to clean of inclusions larger than about 2mm diameter as seen in the lower right of Figure 6. The area fraction on the cope surface is shown in Figure 7, and this has the most surface area of inclusions. When the inclusion formation during filling is visualized using animations, it was observed that the simultaneous filling of the casting from opposing sides (the two runner rigging system shown in Figure 8, left side) results in inclusions being trapped in the part where the two filling streams meet. In order to test whether this was a primary reason for inclusions appearing in the casting, we simulated filling the casting through one side using one runner (as shown in Figure 8 right side image). This allows the inclusions to flow out of the part into the riser on the other side, instead of being trapped in the part. The comparison between area fraction results for the two runner system and the one runner system is shown in Figures 9 and 10 for the cope side surfaces of the middle baffle and collar/top-most surface, respectively. The improvement in using the one runner system is especially noticeable on the middle baffle surface as seen in Figure 9. Figure 10 shows the one runner system to still produce similar inclusion area fraction results on the top of the collar/ring but the improvement on the rest of the cope surface is noticeable. It should be explored if this change is the rigging can be easily made and tested at the foundry.

Performance predictions were made for the FAS muzzle brake using the finite element stress analysis package *ABAQUS* and the fatigue life prediction software *fe-safe*. Note that due to symmetry, only one-quarter of the part is simulated. In ABAQUS, an input deck file for the maximum loading case was provided by Benet Labs, and this was used as the service loading. Therefore a service cycle is defined as "zero load-maximum service load-zero load" step cases. The fatigue is dependent not only on the stress amplitudes in the loading cycle but also on the mean stress (mean stress effects). Therefore, both of these are shown in Figures 11 and 12 for amplitude and mean stress, respectively. Hot spots are observed at the corner near the front baffle, and on the inner ring of the middle baffle as circled in Figure 11. The porosity predicted from the advanced feeding model is imported into the *ABAQUS* stress and *fe-safe* fatigue analyses. The porosity has no effect on stress redistribution in the casting. The stress and

porosity fields are then used in the *fe-safe* fatigue life predictions using strain life fatigue data that is locally dependent on the porosity field (shown previously in Figures 3 and 4). Using sound strain life fatigue properties, the lowest fatigue life is predicted to be on the order of 10^8 cycles at the two stress hotspot locations. Since fatigue properties are measured by defining a run-out test to have occurred at 5 million cycles, this prediction is an infinite life prediction for the sound muzzle brake simulations. Considering the effect of porosity on the fatigue life predictions, the smallest predicted life (where crack initiation "failure" would occur) is reduced to the 10^5 to 10^6 cycle range. Assuming that this maximum loading would occur once per system firing, the predicted fatigue life (100,000 firings) might still be greater than the design number of firings for the brake.

Effect of Sand Core Expansion on Shrinkage of Steel Castings

In order to improve our predictions for casting deformation and defects such as hot tears we have been conducting experiments to measure the properties and interactions between sand molds, cores and steel castings. To determine the effect of sand core expansion on the shrinkage of steel castings, the casting experiment shown in Figure 15 was developed and was run during the past project quarter. Top and front views of the LVDT position probes and thermocouple locations (type B in the casting and type K in the core) are shown in Figure 15 (a) and (b), respectively. The casting geometry is shown in Figure 15 (c); it is a 5" diameter by 4" tall cylinder with a 2" diameter cored out center. Four of the experiments were cast at the University of Northern Iowa Metal Casting Center at the end of August. The metal cast was ASTM A216 grade WCB steel. The mold was made from IL5W silica lake sand and the mold binder was a bio-urethane no-bake. The core was made from 520 washed silica lake sand and the core binder was PUNB at 1.25% by weight with 60:40 Ratio of Part 1 to Part 2 and 8% catalyst. In addition to the four experiments, an additional test casting was poured to determine liquidus temperature of steel in the cylinder #4 casting. Unfortunately, the first casting, cylinder #1, did not completely fill, but we did get good experimental data for on cylinders #2, #3, and #4.

The measured and simulated temperature at the cylinder and core thermocouple locations in cylinder #4 are shown in Figures 16 and 17 for the entire experiment duration and during solidification period, respectively. The cooling rate during solidification is useful in determining the liquidus and solidus temperatures, the measured and simulated cooling rates are shown in Figure 17 using the right hand ordinate axis scale. Note how the maximum inflection point in the cooling rate is used to determine the solidus temperature. The good agreement between measurement and simulation resulted after some small adjustments to property data, solid fraction-temperature curve and boundary conditions.

In Figure 18 the sign convention used in plotting the displacement data on the inner and outer diameters of the casting as measured by quartz rod attached LVDTs is shown. When the outer surfaces contract inward the sign is taken as positive, and when the inner surface moves toward the center the sign is taken as positive. In Figure 19 (a) displacements for the four LVDT sensors versus experiment time to 16,000 seconds (about 4.4 hours) is shown, and in Figure 19 (b) displacements are shown on a time scale up to 2,500 seconds. Note the core expansion effect responsible for negative displacements on the inner surface stops at the end of solidification at about 500 seconds in Figure 19 (b), at which point the displacements change direction on the inner surface. The displacement-temperature plot is given in Figure 20 for cylinder #4. Note the behavior seen at the solid state transformation temperature at about 680°C. Work will continue on the analysis and simulation of the experimental casting during the next quarter. In particular, simulations will be run for cylinders #2 and #3, and additional experiments will be performed to obtain reproducible results.

Measurement of Displacement and Active Forces in Casting a 12x1x1 inch Bar

As described in last quarter's report, we have also been performing experiments to provide data for validating models of displacement (contraction) and stresses (forces) during and after solidification. Last quarter one of these experiments was an in-situ experiment with a 12" long x 1" thick x 1" wide bar with free (unrestrained) and restrained ends similar to that shown in Figure 21. During this quarter, however, the experimental setup was further developed to measure displacements and forces on the 12x1x1 inch steel bar casting in which a load is actively applied to one restrained end (left end in Figure 21) using a turnbuckle. The opposite end is fixed as shown in Figure 21 (right end). Plots of measured temperature (green and blue lines) and contraction versus time for the experiment using the restrained case with actively applied load (dark blue line) and for the unrestrained casting (magenta line) are shown in Figure 22. Unfortunately, as you can see from the data we did not get data for the liquidus temperature during this experiment because of the slow thermocouple response. Notice the turnbuckle is applied from about 100 to 390 seconds. The stress development before, during and after applying the load via the turnbuckle can be seen in Figure 23. Note how a low level of stress begins to develop during solidification, and then when the turnbuckle is first applied (about 1370°C) the stress level steps up. The load is slowly increased until the is a drop near the end of solidification, after which point the steel has more load bearing capability, and the stress level is stepped up over time to about 10 MPa.

During the next quarter, we will continue working on this experiment and analyzing the data. We also hope to begin to simulate the experiment with the applied load case to compare with the measurements.

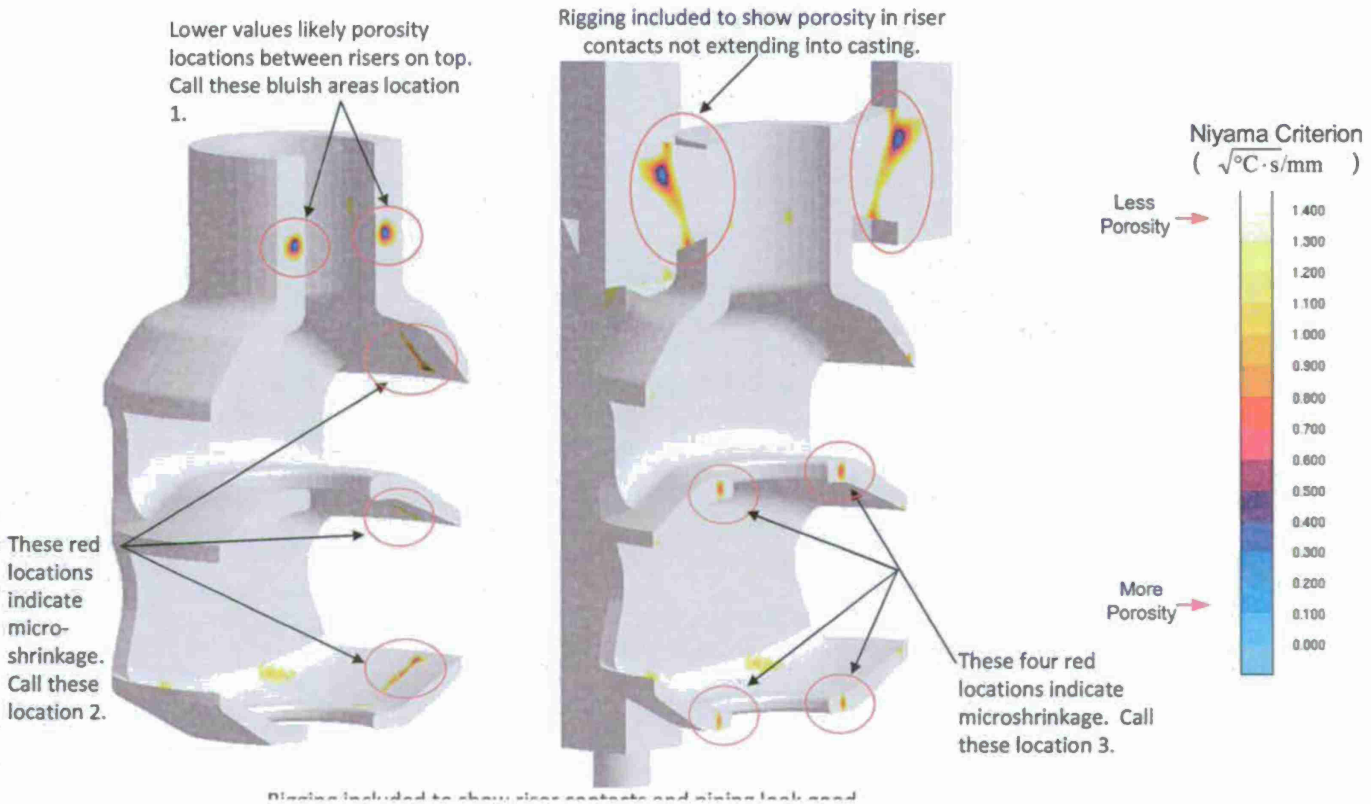

Figure 1 Casting simulation results for Niyama Criterion in two slices across the casting. Note locations 1, 2 and 3 where porosity is predicted. Location 1 should be worse than locations 2 and 3.

Figure 2 Feeding Porosity predictions in center slices across the casting and risers to show riser pipes. Casting had no shrinkage indications by this predictor.

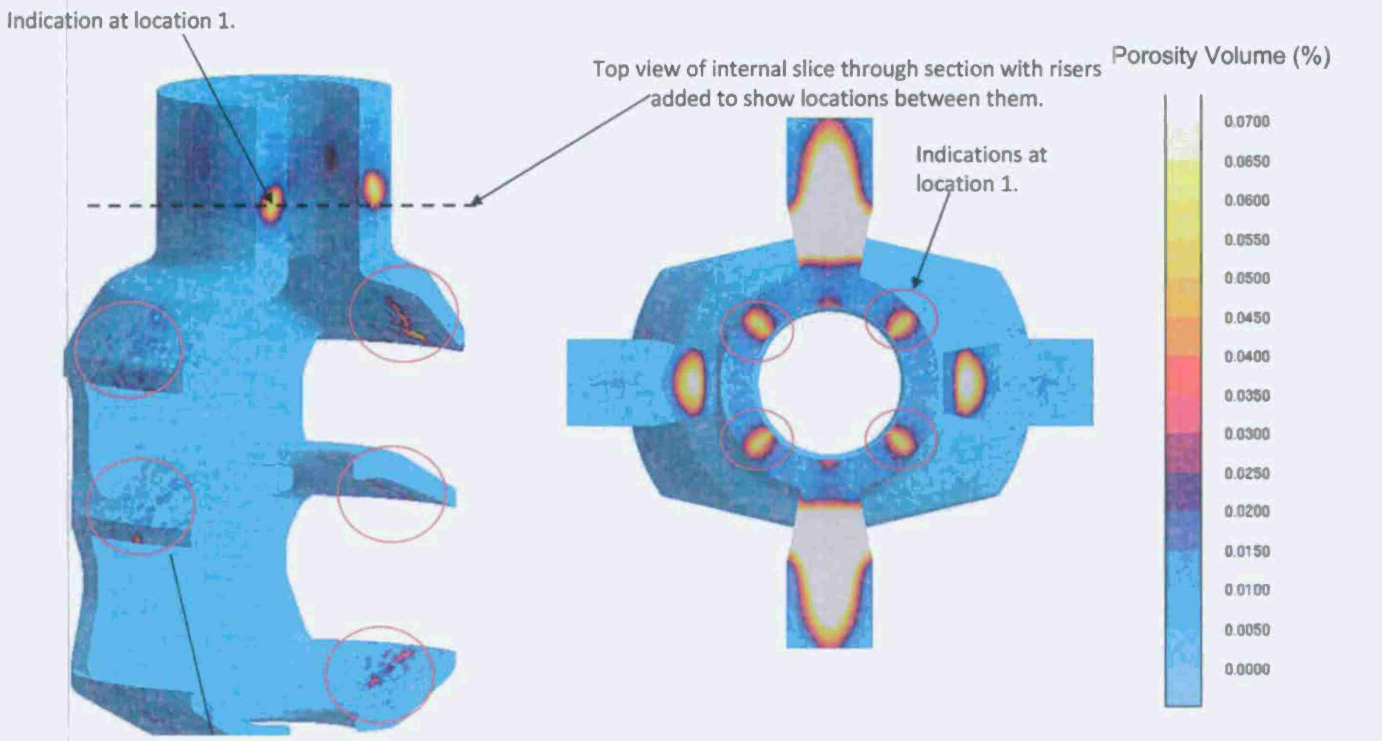

Figure 3 Casting simulation results: Advanced Feeding (AF) - Porosity Volume %, predictions show worst porosity predicted at location 1. Porosity at location 2 is nearly same level, but smaller area.

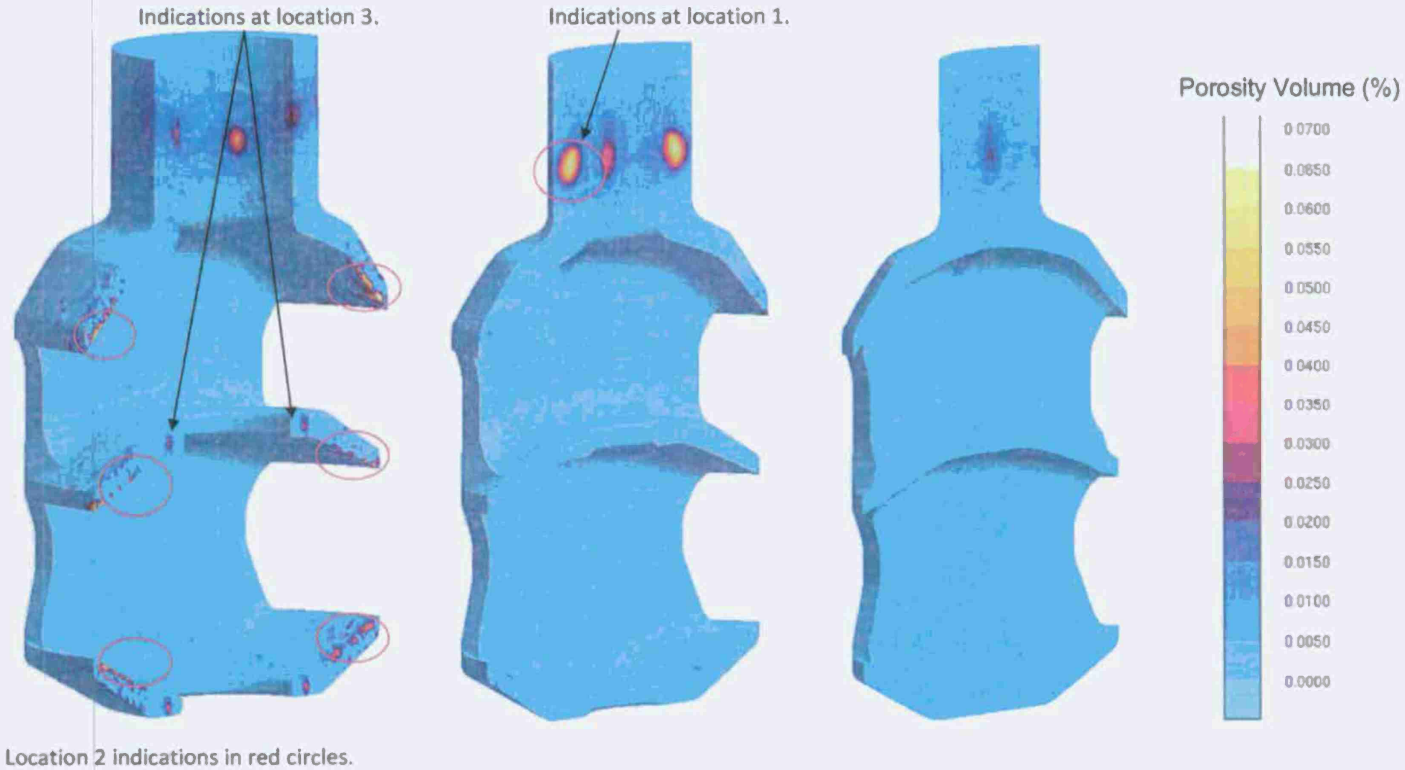

Figure 4 AF porosity predictions in three slices across the casting showing the indications at locations 1, 2 and 3.

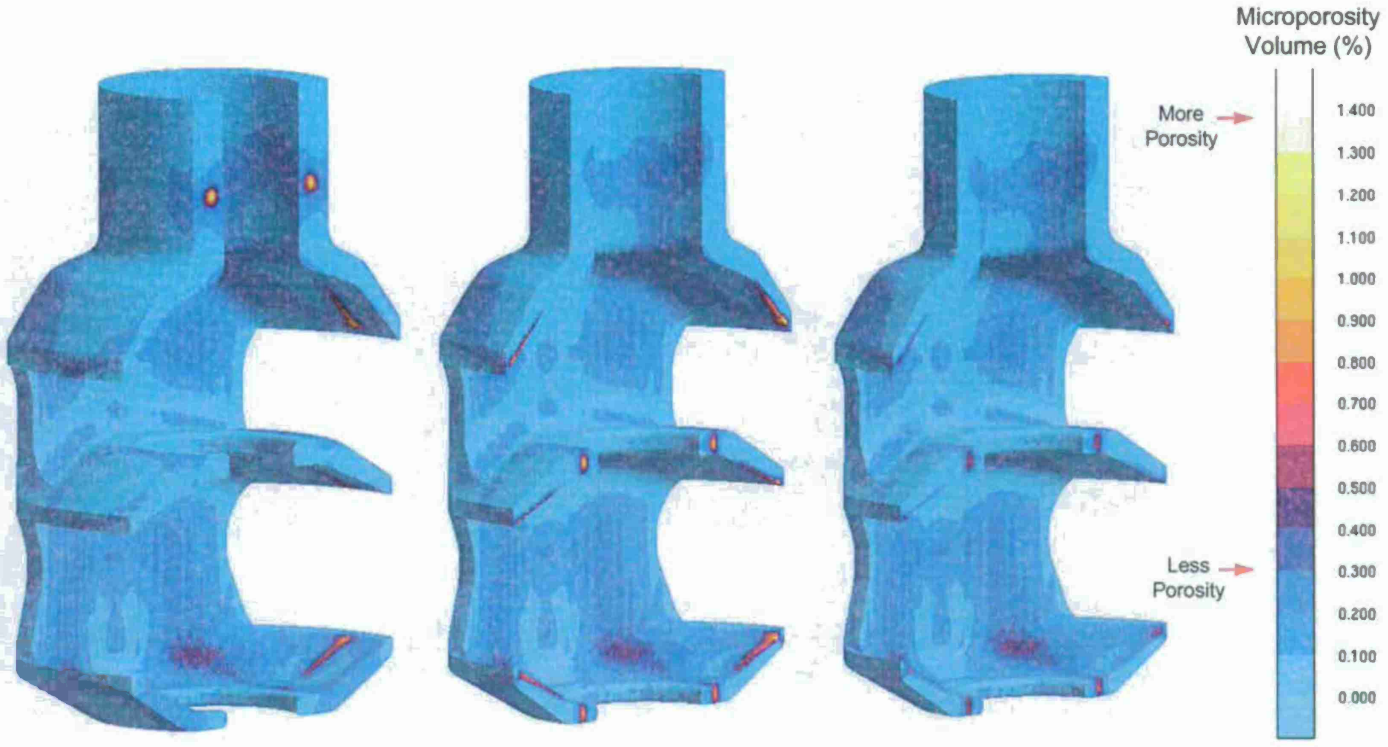

Figure 5 Casting simulation results: Microporosity % predictions at three slices through the casting showing similar level of porosity predicted at locations 1, 2 and 3.

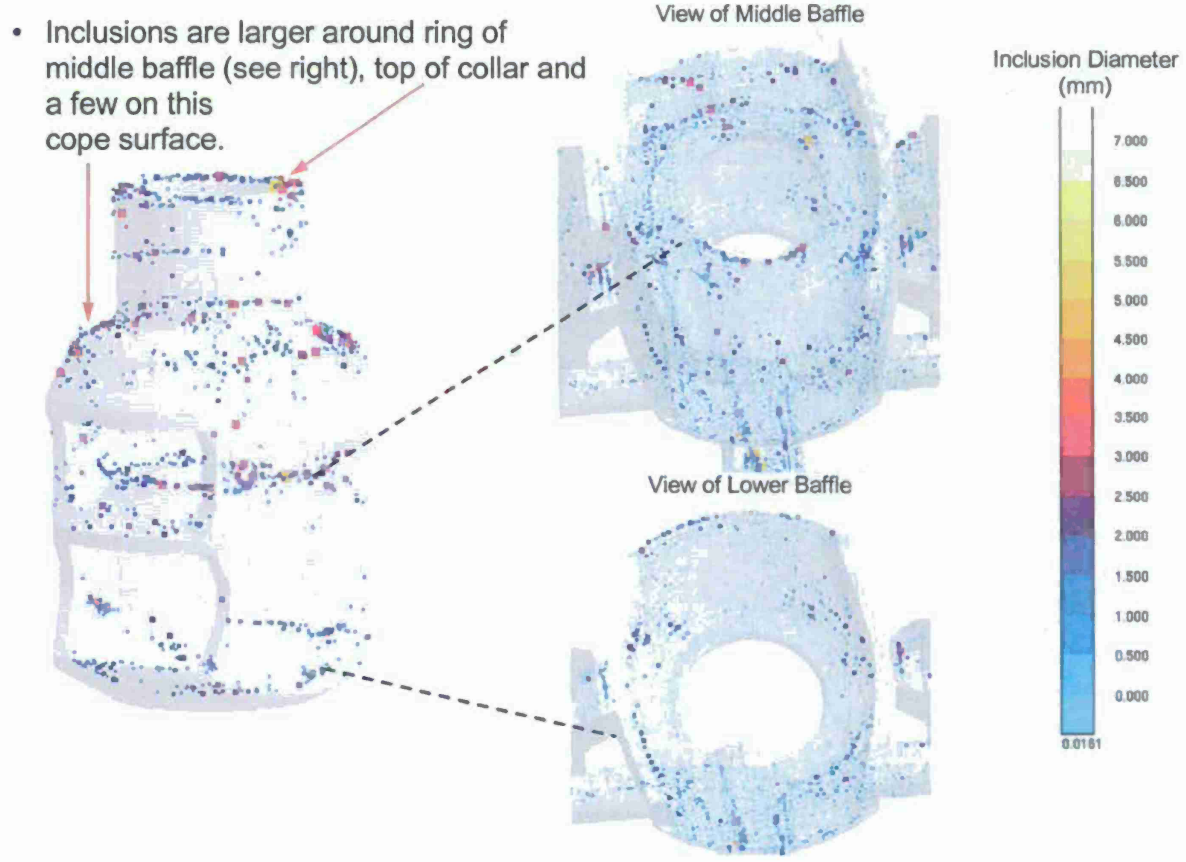

Figure 6 Casting simulation results for reoxidation inclusions diameter prediction.

Figure 7 Casting simulation results for reoxidation inclusions area fraction prediction.

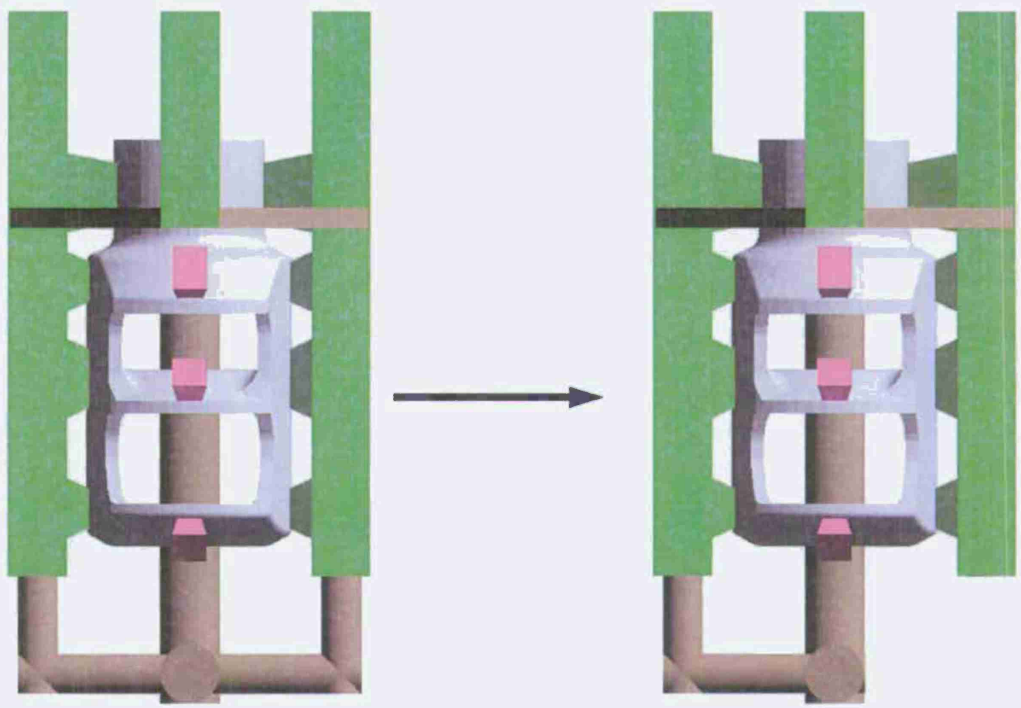

Figure 8 Images showing concept of filling through runner on one side (at right above) rather than two (above left). This allows the inclusions to flow out of the part into the riser on the other side, instead of being trapped in the part where the two filling streams meet.

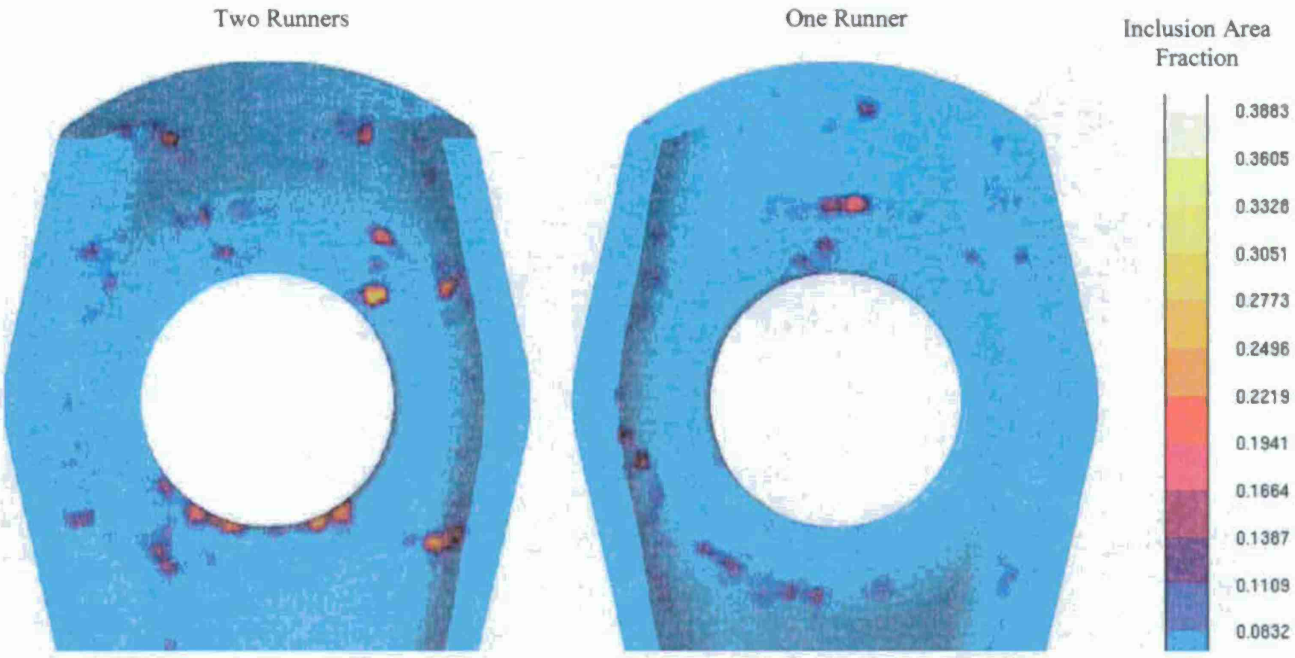

Figure 9 Results for reoxidation inclusion area fraction prediction on the cope surface of the middle baffle for the two filling runners (above left), and one filling runner (above right).

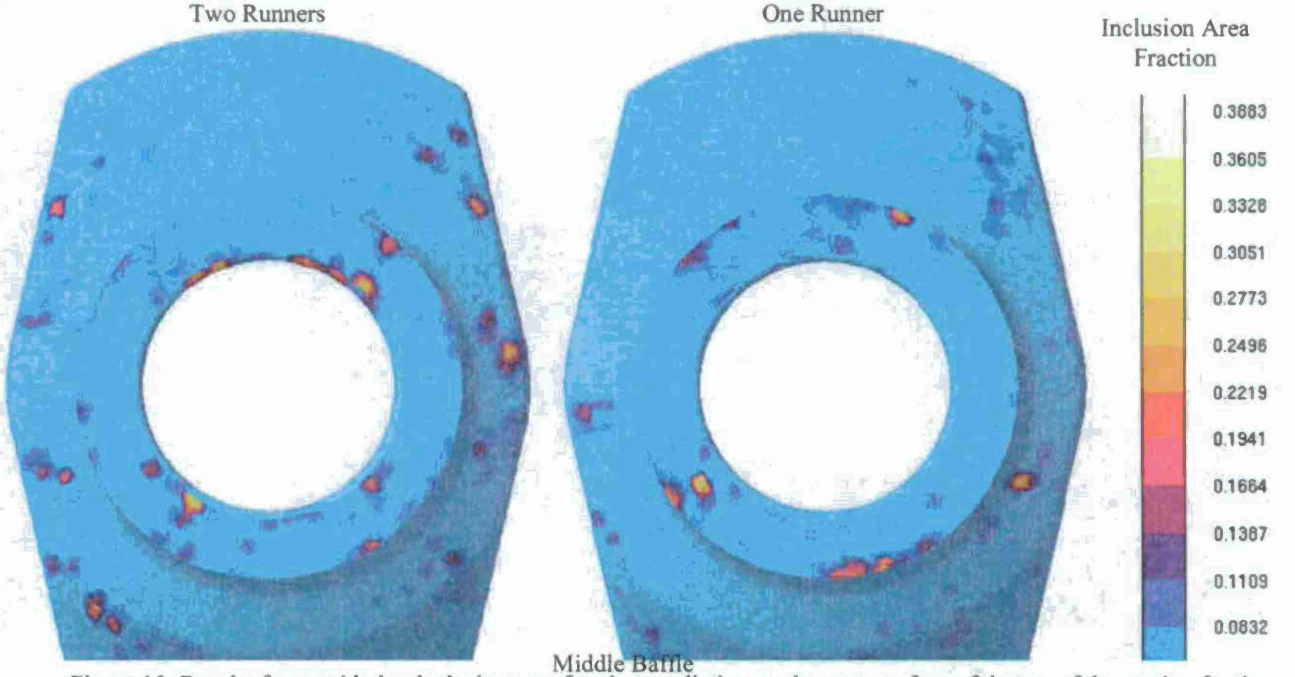

Figure 10 Results for reoxidation inclusion area fraction prediction on the cope surface of the top of the casting for the two filling runners (above left), and one filling runner (above right).

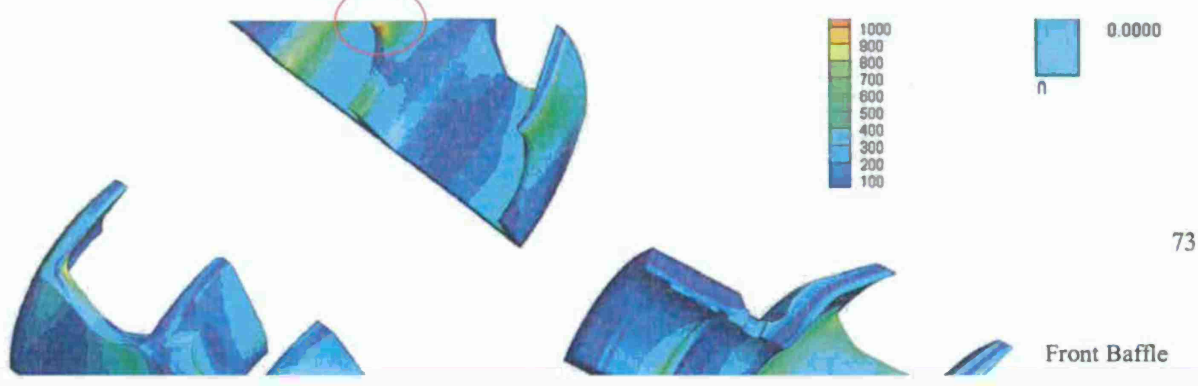

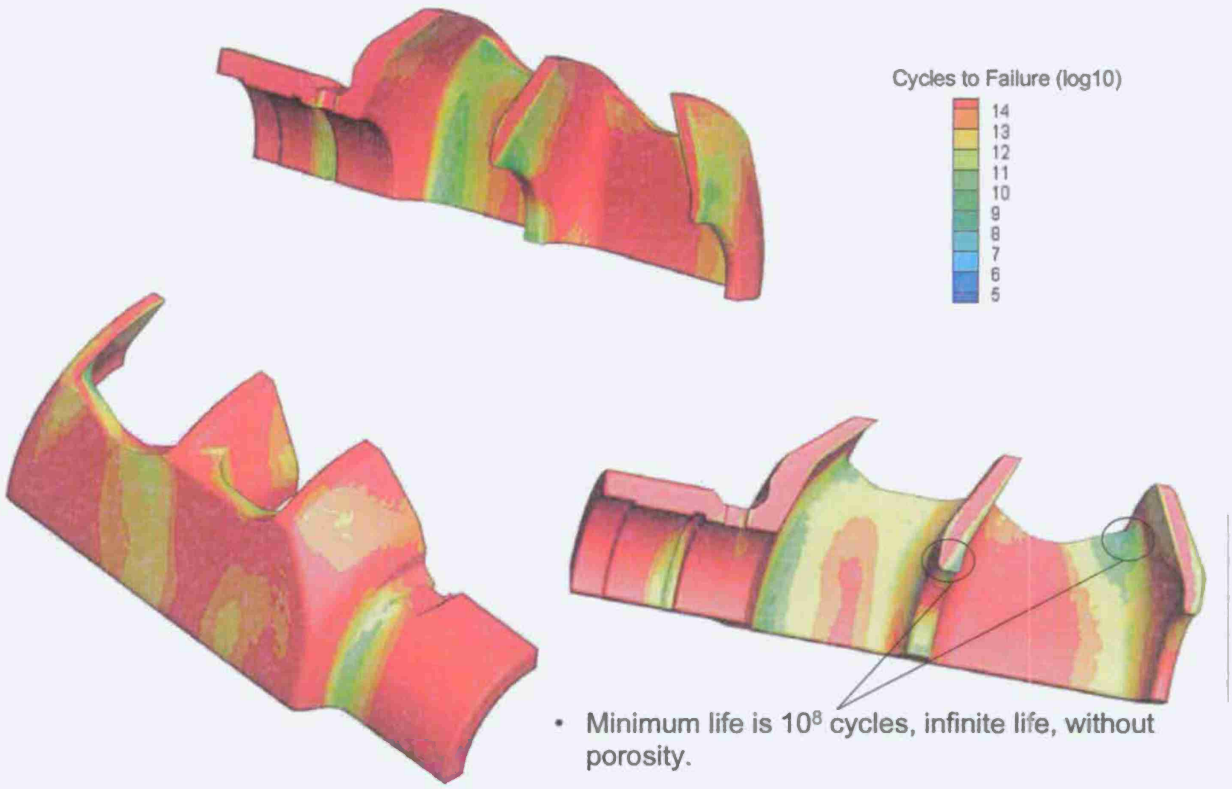

Figure 13 Cycles to failure for sound casting, no porosity field used in the analysis.

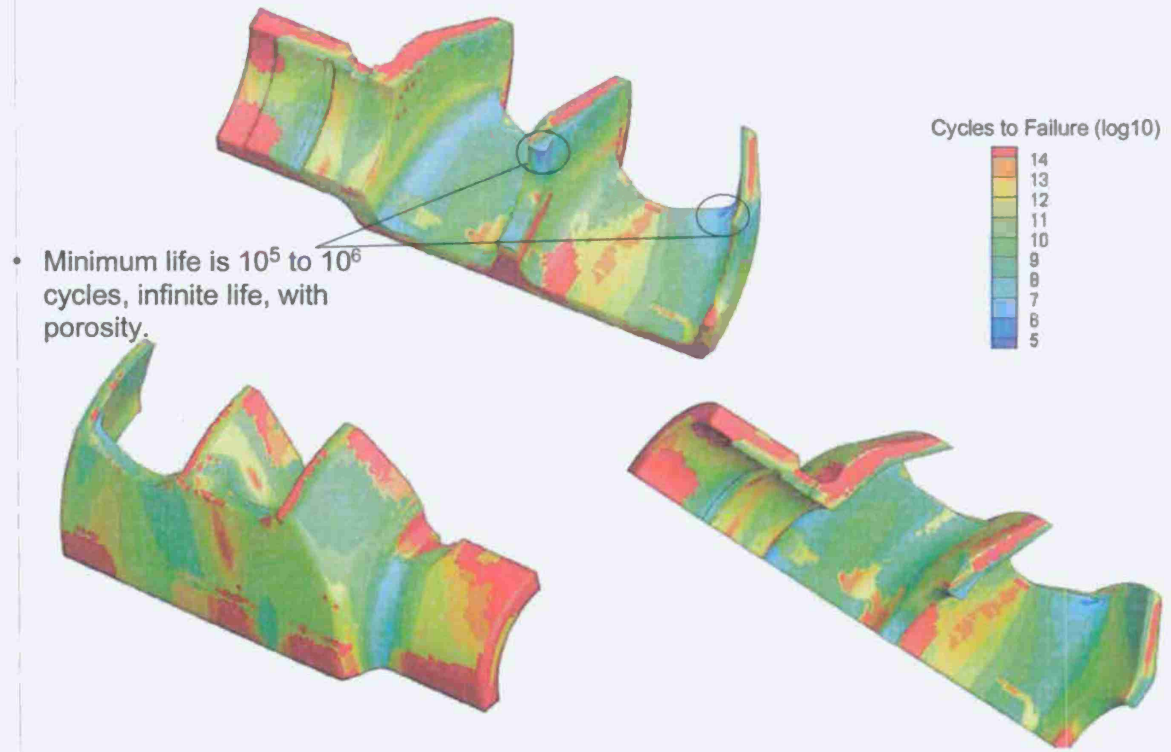

Figure 14 Cycles to failure for sound casting, no porosity field used in the analysis.

Figure 15 Schematic of (a) top view and (b) side view of cylindrical cored casting with locations of thermocouples and LVDT probes. (c) Rendering and dimension of cored casting

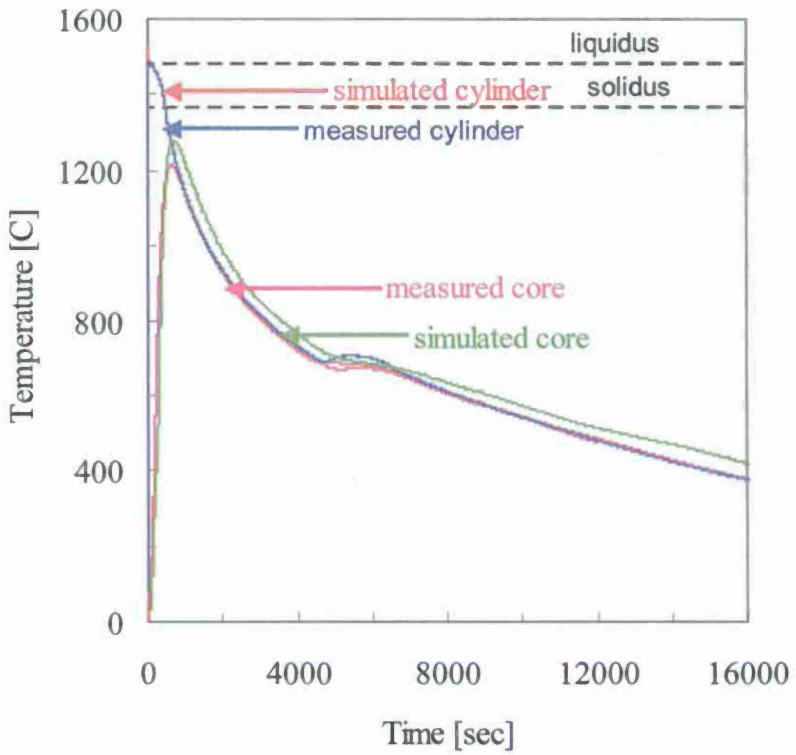

Figure 16 Measured and simulated temperatures versus time in the core center and the casting. Time scale to 16,000 seconds (about 4.4 hours).

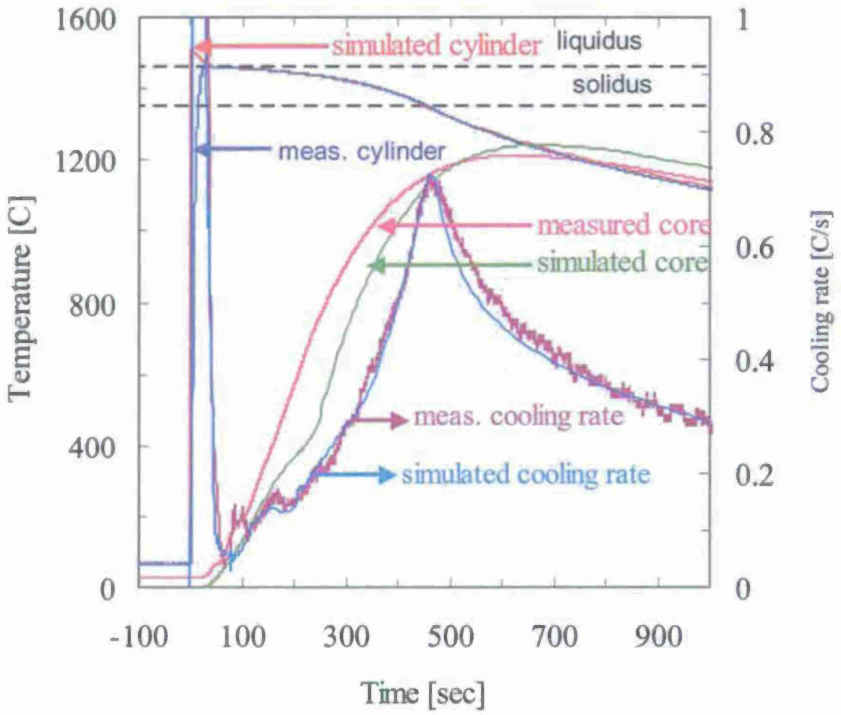

Figure 17 Measured tion. Time scale

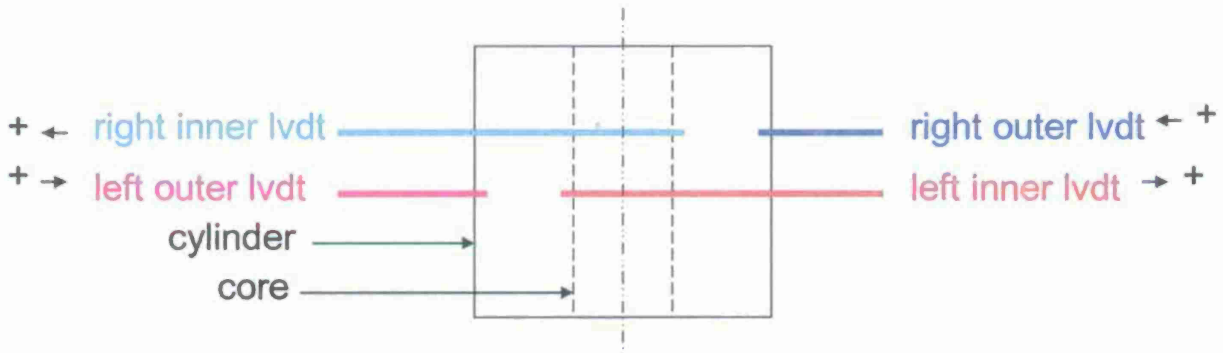

Figure 18 Sign convention used in reporting the LVTD displacements on the inner and outer diameters of the casting.

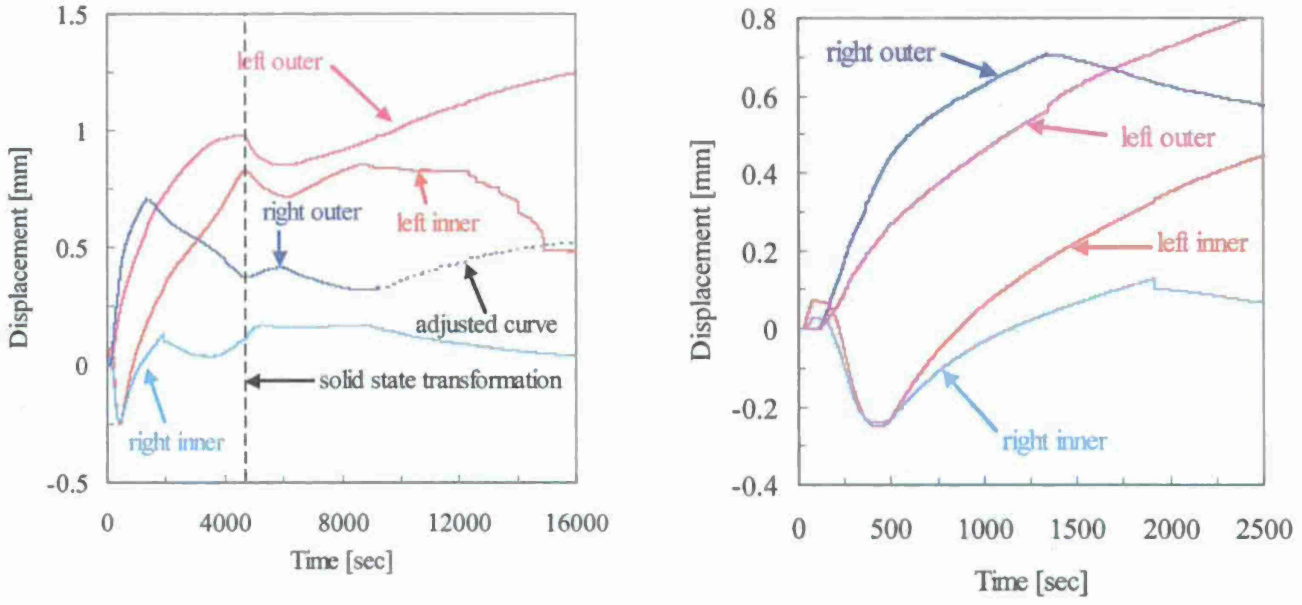

Figure 19 Measured displacements for the four LVDT sensors versus experiment time for (a) time scale to 16,000 seconds (about 4.4 hours), and (b) time scale to 2,500 seconds. Core expansion effect responsible for negative displacements ends at end of solidification at about 500 seconds.

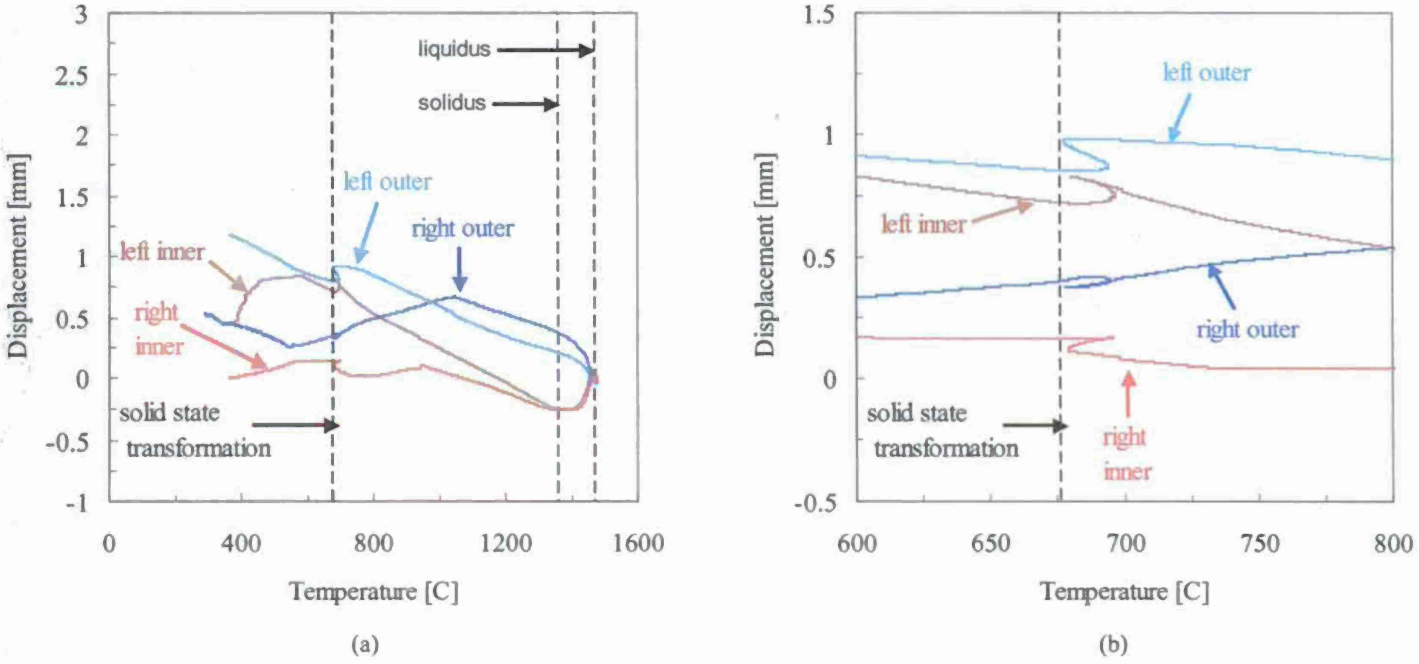

Figure 20 Measured displacements for the four LVDT sensors versus temperature for (a) full range of measured temperatures, and (b) temperature range for the solid state phase transformation.

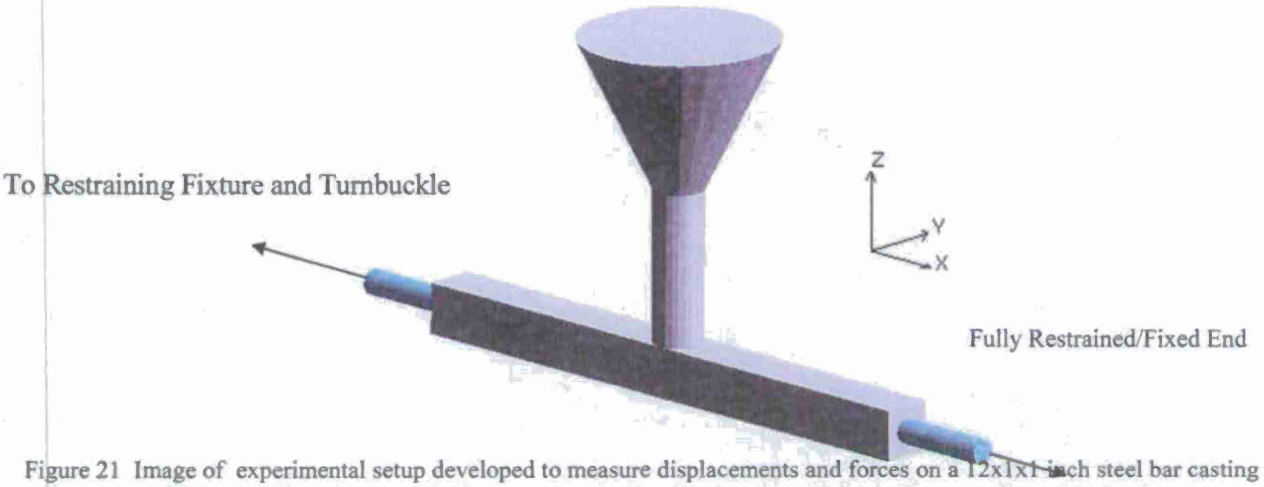

Figure 21 Image of experimental setup developed to measure displacements and forces on a 12x1x1-inch steel bar casting in which a load is actively applied to one restrained end using a turnbuckle. The opposite end is fixed.

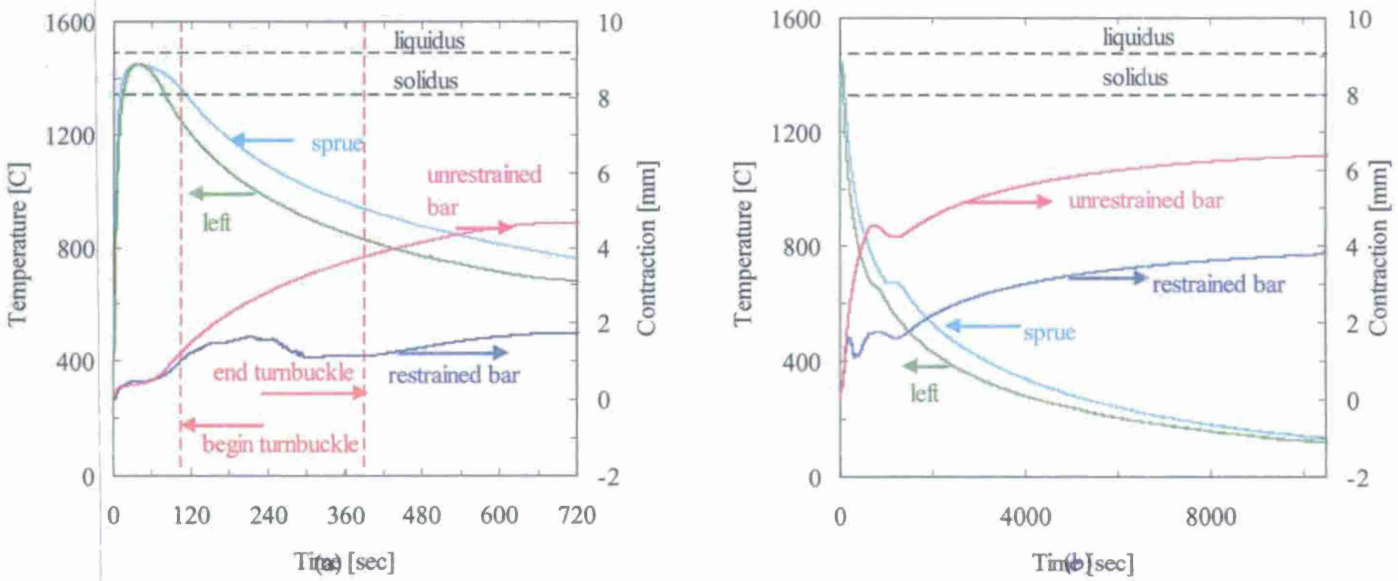

Figure 22 Measured temperatures and contraction versus experiment time for (a) time scale focusing on solidification and application of force, and (b) time scale to end of experiment.

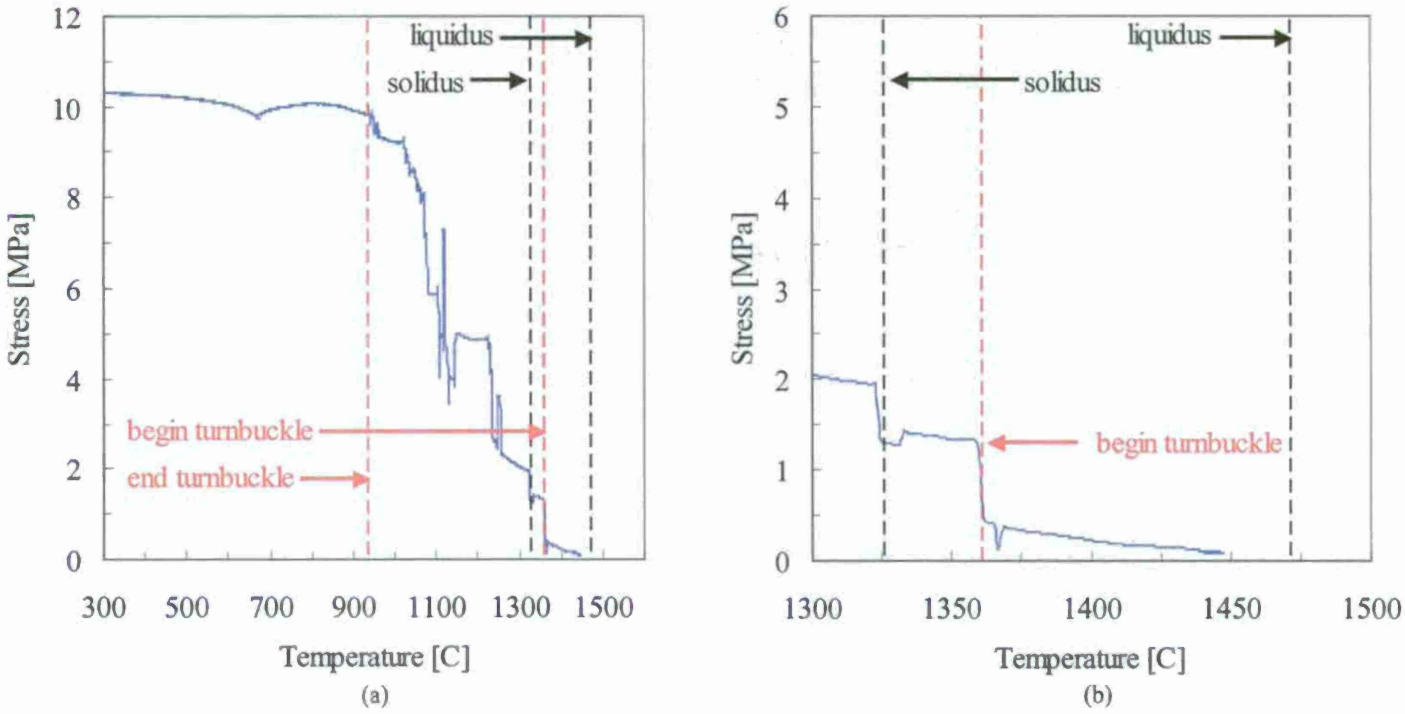

Figure 23 Measured stress versus temperature for (a) entire experimental temperature range, and (b) temperature range focusing on solidification.

Rotor Casting Simulation Deployment

Since the XM360E1 cradle rotor casting component is not currently in production, MAGMAsoft casting simulations were performed to develop a rigging/casting solution for the cradle rotor casting. This rigging would then be simulated using several methods to predict porosity, and the worst porosity predicted would be used to simulate the effect of porosity on casting performance.

It was determined in discussions with SFSA and Benet Labs that an alloy with yield strength greater than 100 ksi should be selected for the part. It was decided that an AISI 41XX alloy would fit this application, and an alloy such as AISI 4130 should be selected. Since our laboratory has a dataset for 4135 that we have confidence in using, this alloy and dataset in MAGMAsoft was used. The thermo-physical and solidification properties used for this alloy are given in Tables 1 through 3. After approximately ten iterations, we arrived at a rigging that produced a casting which should have good soundness, and fills smoothly, which should reduce reoxidation inclusions. This rigging is shown in Figures 1 and 2. The cast component weight is 902 lb (409 kg) and the rigging weighs 644 lb (292 kg), which gives a casting yield of 58%. In our view the yield is satisfactory, but could probably be increased. One area where the rigging might be improved further is reducing the contact area, which for gating and feeders is 175 in^2 (1,132 cm^2). Contact area effects the cleaning costs for the part. As shown in Figure 1, riser sleeves were used; this was found to be necessary to produce a sound casting in the simulations. Chills were added as seen in Figure 1 to reduce predicted indications of porosity between the two risers. These indications would probably not have been of concern to part performance, but were removed using the chills in this preliminary rigging. The round (tile) gating used has a 2" diameter, and the ingates fill the part from the bottom to reduce splashing and inclusions. Figure 2 is provided to give four directional views of the rigging.

Additional conditions for the casting simulation are:

- Casting simulated using our property dataset for AISI 4135, and mold is furan.
- Pouring conditions: inlet temperature 1600 C (2900 F), fill time 40 seconds based on estimated pouring weight.
- Feeding effectivity set to 50% in MAGMAsoft feeding percentage (%) porosity predictions.

Casting simulation results for solidification progression, and porosity by three methods are presented in this report. The three methods of porosity prediction are feeding%, advanced feeding and microporosity. A brief description of these predictive results is given below:

- Feeding Percentage: Determines regions of the casting isolated or cut off from risers that feed shrinkage forming feeding/porosity zones. Feeding zones form shrinkage if there is no open feed path to the riser. Can predict riser shrinkage pipe and hot spots well. Determined by the feeding effectivity (here set to 50%), which can be made more or less conservative by decreasing or increasing it, respectively.

- Advanced Feeding Pore Volume: predicts porosity from the fundamental physics of pore nucleation and growth from the pressure field and flow of liquid in the solidifying metal. Predicts gas and shrinkage porosity.

- Microporosity Predictor: predicts microporosity from a dimensionless thermal criteria developed in our lab. It is very sensitive and predicts quantitative low levels of porosity.

In Figure 3, the progress of solidification in x-ray views of solid fraction is shown from near the start (a) to near the end (e) of solidification. Note the risers are seen to solidify last, and the riser sleeves were found to be necessary for this. The chills assist in freezing the side wall back toward the risers as seen in Figure 3 (b) and (c). The thicker sections appear to be well fed by the risers as seen in Figures 3 (d) and (e).

The feeding percentage predictions of porosity are shown first in Figure 4. Note that the riser shrinkage pipes appear good and have a very conservative safety margin. This indicates the riser size could be reduced. There is an area of feeding% shrinkage (blue) predicted in the part by this method, noted in Figure 5, where only the casting is shown. Given that this method is empirical (depending upon the "feeding effectivity" discussed earlier), increasing the feeding effectivity would cause the indication seen here to disappear. One can determine the relative effects of changing the rigging by keeping the feeding effectivity value and changing the rigging until the indications no longer appear. In this case, Figure 6 shows a modified rigging which gave no feeding indications in the casting for the 50% feeding effectivity. As seen in the changed rigging in Figure 6 (a) the riser contact was extended downward approximately 2 inches, and the feeding indications did not appear (see Figure 6 (b)). If extending the riser downward is acceptable, this modification to the rigging could be made. However, since neither of the other two methods of porosity prediction indicates a problem at this location, in our experience this feeding indication might be a false prediction. Situations like this have led us to develop less empirical and more physics-based methods of porosity prediction.

The advanced feeding prediction method is physics-based, and these results are shown in Figure 7. In the section shown in Figure 7 (a), there is no porosity prediction at the location seen previously in the feeding% results. The riser shrinkage pipes predicted by this method appear similar to those seen in Figure 4, and also appear to be conservatively sized. The only location where porosity is predicted in the part by this method is shown in Figure 7 (b), and is in the side walls. However, it is a very low level of porosity, and appears to be at most about 0.04%. Note that this porosity appears in both side walls and is symmetric.

The casting simulation results for the microporosity predictor are shown in Figure 8. This method gives the largest amount of porosity predicted in the side walls. The outside of the side wall surface is seen in Figure 8 (a), the interior in Figure 8 (b), and the inside wall in Figure 8 (c). There is no porosity predicted at the location seen in Figure 4 in the feeding% results. The level of the porosity is again very low, around 0.4% maximum. Note that Figure 8 (d) shows the casting only. Porosity predicted by this method is the largest, and covers the most volume of the part. Because of this it was decided to use the microporosity prediction when simulating the effect of the porosity on performance.

The main effect of the microporosity will be a reduction in fatigue life. There is no discernable effect on elastic modulus or yield strength for this low level of porosity. A fatigue notch factor is determined from the porosity field for amounts greater than 0.1% according to our methodology. The mapped fatigue notch factor is shown in Figure 9. This fatigue notch factor will be used when we predict the fatigue life, and will reduce the life relative to sound material when the factor is greater than 1.

The porosity is also mapped to the finite element mesh, and is used to locally reduce the elastic properties in the finite element analysis (fea), but the porosity is at such a low level that it has no visible effect on the stress field from the fea. The fea was performed using a load case prepared for us by Benet Labs. The Von Mises stress results from the ABAQUS input case provided by Benet Labs with elastic modulus dependent on porosity is shown in Figure 10. The maximum principal stress for this case is shown in Figure 11. The maximum stresses occur at the corner of the guide slot circled in Figures 10 and 11. Note these stresses are less than $1/3^{rd}$ of yield stress if a steel of 100 ksi yield stress were used.

The stress results from the load case are imported into the *fe-safe* software to predict fatigue life with and without considering the porosity in the casting. A zero load case is used for the start and end of a fatigue cycle, with the peak of the load case stresses used for the cycle peak. Fatigue strain-life properties from the *fe-safe* software database were used for the sound steel properties. Then, for the porosity, the strain-life properties were reduced locally at the fea nodes according to the solution to the Neuber notch and strain-life equations for the fatigue notch factor given by the amount of porosity at the fea nodes. The material properties used in the *fe-safe* analysis were for SAE 4130 steel. These static, cyclic and strain and strain life properties are given below:

Elastic Modulus = 220640 (MPa)
Poisson_Ratio: Poisson's ratio = 0.33
Ultimate_Strength: Ultimate Tensile Strength (MPa or N/mm^2) = 896.4

K_prime: Cyclic Strength Coefficient (MPa) = 1428.0
N_prime: Cyclic strain hardening Exponent = 0.149
Sigma_prime: Fatigue Strength Coefficient (MPa) = 1315.0
B_exponent: Fatigue Strength Exponent = -0.082
Epsilon_prime: Fatigue Ductility Coefficient (MPa) = 1.007
C_exponent: Fatigue Ductility Exponent = -0.651

The predicted fatigue life without and with the porosity field used in the calculations are given in Figure 12, where runout fatigue life is predicted throughout the part without porosity. With porosity, a small hot spot of fatigue life below 1 million cycles is seen at the location of the guide slides (circled). Even though this life is reduced due to porosity, it is on the order of 10^5 cycles, and it greatly exceeds the desired design life which is on the order of 10^4 cycles. The part performance does not appear to be adversely affected by the microporosity predicted in the casting process. Another means the *fe-safe* software uses to visualize fatigue life and part performance is its factor of strength (FOS) calculations. This FOS is the scaling factor applied to the local stresses at an fea node that gives the design fatigue life, in our case set to 5 million cycles. The lower the FOS is, the worse it is, and below 1 means life < 5 million cycles. The FOS is plotted in Figure 13 for the part without and with porosity considered in the calculations. The smallest FOS of 0.6 is seen with porosity, just at the corner of the guide slide. Note this could be a singularity point in the fea, and not realistic. In the neighborhood of this point the FOS is about 1.5. Generally, if just one node gives values dramatically different than the surrounding nodes, the fea results at the node are suspect due to mesh effects and computation issues. Note in Figure 14, for the case with porosity, there are some additional lowered FOS calculations around the support bosses, but these are in the 1.5 range which would still signify a runout condition.

Our conclusion for this quarter's work on the cradle rotor casting is that the part can be cast with good soundness, and only microporosity appears in the predictions for our rigging. This porosity will affect high cycle fatigue life, but this is probably not of concern for this application, where a life on the order of 10,000 firings is a more appropriate performance goal.

Table 1 General solidification parameters used in casting simulations.

Material: AISI4135

General Parameters

Material type:	Steel	
Solidus temperature	1393.00	°C
Liquidus temperature	1496.00	°C
Initial temperature	1600.00	°C
Latent heat	248.0000	kJ/kg
Solidification morphology:	Short Freezing Range	
Feeding effectivity	50.0000	%
Rheology model:	Newtonian	

Table 2 Thermal conductivity (lambda) used in casting simulations.

Lambda as function of Temperature

Temperature [°C]	Lambda [W/mK]
1.00	44.3000
50.00	44.4000
100.00	44.5000
150.00	44.3000
200.00	43.9000
250.00	43.4000
300.00	42.6000
350.00	41.6000
400.00	40.5000
500.00	37.6000
600.00	33.8000
700.00	26.9380
725.00	26.0690
750.00	25.8290
775.00	26.0520
800.00	26.2760
900.00	27.1720
1000.00	28.0710
1100.00	28.9710
1200.00	29.8740

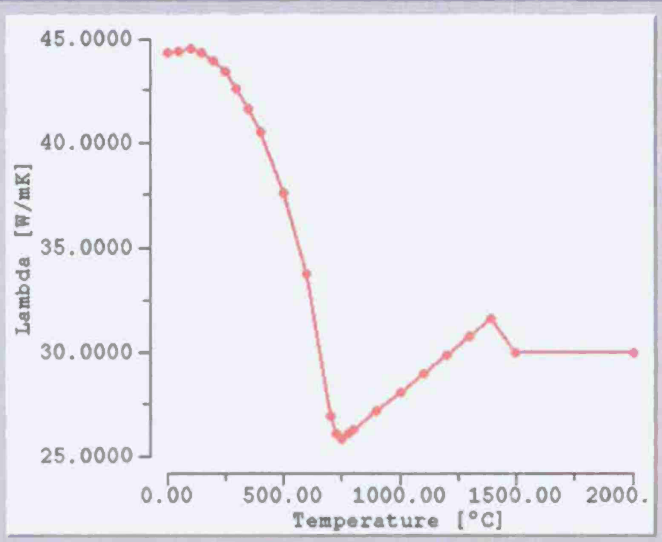

Table 3 Density (Rho), specific heat (Cp) and solid fraction (fs) used in casting simulations.

Rho as function of Temperature

Temperature [°C]	Rho [kg/m³]
1.00	7849.0000
50.00	7840.0000
100.00	7825.0000
150.00	7809.0000
200.00	7792.0000
250.00	7775.0000
300.00	7757.0000
350.00	7739.0000
400.00	7721.0000
500.00	7683.0000
600.00	7644.0000
650.00	7677.7998
700.00	7665.1001
800.00	7625.1001
900.00	7575.0000
1000.00	7524.8999
1100.00	7474.7998
1200.00	7424.7002
1300.00	7374.5000
1375.00	7336.8999

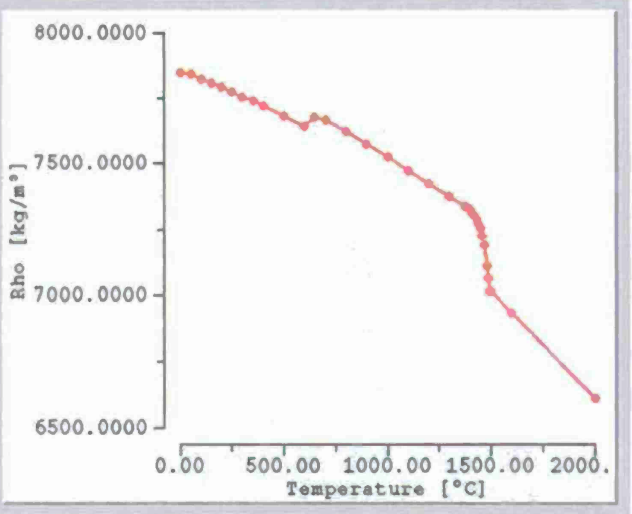

Cp as function of Temperature

Temperature [°C]	Cp [J/kgK]
1.00	451.0000
50.00	470.0000
100.00	503.0000
150.00	528.0000
200.00	543.0000
250.00	554.0000
300.00	577.0000
350.00	601.0000
400.00	621.0000
500.00	688.0000
600.00	800.0000
650.00	643.4800
700.00	626.5400
750.00	588.8000
800.00	596.6000
900.00	612.1000
1000.00	627.7000
1393.00	690.1000
1496.00	750.0000
2000.00	750.0000

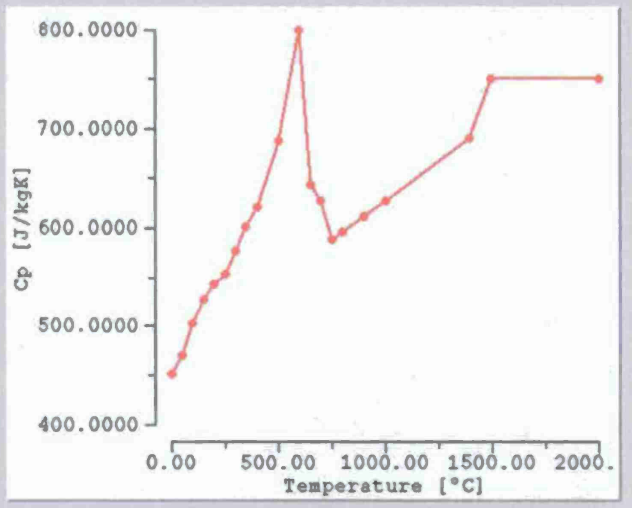

fs as function of Temperature

Temperature [°C]	fs []
1393.00	1.0000
1395.00	0.9944
1400.00	0.9869
1405.00	0.9772
1410.00	0.9649
1415.00	0.9519
1420.00	0.9394
1425.00	0.9248
1430.00	0.9077
1435.00	0.8877
1440.00	0.8644
1445.00	0.8371
1450.00	0.8051
1455.00	0.7673
1460.00	0.7226
1465.00	0.6693
1470.00	0.5992
1475.00	0.4924
1480.00	0.3724
1485.00	0.2883

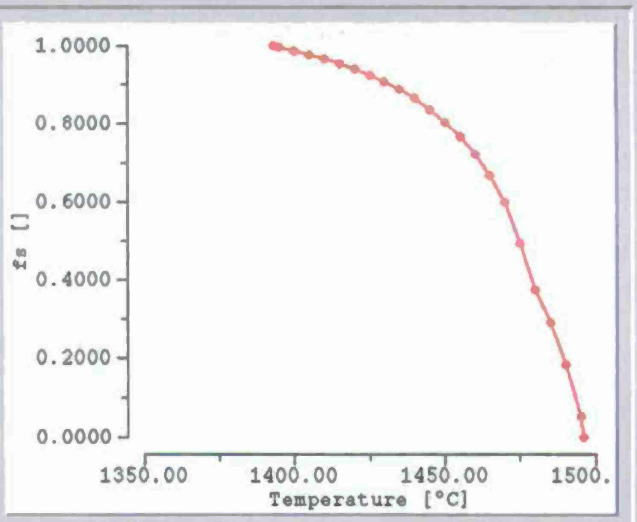

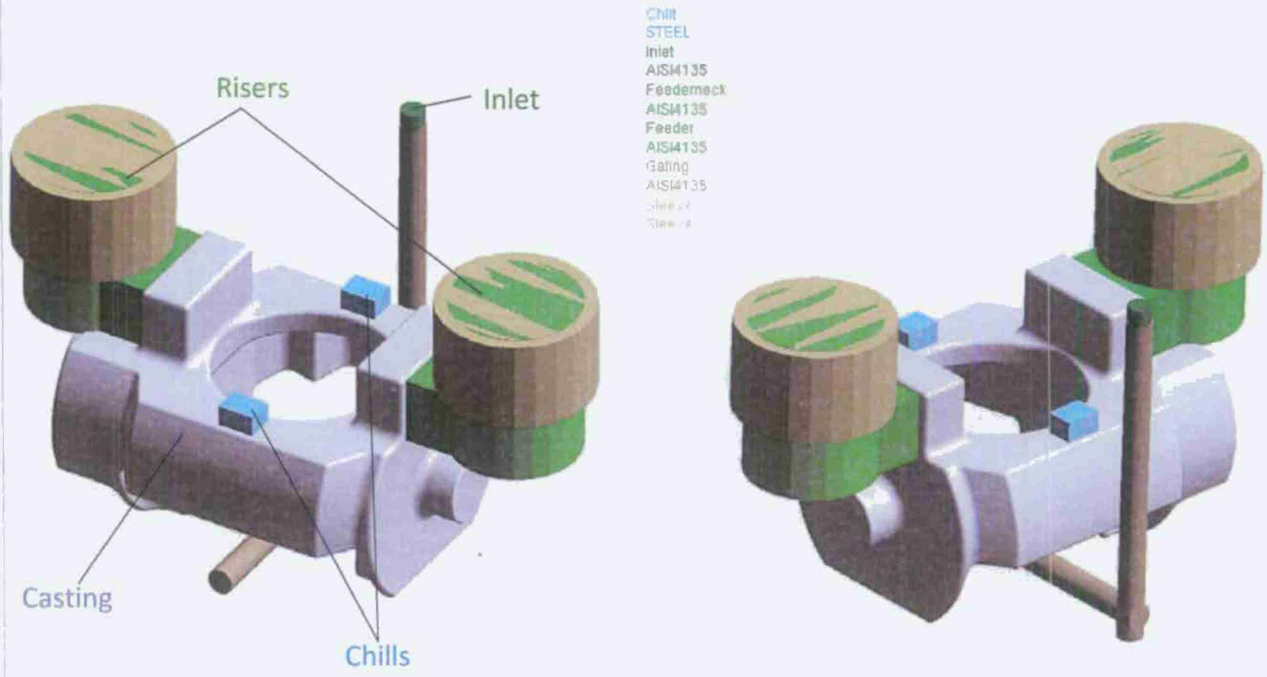

Figure 1 Two views of the rigging found to produce satisfactory simulations results.

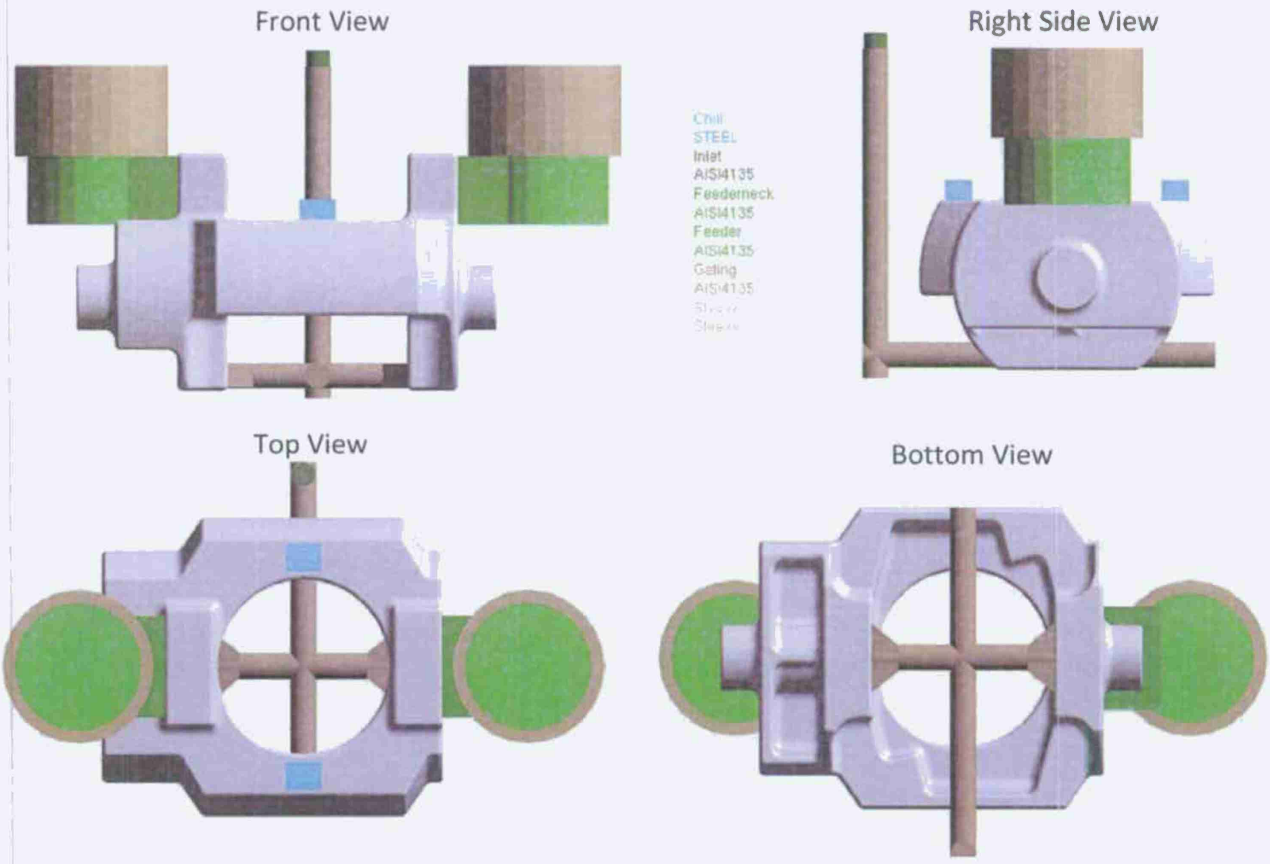

Figure 2 Four directional views of the rigging.

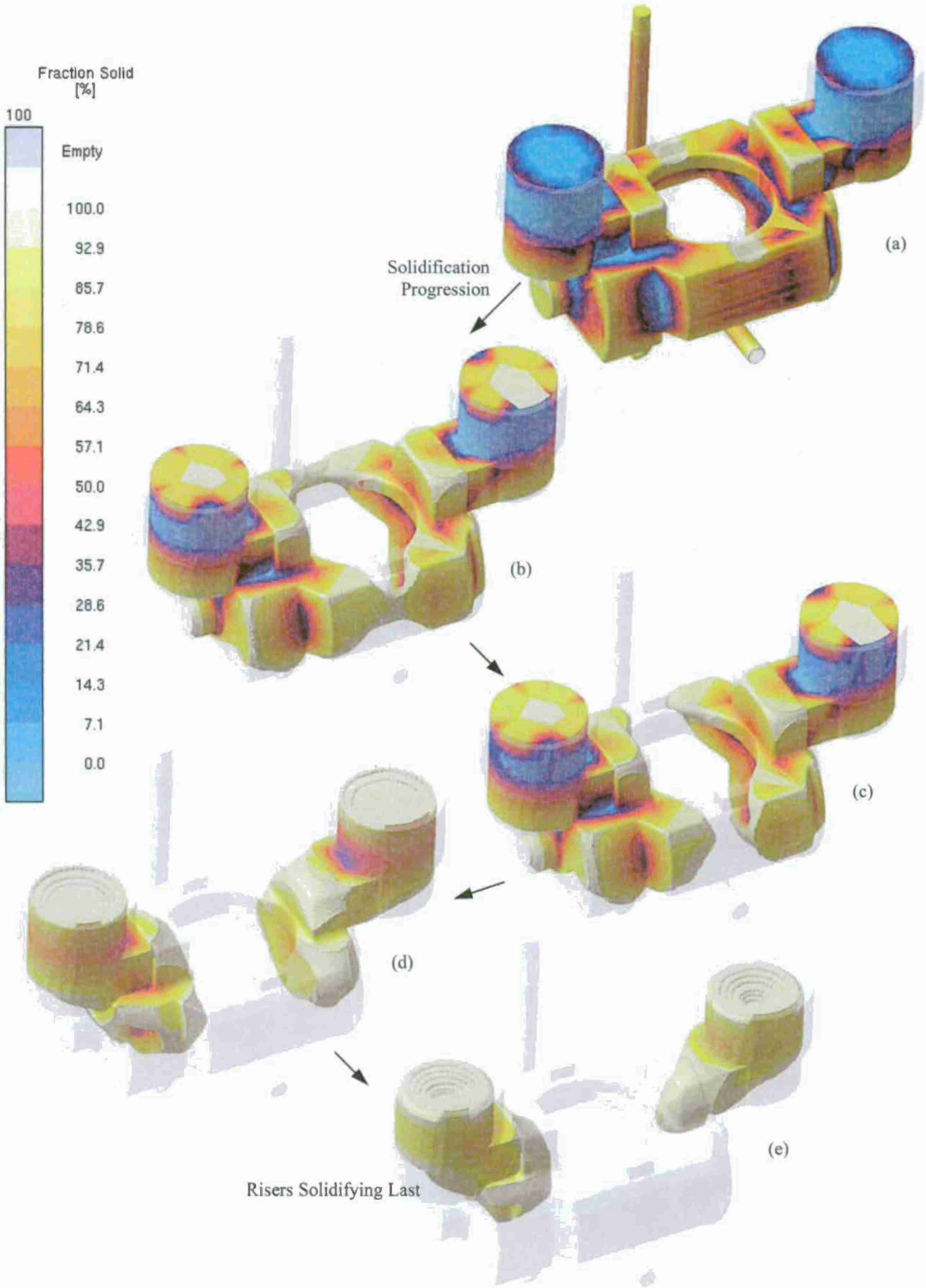

Figure 3 Progress of solidification in x-ray views of solid fraction from (a) near start to (e) near the end of solidification where risers are seen to solidify last.

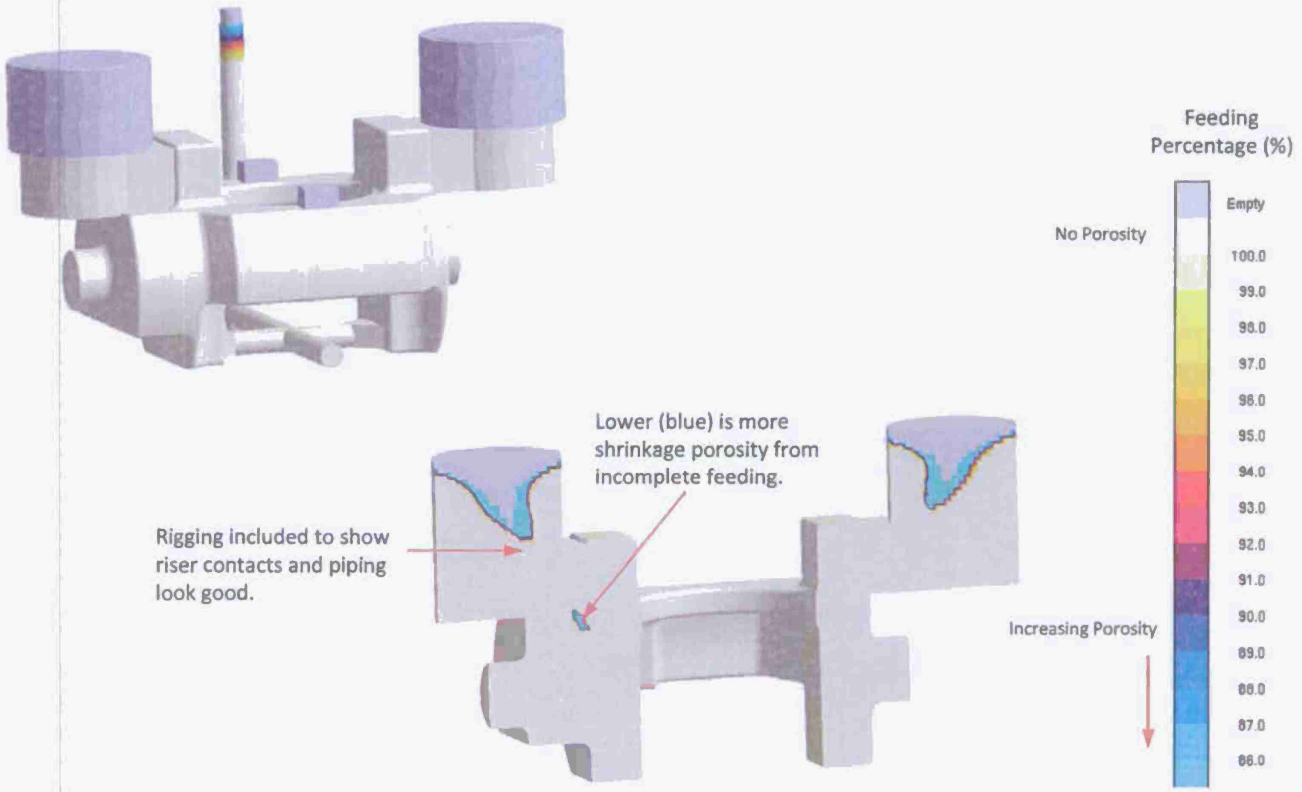

Figure 4 Feeding porosity predictions in center slices across the casting and risers to show riser pipes. Casting has small shrinkage indication at one location by this predictor.

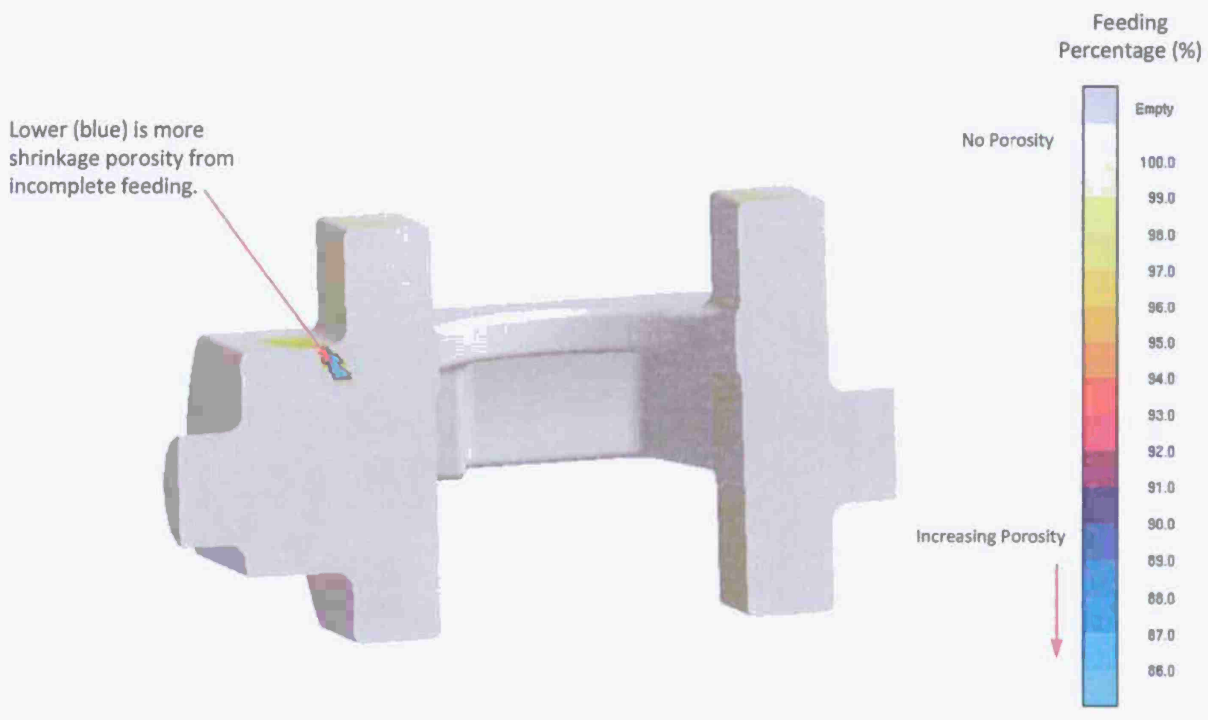

Figure 5 Feeding percentage in section with only the casting shown to clarify porosity location. The rest of the casting is clean of feeding porosity predictions.

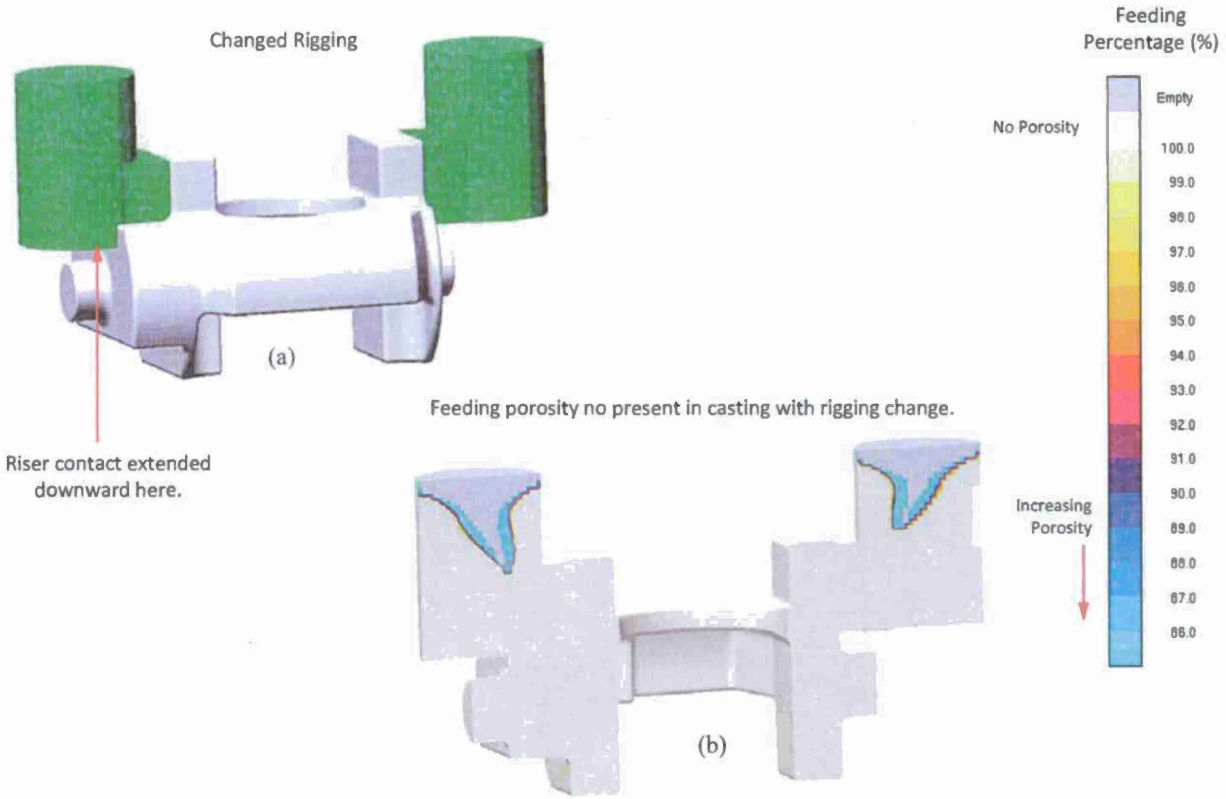

Figure 6 Casting Simulation Results: Feeding %Prediction. Rigging has been changed to remove predicted porosity from the casting.

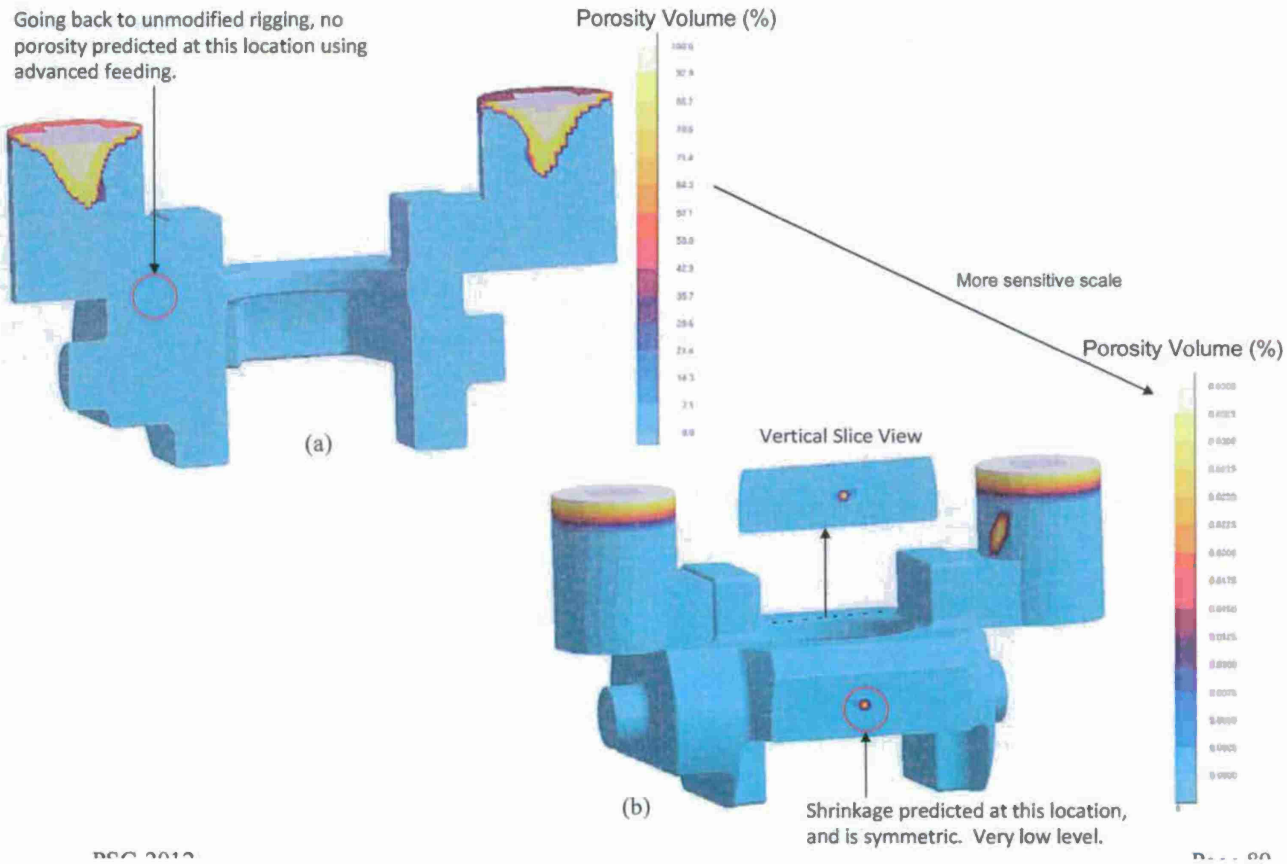

Figure 7 Casting Simulation Results: Advanced Feeding (AF) Porosity Volume % prediction.

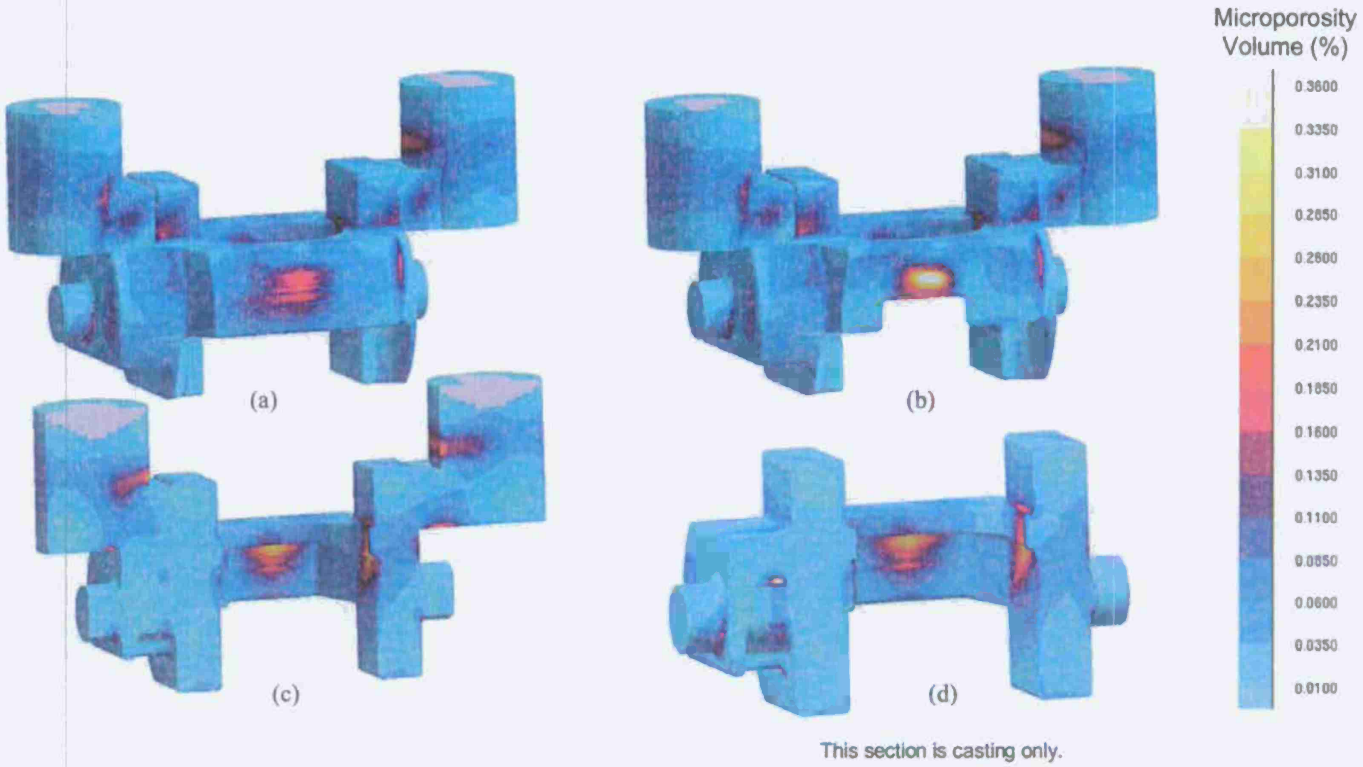

Figure 8 Casting Simulation Results - Microporosity Prediction %: Microporosity predictions on surface and subsurface.

Figure 9 Fatigue notch factor determined from the microporosity results is mapped onto FEA mesh. Microporosity porosity results are used to predict part performance since they appear to be the most sensitive and are worst of the three (most conservative).

Figure 10 Von Mises stress from Benet Labs ABAQUS stress analysis.

Figure 11 Maximum principal stress under loading from Benet Lab stress analysis.

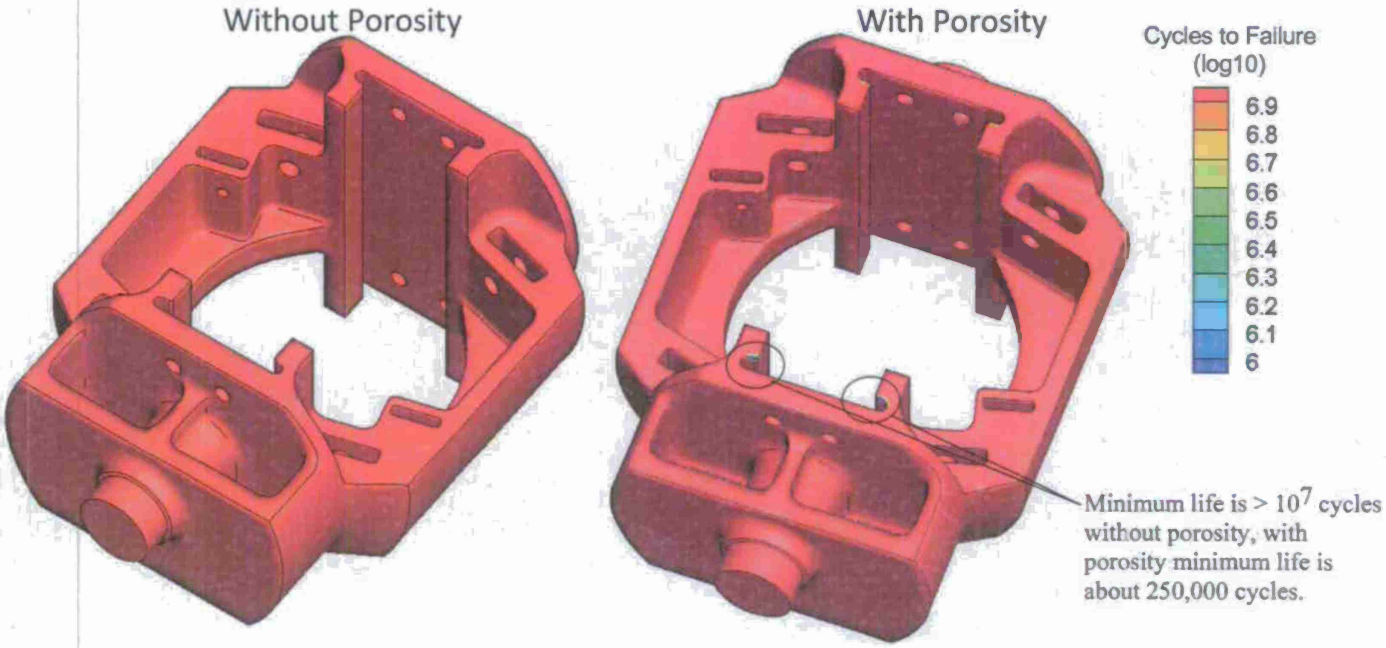

Figure 12 Cycles to failure for casting with and without microporosity field used in the analysis.

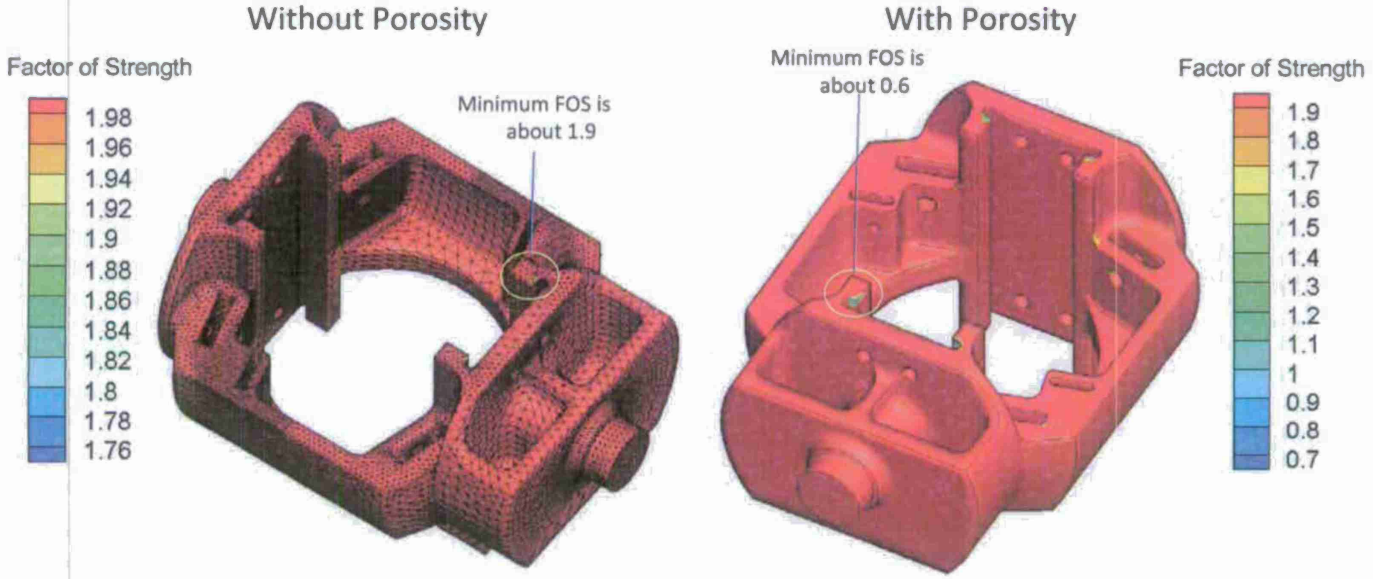

Figure 13 Factor of strength for casting with and without microporosity field used in the analysis. This Factor of Strength (FOS) is the scaling factor applied to the local stresses at an fea node that gives the design fatigue life, 5 million cycles. Lower is worse, below 1 means life < 5 million cycles.

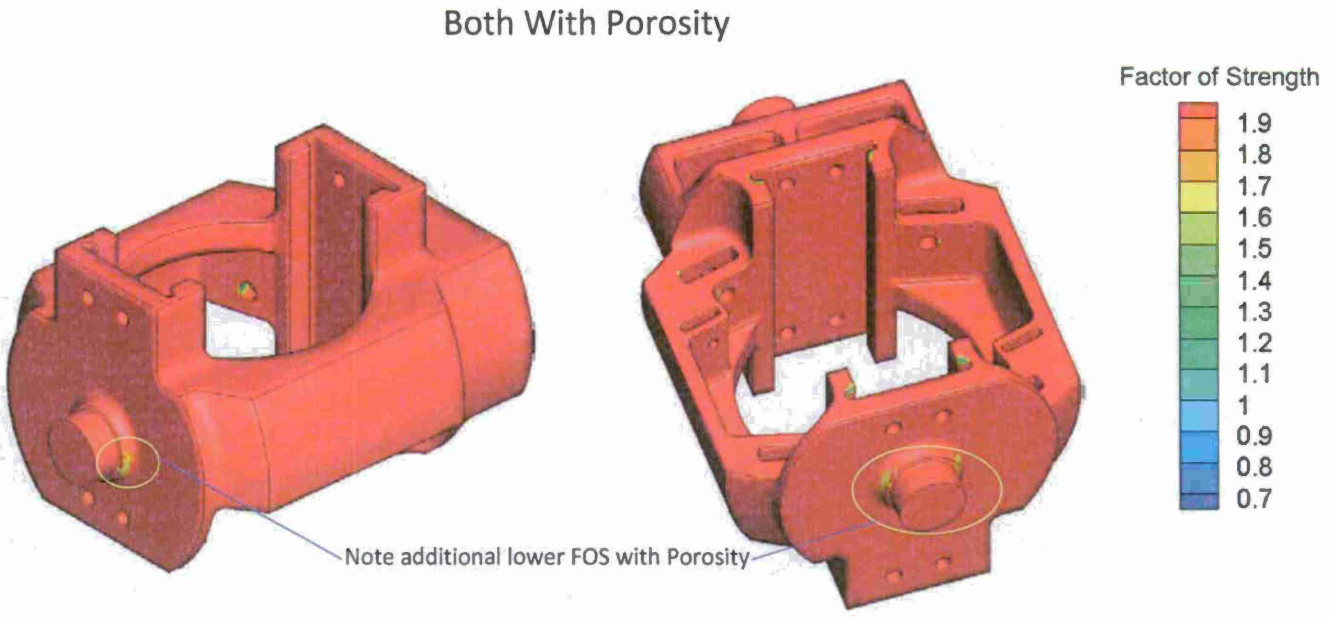

Figure 14 Factor of strength for casting with microporosity field used in the analysis.

Development of Steel Casting Advanced Manufacturing

The Iowa State University research team has worked on three technologies to advance the manufacturing systems used to produce steel castings. These three projects include a rapid patternmaking system, automated finishing of castings, and a software tool to track three dimensional surface data.

To produce a metalcasting via some of the most widely used processes, a pattern is required which is used to make the mold. Often times, production of the patterns takes several weeks which inherently extends the delivery of the final casting. A new patternmaking system has been designed and the machine to be used by the system is being constructed. The intent is that instead of requiring several weeks of craftsman to construct a pattern, the new system can produce a pattern at the touch of a button once the pattern is designed. The system is adopting some techniques from the field of rapid prototyping, but in contrast to rapid prototyping systems, this system will produce a pattern of the same durable materials as traditional patternmaking. The current system is expected to be operational in the first quarter of the next year.

Much of the effort to produce a steel casting includes the post-solidification finishing operations. One of the most labor intensive steps in producing a steel casting is the grinding that occurs after solidification. Grinding is an inherent part of the production process needed to remove the gating and riser contacts and achieve an acceptable surface. The work at ISU has been towards an automated grinding system that has the ability to work on a part without the specific process plan or tool path planning. The research team has developed a small scale prototype of the system that was used to successfully validate the algorithms to accomplish grinding when the part information is not known a priori.

To improve their understanding of the steel casting process, steel casting producers will track the location of surface anomalies. These anomalies are related to process variables, such as molding and pouring parameters, operator variability, and melt composition. While these data have the potential to make valuable improvements in the casting process, the handling of this data is tedious, making it difficult to consistently collect reliable data and in some cases cost prohibitive. This project is developing a system that can be used to record and store the location of surface anomalies on a 3D model along with pertinent process variables. The system will also allow the user to search the database to look for trends in the data based on any of the process variables. The database will be a repository of information that will provide the opportunity to utilize this data that has not been previously available. The data input interface has been developed and current efforts are creating the database and analysis tools.

Rapid Patternmaking

Progress was made in being able to take a pattern model and decompose it to layers for the rapid patternmaking process. To demonstrate partial capabilities of the process, a ¼ scale model of the cope half of the breech nozzle was produced. This was done on a conventional milling machine, and had a machine time of 17.5 hours. There are several opportunities to decrease the cutting time, including the use of a CNC router optimized for cutting wood. The procurement process for a CNC router is currently ongoing, which will lead to a prototype rapid patternmaking machine.

In the previous quarter, a scale model of the cope pattern of the breech nozzle was fabricated using the rapid patternmaking process on a milling machine. The remaining pieces of the pattern and core box were produced this quarter to further demonstrate the capabilities of the process. While utilizing a milling machine can demonstrate the geometry creation capabilities, it is very slow and requires much operator intervention.

The construction of an automated system with a larger build envelope and a much faster material removal rate is planned. As with the prototype method used on the milling machine, the new system is layer based, meaning the pattern is constructed one layer at a time. This system will have a four foot cube build envelope. The major components of the new system have been designed, and construction is about to commence. The major components include a feed elevator to move the sheet material into position, a material transfer device for moving the sheet from the elevator through the glue station and onto the build elevator, the glue station which will automatically apply glue to the sheet material, the build elevator which will hold the new pattern as it being built, and the router which will do the cutting. The CNC router is on order with delivery expected soon which will allow the other system components to be built. Figure 1a shows the machine design.

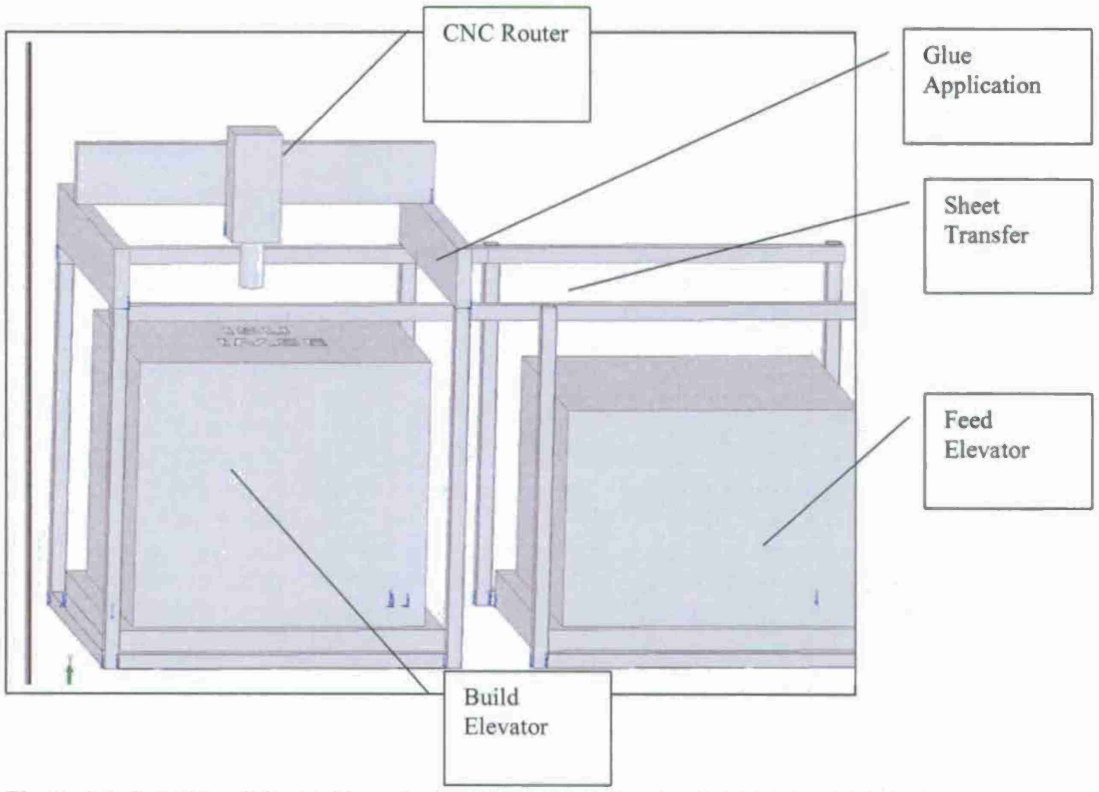

Figure 1a: Drawing of the rapid patternmaking system showing the major system components.

Construction of an automated rapid patternmaking system with a large build envelope and a fast material removal rate is underway. The build volume of the new system will be up to a four foot cube. The major components of the new system have been designed; many have been constructed and/or purchased. The major components include a feed elevator to move the sheet material into position, a material transfer device for moving the sheet from the elevator through the glue station and onto the build elevator, the glue station which will automatically apply glue to the sheet material, the build elevator which will hold the new pattern as it being built, and the router which will do the cutting. The centerpiece of the system is the CNC router, which as been received. Testing has been done to confirm the communication, operation and control of the router in the automated system. In the next quarter, the goal is to integrate all of the pieces and be nearly ready to start building patterns. Figure 1a shows the machine design.

We have been continuing to work to improve and work out bugs in the patternmaking process. All but the final components of a fully integrated system are assembled and integrated. We have been making test patterns to test the functionality of the system components that are operational (see Figure 1b).

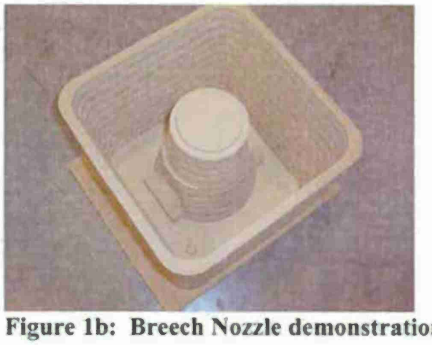

Figure 1b: Breech Nozzle demonstration pattern.

Demonstrated the rapid patternmaking system to produce the tooling for the mortar base plate. Figure 1c provides a pictorial display of all of the pattern pieces produced. This effort required us to work out a few more bugs in the system, but in general the system is working well.

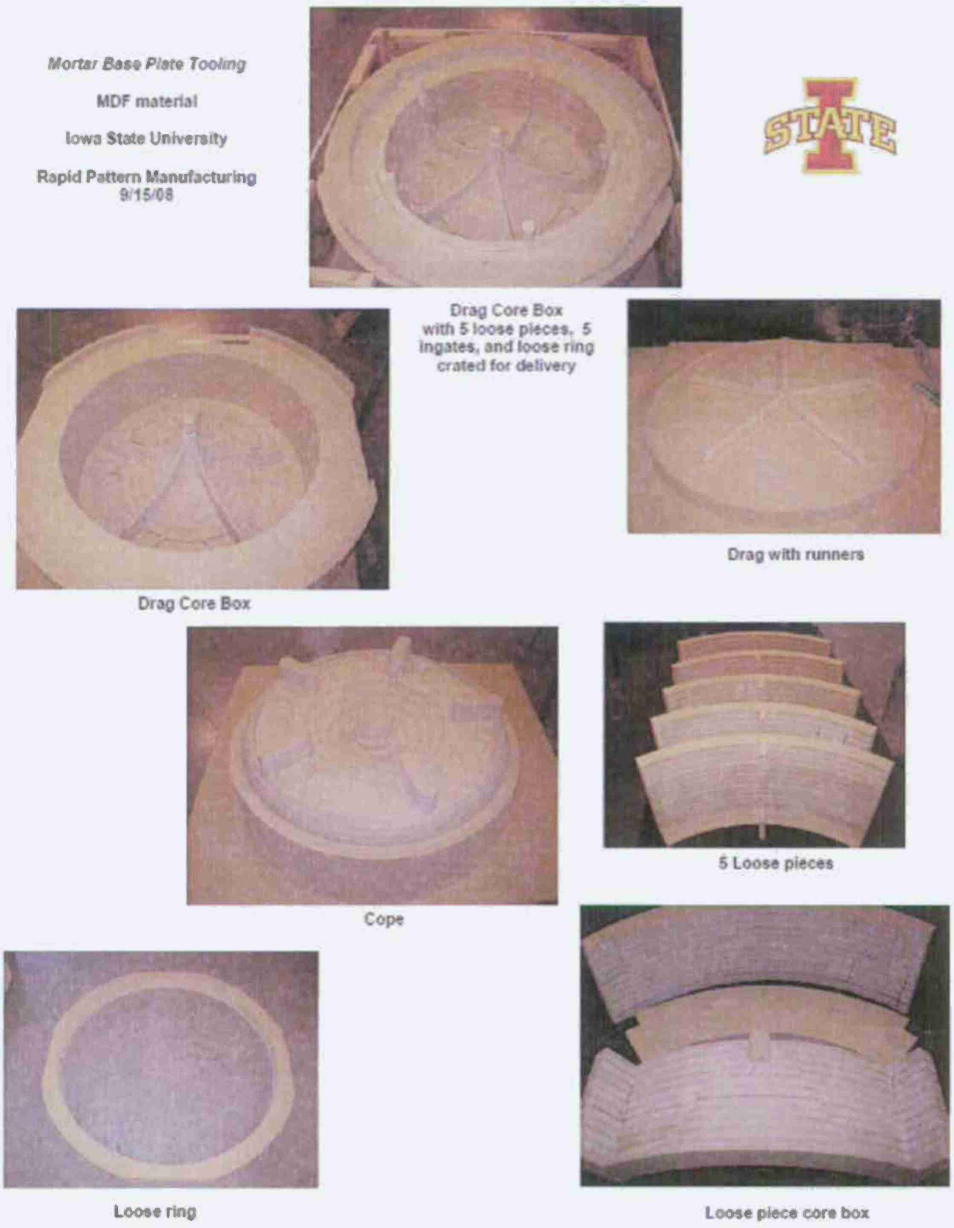

Figure 1c: 120mm mortar baseplate RPM pattern

An innovative two-axis deposition system was designed and implemented. A peristaltic pump coupled with a multi-nozzle print head provides inverted gluing, allowing subsequent in-position machining, Figure 1d. A printing algorithm was developed to increase the speed and efficiency of the gluing raster pattern. A specific adhesive was chosen to balance curing time and strength.

Figure 1d. Gluing system showing print head axis (left); trial showing successful glue deposition in inverted position (right)

All process planning, tool path planning, and machine control software was reviewed and validated, with significant improvements in speed and reliability. Different tool path planning strategies were tested for speed and reliability; these trials led to a machining strategy that reduces processing time by 40% while maintaining high accuracy.

The machine controls were redesigned and relocated to improve safety and reliability, Figure 1e.

A dimensional performance study was done to validate the system output with respect to the design intent. Sources of dimensional errors were defined. Another study evaluated the geometry of 'thin webs' of remaining stock material that may cause problems during machining and need to be avoided. Case studies to demonstrate the effectiveness of the system will be completed as planned on an unfunded basis since timing became a barrier.

Figure 1e. Redesigned machine controls

Automated Finishing Operations

In this quarter, a prototype automated grinding system was completed, Figure 2. This system was constructed on a small gantry system (approximately 1x.1x 1 foot operating volume) and utilizes a small grinder. While this system cannot come close to grinding steel castings, it does demonstrate the capabilities of the algorithms and procedures

that had been previously developed on another project, but remained untested This technology has the potential to replace much of the hand grinding that occurs in steel foundries. Hand grinding is inherently labor intensive, a large ergonomic risk and can lead to delivery delays. Automation options that are currently on the market are not applicable to much of the grinding that is done because it is impossible or infeasible to know the location and orientation of the grinding locations beforehand. This precludes a robot or CNC machine which requires a set machining path.

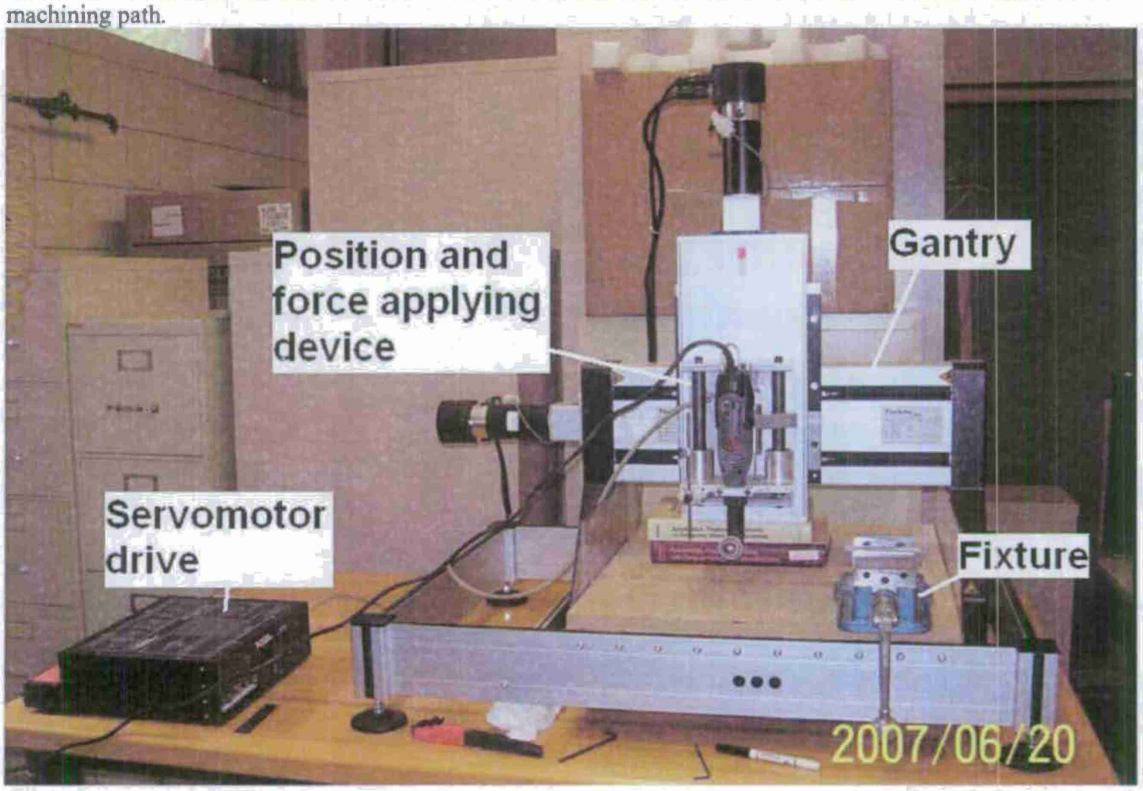

Figure 2: Prototype automated finishing system.

The ISU automated system requires the operator to input some initial information on what to grind, and the system then operates without intervention. The first step is for the user to identify points which surround an anomaly that needs to be removed from the casting surface. This is done by moving the machine to a few anomaly boundary locations, and recording those locations. Since the orientation of the part is unknown, the system must learn what surface is desired under the anomaly area. In the same manner as the anomaly boundary points, the user enters points on the boundary of the desired surface, and the type of surface (planar, concave, convex, saddle). The system will then determines how many points it needs to reconstruct the surface and automatically records the XYZ locations of those surface points. The system then calculates the desired surface in the area of the anomaly.

The system then selects a location in the anomaly area to commence grinding. The grinding wheel is mounted on a spring compliance system which will apply the desired force. As a measure of the force being applied, the compliance system is fitted with a linear transducer. The grinder will start grinding the part. If a large anomaly is encountered, the grinding wheel will lift up. If the wheel is lifted too high as determined by the linear transducer, it indicates that a high force is being applied. This signals the system to lift to a higher layer, and continue grinding. This system will continue navigating the entire area enclosed in the anomaly area in a similar manner until the desired surface is reached, within a user defined tolerance value. This system will determine the grinding path while it is grinding, eliminating the need to program the desired.

Figure 3 shows some parts produced of an epoxy material with excess material above the desired surface (anomalies).

The second row of pictures in Figure 3 shows the same parts after the automated grinding operation on the prototype system. The results of this prototype stage will be presented to the steel casting industry for future direction.

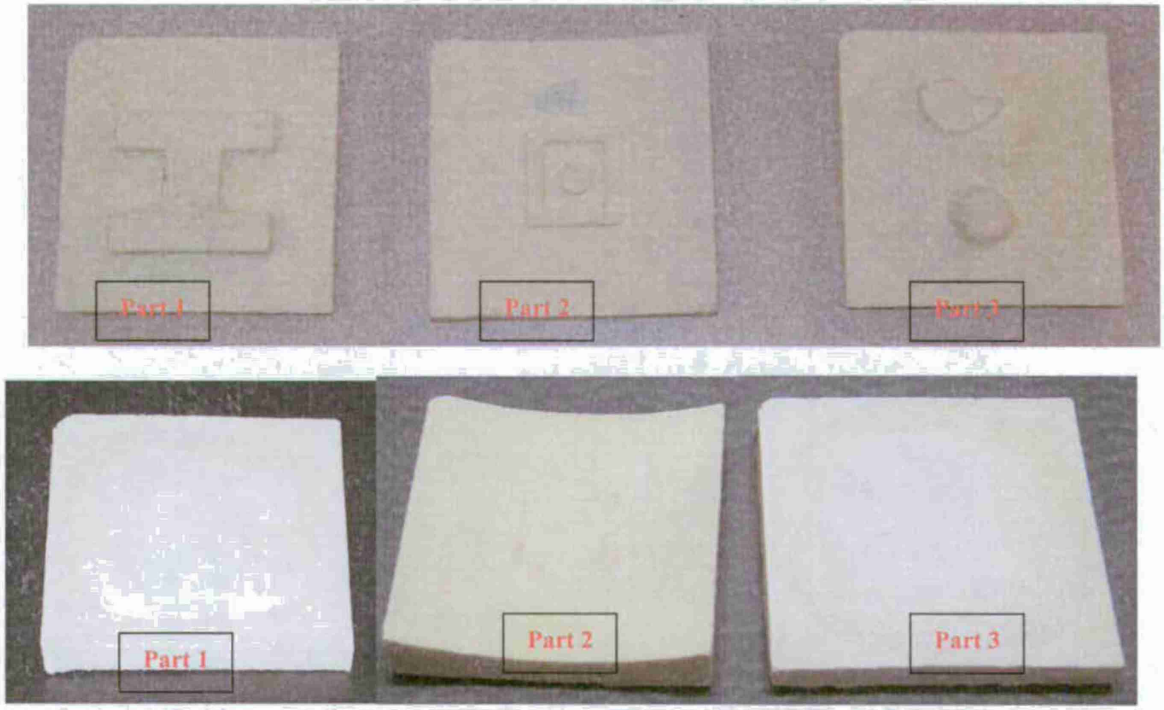

Figure 3: Three examples of parts in the top row with surface anomalies. The second row shows the same parts with the anomalies removed via the automated grinding system.

Anomaly Mapping

Several steel foundries collect data on the location of surface indications, such as inclusions, dirt and hot tears from their castings. The data is recorded on sheets, and a total value for the particular category of indications is often entered in a database. While this data proves invaluable in determining the effect of process changes or other variables over time, there is much more value that could be gained from this data. This project is investigating more effective methods for collecting, storing, and utilizing this information.

The goal is to develop a database to record these indications on a per casting basis. This data then could be for more robust and exacting analysis. For instance, correlations between the occurrence of surface indications in one area could be made to indications in other areas. This database technology and statistically analysis techniques could have much wider applications for studying other data sets such as NDE or wear patterns.

The project will require a user interface for recording the locations of surface indications. A database will be required to store the data that is extracted from the user interface. Statistical analysis tools for this large and valuable dataset then need to be investigated. In the past quarter, several graphical packages for the user interface were investigated. The current direction is to use Adobe Acrobat 3D which has a user interface for recording 3D surface data. The intent is to exploit the capabilities of this package, build a custom interface on top of this software, and then develop methods for extracting and storing data. A prototype user interface is shown in Figure 4.

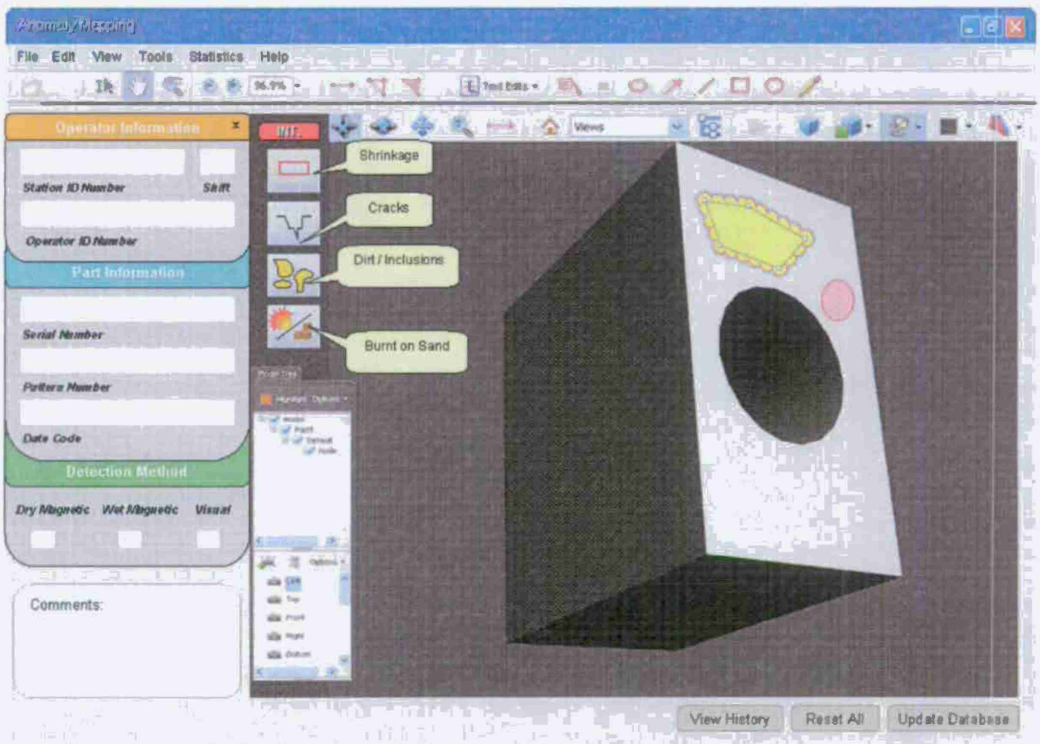

Figure 4: A prototype of the user interface built on the Adobe Acrobat 3D platform.

Surface Finish Characterization: Preliminary work has continued on this part of the project, but nothing more to report this quarter. Efforts have been primarily directed at the other higher priority items.

To improve their understanding of the steel casting process, steel casting producers will track the location of surface anomalies found via visual or NDT methods. These anomalies (i.e., inclusions, dirt, porosity, linear indications, burnt on sand, or shell cracking) are related to process variables such as characteristics of the mold, pouring parameters, operator variability, composition of the melt, and the interaction of the mold with the molten steel.

Potential uses of anomaly data include process tracking and design of experiments for process variables. While these data have the potential to make valuable improvements in the casting process, the handling of this data is tedious, making it difficult to consistently collect reliable data and in some cases cost prohibitive. Anomaly data are typically collected on paper forms by sketching the location of an anomaly on a 2D pre-printed view of the casting, writing textual data, and adding comments. These paper forms are then placed in a file cabinet and rarely accessed because the data is difficult to access and analyze in a meaningful way. Furthermore, the tedious nature of collecting and attempting to interpret data discourages many companies from even collecting data.

This project is developing a system that will help alleviate some of the problems associated with the collection and utilization of surface anomaly data. Using this system, foundries can record and store the location of surface anomalies on a 3D model along with pertinent process variables. The system will also allow the user to search the database to look for trends in the data based on any of the process variables. The database will be a repository of information that will provide the opportunity to utilize this data that has not been previously available.

The system architecture described in Figure 5 supports multiple modes related to responsibilities of the users and the necessary functions that need to be supported.

The Configuration and Anomaly Data Collection components are being implemented in the Adobe Acrobat 3D platform which provides a programming environment based on JavaScript. The primary advantages of using this platform include the commercial availability of Adobe Acrobat, widespread usage of PDF documents and the ability to import CAD models from almost every commercial CAD system.

Future work will develop the analysis module so that the most knowledge can be extracted from the data, with minimal effort.

The analysis module will facilitate multiple output formats in order to extract the most knowledge from the data. Some potential output possibilities include:

- Frequency plots (similar to FEM or solidification time) that show the frequency of anomalies on the part surface. These plots can be separated by the type of anomaly and/or by any processing variables (shift, pouring operator, height of metal in a ladle, gating system).
- Series of plots that show the location of anomalies on the part surface. Each plot in the series would be a particular part. As the user moves through the series, they can identify trends in the plots with respect to time the parts were produced (or any other variable that you sort the plots by.)
- Besides the plots that are more qualitative, quantitative output son the size and/or location of anomalies with respect to any of the variables stored in the database or can be accessed in other databases.
- More sophisticated analysis tools could be developed that would provide correlations between the occurrence of anomalies in one area to another area.
- If the inspection results are recorded for a particular part for more than one of the inspections that the particular part is subjected to, then analysis could be done to compare the original anomalies to those that are identified after a round of welding and grinding. This analysis would be invaluable in eliminating the excessive rework loops that occur at some facilities.

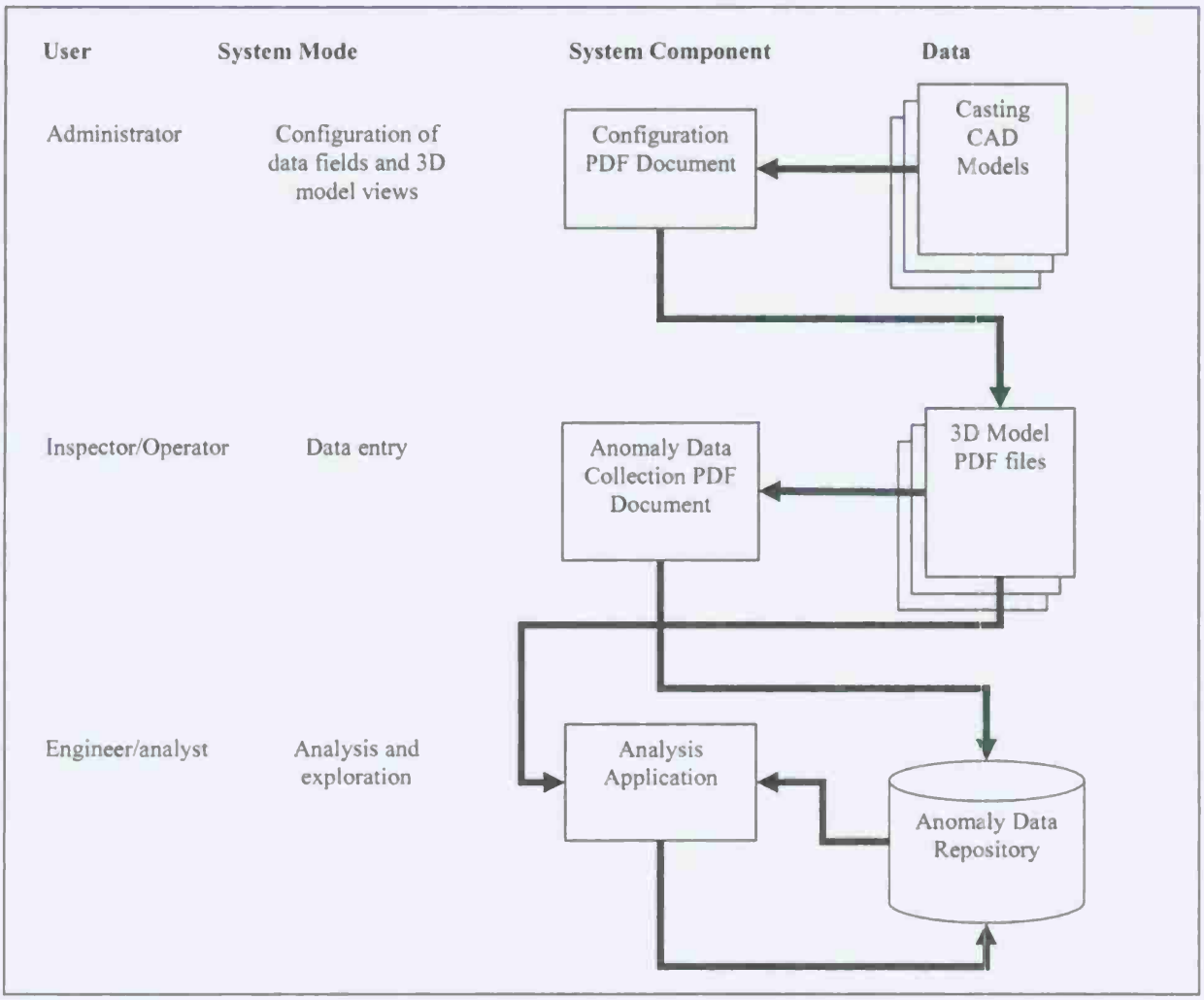

Figure 5: System architecture for the anomaly mapping software.

We finished up some of the output functions to display the anomaly data in frequency maps based on user defined parameters. We have started a case study period with the software by having a researcher working at a partner steel foundry to work out any software issues and demonstrate its effectiveness. This was made possible by the partnering company supporting the student research during the summer.

A case study was conducted during June – August of this year at a steel casting producer. An ISU student worked at the facility and utilized the software to enter surface quality data. This initial data set is being used to help develop and fine tune the analysis tools.

Several statistical analysis tools were developed that utilize the data collected by the new anomaly mapping software. These tools include the automated generation of frequency histograms based on a user defined set of process variables. Statistical tests to determine correlations between anomalies in one area of a casting to another area were developed. Correlation tests were also developed between a user defined set of process variables and anomalies in a geographic region. Principle component analysis tools were used to analyze the database to look for unusually different or very consistent defect patterns. These tools are described in the attached paper that was presented to an industry group.

Development of Sand Properties

Initial work included base line testing of high temperature properties of phenolic urethane no-bake and cold box binder systems. This initial study included the development of stress strain graphs at various temperatures from room to 450C in 100C intervals. Based on recommendations by Dr. Beckermann at the University of Iowa a new specimen core box has been designed and is under construction that will provide a more consistent gage length for physical testing.

The new dog bone sample box and high temperature compression core box were modeled and CNC machined. Test samples were produced from phenolic urethane no bake sand and tested under a nitrogen atmosphere at elevated temperatures to 500°C with soak times up to 45 minutes. A Summary of the results are shown in Figure 1. High temperature expansion tests were conducted under a 7:1 CO2/CO atmosphere and resulting data is currently being processed. Samples contained 3% red iron oxide and are expected to show a crystallographic change prior to the published Crytobolite/Tridimite phase change temperatures.

High temperature testing of the core material in a CO/CO2 atmosphere was initiated but not completed within the reporting period. The test series is expected to be completed within the next operating quarter. Construction of a "blow" cold box core tooling has been started and is expected to be completed early in November of 2007. This will give us the ability to test an amine vapor cured binder system in addition to the liquid cured system already completed.

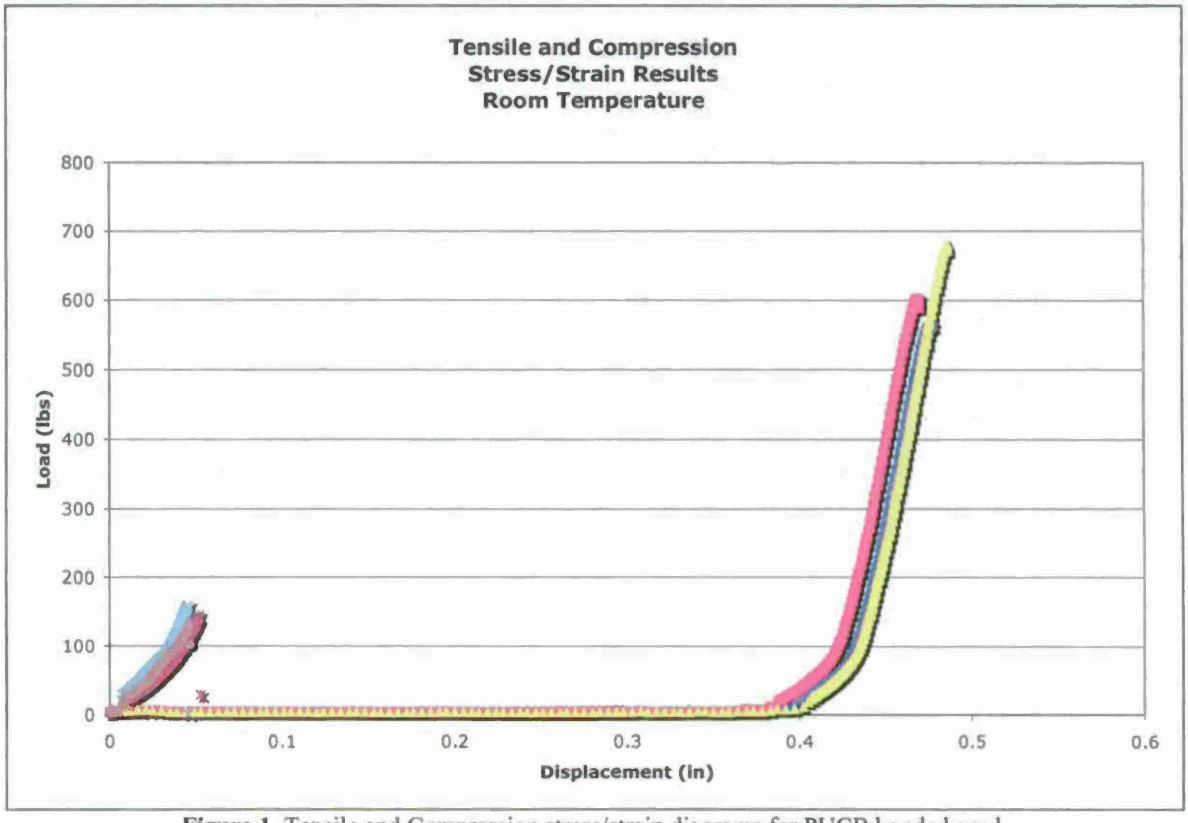

Figure 1. Tensile and Compression stress/strain diagrams for PUCB bonded sand.

Here we can insert a device to measure the force…

PART III - JOINING OF STRESS ACTIVE SECTIONS

Castings of a box design and flanged fittings were employed as stress active systems in this third part of the research on hot tear formation because both mold and section design can result in hindered contraction and the formation of stress to produce hot tearing in steel castings.

The box section castings were varied as to corner design, section tapering, and wall thickness so as to produce different conditions of stress application, stress concentration and hot spots. The flanged fitting studied is indicative of a commercial steel casting and directs attention to typical features of design that are found in commercial castings afflicted with hot tears.

Experimental Practices

The box section of Figure 1, with various design modifications, was employed in the research. The first design modifications examined were variations of the box corners (Figure 2). The effect of tapering the box sections was also investigated with tapers of .035 to .070 inch/inch, as illustrated in Figure 3

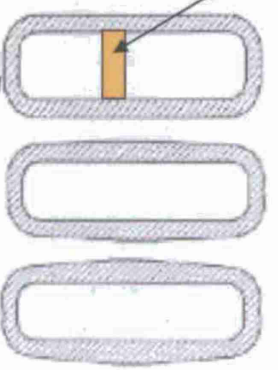

Figure 1—Box section design. (A certain box with various wall sections was also studied.) Box open at top and bottom.

Using the quartz tubes we can measure the displacement of the mold or casting surfaces

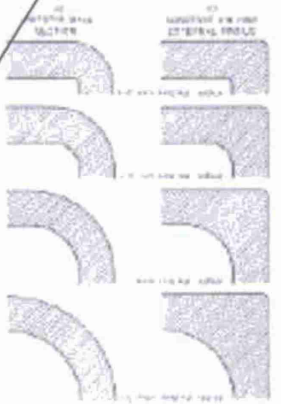

Figure 2—Corner cross section designs studied with the 1-inch thick box casting. Changes applied to 2in.) were also studied for the ½-inch thick box casting.)

All castings were risered at the center of the long walls, and gates entered the risers. Figure 4 illustrates complete cope and drag molds with pattern ready for removal, and Figures 5 and 6 show two typical castings after shakeout.

Molds were hand rammed with AFS No. 60 New Jersey silica sand. Most of the castings were poured into green sand with baked cores. Some green sand cores were used. The green sand was bonded with 4 percent bentonite, 0.5 percent each of corn flour

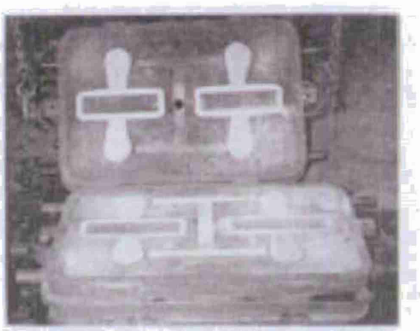

Figure 4—Cope and drag molds of box castings with gates and risers attached to patterns.

Advanced Modeling Dataset

UNI conducted various metallurgical studies to complete the testing for the HY130 and 4330 steels. Work was conducted on the fabrication of an austempering quenching bath and related heat treat furnace. The university also continued to research high temperature properties of molding aggregates and successfully integrated them into stress simulation models using MAGMA casting simulation software. The university continued to assist the University of Iowa with the manufacture of bonded sand specimens and provided additional testing results for high temperature sand properties. This research included developing high temperature sand properties and support of the University of Iowa's efforts to develop and refine casting simulation models.

Refine and develop testing of HY130 and 4300 series medium alloy steel

Three alloys of different compositions were melted in 136 kg (300 lb) capacity air induction furnace. Y blocks were cast in sand moulds and 25.4 mm × 25.4 mm × 203 mm (1"× 1" × 8") rectangular bar was cut from the Y block for the heat-treatment operation. Heat treatment of the material consisted of processing the samples with a normalizing temperature was 926°C (1700°F), for 2 hours followed by air cooling. The heating and cooling rate was measured by inserting a thermocouple at the middle of a 25.4 mm × 25.4 mm × 203 mm rectangular bar. The data acquisition was done using a software control device. The cooling curve yielded a 29°C/min (80°F/min) cooling rate from 926°C - 593°C (1700°F - 1100°F) temperature after that the cooling rate decrease to 4°C/min (25°F /min) up to 93°C (200°F) temperature. Hardening temperature was 846°C (1555°F) for 1 hour, followed by quenching in oil.

Tempering temperature was varied from 176°C (350°F) to 565°C (1050°F) followed by oil quenching. Brinell and Vickers micro hardness were used to determine the hardness variation of as cast and tempered steels. The tensile properties of tempered steels were evaluated in a commercially available tensile testing machine. The tensile properties of tempered steels were determined using smooth cylindrical specimens according to the ASTM designation E 8 [5]. These specimens had a 101.4-mm (4 in.) overall length, a gage length of 25.4-mm (1 in.), and a gage diameter of 6.35-mm (0.25 in.). CVN specimens having 54.96-mm (2.16 in.) length, 10-mm (0.39 in.) width, 10-mm (0.39 in.) thickness, and a notch angle of 45° were machined from the heat-treated materials. . A commercially available pendulum-type impact tester was used to strike the CVN specimens at a location opposite to the notch. A dial indicator attached to this equipment recorded the energy absorbed to fracture the specimens in terms of either Joules or feet-pounds (ft-lbs). Multiple CVN specimens were tested at room temperature. Lateral expansion was determined using the device described in the ASTM standard for that purpose [6]. For metallographic study samples were cut from the tensile specimen. Samples for microstructural study, were prepared by conventional grinding and polishing technique in MCC metallographic laboratory. The samples were etched in 2% nital solution and observed in an optical microscope. The area fraction of various micro-structural phases was determined by image analyzer technique.

Development of high temperature sand properties for molding aggregates

Elevated tensile testing had been previously completed at the university but the limited gage length of the standard AFS tensile test coupon was of a concern when elongation deformation was to be studied. Previous research had identified point loading problems with the AFS tensile specimen design. It was recommended by Dr. Christoph Beckerman and Mr. Charlie Monroe of the University of Iowa that the tensile specimen design be lengthened 1" to provide for an adequate gage length between the test fixture grips. On their recommendation tensile specimen core boxes were produced to increase the gage length of standard AFS tensile test specimens to 1" utilizing the standard grips needed for tensile testing. The 1" gage length would allow the accurate measurement of the elongation of the cores before breaking. The prototype tooling was designed to work with self setting core sands. The elongated dog bone specimens exhibited a slightly lower standard deviation than the original specimens.

An analysis was made to compare the current tensile specimen design to the elongated tensile design. A comparison based on 25 tensile samples showed that the elongated test specimen had an equivalent standard deviation and a slightly higher average strength level. This was thought to be a result of reduced point stresses present in the original specimen design. Tooling for vapor cured specimens was also produced from an iron alloy that makes the use of both chemical and heat activated binders possible. The vapor cured specimens are machine made and cured by passing amine vapor in a nitrogen carrier gas through the core. The polymerization is almost instantaneous as the amine gas is introduced into the core and eliminates variations that would be introduced by a liquid amine catalyst.

An air purge removes the amine vapor before removal from the machine.

Compression samples were produced using standard industry tooling and were comprised of cylinders 1.125 inches in diameter and 2 inches long. The bonded sand specimens were heated in a muffle furnace using a neutral atmosphere consisting of a 7:1 ratio of CO_2 and CO. This gas mixture was found to replicate the mold gas atmosphere found in chemically bonded molds. Three soak times of 15, 30 and 60 minutes were used on the samples to provide time dependent physical properties. The test cores were removed after the desired soak times and immediately placed in the fixture for testing. The samples were compressed until fracture.

Data collected for the compression testing of the samples showed that the relationship between time/temperature and mechanical properties of the sands were not linear. Figure 7 and 8 illustrate the initial testing of sand properties at seven temperatures ranging from 23C to 600C. The sand's physical strength was close to being entirely depleted at the 600C temperature. As the sand's temperature increased from 23C to 100C the strength and elastic modulus decreased as expected. This trend continued until the sand temperature reached 200C decreasing the sand's strength over 60% from the room temperature values. The decrease in strength is thought to be partially related to the loss of solvents in the phenolic urethane binder system causing a decrease in the length of polymer chains. As the sand temperature increased from 200C to 300C the strength and elastic modulus temporarily increased. Increased time at this temperature also caused an increase in both compression strength and elastic modulus of the sands. The increase at 300C may be a secondary polymerization not of the original phenolic urethane but of a heat catalyzed phenolic polymerization of the degraded urethane polymer chains. This caused a temporary increase in both the compression strength and elastic modulus. Continued heating further degraded the polymer chains decreasing both the compression strength and the elastic modulus.

Compression strengths and young's modulus calculations resulting from the deformation under load were compared to known values for bonded sands at room temperature. It was found that the modulus calculated from the deformation was substantially less than results previously published. Close examination of the Twing Albert along with the testing of known property materials yielded the difficulty of the testing method. The extension reported by the Twing Albert is actually the displacement of the testing crosshead. Flexure in the crosshead at even relatively low tensile stresses resulted in displacements in an order of magnitude greater than the actual dog bone deformation. Although strength testing was correct for all temperature levels a new methodology would be required to develop accurate deformation data and resulting young's modulus values. Based on the difficulty associated with the original testing methodology a new more accurate testing methodology was developed. The new testing methodology involved use of a Satec universal testing machine with integrated extensometer.

Samples of Phenolic Urethane Cold Box (PUCB) and Resin Coated Sand (RCS) were produced using addition levels and ratios provided by the manufacturers. The cold box technology is similar to the no bake technology with the exception of the method of introducing the amine catalyst. The PUCB test samples were produced at a 1.2% binder level while the RCS sand was bonded by the manufacturer at a 1.9% resin level. Each of the samples was allowed to cure for a minimum of twenty four hours in a low humidity environment before testing. Elevated temperatures for the samples were provided with a muffle furnace. Samples were placed in aluminum foil and held in a nitrogen atmosphere for the required time at temperature. Difficulties encountered in the testing involved the loosening and degradation of the sand at the surface of the sample causing slippage or false movement of the testing equipment. Three soak times were chosen to give values corresponding to the temperatures involved in the casting process and relate elevated time at temperature rather than the replication of actual casting conditions. Because sand is considered an insulator it is difficult if not impossible to test the tensile stress and strain under casting conditions. Samples were removed from the muffle furnace and tested immediately. A constant loading rate of 200lbs/min was used for all testing and provided a reasonable compromise between the number of data points collected and the cooling of the sample.

Support efforts of the University of Iowa in refining casting simulation models.

The University of Northern Iowa has been supporting the University of Iowa efforts through production of test

specimens. Two sets of multiple specimen tooling was produced to UI specifications. Multiple samples have been produced utilizing phenolic urethane no-bake foundry sand binder. Additional samples were produced including percentages of iron oxide additive to simulate actual sand binder mixes utilized by foundries.

High Strength Low Alloy (HSLA) Steels

Higher strength casting alloys can allow metal casters to lighten casting designs by reducing section thicknesses. By using these high strength alloys, steel castings can achieve strength to weight ratios as high as titanium castings at a fraction of the cost with reduced lead times and overall cost. A study conducted at the University of Northern Iowa evaluated the physical properties of three commercially available low alloy steels and their ability to achieve properties above 956MPa (140 ksi) yield strength while maintaining necessary ductility and toughness. These low alloy compositions were evaluated for their ability to meet 956MPa (140 ksi) yield strength, 6% elongation and 12% reduction of area. The paper discusses induction melting and casting techniques and includes methods for heat treatment and testing. Mechanical testing results are shown for varying tempering temperatures and various heat treatments including standard quench and temper. Results of the mechanical testing show that conventional 4300 series alloys can be effectively heat treated to high strength levels without loss of ductility and toughness. Carbon content was found to be critical in obtaining these high strength levels.

High-strength low-alloy (HSLA) steels are low-carbon steels with up to 1.5% manganese, strengthened by small additions of micro-alloying elements, such as niobium, vanadium or titanium and sometimes by special rolling and cooling techniques which is called thermo-mechanical controlled processing HSLA steel provides many benefits over regular steels. HSLA-steels offer increased strength-to-weight ratios over conventional low-carbon steels for only a modest price premium. Because HSLA alloys are stronger, they can be used in thinner sections, making them particularly attractive for transportation-equipment components where weight reduction is important.In general, HSLA alloys are much stronger and tougher than ordinary plain carbon steel and are designed to handle large amounts of stress, often at very low temperatures. Several commercialized and near-commercialized HSLA steels that exhibit high strength and enhanced formability are being offered around the world for various applications. These steels have the potential to affect cost and weight savings while improving performance.

As a high performance casting material Ti and its alloys are being used today. However a difficulty when manufacturing titanium components is that it is a reactive metal, particularly at high temperatures, taking up oxygen and nitrogen from the atmosphere and hydrogen if moisture is present. The absorption of small amounts causes a reduction in fatigue strength. The cost associated with Ti casting material is also high as compared to steel. Hence, as an alternate of Ti casting high performance structural steel can be used. The strength level of such kind of steels can be determined by the carbon content as well as the alloying addition. High strength is attained at the expense of reduced ductility. In order to improve the ductility and toughness of hardened steel, it is reheated for a relatively short time at the moderate temperature, which is called the tempering operation.However, upon tempering, the high strength steels with predominantly martensitic structure, undergoes temper embrittlement problems in a certain temperature region. The temper embrittlement of martensitic steel is associated with the reduction of toughness properties.

In this present study an attempt has been made to evaluate the physical properties of three commercially available low alloy steels and their ability to achieve properties above 140ksi yield strength while maintaining necessary ductility and toughness. These low alloy compositions were evaluated for their ability to meet 956MPa yield strength, 6% elongation and 12% reduction of area. The paper discusses induction melting and casting techniques and includes methods for heat treatment and testing. Mechanical testing results are shown for varying tempering temperatures and various heat treatments including standard quench and temper.

Three alloys of different compositions were melted in 136 kg (300 lb) capacity air induction furnace. Y blocks were cast in sand moulds and 25.4 mm × 25.4 mm × 203 mm (1"× 1" × 8") rectangular bar was cut from the Y block for the heat-treatment operation, Fig 1. The chemical analysis of each heat is listed in Table 1.

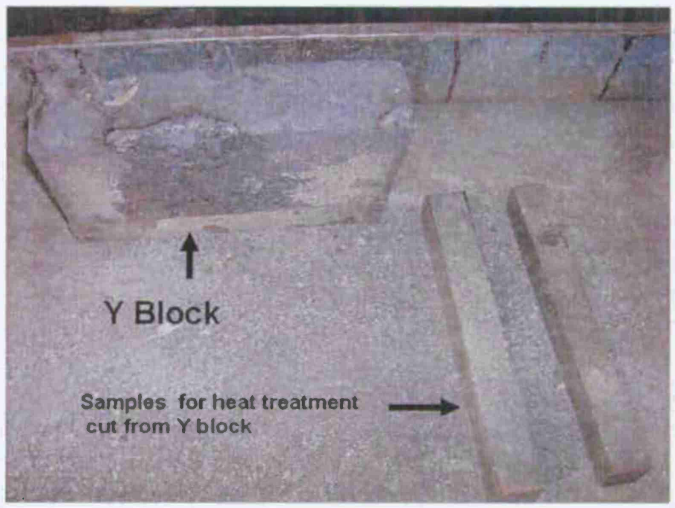

Figure 1 : As cast material

Table 1: Steel compositions: (Weight percent)

	4330	4325	Modified HY-130
C	0.29	.19	0.14
Si	0.57	0.55	0.40
Mn	0.48	0.47	0.57
P	0.024	0.027	0.043
S	0.014	0.017	0.024
Cr	0.52	.52	0.54
Mo	.21	.22	.18
Ni	1.66	1.63	5.2
Al	0.088	0.089	0.05
Cu	0.02	0.03	0.12
Nb	< 00	<0.00	-
Ti	0.003	0.003	<0.001
V	.31	.32	-
Sn	<0.002	<0.002	<0.002
Fe	<95.8	<95.95	<92.5

Heat treatment of the material was done in the following steps.

	4320 &4320	Modified HY-130
Step1	Normalizing	Annealing
Step2	Hardening	Hardening
Step3	Tempering.	Tempering.

The normalizing temperature was 926°C (1700°F), for 2 hours followed by air cooling. The heating and cooling rate was measured by inserting a thermocouple at the middle of a 25.4 mm × 25.4 mm × 203 mm rectangular bar. The data acquisition was done using a software control device. The heating and cooling curve is given in Fig 2.

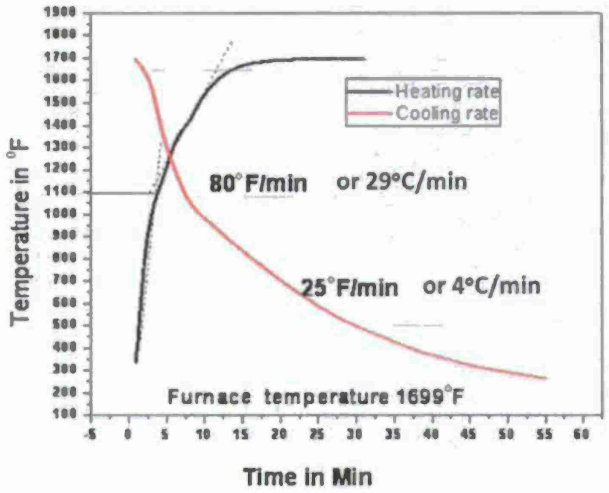

Figure 2: Heating rate in the furnace and air cooling rate of the samples.

The cooling curve shows 29°C/min (80°F/min) cooling rate from 926°C - 593°C (1700°F - 1100°F) temperature after that the cooling rate decrease to 4°C/min (25°F /min) up to 93°C (200°F) temperature. Hardening temperature was 846°C (1555°F) for 1 hour, followed by quenching in oil. The cooling curve obtained in oil quenching is given in Fig3.

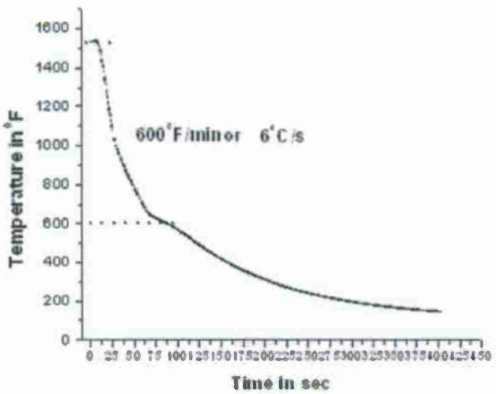

Figure3: Oil quench rate of the samples

Tempering temperature was varied from 176°C (350°F) to 565°C (1050°F) followed by oil quenching. Brinell and Vickers micro hardness were used to determine the hardness variation of as cast and tempered steels. The tensile properties of tempered steels were evaluated in a commercially available tensile testing machine. The tensile properties of tempered steels were determined using smooth cylindrical specimens according to the ASTM designation E 8. These specimens had a 101.4-mm (4 in.) overall length, a gage length of 25.4-mm (1 in.), and a gage diameter of 6.35-mm (0.25 in.). CVN specimens having 54.96-mm (2.16 in.) length, 10-mm (0.39 in.) width, 10-mm (0.39 in.) thickness, and a notch angle of 45° were machined from the heat-treated materials. . A commercially available pendulum-type impact tester was used to strike the CVN specimens at a location opposite to the notch. A dial indicator attached to this equipment recorded the energy absorbed to fracture the specimens in terms of either Joules or feet-pounds (ft-lbs). Multiple CVN specimens were tested at room temperature. Lateral expansion was determined using the device described in the ASTM standard for that purpose. For metallographic study samples were cut from the tensile specimen. The samples for microstructural study, were prepared by conventional grinding and polishing technique in MCC metallographic laboratory. The samples were etched in 2% nital solution and observed in an optical microscope. The

area fraction of various micro-structural phases was determined by image analyzer technique.

The hardness values of the steels in as cast and as quenched conditions are shown in Fig 4. It is observed that, despite of low carbon content, the highest hardness value in as cast condition is obtained for modified HY -130 steel. However after quenching, the increase in hardness value is maximum for 4330 steel (Δ Hardness =176) and that of for modified HY-130 steel and 4320 steel were 83 and 43 respectively. This high increase in hardness value in 4330 steel is due to the high quench stress generated from the interstitial solid solution of carbon into the body centered tetragonal (b.c.t.) iron.

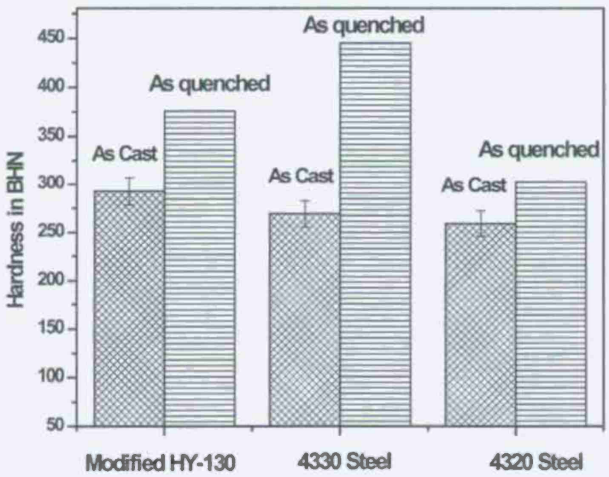

Figure 4 : BHN of the as cast and as quenched 4330 steel.

Figure 5: As cast microstructure of 4330steel in low magnification 200X

The microstructure of the as cast 4330 steel, is shown in Fig 5. The primary and secondary dendrites are revealed in the micrographs. It was interesting to study the variation in mechanical property within the cast structure of 4330 steel. The micro hardness profile was taken from the edge to center of the casting with an interval of 0.635mm (0.025 inch). The variation in micro-hardness from the edge to the center of the casting is shown in Fig 6 (a). Fig 6 (b) shows the

microhardness profile after tempering at 176°C (350°F) temperature. The dotted horizontal line in each graph represents the average hardness of the as cast and tempered at 176°C (350°F) steels taken in Brinell hardness machine. It is interesting to notice a fluctuation of the micro hardness values within the cast structure with respect to the average hardness value. This variation in hardness is due to the

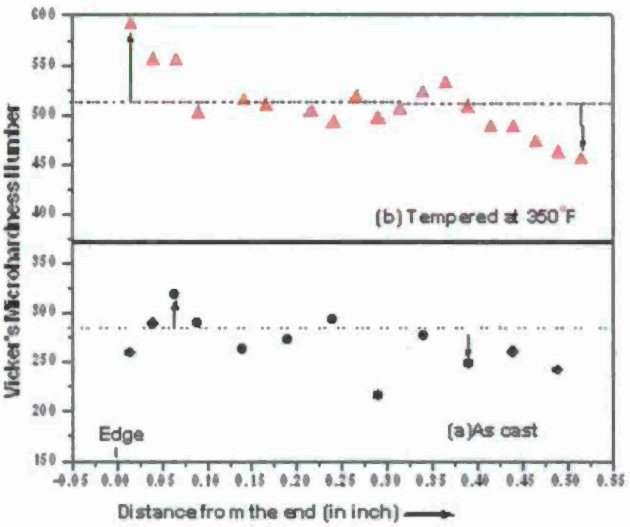

Figure 6 : Cross sectional microhardness profile of 4330 steel.(a) as cast.(b) tempered at 350°F

composition fluctuation, which has occurred during the solidification of metal in the sand mould. It is obvious that the ferrite is the first nucleating phase during solidification process. When the ferrite nucleolus started to grow into the melt the carbon content in ferrite would much less than the average carbon content (0.3 wt %) of the melt. While the ferrite phase grows more and more volume fraction in to the melt, the remaining liquid gets more and more enriched with carbon and other alloying elements and thus, shifts to the lower solidification temperature. It is observed that at the edge the microhardness value is lower than the average BHN value however the hardness value changes with distance, periodically probably maintaining an exponential decay curve. The microstructures were observed at different locations of the cast structures corresponding to different hardness values. It was interesting to observe that the ferrite percentage varies at different locations of the casting as Shown in Fig 7. The area fraction of ferrite at different locations in the as cast structure was calculated with an image analyzer system and is plotted against the corresponding micro hardness values in Fig 8. Considering the Fe-C equilibrium diagram the carbon percentage for a given ferrite fraction was calculated and the carbon percentage at different locations of the casting can be roughly estimated from the microstructural observation. It was observed that the carbon content in the as cast 4330 steel fluctuates in the range of 0.16-0.36 weight percentage.

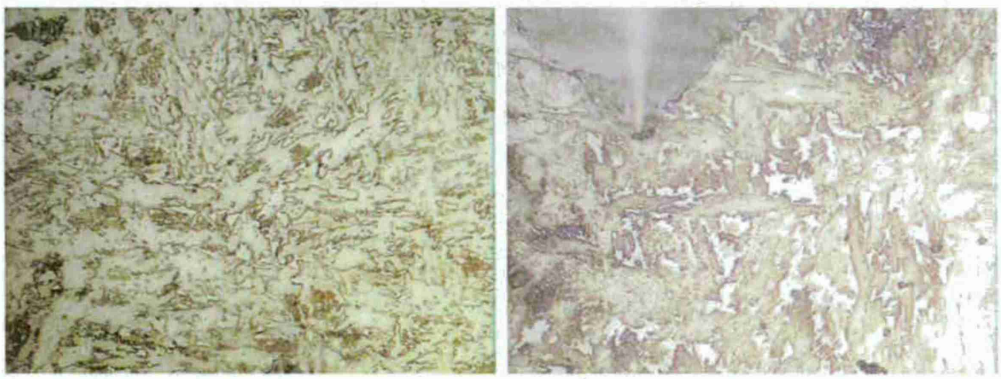

Figure 7: As cast structure of 4330 steel at different locations1000X.(a) at 242 VHN (b) at 318 VHN .

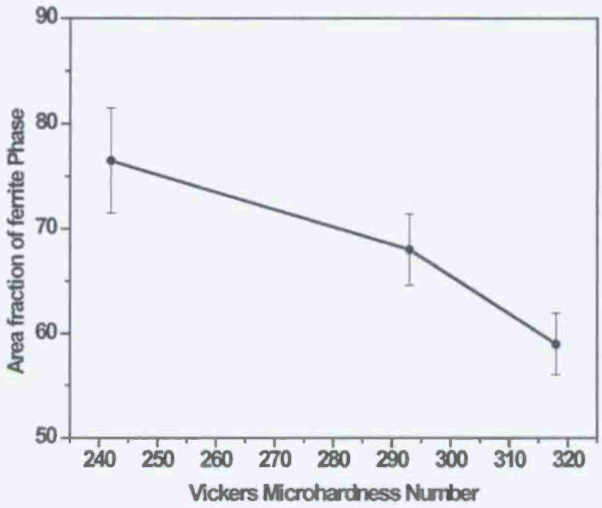

Figure 8: Variation of area fraction of ferrite of 4330 steel with Vickers microhardness number.

Normalizing is a process which is applied to minimize this composition fluctuation of the cast structure as observed earlier. A homogenize chemical composition throughout the structure is obtained by heating it to a single phase region and holding there for a substantial period of time. Thermally activated process i.e. diffusion of the atoms occurs at that elevated temperature and a homogeneous composition profile is obtained in the structure. Fig 6(b), the top portion in Fig6, shows the variation of microhardness of 4330steel after normalizing, hardening and tempering at 176°C (350°F) temperature. It is observed that the variation in microhardness with respect the average Brinell hardness value has become lower than that of as cast condition (over a region 1.27 mm (0.05 inch) to 11.43 mm (0.45 inch)). The high increase in hardness at the edge is contributed to the faster cooling rate at the surface during oil quenching. This microhardness plot in Fig 6(b) is also an indication of the hardenability profile of the 4330 steel.

The variation in microstructure of the 4330 steel due to tempering at different temperature is shown in Figs 9(a) – 9(c). It is observed that at 176°C (350°F) tempering temperature the microstructure is predominantly martensite. Formation invariant plane strain is very much evident in the structure tempered at 176°C (350°F) and it is interesting to observe formation of some bainite in the structure, Fig 9(a). The critical cooling rate for 4330 steel during quenching was reported to be 482°C / min (900 °F/min). For 4330 steel, with lower carbon content than that of 4340 steel, it is expected that the CCT curve would shift more towards left. Hence the critical cooling rate for formation of totally martensite structure would be higher than that of 4340 steel. In this present investigation the oil cooling rate was obtained 315°C / min (600°F/min). Hence some bainite is formed during continuous cooling from austenitizing temperature of 846°C (1555°F). At 343°C (650°F) tempering temperature, appearance of microstructure changes to tempered martensite structure, Fig 9(b). At this stage of tempering, the redistribution of carbon occurs, and precipitation of transition carbides, cementite would precipitate [8]. At higher tempering temperatures of 455°C (850°F) and onwards the softening process takes place and leads to a coarsening of the cementite particles.

(a) 350°F (b) 650°F (c) 850°F

Figure 9: Variation in microstructure of 4330 steel at different tempering temperatures 1000X

The variation in hardness with tempering temperature for three steels is shown in Fig 10. It is interesting to note that the trend in hardness variation with respect to the tempering temperature is same for 4330 and 4320 steel. The hardness value increase form in as quenched condition to 343°C (650°F) tempering temperature and then decrease for higher tempering temperature. The hardness value obtained for 4320 steel is much below the required hardness range. As quench hardness of 4330 steel was much higher than the target hardness range. It drops down to the target hardness range after tempering at 398°C (650°F).

A different trend in hardness variation with tempering temperature was observed in modified HY-130 steel. The as quenched hardness was high enough than the target range however lower than that obtained in as quenched 4330 steel. The hardness values decrease continuously with increasing tempering temperature. The target hardness value was obtained in the tempering temperature range of 398°C (650°F) to 492°C (900°F).

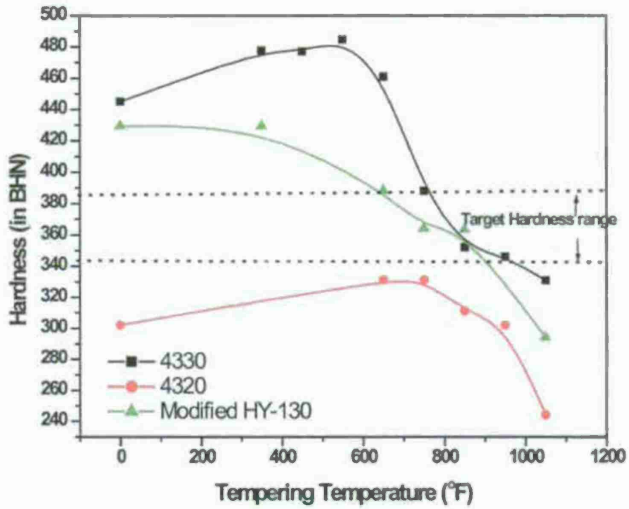

Figure10: Variation in hardness (BHN) with respect to the tempering temperature

It is well known that the ultimate tensile strength (UTS) of a material can be predicted from the hardness variation however harness may not resemble the similar trend in yield strength (YS) property of the material. Hence, it was essential to explore the tensile properties of the steels at different tempering temperatures in perspective of the target yield strength (YS) and the ductility parameters. The tensile properties of 4320 steel, modified HY-130 and 4330 steel are given in Table2, 3 and 4 respectively. The UTS values decrease with increase in tempering temperature and this trend was obtained for all the steels in this investigation. The variation in YS in 4320 steel with tempering temperature was not noticeable and the yield strengths of 4320 steels do not reach the target 956MPa (140 ksi) strength level. However, the ductility parameters (percent elongation and percent reduction in area) were far above the target level. The YS in modified HY-130 steel increase continuously from as quenched condition to 398°C (750°F) tempering temperature and then drops at 455°C (850°F). The continuous increase in YS probably due to strengthening effect resulted from the formation of alloy carbides.(molybdenum carbides) at this tempering temperature region. However transmission electron microscopic observation is required to investigate this phenomenon, which is beyond the scope of the present paper. The target YS value was obtain in modified HY- 130 steel up to the tempering temperature region 398°C (750°F) however the ductility parameter was not satisfactory. For 4340 steel the target tensile properties were achieved in the tempering temperature range of 455°C (850°F) - 510°C (950°F) and the required ductility values were obtained at this tempering region. However, it would necessary to explore, whether this region belongs to the temper embrittlement range of 4330 steel. Temper embrittlement of martensitic steel is an inherent property where a reduced toughness value is observed over a certain temperature region. Hence, the temper embrittlement region of 4330 steel was evaluated. The room temperature impact toughness property of the tempered steel was evaluated and shown in Fig 11.

Table2: Tensile properties of 4320 steel at different tempering temperatures:

	4320 steel			
	UTS (MPa/ ksi)	YS (MPa/ ksi)	%El	%RA
As cast	747 / 108.02	603 / 87.5	1.35	2.68
650	1039 / 150.64	827 / 120	14	14
750	978 / 141.8	805 / 116.7	21	36
850	965 / 140	862 / 125	15	18
950	917 / 133	821 / 119	18	32

Table3: Tensile properties of modified HY-130 steel at different tempering temperatures:

	HY-130 steel			
	UTS (MPa/ ksi)	YS (MPa/ ksi)	%El	%RA
As Quenched	1381/ 200.03	796 / 115.4	5.35	8.18
350	1282 / 186	918 /133.2	3.45	3.57
650	1289 / 187.75	1031/ 149.5	5.8	14.16
750	1225 / 177.7	1070/ 155.2	2.5	9.82
850	1159 / 168.06	965/ 139.9	4.68	3.57

Table4: Tensile properties of 4330 steel at different tempering temperatures

	4330 steel			
	UTS (MPa/ ksi)	YS (MPa/ ksi)	%El	%RA
As cast	779 / 113.4	500/ 72.5	3.4	1.75
650	1690 / 245.1	855 / 124.17	2	6
750	1503 / 218.4	1225 / 177.7	2	6
850	1338/ 194	883 / 128.3	6	16
950	1172 / 170.2	1138 / 165.03	7	20
1050	1048 / 152.5	812 / 117.8	5	15

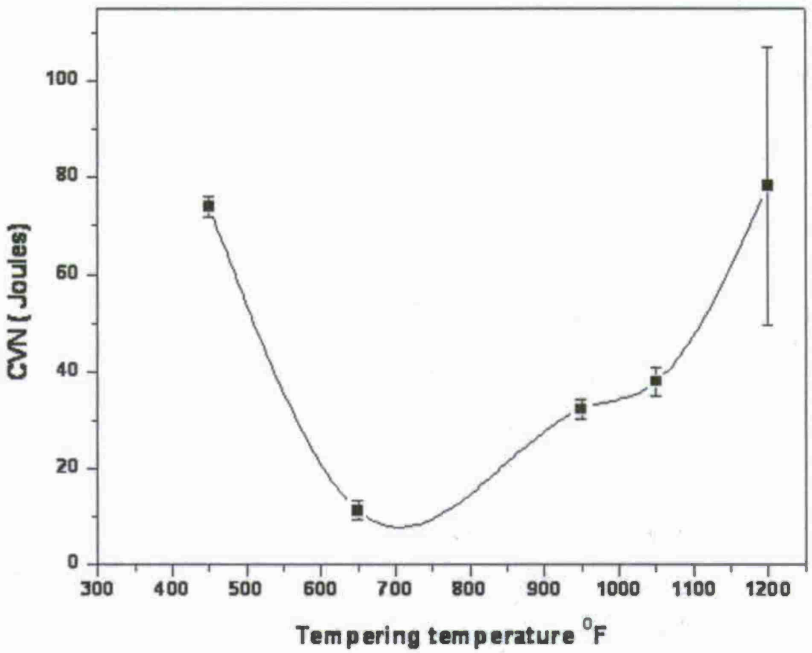

Figure 11: Variation of room temperature impact toughness of 4330 steel due to tempering at different temperatures.

It is observed that the toughness value decrease from 177°C (350°F) tempering temperature to 398°C (650°F) temperature and again a continuous increase in toughness values, up to 649°C (1200°F) was observed. Hence it can be said the temper embrittlement region of 4330 steel is around 398°C (650°F). For further confirmation of this temper embrittlement phenomenon of 4330 steel, the lateral expansion of the fractured specimens was measured and shown in Fig 12. From the Fig it is evident that that the minimum lateral expansion was obtained at 398°C (650°F) tempering temperature and 510°C (950°F) is probably outside of the temper embrittlement region of 4330 steel.

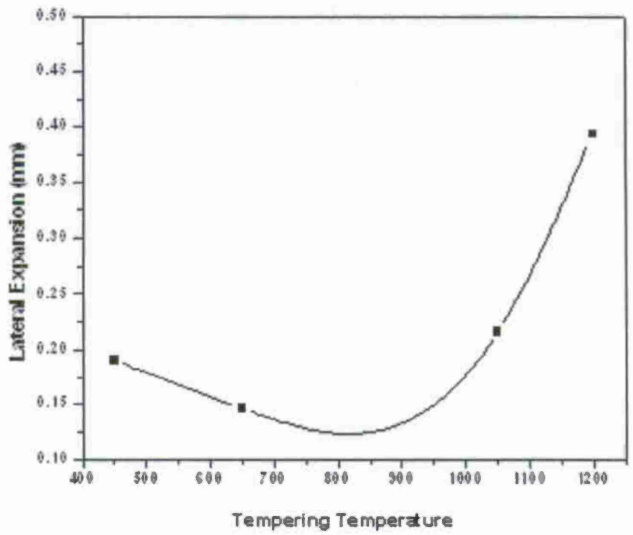

Figure 12. Variation of lateral expansion of 4330 steel due to tempering at different temperatures.

The effect of tempering time on the tensile properties of 4330 steel was also evaluated at 510°C (950°F) tempering temperature and the tensile testing results of the steels tempered at 510°C (950°F) for 1, 3 and 5 hours are given in Table 5. It is observed that the tempering time has negligible effect on the tensile properties of the 4330 steel.

Table 5: Tensile properties of 4330 steel at 950°F tempering temperatures for different hours

	4330 steel			
	UTS	**YS**	**%El**	**%RA**
1	**170.2**	**165**	**7.3**	**20**
3	**171.7**	**150**	**4.2**	**10**
5	**174**	**162**	**8.7**	**22.73**

The target tensile properties were achieved for 4340 steel in the tempering temperature range of 850°F-950°F and the temper embrittlement region of 4330 steel was around 650°F. Minimum impact toughness and lateral expansion were obtained at 650°F tempering temperature for 4330 steel. 510°C (950°F) is probably outside of the temper embrittlement region of 4330 steel. Tempering time at 510oC (950°F) tempering temperature has negligible effect on the tensile properties of the 4330 steel. Microstructural analysis was employed to estimate the fluctuation in carbon content in the as cast 4330 steel. This was found to be in the range of 0.16-0.36 weight percentage. 4320 steel showed much lower strength properties than the target strength level due to lower carbon content in the steel compared to 4330 steel. However the ductility parameters were much higher than the required values. The target YS value was obtain in modified HY- 130 steel up to the tempering temperature region 398°C (750°F) however the ductility parameter was not satisfactory.

Steel Casting and Engineering Support

SFSA has represented the steel castings industrial base for over a century. SFSA's mission is to serve the industry through developing steel casting advanced research, or innovation. SFSA has the active support and leadership of member foundries. SFSA has experience managing diverse and relevant technology development programs, developing new markets and applications, represents the industry nationally and internationally in regulatory and specification development, providing timely and useful business information, and provides state of the art training. SFSA understands meeting the warfighters' needs through steel casting technology and has worked with numerous government and commercial defense activities plus serves on the JDMTP metals subpanel.

SFSA is not a manufacturing entity; however, it has led or been party to numerous federal programs with the DOD, DOE, and DOC for decades. Facilitated by SFSA's direct connection to industry and its peer committee structure, research is managed for relevance to industry and rapidly implemented through its foundry network. SFSA meetings facilitate technology dissemination and with direct foundry involvement in the research, the impact of the project will be immediate.

Sivyer Steel in partnership with the PSC members, has developed an optimized gating system for the breech nozzle. The tooling for the breech nozzle is being completed. The initial prototype will be cast in a grade similar to 8630. Approval of the casting design has been given by Benet along with concurrence to optimize the NDE and testing requirements for the part and its required performance characteristics. Tooling setup will be provided to ISU from the pattern shop to enable a trial application of their rapid tooling process for the breech nozzle; currently looking into machine time at Rock Island Arsenal for the project. Delivery of the first as-cast breech nozzle to Watervliet for machining and assembly is estimated for June.

Site visit made to CTI to discuss prototype work on M777 muzzle brake. Castings were very clean; no indications on x-rays. A few surface discontinuities required welding. Mechanical properties met requirements. The Replicast process, inert shell material and vacuum pouring, lend itself to clean steel. The utilization of solidification software and padding, provide for reduced discontinuities. Prototype casting delivered to Benet. Plan is to develop a domestic source using a similar FoamCast process and to create a prototype for comparison.

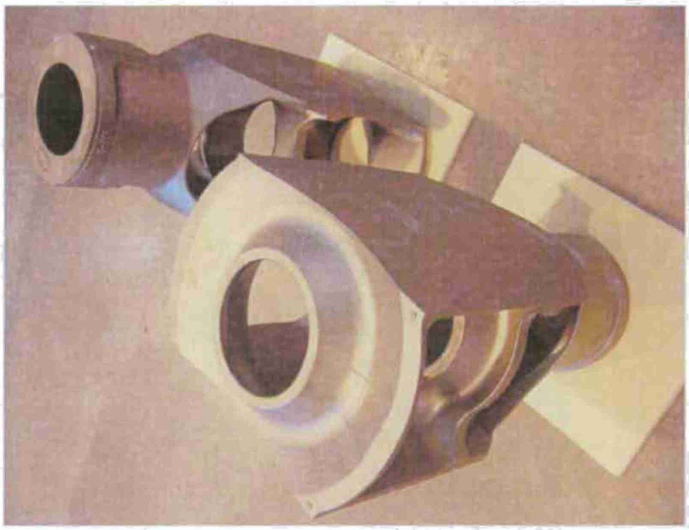

Wisconsin Investcast has run solidification analysis on several iterations of the cleaning mesh holder. The first optimization of the design for casting did not provide enough material at the joint between the tines and the handle. This led to failure of all but one shell while prototyping the next six parts. The same feature also caused the feed path to solidify; thus, leading to a shrinkage void in the "V" of the tines. An attempt to insure setup in a machining fixture led to a revised design, which did pass solidification analysis. This part is being jointly supported by the American Metalcasting Consortium.

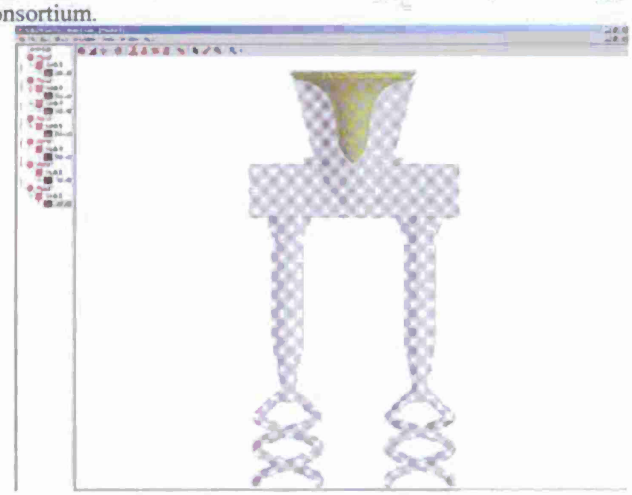

Initial material data on Eglin Steel has been passed along to Benet. The material holds promise for castings in lieu of titanium. Mechanical properties allow for thinner sections; thus, providing weight neutral applications. And, at only a fraction of the cost. HIPing the material provides for slightly higher and more consistent properties. HIPing appears to close up minor microporosity, which generally does not impact the key mechanical performance properties of steel castings. However, it does improve fatigue resistance in this case. The material was originally developed for penetrators by the AFRL at Eglin AFB and was to be made as a forging; a patent is jointly held by AFRL and National Forge. Current attempts to make the material by the forge have missed the mark on material properties; thus, a review of the process is currently underway.

Initial feedback on the mortar baseplate has been provided; awaiting next design iteration. Initial review of a conceptual NLOS-C muzzle brake shows potential for centrifugal casting; waiting on design data to be released. Sources were identified and quotations provided for a maraging steel motor bracket. PCC is providing modifications to the casting design. Mechanical properties of castings are determined in general by cast keel blocks per ASTM. Reference material on how these are determined and the correlation to the casting were provided to Benet. NDE

methods for casting and other manufacturing processes alike are workmanship standards. There is currently no correlation between a certain level and its respective impact on performance characteristics. A paper describing NDE processes and best practices was provided to Benet.

The first prototype breech nozzle was cast at Sivyer Steel in 8630, see figure below. The first run went well and it passed the requirements derived during the design review. Dimensional review of the casting identified two features that were out of tolerance. Benet waived these and the part was shipped for machining.

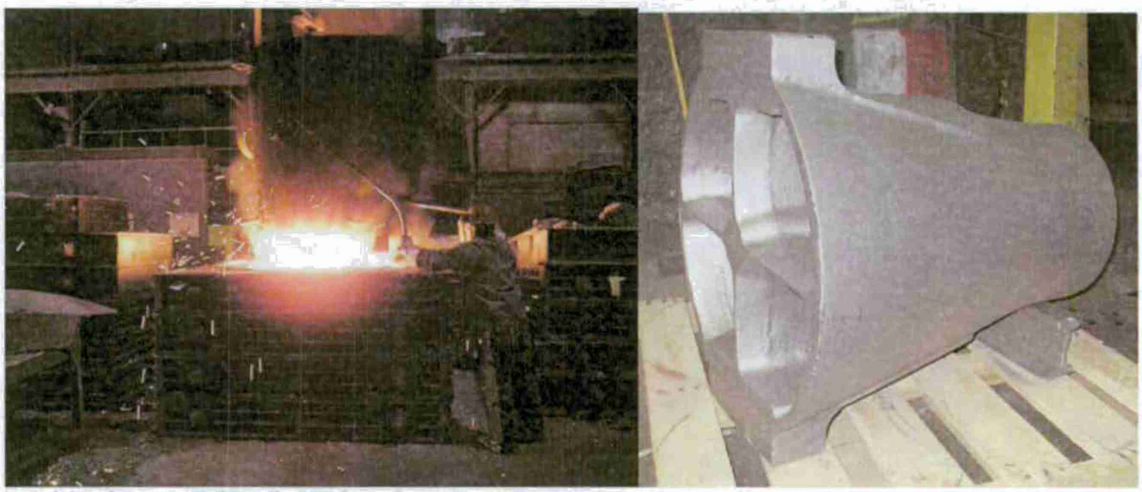

Pouring of prototype breech nozzle and as-cast part.

The tool will be modified to fix the two dimensional issues along with any other concerns noted by the machine shop. Production will begin shortly on making a second prototype breech nozzle in 17-4 PH (CB7Cu).

FoamCast tool is being made at Waukesha to produce a prototype muzzle brake. Technical assistance on cleaning mesh holder design was provided. Advanced steel alloys like cast Eglin Steel and cast Triplex are being investigated for potential Army applications. SFSA participated in the Technikon/Army Metalcasting Forum and continues to coordinate R&D for industry deployment.

The first prototype breech nozzle casting was machined by Ares. Ares noted stock should be added to the exhaust end to machine for setup and to the area where the bolt attaches to allow for more clean-up and fit. Sivyer Steel will coordinate with Ares for any other modifications to the pattern. Review of material options for a precipitation hardenable, corrosion-resistant cast steel such as CB7Cu is pending for manufacturing a second prototype. Final assembly of the RAVEN gun system should occur within the next couple of months.

FoamCast tooling to make the first prototype muzzle brake at Waukesha has been completed as shown in figure below. As-cast prototype should be completed by January 2009. Assistance offered to source cleaning mesh holder. SFSA continues to investigate Army applications for developmental, advanced alloys such as Triplex and Eglin Steel. An overview of the research was given at the SFSA annual meeting to facilitate transition of technology and production support at member steel foundries.

FoamCast pattern for M777 muzzle brake

SFSA and the Iowa universities are investigating a cast steel design for the 120mm mortar baseplate. A teleconference was held to discuss requirements and current design considerations. Technical data for the part has been passed along to the team. The team is currently waiting on a site visit to review the baseplate application to facilitate development of casting design considerations.

The first prototype breech nozzle casting was assembled into the gun system and sent to Ares for testing. Design and material options for the second prototype casting were discussed. Initial firing of gun system was successful and no indications from magnetic particle were identified. Higher pressures and number of rounds will be pursued. Correlation of tests results to FEA and discussion of casting design/manufacturing options will continue.

The FoamCast prototype casting of the muzzle brake was completed at Waukesha. The part along with test data and x-rays were sent to Benet. Initial review of the part is positive. The pouring and as-cast casting are shown in the figure below. SFSA continues to investigate Army applications for developmental, advanced alloys. Research projects were presented at the annual SFSA Technical and Operating Conference. On-site project reviews at all of the universities were held in February. Discussion facilitated the technical steering of the R&D towards industry value and provided key feedback on the continuing research.

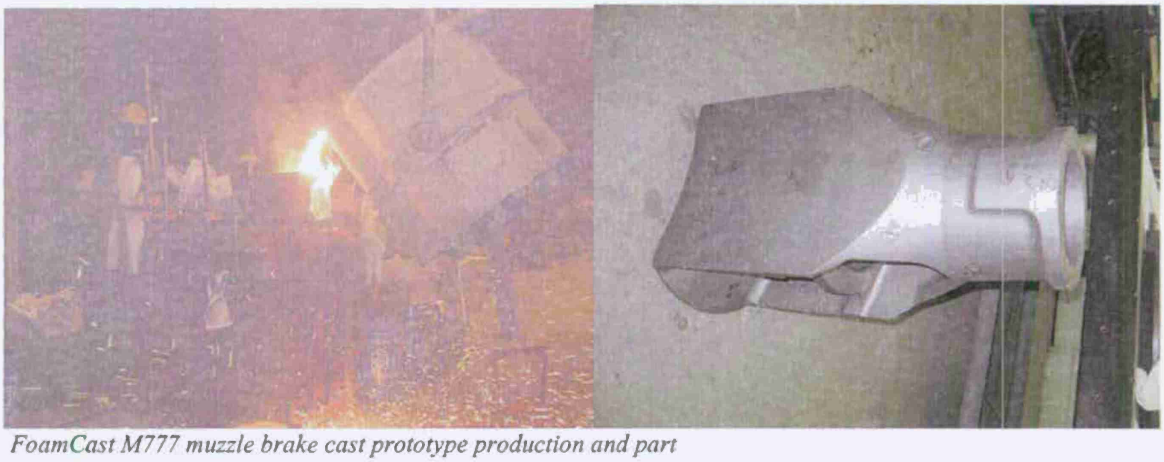

FoamCast M777 muzzle brake cast prototype production and part

SFSA and the Iowa universities have partnered with Benet on the development of a cast steel design for the 120mm mortar baseplate. The operation of the baseplate was viewed at Ft. Benning. Several conference calls have been held to review and discuss the design. Activity under the three universities will be discussed below.

Test data from firing of breech nozzle was reviewed. Crack in vane was analyzed and procedure for weld repair and adding material were provided. Options for creating an improved design for a second prototype were discussed. The FoamCast muzzle brake shortfall on properties was discussed. ASTM material requirements were reviewed. Opportunities for further action were discussed. Conference calls were held to discuss the solid models and

approach for tooling prototypes of the 120mm mortar baseplate. Material options from industry best practices were reviewed.

Options for creating an improved design for a second prototype were discussed. Confirmed properties and tooling changes for making the first prototype. SFSA and Sivyer reviewed tolerances and options to decrease weight to offset increasing vane thickness. SFSA reviewed crack in vane and provided support in developing a weld procedure for repair. Research projects were presented at the annual Carbon and Low Alloy Research Review in July. Discussion facilitated the technical steering of the R&D towards industry value and provided key feedback on continuing research. Issues with tooling solid models were resolved, option to modify design discussed, and problems with development of Rapid Pattern Machine were resolved. ACIPCO was integrated into the team to cast the part out of their high strength alloy and to provide additional post-processing for the cast prototypes.

The National T&O Conference was held in Chicago to disseminate the technology to industry. Discussion were held at meetings at each of the universities in February. A workshop was completed at the T&O to demonstrate the application of the R&D on the Breech Nozzle. The University of Iowa performed the engineering for the second iteration on the breech nozzle design. Three prototypes were poured in Eglin Steel and process improvement was made to the baseplate tooling from ISU. Three prototypes baseplates were processed and machined in Eglin Steel. Tooling was modified and work started on the second prototype of the breech nozzle. Tooling was modified and prototype casting was produced at Sivyer and sent to Ares for machining.

Work initiated on modeling the FAS muzzle brake in conjunction with the effort at Waukesha Foundry. Seminar held for Benet on modeling service performance prediction. Supported allocation for Magma software at Benet. Other activity supporting industry deployment and engineering support to the government included integration of project in industry. Demonstrator steel casting identified with the FAS muzzle brake. Design input provided and sources for manufacturing prototypes identified. Tooling and manufacturing the first production prototype initiated. Also reviewed potential to utilize NLOS-C muzzle brake design for other systems such as the Paladin. Modeling of encapsulated armor tile with cast steel completed by UI. Proprietary porous ceramic process will be utilized to produce ballistic test castings. FOPAT test prototype failed due to both cracking in both the steel and the ceramic. Gating and process need to be optimized to improve encapsulation process. Trial methods for the encapsulation process will be investigated at both Nova and Spokane. Based upon results from ARL work, effort will be spent on promising results of encapsulated tile process versus casting a crate design. Materials and size of plates identified for ballistic testing; tool being produced by Nova.

FAS Crank requirements reviewed and modifications provided. Carbon and Low Alloy Research Review held in Chicago. High Alloy Research Review held in Pittsburgh in conjunction with Foseco. Wollaston and McConway & Torley, for Eglin Steel, have both offered to support deployment with demonstrator castings. Other activity supporting industry deployment and engineering support to the government included integration of project in industry. Plan was discussed at SFSA annual meeting to develop a core group of defense steel foundries to support R&D development and deployment. Supported JDMTP reviews at Benet and in Columbus, OH. Technology transition discussed with Pennsylvania foundry group and facilitated BAE meeting at AFS that centered on Bradley applications. FAS muzzle brake first prototype completed and shipped to Benet. Dimensional inspection was completed via laser scan versus inspection fixture to expedite delivery. The second and third prototypes are in process with completion expected around late September. Tooling fixture completed and will be used to inspect the second two parts. Issue with macro inclusions present on castings #2 and #3; Waukesha will repair weld as required to meet the drawing and continue to work on process improvement to reduce the problem. Results of modeling provided to Nova. Maximum size for porous ceramic process established. Several tests have been run at both Nova and Spokane for encapsulating the tiles. Initial success may be proven via casting CA6NM and alumina tiles. Tooling created at Nova. Waxes sent to Mercury Marine and 15-5 material poured and shipped to ARL. Questek produced material shipped to ARL.

FAS Crank purchase order initiated and castings poured from QuickCast SLAs at Metaltek. Technology transition at the Defense Manufacturing Conference. Supported JDMTP metals subpanel. Developed follow-on research plan for sand characteristics at UNI. Support provided to the development of casting capability at UAB. Worked on the development of RT standard with UI. FAS muzzle brake prototype activity closed out; discussion of options to utilize design on other weapon systems. Effort at Spokane focused on encapsulating alumina tile, which resulted in

a successful prototype that will be sent to ARL. Initial tests of tile encapsulation at Nova have not yielded good tile encapsulation; rigging design change will be completed for additional trials. Material for Eglin Steel and ASTM A487 Grade 10 Class B poured for ballistic test plates; additional alloy from latest MS&T R&D will also be made. Integrated new data into DECAF, developed new report functions, and implemented process for refining the data to get confirmed castings. Deployed Metalcasting Concepts seminar at Warner Robins AFB. On-site support and routine should cost analysis provided.

FAS Crank castings made at Metaltek but failed to meet properties after second heat treat. Due to consumption of test bars, the third part was section to obtain additional samples and the parts were re-heat treated. Fourth SLA and new test bars were made to replace the third part. First and second part were still slightly out of material spec after third iteration of heat treatment. Three parts should ship in April. Obtained quotations for two FAS levers. Discussed implications of risk/cost with prototype parts being manufactured from soft tooling and obtaining tight tolerances (also, impact of business conditions on lead-times). Provided review and assessment of galvanic corrosion with 17-4 PH and low alloy steels. Discussed assistance on component for vertical heat treat furnace (CLIN for application support an option). Discussed the candidate project to develop a cast steel 81mm mortar baseplate through the UI performance modeling. Depending on the status of the RAVEN system, additional design modifications to the breech nozzle could be pursued. Research review at UI with UNI and at ISU. Assisted with industry support for AFS/Saginaw FeMnAl machinability project. Additional modeling for M777 muzzle brake could be added to SOW to support effort at either Waukesha or RIA. Technology transition with Jerry Call at AFS, met with AIST to discuss steel making technology, met with Southern Cast Products, met with Bradken-Chehalis, met with Pacific Steel and supported AFS chapter meeting. Test plates at the range for firing. Identified issue with integration of Aviation data, discussed team use of data at DSCR's joint DLA team meeting, and establish plan to distribute data to AMC partners such as ATI and NFFS. Discussed Metalcasting Concepts seminar at Warner Robins AFB in May and NAVSEA Keyport in August; March seminar at DSCC delayed due to funding. Two on-site DSCC support visits provided and routine should cost analysis supported. Assisted Redstone Arsenal with design input on a 2.75" cone components.

Final FAS Crank casting was made but failed to hit properties likewise; however, was accepted with given properties and shipped to Benet. Sought two additional sources for two FAS levers. Reviewed TDPs for levers and provided recommendations. Provided technical assessment of fixture for vertical heat treat furnace. Preparation for C&LA Research Review. Integration of project within industry including meeting with Waukesha on military supply. Supported JDMTP metals subpanel meeting at Benet. Met with OSD to discuss industry capability. Technology steering at the AFS Metalcasting Congress. Met with Beckerman to discuss transition of R&D. Worked on integration of confirmed castings with surge requirements.

Test module setup for relationship form, working on development of standard queries, determined not to pursue SQL, investigating means to confirm what table is in the POT, and setting a process to prioritize CIS review as conversion nears completion. Casting research training at SFSA T&O and plans set for next Metalcasting Concepts seminar at DSCC in March. On-site DSCC support provided in November. Should cost requests have increased dramatically with the new GFY. Support provided on potential reverse engineering cases for door handle and pump. Continued cost assessment support provided on titanium casting with TSS for DSCP.

Capability for standard query completed along with ability to extract confirmation tables in the POT, uploaded the latest confirmation dataset with the inclusion of ZD047, relationship form incorporated into live database, and work completed by CIS on data conversion and now progressing on unconfirmed parts from PinPoint and other sources with priority set to AMSC G, B, and T items, investigating means to integrate tooling and sourcing websites into government systems, working on VE field for EBS which would include UMR tag for C/F. Metalcasting Concepts seminar and tours provided at DSCC in March, and identified opportunities to update seminar material. On-site DSCC support provided in January and March. Should cost requests remain high while website assistance requests are fairly low. Should cost project done for a family of gun system components. Should cost support provided on Navy diffuser to substantiate a case for reverse engineering. Ability to add C/F tag in IBMS for surge is awaiting action by contractor. Pump not being pursued for reverse engineering due to complexity and lack of savings. 7.62 suppressor casting design and sourcing support provided to Picatinny. Identified new opportunities to pursue RSW assistance, process/material marketbasekets, and request for foundry source in contract.

Program management utilities developed in DECAF, which should enable direct input of data fields into VE Stars for tracking, CIS working on new unconfirmed parts to increase population of parts in DECAF, utilizing data in DECAF to develop "big ideas" for the site, and setting up a macro to export snapshot of database. Metalcasting Concepts seminar provided at Warner Robins AFB. Support was provided to DSCC in conjunction with the AFS Metalcasting Congress and the DLA Land and Maritime Supplier Conference in addition to a joint supply center team meeting. Should cost requests continue at a higher pace, which matches a higher utilization of this activity by buyers. Website assistance requests are fairly low due to an inadvertent error in the contact form. Working on three big ideas to support DSCC's command initiative. C/F tag in IBMS for surge is complete and ready for integration into the LTC/surge process. Casting support provided to Picatinny for a Firing Platform.

Cast Steel Encapsulated Ceramic Armor Tile

Three major objectives were identified in this project. One,to encapsulate ceramic Armor tiles with the new investment casting pattern material, FOPAT. Two, to inspect the ceramic tile by x-rays in the as-injected and shelled condition prior to investment casting. Three, to investment cast metal around the Silicon Carbide (SiC) tile on a best effort basis.

An aluminum tool was made that would enable a SiC disc (provided by ARL) to be positioned in the die and allow approximately 0.125" of FOPAT investment casting pattern material to be injected around the disc. Approximately 4 SiC discs, 2 each of fully machined and 2 each of as-pressed were encapsulated into FOPAT and sent to MetalTek Investcast in Watertown, Wisconsin for casting. Triplex (FeMnAl) alloy was selected by the project team as the casting alloy. The preheat temperature was 2000 F and the mold was heavily covered with Kaowool insulating blanket to hold in the heat to minimize the thermal difference between the metal, shell and SiC disc.

The results are shown below. As seen in the photos below, the first two project objectives were successfully completed, however, the casting had hot tears. In order to improve the casting results, a single gate may be a better option and looks like it could have prevented the tearing at the top. The alloy still split at the seams of the silicon carbide probably due to residual stresses from the sharp edge. We would suggest that those edges be rounded or chamfered in the future.

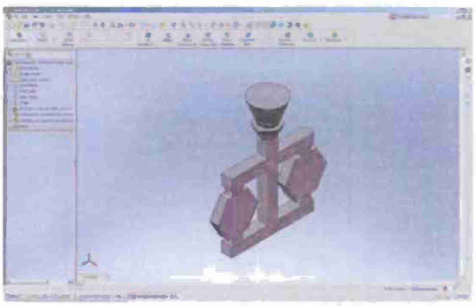

CAD View or 3D Visual of the Assembly of the Two Parts to be Cast

SiC Armor Disc Encapsulated with FOPAT Patterns with Stainless Steel Locating Pins

FOPAT Patterns with Gating, Sprues and Pour Cup

Investment Casting Ceramic Shell

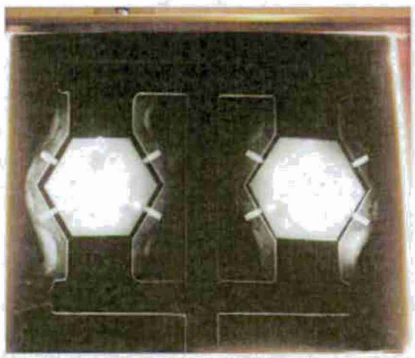

X-ray of Shell Showing Good Positioning of the SiC Discs

Casting After Pouring Just After Shell Removal Showing the Hot Tearing

Additional trials to encapsulate armor tiles were completed at Nova Precision Castings and

Spokane Industries. From these trials one critical technical hurdle was identified, the reaction created by molten steel contacting the Si-C tile. Both silicon and carbon are components of cast steel; thus, they readily react which causes both a chemical reaction and leads to tearing of the metal. The sharp edges on the tiles may also be creating a higher propensity for hot tearing of the metal, and could adversely impact the ballistics.

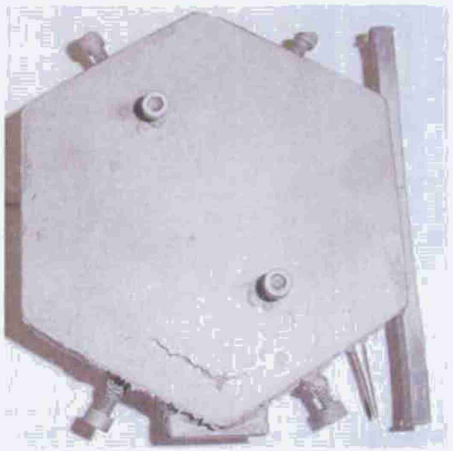

Nova pour 1 with CF8M to reduce hot tearing and test rigging

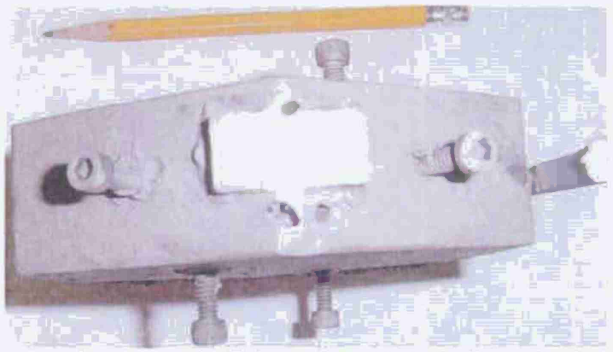

Nova pour 1 with some gas bubbles on top side indicating potential reaction

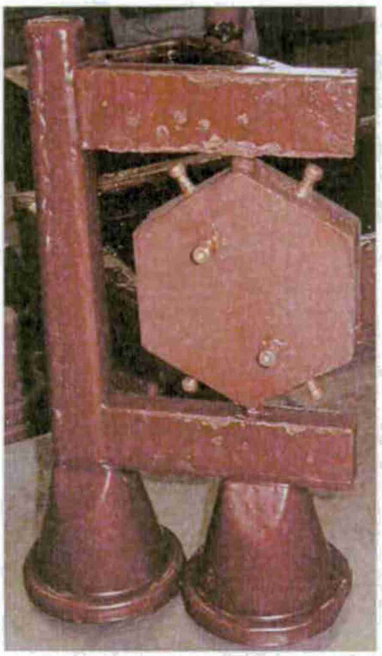

Nova rigging for encapsulated ceramic tile

Nova wrapped investment shell

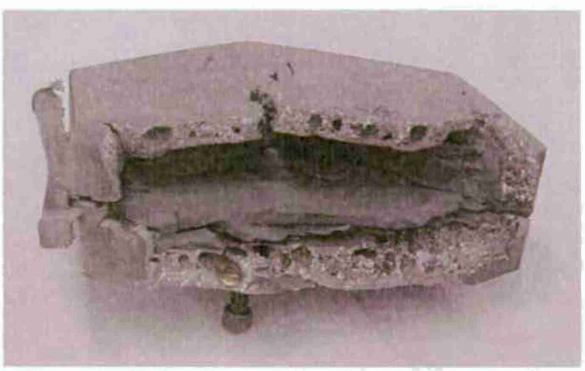

Nova pour 2 showing metal cracking and gas reaction

Spokane pour 1 in 8630 – no visible metal cracks

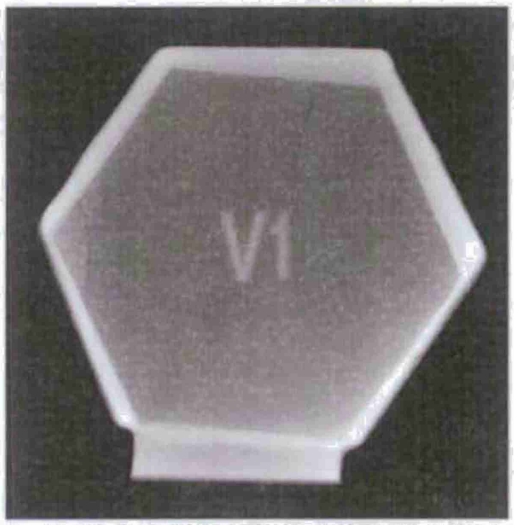

Spokane pour 1 with alumina tiles – two cracks and tile shifted appear in x-ray

Spokane pour 2 with 8630 and Si-C shows both reaction and cracking of both metal and tile

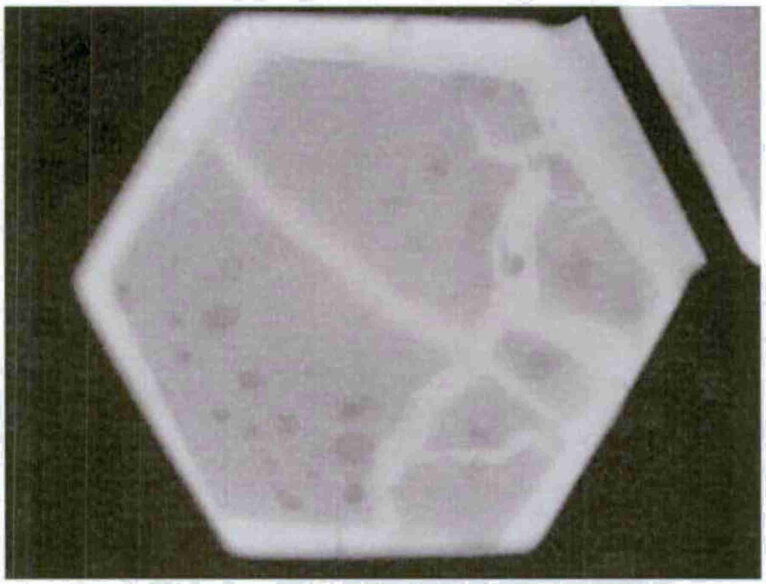

Spokane pour 2 x-ray shows reaction pores and cracking

Nova did not pursue casting an egg crate casting to press fit tiles as this approach was deemed not cost-effective compared to existing technology, which does the same with titanium. Utilizing the Eglin Steel alloy, this approach has resurfaced in conjunction with both M Cubed and REL to enable the use of nonferrous alloys, which serves as the means of contact between the tile and metal. Nova also cast ballistic test plates in 4325 and Eglin Steel to acquire data on the performance of the material. These same plates were also cast by Mercury Marine in their as-cast 15-5 PH alloy that is used for boat propellers.

Ferrium C61 and Ferrium M54 Ballistic Performance

The objective of this effort was to deliver plates of Ferrium C61 and Ferrium M54 for ballistic testing. Panels were to be delivered in sets of three with approximate dimensions of 0.25" x 6" x 12". The data should be compared against current available test data to determine if equivalent performance with cost reduction or enhanced performance can be achieved. The plates are to be delivered to the Army Research Laboratory for ballistic testing and compared to prior data. An example of the prior test data is shown in the Figure below.

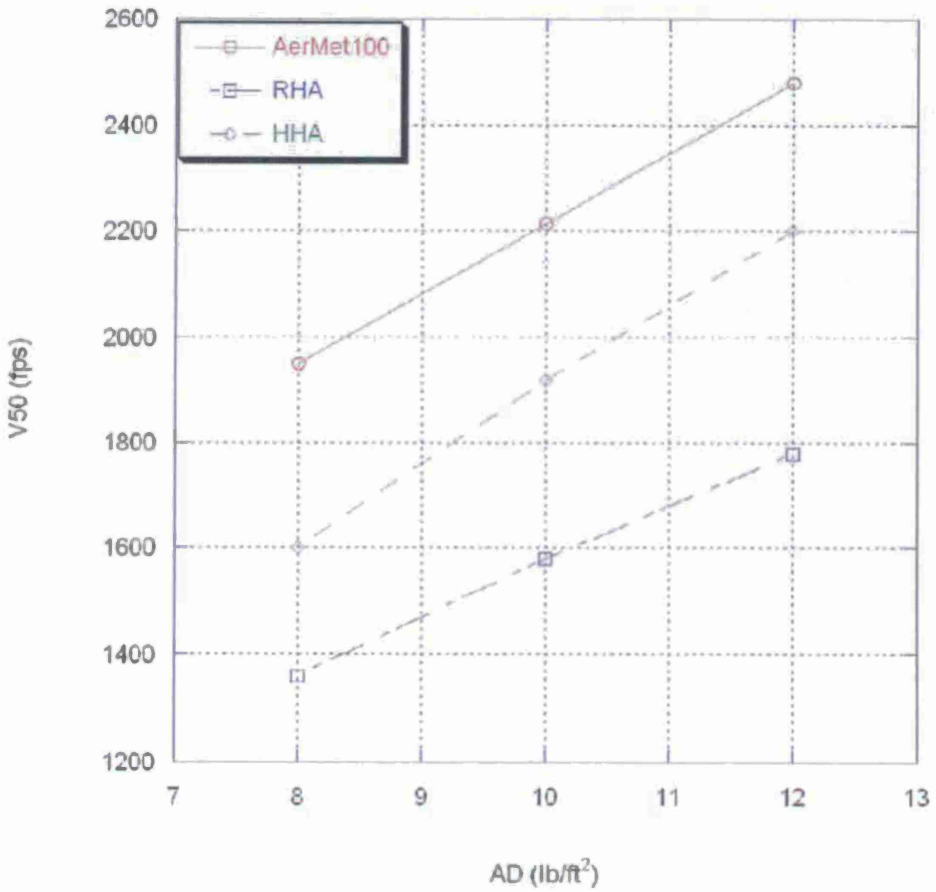

Figure V50 values for various materials as a function of aerial density

A summary of the test plate production is given within this document. There are three case-hardened Ferrium C61 plates that have a surface hardness of ~60HRC with a case depth of ~0.040" (measured at 52HRC) and a core hardness of ~49HRC. The dimensions of the plates are ~0.25" x 6" x 12". There are three Ferrium M54 plates that have a hardness of 54HRC, and is most similar to AerMet® 100 in material properties but with a lower procurement cost.

This technical memorandum details the processing of three plates each of Ferrium® C61™ and Ferrium® M54™ for ballistic testing.

Ferrium® C61™ Plate Processing

Test plates of Ferrium C61 were produced from rolled plate stock. The original plate size was ~0.45" x ~7" x ~25" and was from heat number HB72. Three plates were cut from this stock to produce 6" x 12" rectangular plates. To remove the decarburized layer produced during the rolling process, the plates were ground ~0.090 on each side to produce plates that were ~0.275" thick. The three plates, ~0.275" x 6" x 12", then received thermal processing at Solar Atmospheres (Souderton, PA). The plates vacuum carburized at 1832F, gas-quenched, sub-zero cooled at -100F for 1 hour, tempered at 975F for 2 hours, and a second temper at 900F for 12 hours. The original heat temper treatment intended was 900F for 16 hours, but there was an error in the purchase order and a furnace control issue during processing. While there was a variance from the intended processing, there does not appear to be an adverse impact on the structure or hardness of the test plates. The thermal processing charts can be viewed in the appendix with a description of the tempering cycle.
Superficial hardness measurements were completed on one plate, while hardness profile and microstructure were evaluated using a carrier piece that was 1" RD x 0.5" thick. The superficial hardness measured was 77 to 78 HR30N (~59-60HRC). Results from the carrier piece are shown in Figure 1 Figure 2 below.

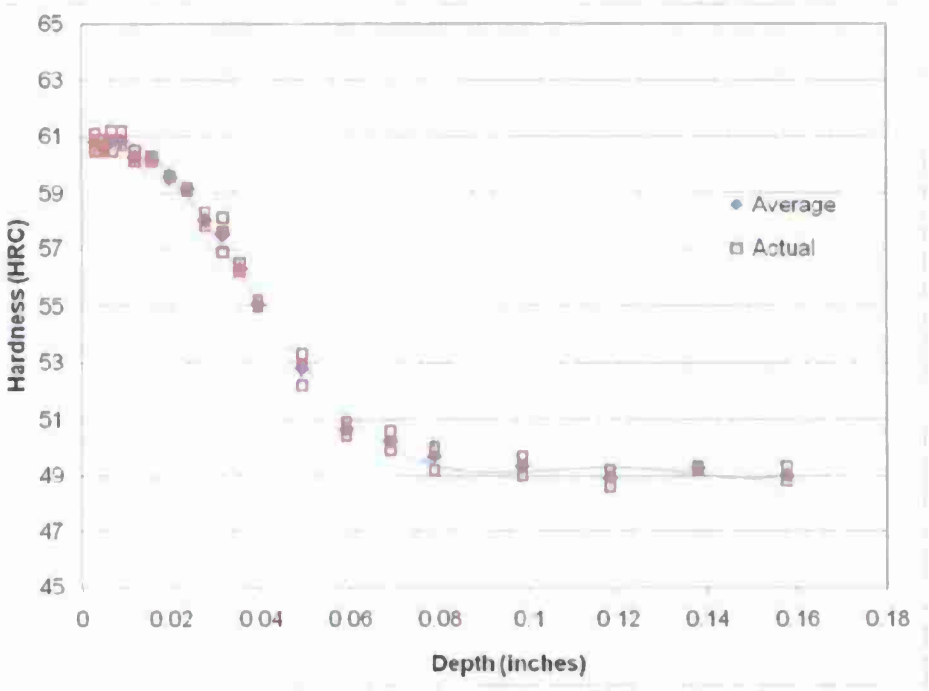

Figure 1 Microhardness profile of carrier specimen for Ferrium C61 ballistic plates indicating a 60HRC surface hardness with a depth of 0.04" at 52HRC (superficial hardness measurements on plates measured 59 - 60HRC)

Figure 2 Micrograph of carrier puck showing a microstructure free of primary carbides.

After thermal processing, the test plates were then ground up to 0.008" to remove any surface oxide or decarburization layer that may have occurred during processing. The ground surface of the plates are to be ballistic tested. An image of two plates showing the ground side and one plate showing the back with labeling is shown in Figure 3 below.

Figure 3 Left: Machined, side for ballistic testing; Right: non-machined, labeled "Ferrium C61 (backside)" not intended for ballistic testing

Ferrium® M54™ Plate Processing

Test plates of Ferrium M54 were produced from bar stock. The original bar stock was 7.5" x 7.5" x 12" and was from heat number A0029. Three plates were wire EDM cut from this stock to produce 0.285"x

6" x 12" rectangular plates. The three plates, 0.285" x 6" x 12", then received thermal processing at Bodycote Thermal Processing (Sturtevant, WI). The plates vacuum solution treated at 1940F for 1.5 hours, gas-quenched, sub-zero cooled at -100F for 1 hour, and tempered at 977F for 6 hours. Hardness measurements and microscopy were completed on a carrier piece of material that was of the same thickness and from the same heat as the plates. The original hardness profile indicated that there was a remnant layer still left from the wire EDM operation that was ~0.05" in depth (Figure 4). To remove this, the three plates had 0.055" ground from the ballistic test side and 0.005" ground from the backside (required for alignment in Blanchard grinder). After grinding, the final dimensions of the three test plates are 0.24" x 6" x 12". The hardness of the test surface was measured to be 54HRC in carrier specimen. The micrograph shows a lath martensitic structure with no inclusions (Figure 5).

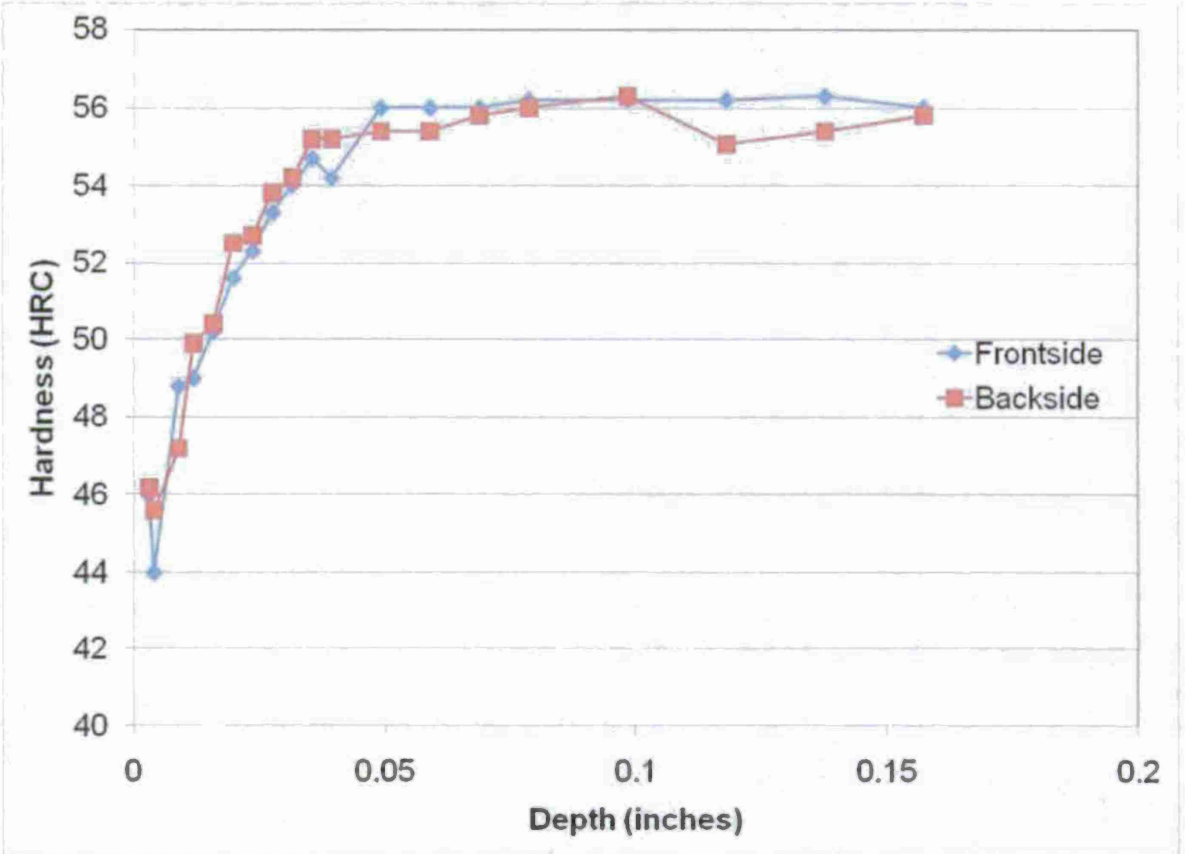

Figure 4 Microhardness trace from edge of plate toward center showing an interaction/decarb layer of 0.050" that needs to be removed from test side.

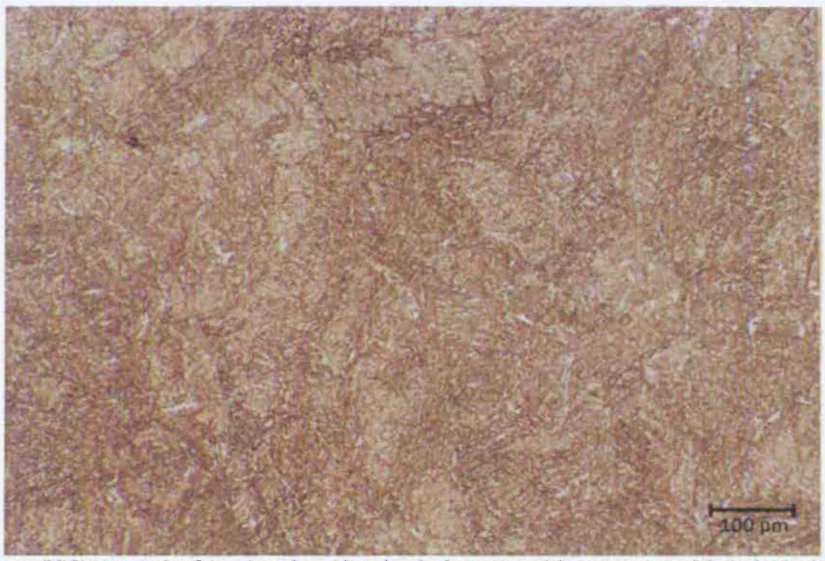

Figure 5 Micrograph of carrier piece showing lath-martensitic structure with no inclusions.

The ground surface (machined side, 0.055" removal) of the plates are to be ballistic tested. An image of two plates showing the ground side and one plate showing the back with labeling is shown in Figure 3 below.

Figure 6 Left: Machined side for ballistic testing; Right: non-machined, labeled "Ferrium M54 (backside)" not intended for ballistic testing

Development of Casting Procurement Tools

NFFS has an established bid matching service to monitor government solicitations for those items in the cast tooling database and the confirmed casting database were the national stock number has been identified. In addition to the DLA Internet Bid Board System (DIBBS), other procurement sites are included in this process to include, but not limited to, Fedbizopps.gov, Army Acquisition Business Website, and Navy Electronic Commerce Online.

Solicitations for parts that are in the tooling database are directed to the foundries that already have tooling available on the day that the solicitation is posted. During the 1st quarter of 2011, NFFS directed 409 solicitations with an estimated value of $7.1 million (based on prior procurements) to foundries that already have tooling. Of the 409 solicitations, there were solicitations for 97 parts that had not been purchased in the last 5 years, and 50 of the 97 had not been procured in the past 10 years. Therefore, nearly 25% of the parts in these solicitations have not been procured in 5-10 years which would indicate that without the procurement solutions network, there is a greater risk for these items to have fragmented supply chains and may require significant cost and lead-times to establish new casting sources. NFFS tracks each of these solicitations and will review each of these with the foundry participants to assess how many were awarded to the foundry and the impact on costs and lead-times.

For government parts identified as confirmed castings but the tooling source is not known, NFFS utilizes the defense casting suppliers database and directs the solicitation to the foundries that are uniquely qualified to respond to the bid based upon that company's profile. This enables the foundries to make a timely and informed business decision on determining which solicitations to pursue and has been proven to be an effective resource that has assisted many foundries in securing new business. During the quarter, NFFS directed 14 confirmed casting solicitations to approximately 40 foundries (on average) from the Defense Casting Suppliers Database per solicitation. Not all confirmed casting solicitations are sent out and are filtered based on anticipated dollar value, time since prior procurement, and acquisition method code.

NFFS sent out the bi-annual updates to all of the companies in the tooling database via e-mail. A spreadsheet of all the pattern records is distributed to each company twice a year for review. The companies will update NFFS on new patterns, scrapped patterns, and change in information on existing patterns. The update went out in early March and typically takes several weeks to receive everyone's update and incorporate all of the changes. As of the end of March, there were approximately 200 new defense patterns listed and some 140 patterns where the foundry indicated they no longer had the tooling. The importance of this is while the tooling location may no longer be available for these items, it is still useful to know what parts that the foundry has manufactured in the past.

During the quarter, NFFS received a total of 22 inquiries from defense contractors (not including inquiries to DSCR) searching for tooling and casting sources. NFFS was able to find a match to existing tooling for 10 of the 22 inquiries. In addition, NFFS offered assistance in helping the contractors to find potential casting source based upon the part in addition to leveraging the

casting supplier database.

In January, NFFS completed the implementation of a new bid matching software system. The new system provides a number of features that enhance the efficiencies and capabilities of the procurement solution tools. One feature is the ability to categorize lists of NSN's within the software and color code solicitations so that the user can quickly identify, by color, which category the part belongs such as tooling, confirmed casting, suspect, etc. Secondly, the software connects the DLA's cFolders system and automatically downloads and stores all available drawings for each solicitation. This enables staff to review tech data packages in a more timely fashion to both confirm casting content and identify material and process for existing tooling database records.

In an effort to increase confirmed cast NSN's, the bid matching software company also completed a study for NFFS on researching all Federal Logistics Information System (FLIS) records for the word 'cast' in 3 specific fields: Procurement Item Description, Technical Characteristics, and Drawing/Specification Title fields. The study resulted in more than 80,000 parts with national stock numbers returned. The initial focus is to monitor items within the list that have a higher probability of being a confirmed cast part – particularly looking at those items with 'cast' tech. characteristics or drawing title fields. The initial population to research resulted in more than 20,000 items.

The new population was appended to the population of the casting NSN list that NFFS monitors for solicitations. As a result, there were more than 1,800 solicitations reviewed during the quarter, 409 of which were matched to tooling and directed to the appropriate metalcasting facilities. The balance of the solicitations were reviewed to confirm casting content and update the part search database and distributed accordingly. As of the end of the quarter, 125 new NSN's were confirmed with castings. In addition, NFFS confirmed 25 new NSN's by matching available part drawings to orphan part numbers in the tooling database. Finally, approximately 170 tooling records have had the material and process fields updated based upon information from the drawings.

Deployment of Casting Procurement Tools

NFFS has an established bid matching service to monitor government solicitations for those items in the cast tooling database and the confirmed casting database were the national stock number has been identified. In addition to the DLA Internet Bid Board System (DIBBS), other procurement sites are included in this process to include, but not limited to, Fedbizopps.gov, Army Acquisition Business Website, and Navy Electronic Commerce Online.

Solicitations for parts that are in the tooling database are directed to the foundries that already have tooling available on the day that the solicitation is posted. During the 4th quarter of 2011, NFFS directed 434 solicitations with an estimated value of $7.4 million (based on prior procurements) to foundries that already have tooling. Of the 434 solicitations, there were solicitations for 95 parts that had not been purchased in the last 5 years, and 40 of the 95 had not been procured in the past 10 years. Therefore, more than 21% of the parts in these solicitations have not been procured in 5-10 years which would indicate that without the procurement

solutions network, there is a greater risk for these items to have fragmented supply chains and may require significant cost and lead-times to establish new casting sources. NFFS tracks each of these solicitations and will review each of these with the foundry participants to assess how many were awarded to the foundry and the impact on costs and lead-times.
For government parts identified as confirmed castings but the tooling source is not known, NFFS utilizes the defense casting suppliers database and directs the solicitation to the foundries that are uniquely qualified to respond to the bid based upon that company's profile. This enables the foundries to make a timely and informed business decision on determining which solicitations to pursue and has been proven to be an effective resource that has assisted many foundries in securing new business. During the quarter, NFFS directed 12 confirmed casting solicitations to approximately 40 foundries (on average) from the Defense Casting Suppliers Database per solicitation. Not all confirmed casting solicitations are sent out and are filtered based on anticipated dollar value, time since prior procurement, and acquisition method code.

Solicitations for parts that are in the tooling database are directed to the foundries that already have tooling available on the day that the solicitation is posted. During the 1st quarter of 2012, NFFS directed 438 solicitations with an estimated value of $10.9 million (based on prior procurements) to foundries that already have tooling. Of the 438 solicitations, there were solicitations for 100 parts that had not been purchased in the last 5 years, and 28 of the 100 had not been procured in the past 10 years. Therefore, 23% of the parts in these solicitations have not been procured in 5-10 years which would indicate that without the procurement solutions network, there is a greater risk for these items to have fragmented supply chains and may require significant cost and lead-times to establish new casting sources. NFFS tracks each of these solicitations and will review each of these with the foundry participants to assess how many were awarded to the foundry and the impact on costs and lead-times.

For government parts identified as confirmed castings but the tooling source is not known, NFFS utilizes the defense casting suppliers database and directs the solicitation to the foundries that are uniquely qualified to respond to the bid based upon that company's profile. This enables the foundries to make a timely and informed business decision on determining which solicitations to pursue and has been proven to be an effective resource that has assisted many foundries in securing new business. During the quarter, NFFS directed 10 confirmed casting solicitations to approximately 45 foundries (on average) from the Defense Casting Suppliers Database per solicitation. Not all confirmed casting solicitations are sent out and are filtered based on anticipated dollar value, time since prior procurement, and acquisition method code.

Solicitations for parts that are in the tooling database are directed to the foundries that already have tooling available on the day that the solicitation is posted. During the month of April 2012, NFFS directed 190 solicitations with an estimated value of $1.63 million (based on prior procurements) to foundries that already have tooling. Of the 190 solicitations, there were solicitations for 42 parts that had not been purchased in the last 5 years, and 20 of the 42 had not been procured in the past 10 years. Therefore, 22% of the parts in these solicitations have not been procured in 5-10 years which would indicate that without the procurement solutions network, there is a greater risk for these items to have fragmented supply chains and may require significant cost and lead-times to establish new casting sources. NFFS tracks each of these solicitations and will review each of these with the foundry participants to assess how many

were awarded to the foundry and the impact on costs and lead-times.

For government parts identified as confirmed castings but the tooling source is not known, NFFS utilizes the defense casting suppliers database and directs the solicitation to the foundries that are uniquely qualified to respond to the bid based upon that company's profile. This enables the foundries to make a timely and informed business decision on determining which solicitations to pursue and has been proven to be an effective resource that has assisted many foundries in securing new business. During the month, NFFS directed 3 confirmed casting solicitations to approximately 40 foundries (on average) from the Defense Casting Suppliers Database per solicitation. Not all confirmed casting solicitations are sent out and are filtered based on anticipated dollar value, time since prior procurement, and acquisition method code.

In summary, NFFS directed 1,062 solicitations with an estimated value of $20 million (based on prior procurements) to foundries with tooling.

NFFS distributes spreadsheets of pattern records for each company in the tooling database twice a year for review. The companies will update NFFS on new patterns, scrapped patterns, and change in information on existing patterns. The update is scheduled for February 2012.

NFFS sent out the bi-annual updates to all of the companies in the tooling database via e-mail. A spreadsheet of all the pattern records is distributed to each company twice a year for review. The companies will update NFFS on new patterns, scrapped patterns, and change in information on existing patterns. The update went out in early March and typically takes several weeks to receive everyone's update and incorporate all of the changes. As of the end of March, NFFS had received responses from more than half of the companies in the database and plans to follow-up with the other companies in April.

NFFS received a tooling list from Rock Island Arsenal in late March to be added to the tooling database. The list contains records for approximately 235 sand and investment cast patterns. Staff began research to complete the records to identify national stock number and material.

In summary, Bi-annual tooling database record update was completed.

During the quarter, NFFS received a total of 32 inquiries from defense contractors (not including inquiries to DSCR) searching for tooling and casting sources. NFFS was able to find a match to existing tooling for 15 of the 32 inquiries, nearly a 50% success rate. In addition, NFFS offered assistance in helping the contractors to find potential casting source based upon the part in addition to leveraging the casting supplier database.

During the quarter, NFFS received a total of 21 inquiries from defense contractors (not including inquiries to DSCR) searching for tooling and casting sources. NFFS was able to find a match to existing tooling for 3 of the 21 inquiries. In addition, NFFS offered assistance in helping the contractors to find potential casting source based upon the part in addition to leveraging the casting supplier database.

During the quarter, NFFS received a total of 7 inquiries from defense contractors (not including

inquiries to DSCR) searching for tooling and casting sources. NFFS was able to find a match to existing tooling for 1 of the 7 inquiries. In addition, NFFS offered assistance in helping the contractors to find potential casting source based upon the part in addition to leveraging the casting supplier database.

In summary, NFFS received a total of 60 inquiries from defense contractors (not including inquiries to DSCR) searching for tooling and casting sources. NFFS was able to find a match to existing tooling for 17 of the 60 inquiries.

Of the 30,000 National Stock Numbers of both confirmed and unconfirmed cast parts that NFFS monitors for bid solicitation activity, there were more than 1,800 solicitations reviewed during the quarter, 434 of which were matched to tooling and directed to the appropriate metalcasting facilities. The balance of the solicitations were reviewed to confirm casting content and update the part search database and distributed accordingly. As of the end of the quarter, 160 new NSN's were confirmed with castings. In addition, NFFS confirmed 20 new NSN's by matching available part drawings to orphan part numbers in the tooling database. Finally, approximately 240 tooling records have had the material and/or process fields updated based upon information from the drawings.

Of the 30,000 National Stock Numbers of both confirmed and unconfirmed cast parts that NFFS monitors for bid solicitation activity, there were more than 2,000 solicitations reviewed during the quarter, 438 of which were matched to tooling and directed to the appropriate metalcasting facilities. The balance of the solicitations were reviewed to confirm casting content and update the part search database and distributed accordingly. As of the end of the quarter, 180 new NSN's were confirmed with castings. In addition, NFFS confirmed 35 new NSN's by matching available part drawings to orphan part numbers in the tooling database. Finally, approximately 300 tooling records have had the material and/or process fields updated based upon information from the drawings.

Of the 30,000 National Stock Numbers of both confirmed and unconfirmed cast parts that NFFS monitors for bid solicitation activity, there were more than 500 solicitations reviewed during the month, 190 of which were matched to tooling and directed to the appropriate metalcasting facilities. The balance of the solicitations were reviewed to confirm casting content and update the part search database and distributed accordingly. As of the end of the April, 45 new NSN's were confirmed with castings. In addition, NFFS confirmed 5 new NSN's by matching available part drawings to orphan part numbers in the tooling database. Finally, approximately 75 tooling records have had the material and/or process fields updated based upon information from the drawings.

In summary, NFFS confirmed 60 new NSN's by matching available part drawings to orphan part numbers in the tooling database, approximately 615 records in the tooling database had the material and/or process fields updated based upon information from the drawings, and NFFS researched tech data packages of 'suspect cast parts list' and confirmed 385 NSNs that contained castings.

Conclusions

SFSA is uniquely positioned through its industry leadership steel casting R&D to assume a prominent role in the development of industry-ready, performance steel casting technology. SFSA is an approved supplier of steel casting R&D to the steel foundry industry and the markets they support.

SFSA provides many critical cast steel system components to the Department of Defense such as cleats, ejection chutes, control arms, muzzle brakes, mortar components, clevises, tow bar clamps, ammo conveyor elements, hydraulic accumulators, etc. Steel castings also provide many critical commercial products such as pumps and valves, nuclear components, and railroad couplers, side frames, and bolsters. Development of new technology for this manufacturing sector is critical to the continued longevity of the industry and the ability to produce complex metal shapes.

This program strengthened SFSA's capability and allowed us to better serve the DOD's requirements to support improved reliability, light weight, high performance weapon systems. The approach taken by SFSA in this initiative was to apply the latest technologies to improve the steel casting design and manufacturing.

Appendix A: SF 298

REPORT DOCUMENTATION PAGE	

PLEASE DO NOT RETURN YOUR FORM TO THE ABOVE ADDRESS.

1. REPORT DATE	2. REPORT TYPE	3. DATES COVERED
30-09-2012	Final Report	03 Nov 2006 - 30 Jun 2012

4. TITLE AND SUBTITLE Performance Steel Castings	5a. CONTRACT NUMBER W15QKN-08-2-0007
	5b. GRANT NUMBER
	5c. PROGRAM ELEMENT NUMBER
6. AUTHOR(S) Poweleit, David, R. Monroe, Raymond, W.	5d. PROJECT NUMBER
	5e. TASK NUMBER
	5f. WORK UNIT NUMBER
7. PERFORMING ORGANIZATION NAME(S) AND ADDRESS(ES) Steel Founders' Society of America (SFSA) 780 McArdle Dr Unit G Crystal Lake IL 60014	8. PERFORMING ORGANIZATION REPORT NUMBER PSC-2012
9. SPONSORING/MONITORING AGENCY NAME(S) AND ADDRESS(ES) US Army JM&L LCMC Acquisition Center AMSML-AQ-JA Bldg 10 Picatinny Arsenal, NJ 07806-5000	10. SPONSOR/MONITOR'S ACRONYM(S) ARDEC Benet Labs
	11. SPONSOR/MONITOR'S REPORT NUMBER(S)

12. DISTRIBUTION/AVAILABILITY STATEMENT

Distribution Statement A

13. SUPPLEMENTARY NOTES

14. ABSTRACT

Weapon system designers and builders need advanced steel casting technology to achieve the performance goals required for new systems. The dramatic reduction in weight and increase in capability will require high performance components with complex geometries. SFSA combined the latest developments in technology to improve the design and manufacturing of steel castings for improved weapon system reliability. SFSA developed innovative casting design and manufacturing processes for high performance parts. SFSA is uniquely positioned through its industry leadership steel casting R&D to assume a prominent role in the development of industry-ready, performance steel casting technology. R&D led to innovative capability to simulate the steel casting applications, manufacture short run tooling, and acquire advanced sand properties for modeling. SFSA developed the initial thrust on encapsulated ceramic armor tiles through steel casting. SFSA provided technical support and technology tools, including sourcing and tooling, to support the procurement of castings, which provided a benefit through facilitating a robust supply chain while minimizing cost and

15. SUBJECT TERMS

steel, casting, modeling, performance, rapid tooling, sand, armor, alloys, foundry, muzzle brake, supply center, tooling, sources

16. SECURITY CLASSIFICATION OF:			17. LIMITATION OF ABSTRACT	18. NUMBER OF PAGES	19a. NAME OF RESPONSIBLE PERSON
a. REPORT	b. ABSTRACT	c. THIS PAGE			David Poweleit
U	U	U	SAR	141	19b. TELEPHONE NUMBER 815-455-8240 x204

Standard Form 298